Feynman-Vernon influence functional approach to quantum transport in interacting nanojunctions: An analytical hierarchical study

Luca Magazzù and Milena Grifoni

Institute for Theoretical Physics, University of Regensburg, 93040 Regensburg, Germany

(Dated: April 30, 2021)

We present a non perturbative and formally exact approach for charge transport in interacting nanojunctions based on a real time path integral formulation of the reduced system dynamics. For reservoirs of noninteracting fermions, the exact trace over the leads' degrees of freedom results in the nonlocal in time Feynman-Vernon influence functional, which induces time correlations between tunneling transitions in and out of the nanojunction. An expansion of the influence functional in terms of the number of tunneling transitions, and integration of the Grassmann variables between the tunneling times, allows us to obtain a still exact generalized master equation (GME) for the populations of the reduced density matrix (RDM) in the occupation number representation, as well as a formally exact expression for the current. To this extent, we exploit that in the occupation number representation each single-particle fermionic degree of freedom can be only empty or occupied, and that this change can only occur upon tunneling. By borrowing the nomenclature of the famous spin-boson problem, we characterize the two-state dynamics of such degrees of freedom on the forward and backward branches in terms of single four-state paths with alternating blips and sojourns. This allows a diagrammatic representation of the GME kernel and its parametrization in terms of sequences of blips and sojourns.

We apply our formalism to the exactly solvable resonant level model (RLM) and to the the single impurity Anderson model (SIAM), the latter being a prototype system for studying strong correlations. For both systems, we demonstrate a hierarchical diagrammatic structure of the exact GME kernel. While the hierarchy closes at the second-tier level for the RLM, this is not the case for the interacting SIAM. Upon inspection of the GME, known results from various perturbative and nonperturbative approximation schemes to quantum transport in the SIAM are recovered. For example, a truncation to the second tier reproduces the resonant tunneling approximation applicable for temperatures well above the Kondo temperature $T_{\rm K}$. Finally, a noncrossing approximation for the hierarchical kernel is developed, which enables us to systematically decrease temperature at each next level of the approximation. Analytical results for a simplified fourth-tier scheme are presented.

I. INTRODUCTION

The qualitative understanding and quantitative description of transport properties of interacting nanojunctions is one of the core problems of nonequilibrium condensed matter physics. Interacting nanojunctions describe the general class of open systems whereby a quantum system S of interest (a molecule, a quantum wire, a set of quantum dots etc.) is coupled via tunneling to two or more fermionic reservoirs held at different chemical potential and/or temperature, see Fig. 1. Relevant observables of interest are typically the average current flowing through the junctions, or its higher-order cumulants, which result from a nonequilibrium configuration in the leads.

The presence of many-body electronic interactions in the central system, in combination with the large number of degrees of freedom in the fermionic reservoirs, renders the solution of the transport problem a challenge. Not even for the archetypal single-impurity Anderson model (SIAM) [1], where the central system is a single orbital which can accommodate two electrons of opposite spin, the current-voltage characteristics for this model has yet been obtained in closed analytic form in the whole regime of parameters. The SIAM is a prototypical example to investigate the interplay between strong correlations in the central system and a continuum of degrees of freedom

provided by the leads electrons. Below a critical temperature, known as Kondo temperature $T_{\rm K}$, this interplay gives rise to the emergence of the Kondo singlet, a bound state at the Fermi level signaling the screening of the unpaired impurity spin by the conduction electrons [2–6]. Importantly, the Kondo temperature depends exponentially on the tunneling coupling, showing the need of nonperturbative approaches in the tunneling to capture this effect [4].

The necessity to develop approximation schemes enabling the treatment of tunneling and interactions on the same footing is at the core of various approaches to interacting quantum transport which have been proposed in the literature. In order to understand the novelty of the method proposed in this work, and to put it in a proper context, we shortly summarize the very essence of the main approaches available so far. We start by distinguishing between numerically exact methods and analytical or semi-analytical schemes. In equilibrium, numerically exact methods such as the numerical renormalization group (NRG) [7, 8] or the density matrix renormalization group (DM-NRG) [9, 10] are well-established to evaluate the linear conductance through nanojunctions with only few degrees of freedom of the central system. In this work we shall use results from DM-NRG simulations to benchmark various approximation routes for the SIAM. Numerical schemes also applicable in nonequilib-

rium situations are being developed and involve, among others, time-dependent DM-NRG methods [11, 12], iterative [13] and Monte Carlo [14] path integral schemes, and hierarchical equation of motion approaches [15, 16], also based on the path integral approach, or auxiliary function methods [17–19]. See also [20] for a more detailed review and comparative study of some of these approaches. The computational effort however grows exponentially with the number of degrees of freedom of the central system, which renders numerical approaches impractical for interacting nanojunctions with more than few degrees of freedom.

For this reason, also semi-analytical and analytical schemes have attracted much interest to address the transport problem. These encompass frameworks where the expression for the current involves the calculation of nonequilibrium Greens' functions and associated self-energies [21–27] to ones where the current results from a statistical average, and thus the central quantities are the density operator or the reduced density matrix (RDM) of the open system, see e.g. [28–31]. Given the large variety of methods and their different range of applicability, it is rather difficult to keep focus of the enormous amount of literature by now available, so that comparison between various schemes and short topical reviews become very valuable [32–38].

From the perspective of this work, it is convenient to separate the available methods in two main groups. In the first one, and by far the most popular, starting point are dynamical equations for the relevant quantities, which are solved by truncating a hierarchy of equations, or by systematic perturbation schemes. The most known dynamical schemes involve equations of motions for the Green's functions [33, 39–43], kinetic equations for the density matrix [44, 45] or the reduced density operator [29, 46–52], and perturbative RG-schemes [53–59]. In the second and much less explored one, starting point are formally exact expressions for generating functions or for the reduced density matrix obtained with field integral methods. Here the relevant information on the time-evolution of the open system is captured e.g. by Keldysh effective actions [60, 61] or double-path Feynman-Vernon influence functionals [62, 63], resulting from an exact trace over the reservoir degrees of freedom. The advantage of these approaches is to enable analytical solutions being intrinsically nonperturbative in both the tunneling and interaction. For example, generating functional methods have been used to treat zero-bias anomalies in metallic islands [64], and the nonequilibrium Kondo effect in the SIAM [65, 66] and in carbon nanotube-based quantum dot [67–69]. However, a treatment of interacting nanojunctions based on an exact path integral expression for the junction's RDM has not been discussed yet. In this work we wish to bridge this gap.

Here we propose an analytical method, based on the Feynman-Vernon influence functional approach for fermionic reservoirs. This approach provides an exact expression for the RDM in the fermionic coherent-state representation [70, 71] and has been used to investigate transient and stationary transport in noninteracting nanojunctions [63, 72–74].

Here we show that the influence functional is also a powerful tool to treat interaction effects all the way down to low temperatures for a generic nanojunction linearly coupled to nonequilibrium fermionic reservoirs. Starting from the exact formal expression for the system's RDM, we derive a still exact quantum master equation for the same object. Importantly, and one major result of this work, a nested hierarchical structure of the quantum master equation kernel is recognized which allows for devising systematic, non perturbative schemes in the calculation of the kernel. Similarly, a path-integral expression for the current through the nanojunction is obtained and its relation to current formulae in terms of nonequilibrium Green's functions [21] elucidated. We apply then our formalism to two archetypal examples. The first one, the exactly solvable resonant level model (RLM) [36], is used to show that the nesting in the hierarchical structure is finite for noninteracting models, and thus a closed analytical form for the current can be obtained. The second is the SIAM, where the combined effect of interactions and tunneling coupling imply a complex, infinite, hierarchical structure. On the one hand, by performing an expansion of the kernel in powers of the tunneling coupling, Coulomb blockade physics, single electron tunneling and cotunneling effects occurring in the weak coupling limit [75] can be described, in agreement with established diagrammatic perturbative schemes, see e.g. [34, 47]. On the other hand, by truncating the hierarchy to the second tier, approximation schemes for the SIAM obtained from equation of motion approaches (EOM) for Green's function [76], or the diagrammatic resonant tunneling approximation (RTA) [47] are recovered. Such schemes foresee the onset of the Kondo zero-bias anomaly, but are plagued by a pinning problem of the self-energy at the particle-hole symmetry point when decreasing the temperature, see e.g. [40]. Further, the temperature for the onset of the anomaly differs from the proper Kondo temperature, see e.g. [49]. Thus higher-oder tiers are required. In this work, we develop an infinite-tier scheme whereby the problem of finding the self-energies, and thus the retarded Green's function, is reduced to a geometrical problem involving the inversion of matrices of dimension 4×4, at most, for the SIAM. Exemplarily, we discuss a fourth-tier scheme whose simplified version allows for an analytical solution that improves over the second-tier schemes.

The paper is structured as follows. In Sec. II we introduce the generic model for interacting nanojunctions and derive formally exact path integral expressions in the coherent-state representation [70] for both the RDM and for the current at a given lead [63, 72]. Here, as a result of the trace over the fermionic reservoirs, tunneling events in and out of the central system become correlated through the action of the time-nonlocal Feynman-Vernon influence functional. How to then obtain an exact master

equation for the RDM in the case of noninteracting nano-junctions is further discussed in [63, 72]. Since our focus is on the interplay of interactions and tunneling, we perform a first crucial step by expressing the exact propagator in the *occupation number representation* starting from the coherent-state picture. This transformation paves the route for the expansion of the influence functional in series of tunneling transitions discussed in Sec. III, and for the diagrammatic representation of the propagator in terms of *blips* and *sojourns* illustrated in Sec. IV. Here, borrowing the nomenclature from the famous spin-boson problem [77], we show that by expanding the influence functional and integrating out the Grassmann variables we can view a path as a sequence of blips/sojourns as for the two-state system in the spin-boson problem; the two states of the spin correspond here to (fermionic) degrees of freedom of the central system being empty or singly occupied. In Sec. V this knowledge is used to obtain an exact generalized master equation for the diagonal elements (populations) of the RDM, as well as an integral equation for the current. The hierarchical structure of the populations kernel in Laplace space and the Dyson equation for its propagator are derived in the central Sec. VI. Specializing to the case of proportional coupling, the connection between the current kernel and the retarded Green's function is established in Sec. VII. There, the Meir-Wingreen formula for the current is recovered. There follow two sections where we apply our general formalism to the exactly solvable RLM, Sec. VIII, and to the SIAM, Sec. IX. Since the RLM accommodates at most one electron, interactions effects play no role here, and the Dyson equation for the propagator is solved exactly at the second-tier level. In the SIAM in contrast, the hierarchy of equations for the propagator does not close, and approximation schemes are required. We show how to recover within our formalism various common approximation schemes for the SIAM and discuss further a novel infinite-tier scheme. Analytical results are then obtained within a truncation of this scheme to the fourth tier, with some additional simplifications. Finally, conclusions are drawn in Sec. X. Some of the detailed derivations are deferred to the appendices.

II. PATH INTEGRAL REPRESENTATION FOR THE REDUCED DENSITY MATRIX AND THE CURRENT

We consider the general transport setting depicted in Fig. 1, where a central interacting region, with a number N of available electron states, indexed by i or j in what follows, is connected via tunnel coupling to non-interacting fermionic leads, held in general at different chemical potentials and/or different temperatures. This general setting can describe molecular junctions [26, 27], manufactured nanostructures, such as lateral quantum dots [78], or other complex junctions [79].

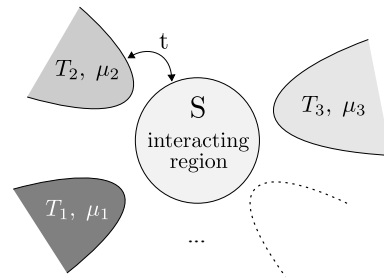The Hamiltonian of this transport setup consists of

FIG. 1. General transport setting where a central interacting region, the system S, is tunnel-coupled to several noninteracting fermionic leads with given temperature and chemical potential.

three terms, corresponding to the partition in central system (S) plus leads coupled via a particle exchange term, and reads

$$
\begin{aligned}
H =& H_S + \sum_{\alpha k \sigma} \epsilon_{\alpha k} c^\dagger_{\alpha k \sigma} c_{\alpha k \sigma} \\
&+ \sum_{i \alpha k \sigma} \left[t_{i \alpha k \sigma} a^\dagger_i c_{\alpha k \sigma} + t^*_{i \alpha k \sigma} c^\dagger_{\alpha k \sigma} a_i \right] .
\end{aligned}
\tag{1}
$$

The central system part is left unspecified at the present stage, being some function of the fermionic creation and annihilation operators $a^\dagger_i$ and a_i relative to the single-particle basis $\{|i\rangle\}$ in S. It contains in principle interaction terms which are quartic in these operators. Further, for simplicity, H_S is assumed to be time-independent, although the inclusion of time-dependent terms in a real-time path integral formalism is straightforward [62, 80]. The second term is the free leads part with creation and annihilation operators $c^\dagger_{\alpha k \sigma}$ and $c_{\alpha k \sigma}$, where α runs over the leads, σ is the spin degree of freedom, and k denotes the kth electronic state in the lead α. The third term in Eq. (1) describes the exchange of particles between dot and leads, with the energies $t_{i \alpha k \sigma}$ giving the amplitude of the tunnel coupling. In the continuum limit, denoting with $\varrho_{\alpha \sigma}(\epsilon)$ the density of states of lead α in energy space, we set $\sum_{\alpha k \sigma} \rightarrow \sum_{\alpha \sigma} \int d\epsilon \varrho_{\alpha \sigma}(\epsilon)$. Then, the tunnel coupling is characterized by the energy-dependent hybridization matrix $\mathbf{\Gamma}(\epsilon) = \sum_\alpha \mathbf{\Gamma}_\alpha(\epsilon)$ whose elements are

$$
[\mathbf{\Gamma}_\alpha(\epsilon)]_{ij} := 2\pi \sum_\sigma \varrho_{\alpha \sigma}(\epsilon) t_{i\alpha}(\epsilon) t^*_{j\alpha}(\epsilon) .
\tag{2}
$$

A. Reduced density matrix and current

Let us denote with ρ the reduced density matrix (RDM) of the central system. The RDM is obtained from $\rho_{\text{tot}}(t)$, the total density matrix, by tracing out the leads degrees of freedom $\rho(t) = \text{Tr}_{\text{leads}}[\rho_{\text{tot}}(t)]$, with the time evolution of ρ_{tot} being governed by the evolution operator associated to the Hamiltonian (1). Since

we have assumed noninteracting leads, this trace can be performed exactly in the coherent-state representation using standard path integral techniques [70, 72]. We assume for simplicity an initially factorized density matrix $\rho_{\text{tot}}(t_0) = \rho(t_0) \otimes \rho_{\text{leads}}^{\text{th}}$, where $\rho_{\text{leads}}^{\text{th}} = \bigotimes_\alpha \rho_\alpha^{\text{th}}$, with the lead α in the grand-canonical equilibrium state at a given temperature T_α and chemical potential μ_α, see Fig. 1. The propagator $\mathcal{J}$ yields the matrix elements of the RDM in the coherent-state representation at time t according to

$$\langle \boldsymbol{\xi}_a | \rho(t) | \boldsymbol{\xi}_b \rangle = \int d^2\boldsymbol{\xi}_0 d^2\bar{\boldsymbol{\xi}}_0 \mathcal{J}(\boldsymbol{\xi}_a^*, \boldsymbol{\xi}_b, t; \boldsymbol{\xi}_0, \bar{\boldsymbol{\xi}}_0^*, t_0) \rho_{\boldsymbol{\xi}_0 \bar{\boldsymbol{\xi}}_0}(t_0) , \tag{3}$$

where $\rho_{\boldsymbol{\xi}_0 \bar{\boldsymbol{\xi}}_0}(t_0) = \langle \boldsymbol{\xi}_0 | \rho(t_0) | \bar{\boldsymbol{\xi}}_0 \rangle$. The Grassmann variables $\boldsymbol{\xi} = (\dots, \xi^i, \dots)$ and $\boldsymbol{\xi}^* = (\dots, \xi^{i*}, \dots)$ have one component for each electronic state which is defined by $\hat{a}_i | \boldsymbol{\xi} \rangle = \xi^i | \boldsymbol{\xi} \rangle$ and $\langle \boldsymbol{\xi} | \hat{a}_i^\dagger = \xi^{i*} \langle \boldsymbol{\xi} |$. Following the procedure outlined in Appendix A, the propagator acquires the formal, exact path integral expression in the coherent-state representation

$$\mathcal{J}(\boldsymbol{\xi}_a^*, \boldsymbol{\xi}_b, t; \boldsymbol{\xi}_0, \bar{\boldsymbol{\xi}}_0^*, t_0) = \int_{\boldsymbol{\xi}_0}^{\boldsymbol{\xi}_a^*} D\boldsymbol{\xi} \int_{\bar{\boldsymbol{\xi}}_0^*}^{\boldsymbol{\xi}_b} D\bar{\boldsymbol{\xi}} \\ \times e^{\frac{i}{\hbar}[S_S(\boldsymbol{\xi}^*, \boldsymbol{\xi}) - S_S^*(\bar{\boldsymbol{\xi}}^*, \bar{\boldsymbol{\xi}})]} \mathcal{F}(\boldsymbol{\xi}^*, \boldsymbol{\xi}, \bar{\boldsymbol{\xi}}^*, \bar{\boldsymbol{\xi}}) , \tag{4}$$

where $\int D\boldsymbol{\xi} = \int \prod_{k=1}^K d\boldsymbol{\xi}(t_k)^* d\boldsymbol{\xi}(t_k)$ and $\int D\bar{\boldsymbol{\xi}} = \int \prod_{k=1}^K d\bar{\boldsymbol{\xi}}(t_k)^* d\bar{\boldsymbol{\xi}}(t_k)$ denote the sums over paths in the forward and backward time branches, respectively, with fixed end-points and $K \to \infty$. The action of the central system is given by the time-discretized expression ($\boldsymbol{\xi}_k \equiv \boldsymbol{\xi}(t_k)$ and $t_{k+1} = t_k + \delta t$)

$$e^{\frac{i}{\hbar}S_S(\boldsymbol{\xi}^*, \boldsymbol{\xi})} = \prod_{k=0}^K e^{-\boldsymbol{\xi}_k^* \cdot \boldsymbol{\xi}_k + \boldsymbol{\xi}_{k+1}^* \cdot \boldsymbol{\xi}_k - \frac{i}{\hbar} H_S(\boldsymbol{\xi}_{k+1}^*, \boldsymbol{\xi}_k)\delta t} ,$$
$$e^{\frac{i}{\hbar}S_S^*(\bar{\boldsymbol{\xi}}^*, \bar{\boldsymbol{\xi}})} = \prod_{k=0}^K e^{-\bar{\boldsymbol{\xi}}_k^* \cdot \bar{\boldsymbol{\xi}}_k + \bar{\boldsymbol{\xi}}_k^* \cdot \bar{\boldsymbol{\xi}}_{k+1} + \frac{i}{\hbar} H_S(\bar{\boldsymbol{\xi}}_k^*, \bar{\boldsymbol{\xi}}_{k+1})\delta t} , \tag{5}$$

with $\boldsymbol{\xi}^*(t_{K+1}) \equiv \boldsymbol{\xi}_a^*$ and $\bar{\boldsymbol{\xi}}(t_{K+1}) \equiv \boldsymbol{\xi}_b$. Due to the trace over the leads, these paths are coupled by the Feynman-Vernon influence functional [62] $\mathcal{F}(\boldsymbol{\xi}^*, \boldsymbol{\xi}, \bar{\boldsymbol{\xi}}^*, \bar{\boldsymbol{\xi}}) = \exp[\Phi(\boldsymbol{\xi}^*, \boldsymbol{\xi}, \bar{\boldsymbol{\xi}}^*, \bar{\boldsymbol{\xi}})]$ whose phase can be given in the following symmetric form, see Appendix B,

$$\Phi(\boldsymbol{\xi}^*, \boldsymbol{\xi}, \bar{\boldsymbol{\xi}}^*, \bar{\boldsymbol{\xi}}) = -\int_{t_0}^t dt' \int_{t_0}^{t'} dt'' \Big[\\ \boldsymbol{\xi}^*(t') \cdot \mathbf{g}_-(t' - t'') \cdot \boldsymbol{\xi}(t'') + \boldsymbol{\xi}(t') \cdot \mathbf{g}_+^*(t' - t'') \cdot \boldsymbol{\xi}^*(t'') \\ -\bar{\boldsymbol{\xi}}(t') \cdot \mathbf{g}_-^*(t' - t'') \cdot \bar{\boldsymbol{\xi}}^*(t'') - \bar{\boldsymbol{\xi}}^*(t') \cdot \mathbf{g}_+(t' - t'') \cdot \bar{\boldsymbol{\xi}}(t'') \\ +\bar{\boldsymbol{\xi}}^*(t') \cdot \mathbf{g}_-(t' - t'') \cdot \boldsymbol{\xi}(t'') + \bar{\boldsymbol{\xi}}(t') \cdot \mathbf{g}_+^*(t' - t'') \cdot \boldsymbol{\xi}^*(t'') \\ -\boldsymbol{\xi}(t') \cdot \mathbf{g}_-^*(t' - t'') \cdot \bar{\boldsymbol{\xi}}^*(t'') - \boldsymbol{\xi}^*(t') \cdot \mathbf{g}_+(t' - t'') \cdot \bar{\boldsymbol{\xi}}(t'') \Big] . \tag{6}$$

The correlation matrices $\mathbf{g}_\pm$ have elements

$$g_{ij,\pm}(t) = \frac{1}{\hbar^2} \sum_{\alpha k \sigma} t_{i\alpha k \sigma} t_{j\alpha k \sigma}^* f_\pm^\alpha(\epsilon_k) e^{-\frac{i}{\hbar}\epsilon_{\alpha k} t} , \tag{7}$$

where $f_+^\alpha(\epsilon_k) = [1 + e^{\beta_\alpha(\epsilon_{\alpha k} - \mu_\alpha)}]^{-1}$ is the Fermi function of lead α and $f_-^\alpha(\epsilon_k) := 1 - f_+^\alpha(\epsilon_k)$. As shown in Appendix C, these matrix elements are the correlation functions of the leads' force operator.

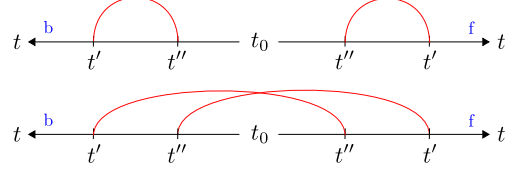The phase of the influence functional, Eq. (6), displays

FIG. 2. The elementary processes displayed in the phase of the influence functional, Eq. (6): Each line joining a pair of tunneling transitions represents either a creation/annihilation or annihilation/creation process, giving a total of eight elementary processes. In the lower panel, the paths in the forward (f) and backward (b) time branch are coupled by the influence phase Φ.

the eight fundamental processes involved in the transport setup consisting of pairs of tunneling events, each creating or annihilating one electron in the central system, connected by a fermion line. These processes are shown in Fig. 2. A fermion line is mathematically represented by the time-dependent part of the correlation function calculated at the difference between the times of the two events, see Eq. (7). To the two tunneling transitions coupled by a correlation matrix $\mathbf{g}$ we attributed the product of the two tunnel amplitudes with the appropriate Fermi function, as given by the prefactors of $\mathbf{g}$. As an example of process in the phase of the influence functional, consider $\xi^{i*}(t') g_{ij,-}(t' - t'')\xi^j(t'')$, which is one of the terms generated by the scalar product in the first term of the sum in Eq. (6). This is the forward process depicted in the upper-right part of Fig. 2 and consists in the destruction of one electron in the state j of the central system at time t'' followed by the creation of one electron at a later time t' in the state i. Note that this is actually a collection of processes, as there is a sum over the leads and their states in the correlation function. Likewise, $\bar{\xi}^i(t') g_{ij,-}^*(t' - t'')\bar{\xi}^{j*}(t'')$ gives the creation of one electron in the dot at time t'' followed by the annihilation of an electron at a later time t' in the backward time branch, see the upper-left part of Fig. 2.

As can be seen from Eq. (6), in the influence functional, forward and backward paths of the individual degrees of freedom are self-interacting and also coupled to each other in a time-nonlocal fashion. The latter feature ensures that the Feynman-Vernon approach takes fully into account the back-action due to the leads in the system evolution.

B. Current

We define the particle current in lead l as the expectation value of $\hat{\dot{N}}_l(t)$, the time derivative of the particle number operator of lead l. In the Heisenberg picture $\hat{N}_l(t) = \sum_{k\sigma} c_{lk\sigma}^\dagger(t) c_{lk\sigma}(t)$ so that, with the general Hamiltonian in Eq. (1),

$$
\begin{aligned}
\hat{\dot{N}}_l(t) &= -\frac{i}{\hbar}\left[\hat{N}_l(t), H(t)\right] \\
&= -\frac{i}{\hbar}\sum_{ik\sigma}\left[t_{ilk\sigma}^* c_{lk\sigma}^\dagger(t) a_i(t) - t_{ilk\sigma} a_i^\dagger(t) c_{lk\sigma}(t)\right].
\end{aligned}
\tag{8}
$$

The electron current $I_l(t) = -e\langle\hat{\dot{N}}_l(t)\rangle$, where $\langle\hat{\dot{N}}_l(t)\rangle = \text{Tr}[\hat{\dot{N}}_l(t)\rho_{\text{tot}}]$, assumes the form

$$
\begin{aligned}
I_l(t) &= e\frac{i}{\hbar}\sum_{ik\sigma}\left[t_{ilk\sigma}^*\langle c_{lk\sigma}^\dagger(t) a_i(t)\rangle - t_{ilk\sigma}\langle a_i^\dagger(t) c_{lk\sigma}(t)\rangle\right] \\
&\equiv e 2\text{Re }\text{Tr}_{\text{S}}[\boldsymbol{\mathcal{A}}_l(t)],
\end{aligned}
\tag{9}
$$

where, using $\hat{O}_H(t) = U^\dagger(t, t_0)\hat{O}_S U(t, t_0)$, we have defined the system operator $\mathcal{A}_l(t)$ as the following trace over the leads

$$
[\boldsymbol{\mathcal{A}}_l(t)]_{ii} := -\frac{i}{\hbar}\sum_{k\sigma} t_{ilk\sigma}\text{Tr}_{\text{leads}}\left[a_i^\dagger c_{lk\sigma}\rho_{\text{tot}}(t)\right].
\tag{10}
$$

The system operator $\mathcal{A}_l(t)$ admits a path integral representation similar to the one carried out for the RDM, namely

$$
\langle\boldsymbol{\xi}_a|\boldsymbol{\mathcal{A}}_l(t)|\boldsymbol{\xi}_b\rangle = \int d^2\boldsymbol{\xi}_0 d^2\bar{\boldsymbol{\xi}}_0 \mathcal{J}_l^I(\boldsymbol{\xi}_a^*, \boldsymbol{\xi}_b, t; \boldsymbol{\xi}_0, \bar{\boldsymbol{\xi}}_0^*, t_0)\rho_{\boldsymbol{\xi}_0\bar{\boldsymbol{\xi}}_0}(t_0).
\tag{11}
$$

The current propagator is given by [63, 72]

$$
\begin{aligned}
\mathcal{J}_l^I(\boldsymbol{\xi}_a^*, \boldsymbol{\xi}_b, t; \boldsymbol{\xi}_0, \bar{\boldsymbol{\xi}}_0^*, t_0) &= \int_{\boldsymbol{\xi}_0}^{\boldsymbol{\xi}_a^*} D\boldsymbol{\xi}\int_{\bar{\boldsymbol{\xi}}_0^*}^{\boldsymbol{\xi}_b} D\bar{\boldsymbol{\xi}} \\
&\times e^{\frac{i}{\hbar}[S_{\text{S}}(\boldsymbol{\xi}^*, \boldsymbol{\xi}) - S_{\text{S}}^*(\bar{\boldsymbol{\xi}}^*, \bar{\boldsymbol{\xi}})]}\mathcal{I}_l(\boldsymbol{\xi}^*, \boldsymbol{\xi}, \bar{\boldsymbol{\xi}})\mathcal{F}(\boldsymbol{\xi}^*, \boldsymbol{\xi}, \bar{\boldsymbol{\xi}}^*, \bar{\boldsymbol{\xi}}).
\end{aligned}
\tag{12}
$$

This expression is similar to that of the propagator for the system RDM, Eq. (4), the difference being the multiplicative current functional

$$
\begin{aligned}
\mathcal{I}_l(\boldsymbol{\xi}^*, \boldsymbol{\xi}, \bar{\boldsymbol{\xi}}) = -\int_{t_0}^t dt'\, \boldsymbol{\xi}^*(t)\big[&\mathbf{g}_{l,-}(t - t')\boldsymbol{\xi}(t') \\
&-\mathbf{g}_{l,+}(t - t')\bar{\boldsymbol{\xi}}(t')\big]
\end{aligned}
\tag{13}
$$

(compare with the phase of the influence functional given by Eq. (6)). Here, the correlation matrices bear the index l (which is not summed over) of the lead considered for the calculation of the current, with $\mathbf{g}_\pm(t) = \sum_\alpha \mathbf{g}_{\alpha,\pm}(t)$. Moreover, there is one single time integral and the last Grassmann variable has the time argument fixed at the final time t while the argument of the first runs from t_0 to t. Finally, the structure of the integrand in $\mathcal{I}$ is similar

to that of Φ, the exponent of the influence functional $\mathcal{F}$ given in Eq. (6), except for the two constraints that fix the nature of the last Grassmann variable, reflecting the fact that the operator $a_i^\dagger$ is fixed in the calculation of $\mathcal{A}_l$, see Eq. (10). In Appendix D, we show the connection between the path integral expression for the current and the Green's functions.

C. Propagators in the occupation number representation

For a system with N electronic states $i = 1, \ldots, N$, we introduce the composite index $\boldsymbol{n} = (n_1, \ldots, n_N)$ collecting the occupations of the states in the occupation number representation, with $n_i = 0, 1$ for state i. The anticommutation relation obeyed by any two Grassmann variables yields the property [70]

$$
\int d\xi^* d\xi\left\{\xi^*\xi,\ \xi^*,\ \xi,\ 1\right\} = \left\{-1,\ 0,\ 0,\ 0\right\}.
\tag{14}
$$

Note that ξ^* and ξ are independent Grassmann variables. The definition of coherent states

$$
|\boldsymbol{\xi}\rangle = \prod_{i=1}^N(1 - \xi^i a_i^\dagger)|0_i\rangle
$$

and the property of the Grassmann integrals, Eq. (14), allow us to define the projectors that map the system state from the coherent-state to the occupation number representation. For example, in the case of a single electron state ($N = 1$) an element of the RDM reads in the coherent-state representation

$$
\langle\xi|\rho(t)|\bar{\xi}\rangle = \rho_{00}(t) + \rho_{01}(t)\bar{\xi} + \rho_{10}(t)\xi^* + \rho_{11}(t)\xi^*\bar{\xi},
\tag{15}
$$

where we have used $\langle 0|\xi\rangle = \langle 0|(1 - \xi a^\dagger)|0\rangle = 1 - \langle 0|\xi|1\rangle = 1 - \xi\langle 0|1\rangle = 1$ and $\langle 1|\xi\rangle = \langle 0|a|\xi\rangle = \langle 0|\xi|\xi\rangle = \xi\langle 0|\xi\rangle = \xi$. The elements of the RDM in the occupation number representation are then recovered by performing the Grassmann integrals

$$
\rho_{nn'}(t) = \Pi(n')\Pi^*(n)\ \langle\xi|\rho(t)|\bar{\xi}\rangle,
\tag{16}
$$

where the projectors $\Pi^*(n)$ and $\Pi(n)$ integrate out the Grassmann variables to the left and to the right of the operator $|0\rangle\langle 0|$, respectively. Their definitions are

$$
\begin{aligned}
\Pi^*(0) &= \int d\xi^*\xi^*,\quad \Pi^*(1) = \int d\xi^*, \\
\Pi(0) &= \int d\bar{\xi}\,\bar{\xi},\qquad \Pi(1) = \int d\bar{\xi},
\end{aligned}
\tag{17}
$$

as can be checked by applying the rules in Eq. (14) for the Grassmann integrals. In the general case, the populations, identified by the occupations $n_1, \ldots, n_N$, are given by $P_{\boldsymbol{n}}(t) = \rho_{\boldsymbol{nn}}(t) = \Pi_b(\boldsymbol{n})\Pi_a^*(\boldsymbol{n})\,\rho_{ab}(t)$, where

$$
\Pi(\boldsymbol{n}) = \prod_{i=1}^N \Pi^i(n_i),\qquad \Pi^*(\boldsymbol{n}) = \prod_{i=N}^1 \Pi^{i*}(n_i).
\tag{18}
$$

The propagator for the populations in the occupation number representation gives the population vector at time t according to

$$P_{\boldsymbol{n}'}(t) = \sum_{\boldsymbol{n}''} J_{\boldsymbol{n}'\boldsymbol{n}''}(t,t_0) P_{\boldsymbol{n}''}(t_0) . \qquad (19)$$

Thus, the matrix element $(\boldsymbol{n}', \boldsymbol{n})$ of the propagator is obtained by fixing the initial state to $\rho(t_0) = |\boldsymbol{n}\rangle\langle\boldsymbol{n}|$ so that $P_{\boldsymbol{n}''}(t_0) = \delta_{\boldsymbol{n}''\boldsymbol{n}}$. Then

$$J_{\boldsymbol{n}'\boldsymbol{n}}(t,t_0) = \Pi_b(\boldsymbol{n}')\Pi_a^*(\boldsymbol{n}') \int d^2\boldsymbol{\xi}_0 d^2\bar{\boldsymbol{\xi}}_0 \mathcal{J}(\boldsymbol{\xi}_a^*, \bar{\boldsymbol{\xi}}_b, t; \boldsymbol{\xi}_0, \bar{\boldsymbol{\xi}}_0^*, t_0)$$
$$\times \langle\boldsymbol{\xi}_0|\boldsymbol{n}\rangle\langle\boldsymbol{n}|\bar{\boldsymbol{\xi}}_0\rangle , \qquad (20)$$

where we use Eq. (15) to calculate the matrix element of the RDM at t_0 in the coherent-state representation. Equation (20) provides the recipe to obtain the propagator in the occupation number representation starting from the coherent-state path integral picture.

Likewise, the diagonal elements of the current propagator in Eq. (11) are obtained as

$$J_{l,\boldsymbol{n}'\boldsymbol{n}}^I(t,t_0) = \Pi_b(\boldsymbol{n}')\Pi_a^*(\boldsymbol{n}') \int d^2\boldsymbol{\xi}_0 d^2\bar{\boldsymbol{\xi}}_0 \mathcal{J}_l^I(\boldsymbol{\xi}_a^*, \bar{\boldsymbol{\xi}}_b, t; \boldsymbol{\xi}_0, \bar{\boldsymbol{\xi}}_0^*, t_0)$$
$$\times \langle\boldsymbol{\xi}_0|\boldsymbol{n}\rangle\langle\boldsymbol{n}|\bar{\boldsymbol{\xi}}_0\rangle . \qquad (21)$$

III. TUNNELING EXPANSION OF THE INFLUENCE FUNCTIONAL

The influence functional couples the processes within and between the forward and backward time branches of the propagators. To move forward in the actual calculations, first we unify the two time branches in a single one and then discretize the paths of the central system in this unique time branch by expanding the influence functional in the number of processes, namely in powers of Γ, see Eq. (2). This expansion gives rise to a diagrammatic unraveling of the propagator. The peculiarity of the present approach is the parametrization of the paths of S in terms of N paths of reduced density matrices of individual two-state systems, one for each electron state of the central system.

A. Diagrammatic unravelling of the propagator from the expansion of the influence functional

Adopting the following notation

$$\boldsymbol{\xi}_{+1}^{+1} = \boldsymbol{\xi} , \quad \boldsymbol{\xi}_{+1}^{-1} = \boldsymbol{\xi}^* , \quad \boldsymbol{\xi}_{-1}^{+1} = \bar{\boldsymbol{\xi}} , \quad \boldsymbol{\xi}_{-1}^{-1} = \bar{\boldsymbol{\xi}}^* ,$$
$$\mathbf{g}_{+1}^{+1} = \mathbf{g}_+ , \quad \mathbf{g}_{+1}^{-1} = \mathbf{g}_+^* , \quad \mathbf{g}_{-1}^{+1} = \mathbf{g}_- , \quad \mathbf{g}_{-1}^{-1} = \mathbf{g}_-^* ,$$
$$(22)$$

where the lower index identifies the time branch (sign of the Fermi function) and the upper index performs

the complex (Hermitian) conjugation for the Grassmann-valued paths (correlation matrices), the phase of the influence functional, Eq. (6), can be expressed in the compact form $\Phi(\boldsymbol{\xi}^*, \boldsymbol{\xi}, \bar{\boldsymbol{\xi}}^*, \bar{\boldsymbol{\xi}}) = \int_{t_0}^{t} dt' \int_{t_0}^{t'} dt'' \, F(t', t'')$, where

$$F(t', t'') = - \sum_{x,y,z=\pm 1} x \, \boldsymbol{\xi}_y^z(t') \mathbf{g}_{xz}^{-z}(t' - t'') \boldsymbol{\xi}_x^{-z}(t'') . \quad (23)$$

The eight elementary processes comprised by the phase of the influence functional are rendered by the sum over the three binary indexes $x, y,$ and z. As these processes consist of couples of tunneling transitions, the expansion in the tunnel coupling is given by the sum over the number m of pairs of transitions

$$\mathcal{J}(\boldsymbol{\xi}_a^*, \boldsymbol{\xi}_b, t; \boldsymbol{\xi}_0, \bar{\boldsymbol{\xi}}_0^*, t_0) = \sum_{m=0}^{\infty} \mathcal{J}^{(m)}(\boldsymbol{\xi}_a^*, \boldsymbol{\xi}_b, t; \boldsymbol{\xi}_0, \bar{\boldsymbol{\xi}}_0^*, t_0) .$$

The term with $2m$ transitions (order m in Γ, cf. Eq. (2)) reads

$$\mathcal{J}^{(m)}(\boldsymbol{\xi}_a^*, \boldsymbol{\xi}_b, t; \boldsymbol{\xi}_0, \bar{\boldsymbol{\xi}}_0^*, t_0) = \int \mathcal{D}\{t\}_m \int_{\boldsymbol{\xi}_0}^{\boldsymbol{\xi}_a^*} D\boldsymbol{\xi} \int_{\bar{\boldsymbol{\xi}}_0^*}^{\boldsymbol{\xi}_b} D\bar{\boldsymbol{\xi}}$$
$$\times e^{\frac{i}{\hbar}[S_S(\boldsymbol{\xi}^*, \boldsymbol{\xi}) - S_S^*(\bar{\boldsymbol{\xi}}^*, \bar{\boldsymbol{\xi}})]} \sum_{\mathcal{P}_m} \prod_{p=1}^{m} F_{k_p, l_p} ,$$
$$(24)$$

where $\mathcal{P}_m$ denotes one of the $(2m)!/(2^m m!)$ possible arrangements of $2m$ time indexes in groups of 2 with no repetitions, meaning that two transitions at the same time instant are not allowed. The symbol $\int \mathcal{D}\{t\}_m$ comprises the nested time integrations over the $2m$ transition times. Explicitly

$$\int \mathcal{D}\{t\}_m := \int_{t_0}^{t} dt_{2m} \int_{t_0}^{t_{2m}} dt_{2m-1} \cdots \int_{t_0}^{t_2} dt_1 . \quad (25)$$

In Eq. (24), we have introduced the Grassmann-valued functions

$$F_{kl} = - \sum_{i,j=1}^{N} \sum_{x,y,z=\pm 1} x \, [\xi_k^i]_y^z \, [g_{ij}(t_k - t_l)]_{xz}^{-z} \, [\xi_l^j]_x^{-z} . \quad (26)$$

Thus, in the present *time-discretized* picture of the influence functional, the Grassmann-valued paths, which are expressed in terms of a set of Grassmann numbers associated to the specific time instants of the tunneling transitions, consist of individual transition at specific times (the sequence of times being ordered). The nested time integrals in Eq. (25) reproduce all the possibilities for the sequences of processes. Finally, the sum over the set of coefficients $x, y,$ and z in Eq. (26) and the sum over the system states, implicit in the scalar products with the correlation matrix, produce the sum-over-paths.

To deal with the forward and backward paths with a single parametrization, it is convenient to use a single time direction for the two time branches depicted in

Fig. 2. In order to do so, it is necessary to make the associations

$$\begin{aligned} \xi^*/\xi & \quad \text{creation/annihilation in S} \\ \bar{\xi}^*/\bar{\xi} & \quad \text{annihilation/creation in S ,} \end{aligned} \tag{27}$$

as suggested by Fig. 3.

The resulting diagrammatic notation is more compact

FIG. 3. Forward (non-barred) and backward (barred) Grassmann variables arranged in a single (forward) time axis with reversal of the time direction for the backward branch. This requires associating to $\bar{\xi}^*$ the annihilation and to $\bar{\xi}$ the creation of an electron in the central system.

and the topology of the diagrams is different with respect to the Keldysh formalism. For example, diagrams displaying crossings in the Keldysh contour, as e.g. in the seminal work by König *et al.* [47], can be crossing-free when the time branches are collapsed in a single one, as in the present treatment, see also e.g. [37, 81].

Two examples of paths, comprising two tunneling transitions each, are detailed in Fig. 4 where the Grassmann variables associated to the transition times t_k and t_l and contained in the functions F_{kl} are highlighted. Both pro-
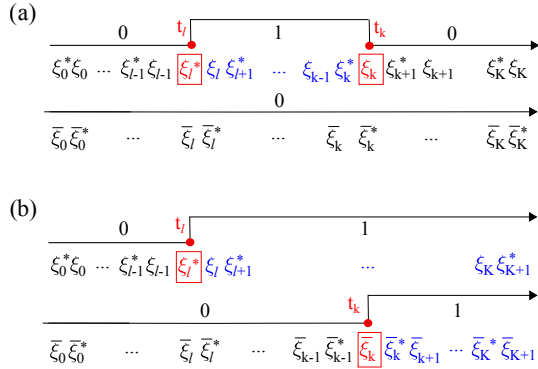
FIG. 4. Two examples of paths of an individual electron state in the central system. The transition times and the corresponding Grassmann variables $\xi_k \equiv \xi(t_k)$ contained in the influence functions, Eq. (26), are highlighted by red boxes. Zeros and ones indicate the occupation of the state in the forward and backward branches.

cesses in Fig. 4 fall in the class succinctly represented by the only diagram generated by the first order term in the expansion of the influence function, namely

$$F_{21} \rightarrow \quad \overparen{\qquad} \quad . \tag{28}$$

As a further example, the 2nd order term in the expansion of the influence functional gives

$$\sum_{\mathcal{P}_2} \prod_{p=1}^{2} \mathrm{F}_{k_p\, l_p} = \mathrm{F}_{21}\mathrm{F}_{43} + \mathrm{F}_{32}\mathrm{F}_{41} + \mathrm{F}_{31}\mathrm{F}_{42}$$

$$\rightarrow \underbrace{\overparen{\quad}\ \overparen{\quad}}_{} + \underbrace{\overparen{\overparen{\quad}}}_{} + \underbrace{\overparen{\overparen{\quad}}}_{} \ ,$$

where we provided a diagrammatic picture of the three terms resulting from the sum over the permutations. Note that each function F_{kl} contains a pair of Grassmann-valued (vector) variables and therefore the functions F commute with each other.

IV. STATE-CONSERVING TUNNELING AND DIAGRAMMATIC RULES

A. Diagonal hybridization matrix

The expansion in terms of the influence functions F_{kl} given in Eq. (24) is very general and only relies on the properties of Grassmann numbers. In the remaining of this work we focus for simplicity on the case in which the correlation matrices are diagonal in the basis $\{|i\rangle\}$ of single-electron states of the central system S, namely

$$[\mathbf{g}_{\alpha,\pm}(t)]_{ij} = \frac{1}{\hbar^2} \sum_{k\sigma} |\mathrm{t}_{i\alpha k\sigma}|^2 f_{\pm}^{\alpha}(\epsilon_k) e^{-\frac{i}{\hbar}\epsilon_{\alpha k} t} \delta_{ij} \ , \tag{29}$$

with $\mathbf{g}_{\pm}(t) = \sum_{\alpha} \mathbf{g}_{\alpha,\pm}(t)$. This implies that the paths of the different electron states in S are correlated only via the interaction term at the level of the system Hamiltonian and are otherwise independent. As a result, the energy-dependent hybridization matrix of lead α, Eq. (2), specializes to

$$[\mathbf{\Gamma}_{\alpha}(\epsilon)]_{ij} = 2\pi \sum_{\sigma} \varrho_{\alpha\sigma}(\epsilon)|\mathrm{t}_{i\alpha\sigma}(\epsilon)|^2 \delta_{ij} \ , \tag{30}$$

which is still state-dependent, i.e. not proportional to the identity. Note that the hybridization matrices of the different leads are simultaneously diagonal in the occupation basis $\{|n_1, \ldots, n_N\rangle\}$. Archetype examples of systems to which Eq. (29) applies are the resonant level model (RLM) and the single impurity Anderson model (SIAM) discussed in Secs. VIII and IX, respectively.

Due to the diagonal correlation matrices, Eq. (29), the influence functional is factorized and the fermion lines only connect transitions which change the occupation of individual states. As a result, if no coherences are present at the initial time t_0, none will be produced at later times. This is not true for non-diagonal correlation matrices, where coherences can develop and couple to the populations. This aspect is crucial for example in the so-called spin-valve setup [82–86] and for interacting nanojunctions displaying interference effects [44, 87, 88].

With the correlation matrices given by Eq (29), the

Grassmann-valued functions in Eq. (26) specialize to $F_{kl} = \sum_{i=1}^{N} F_{kl}^i$, where

$$F_{kl}^i = \sum_{x,y,z=\pm 1} -x \, [\xi_k^i]_y^z [g_{ii}(t_k - t_l)]_{xz}^{-z} [\xi_l^i]_x^{-z} . \tag{31}$$

The assumption of diagonal correlation matrices allows us to establish diagrammatic rules for the paths of individual fermionic single-particle states i and to express the contribution of a composite diagram, involving different electron states, in terms of the individual diagrammatic contributions and of a *common* phase factor accounting for the interactions.

B. Parametrization for a single degree of freedom (resonant level model)

Before considering the general case, we focus our attention on an individual degree of freedom of the central system S or, equivalently, on the simplest case of a *spinless level* coupled to electronic reservoirs, the so-called resonant level model, see Fig. 15 below.

To this extent we notice that a single fermionic degree of freedom is characterized, in the occupation number representation, by the two values $0, 1$, for the state being empty or occupied, respectively. Thus, one can consider the degree of freedom as a two-state system; the corresponding time evolution of generic forward and backward paths for such pseudo-spin, or qubit, is shown in Fig. 5. Borrowing ideas from the path integral formulation of the famous spin-boson problem [62], we conveniently collapse the two-state paths on the forward and backward branches into a single four-state path. As shown in Fig. 5, in analogy to the spin-boson nomenclature, we call sojourns the states $(0, \bar{0})$ and $(1, \bar{1})$, and blips the combinations $(0, \bar{1})$ and $(1, \bar{0})$. This is done under the assumption
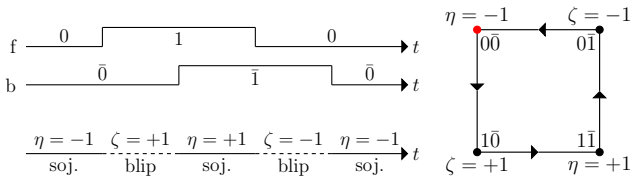
FIG. 5. Blip/sojourn parametrization. Left – Forward and backward paths associated to the occupation of an individual electron state with the corresponding collapsed, single-branch path parametrized in terms of blip and sojourns (below). Right – The time evolution now occurs along the four sides of the square, whose corners define the four elements of the density matrix of a two-state system. The red full dot on the top-left corner denotes the starting (and final) state of the path.

of instantaneous tunneling events that change the occupation number of the electron states in S. A sojourn state corresponds to having the same occupation of the electron state both in the forward and in the backward path,

meaning that the state is either empty ($\eta = -1$) or occupied ($\eta = +1$) in both branches. On the contrary, a blip state refers to different occupation of the two branches, namely occupied in the forward and empty in the backward ($\zeta = +1$) or *vice-versa* ($\zeta = -1$), see the right panel of Fig. 5. In the present case, since $N = 1$, we disregard the state index i, and Eq. (31) reduces to $F_{kl}^i \to F_{kl}$.

To proceed, we perform the integration of the Grassmann variables associated to the time instants *between* transitions, as done explicitly in Appendix. F. This results in the phase factors related to the central system S which are discussed below. The residual Grassmann variables are the ones associated to the transition times, as shown in Fig. 6 for a collapsed path which comprises four tunneling transitions.
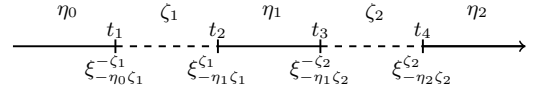

FIG. 6. Sequence of Grassmann variables associated to the transition times of an individual degree of freedom of the central system in the blip/sojourn parametrization, see Eqs. (22) and (27).

A path of the electron state with $2m$ transitions starting and ending in a sojourn, has $m + 1$ sojourn intervals $(\eta_0, \ldots, \eta_m)$ and m blip intervals $(\zeta_1, \ldots, \zeta_m)$. The path is thus uniquely identified by the corresponding sequence

$$\eta_0, \zeta_1, \eta_1, \ldots, \zeta_k, \eta_k, \ldots, \zeta_m, \eta_m.$$

With the associations made in Eqs. (22) and (27), to this sequence of blip/sojourn indexes there correspond the following sequence of Grassmann variables

$$\xi_{-\eta_0 \zeta_1}^{-\zeta_1}, \xi_{-\eta_1 \zeta_1}^{\zeta_1}, \ldots, \xi_{-\eta_{k-1} \zeta_k}^{-\zeta_k}, \xi_{-\eta_k \zeta_k}^{\zeta_k}, \ldots, \xi_{-\eta_m \zeta_m}^{\zeta_m} ,$$

as shown in Fig 6. To each transition to a blip state (odd transition times t_{2k-1}) is associated the Grassmann variable $[\xi_{2k-1}]_{-\eta_{k-1}\zeta_k}^{-\zeta_k} \equiv \xi_{-\eta_{k-1}\zeta_k}^{-\zeta_k}$ and to a transition to a sojourn (even transition times t_{2k}) is associated $[\xi_{2k}]_{-\eta_k \zeta_k}^{\zeta_k} \equiv \xi_{-\eta_k \zeta_k}^{\zeta_k}$. Grassmann variables at different times are independent, otherwise a path with two Grassmann variables of the same type (e.g. creation in the forward path) would yield a vanishing contribution due to the property $(\xi^*)^2 = \xi^2 = 0$. Note that to a given path there correspond different arrangements of the functions F_{kl} (fermion lines) attached to couples of transitions.

From Eq. (31), and using $(\zeta_k)^2 = 1$, according to the type of transitions being involved at times t_k and t_l (blip-sojourn, sojourn-blip, blip-blip, or sojourn-sojourn), the
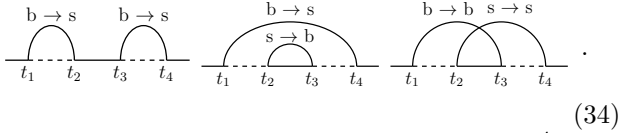
function F_{kl} acquires one of the forms

$$
\begin{aligned}
(b \to s) \qquad & F_{2k\,2l-1} = \xi^{\zeta_k}_{-\eta_k\zeta_k}\, f_{2k\,2l-1}\, \xi^{-\zeta_l}_{-\eta_{l-1}\zeta_l} \\
(s \to b) \qquad & F_{2k-1\,2l} = \xi^{-\zeta_k}_{-\eta_{k-1}\zeta_k}\, f_{2k-1\,2l}\, \xi^{\zeta_l}_{-\eta_l\zeta_l} \\
(b \to b) \quad & F_{2k-1\,2l-1} = \xi^{-\zeta_k}_{-\eta_{k-1}\zeta_k}\, f_{2k-1\,2l-1}\, \xi^{-\zeta_l}_{-\eta_{l-1}\zeta_l} \\
(s \to s) \qquad & F_{2k\,2l} = \xi^{\zeta_k}_{-\eta_k\zeta_k}\, f_{2k\,2l}\, \xi^{\zeta_l}_{-\eta_l\zeta_l}\ ,
\end{aligned} \tag{32}
$$

where

$$
\begin{aligned}
f_{2k\,2l-1} &= \eta_{l-1}\zeta_l\, g^{-\zeta_l}_{-\eta_{l-1}}(t_{2k} - t_{2l-1})\delta_{\zeta_k,\zeta_l} \\
f_{2k-1\,2l} &= \eta_l\zeta_l\, g^{\zeta_l}_{\eta_l}(t_{2k-1} - t_{2l})\delta_{\zeta_k,\zeta_l} \\
f_{2k-1\,2l-1} &= \eta_{l-1}\zeta_l\, g^{-\zeta_l}_{-\eta_{l-1}}(t_{2k-1} - t_{2l-1})\delta_{\zeta_k,-\zeta_l} \\
f_{2k\,2l} &= \eta_l\zeta_l\, g^{\zeta_l}_{\eta_l}(t_{2k} - t_{2l})\delta_{\zeta_k,-\zeta_l}\ .
\end{aligned} \tag{33}
$$

Equation (32) is the combined result of the parametrization of the paths shown in Figs. 5 and 6 and the form of the influence functions in Eq. (31). This result is essential to establish the diagrammatic rules discussed in the next section once the residual Grassmann variables are integrated out. The following scheme clarifies the associations in Eq. (32) in the case $m = 2$

$$ \tag{34} $$

Besides depending on the influence functions F^i_{kl}, the propagator also depends on the action of the central system $S_S(\boldsymbol{\xi}^*, \boldsymbol{\xi})$, see Eq. (4). Upon integrating out the Grassmann variables between transitions, this action produces the phase factors b_{kl} associated to the influence functions in Eq. (32). For a central system with a single spinless level of energy ϵ these phase factors are schematized by

$$
\begin{aligned}
(b \to s) \quad & e^{-\frac{i}{\hbar}\zeta_l\epsilon\,(t_{2k}-t_{2l-1})} \\
(s \to b) \quad & e^{+\frac{i}{\hbar}\zeta_l\epsilon\,(t_{2k-1}-t_{2l})} \\
(b \to b) \quad & e^{-\frac{i}{\hbar}\zeta_l\epsilon\,(t_{2k-1}-t_{2l-1})} \\
(s \to s) \quad & e^{+\frac{i}{\hbar}\zeta_l\epsilon\,(t_{2k}-t_{2l})}\ .
\end{aligned} \tag{35}
$$

Note that the sign of the exponent is determined by the state (blip/sojourn) from which the fermion line departs, see the scheme (34). Applying Eq. (20) to the propagator order by order, Eq. (24), we are left with the following expansion of the propagator for the populations in the resonant level model: $J_{\eta'\eta}(t; t_0) = \sum_{m=0}^{\infty} J^{(m)}_{\eta'\eta}(t; t_0)$, where

$$
J^{(m)}_{\eta'\eta}(t; t_0) = \sum_{\text{paths}_m} \int \mathcal{D}\{t\}_m \sum_{\mathcal{P}} \mathcal{B}_m(\mathcal{P})\Phi_m(\mathcal{P})\ . \tag{36}
$$

Here, the sum over the permutations $\mathcal{P}$ accounts for the different ways in which the fermion lines can connect m pairs of tunneling transitions within the path joining the

two sojourns η and η', see Eq. (34). The central system and influence functional part are given by

$$
\begin{aligned}
\mathcal{B}_m(\mathcal{P}) &= \prod_{p=1}^{m} b_{k_p\,l_p}\ , \\
\Phi_m(\mathcal{P}) &= \int \mathcal{D}\{\xi\}_m \prod_{p=1}^{m} F_{k_p\,l_p}\ ,
\end{aligned} \tag{37}
$$

respectively.

The sum over paths in Eq. (36) amounts to summing over the possible values of the intermediate blip and sojourn state with $2m$ tunneling transitions. For example, in the case $m = 2$

$$ \tag{38} $$

Finally, the symbol $\int \mathcal{D}\{\xi\}_m$ performs the integration over the residual Grassmann variables associated to the $2m$ transition times

$$
\int \mathcal{D}\{\xi\}_m := \int \prod_{k=1}^{m} (-\zeta_k\eta_k) d\xi^{-\zeta_k}_{-\eta_{k-1}\zeta_k} d\xi^{\zeta_k}_{-\eta_k\zeta_k}\ . \tag{39}
$$

The factors $-\eta_k\zeta_k$ in the above integration measure reflect the non-commuting nature of the symbols $d\xi$ and are introduced to keep track of the order in which the Grassmann-valued coordinates appear originally in the integration measure, i.e. $\prod_k d^2\xi(t_k)d^2\bar{\xi}(t_k) = \prod_k d\xi^*(t_k)d\xi(t_k)d\bar{\xi}^*(t_k)d\bar{\xi}(t_k)$, with the $*$-numbers to the left within the two classes of forward and backward variables, and with the backward variables to the right of the forward. This is exemplified in Appendix G.

C. Parametrization for N degrees of freedom

Due to the diagonal hybridization matrices introduced in Sec. IV A, the influence functional factorizes in the product of functionals for the individual electron states i, or, equivalently, the phase of the influence functional, Eq. (6), is the sum over the electron states i. As a result, the above description of the resonant level model generalizes in a straightforward fashion to N electronic states. In this case, the populations are identified with the string of sojourns associated to the different electron states via the vector index $\boldsymbol{\eta} = \{\eta^i\}$, with the correspondences $n_i = 0 \leftrightarrow \eta^i = -1$ and $n_i = 1 \leftrightarrow \eta^i = +1$. The propagator for the populations now reads $J_{\boldsymbol{\eta'\eta}}(t; t_0) = \sum_{m=0}^{\infty} J^{(m)}_{\boldsymbol{\eta'\eta}}(t; t_0)$, where

$$
J^{(m)}_{\boldsymbol{\eta'\eta}}(t; t_0) = \sum_{\text{paths}_m} \int \mathcal{D}\{t\}_m \prod_i \sum_{\mathcal{P}_i} \mathcal{B}^i_{m_i}(\mathcal{P}_i)\Phi^i_{m_i}(\mathcal{P}_i)\ , \tag{40}
$$

with $\sum_i m_i = m$, and where

$$\mathcal{B}^i_{m_i}(\mathcal{P}) = \prod_{p=1}^{m_i} \mathrm{b}^i_{k_p\, l_p} \ ,$$

$$\Phi^i_{m_i}(\mathcal{P}_i) = \int \mathcal{D}\{\xi\}_{m_i} \prod_{p=1}^{m_i} \mathrm{F}^i_{k_p\, l_p} \ . \tag{41}$$

The sum over the permutations $\mathcal{P}_i$ accounts now for the different ways in which the fermion lines can connect m_i pairs of tunneling transitions within the same path, that of the electron state i joining the two sojourns η^i and $\eta^{i\prime}$.

While the influence functions $\Phi^i_{m_i}$ depend exclusively on the path of the individual state i, the phase factors in $\mathcal{B}^i_{m_i}$ couple the paths of the different states via the interaction. Specifically, the constant single-particle energies ϵ_i turn into the path-dependent energies E_i; they depend on the instantaneous states of all degrees of freedom $\{\eta^j\}_n$ during the time interval τ_n between consecutive transitions, not necessarily of the same electron state. For example, assume that a fermion line associated to the state i departs form a blip state at time t_l and encompasses W intervals with $\sum_n^W \tau_n = t_k - t_l$. Then the corresponding phase factor reads

$$\mathrm{b}^i_{kl} := \prod_{n=1}^{W} e^{-\frac{i}{\hbar}\zeta_l E_i(\{\eta\}_n)\tau_n} \ , \tag{42}$$

which reduces for a noninteracting system to

$$\mathrm{b}^i_{kl} = \prod_{n=1}^{W} e^{-\frac{i}{\hbar}\zeta_l \epsilon_i \tau_n} = e^{-\frac{i}{\hbar}\zeta_l \epsilon_i (t_k - t_l)} \ . \tag{43}$$

Thus, in the noninteracting case, the integrand in Eq. (40) is actually factorized in the system's degrees on freedom.

Finally, the sum over paths in Eq. (40) now takes into account the different possibilities to distribute $2m$ transitions among the paths of the N individual states i connecting the initial and final sojourn states $\boldsymbol{\eta}$ and $\boldsymbol{\eta}'$ with $\sum_i m_i = m$.

To exemplify how these phase factors and the sum-over-paths work in the case of a multi-state system ($N > 1$), consider the case of the SIAM. As it describes an interacting central system which is a single, spinful level, we have $N = 2$ and $i \equiv \sigma = \uparrow, \downarrow$, cf. Eq. (147) below. In this specific case, denoting with $\bar\sigma$ the opposite spin state with respect to σ, the energies associated to the spin σ in the phase factors read

$$\begin{aligned} E_\sigma(\eta) &= \epsilon_\sigma + (1+\eta)U/2 & (\text{blip}-\text{soj.}) \\ E_\sigma &= \epsilon_\sigma + U/2 & (\text{blip}-\text{blip}) \ , \end{aligned} \tag{44}$$

Thus, for example, if the path of $\bar\sigma$ is in a sojourn state with $\eta = +1$, then $E_\sigma = \epsilon_\sigma + U$: This is the addition energy to be payed for adding a further electron to the dot. The presence of the term $U/2$ in the second line

of Eq. (44) implies that overlap of different fermion lines can produce the energy U according to the relative sign of the index ζ, see Appendix F for details. In Fig. 7 an example which shows the energies E_σ is provided for a path with two transition for each spin path.

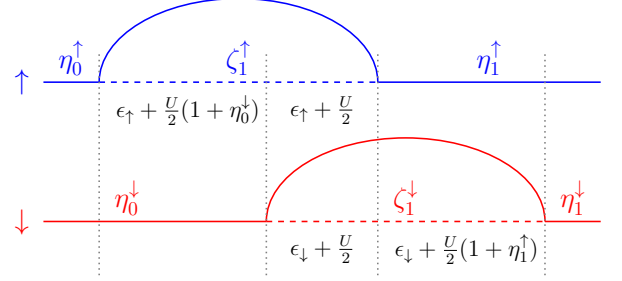The sum over paths with 4 transitions connecting the

FIG. 7. Path-dependent energies in the SIAM. The energies E_σ in the phase factors, Eq. (42), associated to the overlap of blip and sojourn of the two electron states $\sigma = \uparrow, \downarrow$ are $E_\sigma(\eta) = \epsilon_\sigma + (1+\eta)U/2$ for blip-sojourn overlap and $E_\sigma = \epsilon_\sigma + U/2$ for blip-blip overlap. The time axis is divided in 5 intervals τ_k separated by 4 tunneling transitions ($m = 2$) distributed between the two paths. The phase factors descend from the action of the central system, see Eqs. (4) and (5), after integrating-out the Grassmann variables between the tunneling transitions.

populations $\boldsymbol{\eta} = (\eta^\uparrow, \eta^\downarrow)$ and $\boldsymbol{\eta}' = (\eta'^\uparrow, \eta'^\downarrow)$ is given by

$$\tag{45}$$

Note that if $\eta'^\downarrow \neq \eta^\downarrow$, then the uppermost line of Eq. (45) does not contribute to the sum -over-paths. The same holds for $\sigma = \uparrow$ and the bottom line. If initial and final sojourns, $\boldsymbol{\eta}$ and $\boldsymbol{\eta}'$, differ for both spin states, then only the central line contributes to the sum.

Finally, the Grassmann variables and blip/sojourn indexes in the symbol $\int \mathcal{D}\{\xi\}_{m_i}$ acquire the state index i

$$\int \mathcal{D}\{\xi\}_{m_i} := \int \prod_{k=1}^{m_i} (-\zeta^i_k \eta^i_k) d\xi^{-\zeta^i_k}_{-\eta^i_{k-1}\zeta^i_k} d\xi^{\zeta^i_k}_{-\eta^i_k \zeta^i_k} \ , \tag{46}$$

cf. Eq. (39).

Using the parametrization of the paths in Fig. 6 for the individual degrees of freedom i and the integration

measure in Eq. (46) for the residual Grassmann variables associated to the transition times, we are able to automatically carry out the integrations over these variables: The result is simply an overall sign given by the anticommutation property of the ξ's, as detailed in Appendix F. In other words, we find from Eq. (32) the simple form

$$\Phi^i_{m_i}(\mathcal{P}_i) = \text{sgn}_{\mathcal{P}_i} \prod_{k=1}^{m_i} \zeta^i_k \eta^i_k \prod_{p=1}^{m_i} f^i_{k_p l_p} , \qquad (47)$$

where $\text{sgn}_{\mathcal{P}_i}$ is an overall sign given by the integration over the Grassmann variables associated to the transitions. This sign depends on the order of the transitions, and thus on the permutation $\mathcal{P}$, due to the noncommuting character of the Grassmann variables. Importantly, Eq. (47) allows us to establish diagrammatic rules, whereby the explicit form of the functions f_{kl} is obtained by just looking at the arrangement of the fermion lines in the associated diagram, cf. Eq. (33). The diagrammatic rules are summarized below.

D. Diagrammatic rules in the time domain for the individual electron states

Once specified a path of the full system with $2m$ transitions, the individual influence functions $\Phi^i_{m_i}$, Eq. (41), are the sums over the different arrangements of fermion lines f^i_{kl} connecting $2m_i$ transitions, where $\sum_i m_i = m$. Each of these arrangements of fermion lines constitutes a diagram relative to the state i. In this section we establish diagrammatic rules individually for each state. This is convenient because, since the Pauli exclusion principle applies separately to the different states in the central system, the overlap of fermion lines yields different diagrammatic contributions according to whether the lines involve the same or different electron states. Diagrams relative to different states are then coupled by the phase factors in $\mathcal{B}^i_{m_i}$, see Eqs. (41) and (42). Each diagrammatic contribution $\mathcal{B}^i_{m_i}(\mathcal{P}_i)\Phi^i_{m_i}(\mathcal{P}_i)$ to Eq. (40) consists of (from here on the state index i is understood)

- The overall sign $(-1)^{\text{n. crossings}}$ due to the integration of the Grassmann variables in Φ_m, see Eqs. (32), (41), and Eq. (47).

- The product $\prod_{k=1}^m (-\zeta_k \eta_k)$, from the normal ordering of the Grassmann integration measure, see Eqs. (39) and (46).

- The product of the functions f_{kl}, Eq. (33), representing the fermion lines which connect two tunneling transitions, times the corresponding phase factor b_{kl} of the central system, Eqs. (35) and (42). To each fermion line is associated the constraint on the ζ's connected by the line, according to the scheme in Eq. (33).

Below we show examples with m from 0 to 2. More examples, with higher order diagrams, are shown in Appendix H. For $m = 0$ there are no tunneling transitions. Hence

$$(0) \underline{\hspace{2cm}} \qquad \delta_{\eta',\eta} \qquad (48)$$

For $m = 1$ there is only one fermion line connecting two tunneling times

$$(1) \underset{\eta_0 \zeta_1}{\text{⌒----}} \qquad (+1)(-\zeta_1 \eta_1) \, f_{21} b_{21}$$

$$= (-\zeta_1 \eta_1) \, \eta_0 \zeta_1 g^{-\zeta_1}_{-\eta_0}(t_2 - t_1) b_{21} \qquad (49)$$

$$= \eta' \eta \, [-g^{-\zeta_1}_{-\eta}(t_2 - t_1)] b_{21} .$$

Here we used $(\zeta_1)^2 = 1$ and identified $\eta_0 = \eta$ and $\eta_1 = \eta'$. The full dot in the above diagram indicates the vertex, here associated to the transition from which the fermion line departs. Analogously, with $m = 2$

$$(2a) \underset{\eta_0 \zeta_1 \qquad \eta_1 \zeta_2}{\text{⌒----⌒----}}$$

$$(+1)\zeta_1 \eta_1 \zeta_2 \eta_2 \, f_{21} b_{21} f_{43} b_{43}$$

$$= \zeta_1 \eta_1 \zeta_2 \eta_2 \, \eta_0 \zeta_1 g^{-\zeta_1}_{-\eta_0}(t_2 - t_1) b_{21} \qquad (50)$$

$$\times \eta_1 \zeta_2 \, g^{-\zeta_2}_{-\eta_1}(t_4 - t_3) b_{43}$$

$$= \eta' \eta \, [-g^{-\zeta_1}_{-\eta}(t_2 - t_1)] b_{21} [-g^{-\zeta_2}_{-\eta_1}(t_4 - t_3)] b_{43} ,$$

$$(2b) \underset{\eta_0 \zeta_1 \quad \zeta_1 \eta_1}{\text{⌒--⌒----}}$$

$$(+1)\zeta_1 \eta_1 \zeta_2 \eta_2 \, f_{41} b_{41} f_{32} b_{32}$$

$$= \zeta_1 \eta_1 \zeta_2 \eta_2 \, \eta_0 \zeta_1 \, g^{-\zeta_1}_{-\eta_0}(t_4 - t_1) b_{41}$$

$$\times \zeta_1 \eta_1 \, g^{\zeta_1}_{\eta_1}(t_3 - t_2) b_{32} \delta_{\zeta_2,\zeta_1}$$

$$= \eta' \eta \delta_{\zeta_2,\zeta_1} \, [-g^{-\zeta_1}_{-\eta}(t_4 - t_1)] b_{41} \, [-g^{\zeta_1}_{\eta_1}(t_3 - t_2)] b_{32} , \qquad (51)$$

$$(2c) \underset{\eta_0 \zeta_1 \quad \zeta_1 \eta_1}{\text{⌒--⌒----}}$$

$$(-1)\zeta_1 \eta_1 \zeta_2 \eta_2 \, f_{31} b_{31} f_{42} b_{42}$$

$$= \zeta_1 \eta_1 \zeta_2 \eta_2 \, \eta_0 \zeta_1 \, g^{-\zeta_1}_{-\eta_0}(t_3 - t_1) b_{31}$$

$$\times \zeta_1 \eta_1 \, g^{\zeta_1}_{\eta_1}(t_4 - t_2) b_{42} \delta_{\zeta_2,-\zeta_1}$$

$$= \eta' \eta \, [-g^{-\zeta_1}_{-\eta}(t_3 - t_1)] b_{31} \, [-g^{\zeta_1}_{\eta_1}(t_4 - t_2)] b_{42} \delta_{\zeta_2,-\zeta_1} , \qquad (52)$$

where we used $\zeta_1 \zeta_2 \delta_{\zeta_2,-\zeta_1} = -\delta_{\zeta_2,-\zeta_1}$.

Noticeably, for all second-order diagrams, the product of the inner sojourns and blips results in a factor $+1$. Multiplication by internal sojourn indexes emerges as we go to higher orders and overlap of more than two fermion

lines. This is exemplified by the following diagram of order $m = 3$ (see also the complete list in Appendix H)

$$(3) \quad$$

$$\prod_{k=1}^{3}(-\zeta_k\eta_k)\eta_0\zeta_1 \, \mathrm{g}_{-\eta_0}^{-\zeta_1}(6,1)\mathrm{b}_{61} \, \zeta_1\eta_1\mathrm{g}_{\eta_1}^{\zeta_1}(5,2)\mathrm{b}_{52} \quad (53)$$

$$\times \, \eta_1\zeta_2\mathrm{g}_{-\eta_1}^{-\zeta_2}(4,3)\mathrm{b}_{43}\delta_{\zeta_3,\zeta_1}$$

$$= \eta'\eta\eta_1\eta_2 \, [-\mathrm{g}_{-\eta}^{-\zeta_1}(6,1)]\mathrm{b}_{61} \, [-\mathrm{g}_{\eta_1}^{\zeta_1}(5,2)]\mathrm{b}_{52}$$

$$\times \, [-\mathrm{g}_{-\eta_1}^{-\zeta_2}(4,3)]\mathrm{b}_{43}\delta_{\zeta_3,\zeta_1} \,,$$

where, for the sake of compactness, we set $\mathrm{g}(t_k - t_l) \equiv \mathrm{g}(k, l)$.

By applying the above rules we notice that the multiplicative factors ζ are always compensated by the product $\prod_{k=1}^{m}(-\zeta_k\eta_k)$ and by the constraints $\delta_{\zeta_k,\pm\zeta_l}$ contained in the functions f_{kl}, Eq. (33). The multiplicative sojourn indexes are instead compensated solely by the products $\zeta_l\eta_l$ or $\eta_{l-1}\zeta_l$ associated to each departing line (i.e. to the vertexes). As a result, each diagram presents, as a multiplicative factor, the product $\eta'\eta$ of the last and first sojourn indexes times the product of the η_k's of the internal sojourns which are not compensated, i.e. the ones with zero or two departing lines.

We are now in the position to set the diagrammatic rules for the individual states (to a full diagram will correspond the product of the diagrammatic contributions from each state, see Eq. (40) and the examples in Sec. IV E). To each diagram we associate

1. An overall sign $(-1)^{\text{n. crossings}}$.

2. A sign given by the products of the non-compensated ζ indexes (namely the ones of the blip states with zero or two vertexes) times the corresponding constraints. For example $\zeta_k\zeta_l\delta_{\zeta_k,-\zeta_l} = -\delta_{\zeta_k,-\zeta_l}$ and $\zeta_k\zeta_l\delta_{\zeta_k,\zeta_l} = \delta_{\zeta_k,\zeta_l}$, (because $\zeta = \pm 1$). These constraints make the corresponding sums in the sum-over-paths collapse.

3. The product $\eta'\eta$ times the product of the non-compensated η indexes, namely the ones of the sojourn states with zero or two vertexes.

4. The products of the correlators $-\mathrm{g}_x^y(t_k - t_l)$ and the associated phase factors b_{kl} of the central system for each fermion line.

To exemplify this, we consider the following 3rd-order diagram

$$(54)$$

$$- \eta'\eta\eta_1\eta_2[-\mathrm{g}_{-\eta}^{-\zeta_1}(4,1)]\mathrm{b}_{41} \, [-\mathrm{g}_{\eta_1}^{\zeta_1}(6,2)]\mathrm{b}_{62}$$

$$\times [-\mathrm{g}_{-\eta_1}^{-\zeta_1}(5,3)]\mathrm{b}_{53}\delta_{\zeta_3,-\zeta_1}\delta_{\zeta_2,\zeta_1} \,,$$

where, as in Eq. (52), we used $\zeta_1\zeta_3\delta_{\zeta_3,-\zeta_1} = -\delta_{\zeta_3,-\zeta_1}$. Another example is given by

$$(55)$$

$$- \eta'\eta\eta_1\eta_2[-\mathrm{g}_{-\eta}^{-\zeta_1}(4,1)]\mathrm{b}_{41} \, [-\mathrm{g}_{\eta_1}^{\zeta_1}(5,2)]\mathrm{b}_{52}$$

$$\times [-\mathrm{g}_{-\eta_1}^{-\zeta_1}(6,3)]\mathrm{b}_{63}\delta_{\zeta_3,\zeta_1}\delta_{\zeta_2,\zeta_1} \,,$$

where we used $\zeta_1\zeta_3\delta_{\zeta_3,\zeta_1} = \delta_{\zeta_3,\zeta_1}$.

By inspection of the diagrams in Eqs. (53)-(55), one sees that none of the correlators g bears the index η_2. If also the phase factors b_{kl} do not depend on η_2, as e.g. in the case of the resonant level model, or in the non-interacting case, see Eq. (42), then by performing the sum over paths the diagrams with this topology *vanish collectively* due to the sum over η_2. A similar argument holds for all the diagrams with more than two overlapping fermion lines of the same state i because overlap of more than two fermion lines entails the presence of sojourns with no vertexes. This means, in particular, that:
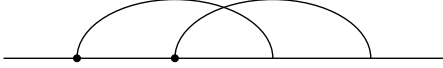
- The exact propagator for the resonant level model is reproduced by the diagrams with at most two overlapping fermion lines.

- For the non-interacting spinful level the exact propagator is reproduced by the diagrams with at most four overlapping fermion lines, of which no more that two can belong to the same spin.

These results are in agreement with what has been proved using a Liouville space approach in [45].
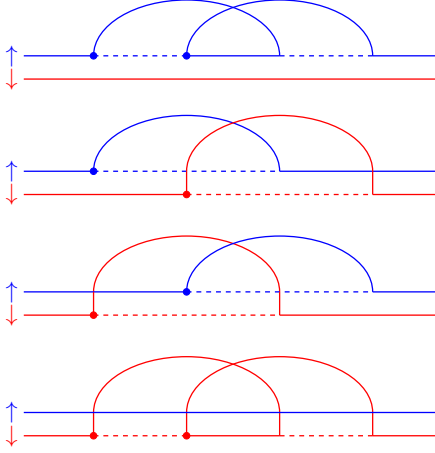
E. Diagrams for N-state systems

A full diagram for $N > 1$ and with diagonal hybridization matrices is given by the arrangements of fermion lines, with some fixed topology, connecting the transitions within the paths of the individual system states i. As an example, consider again the SIAM. A so-called
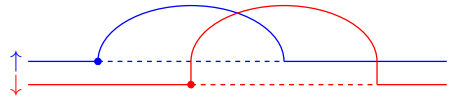
crossing diagram ($m = 2$, with crossing fermion lines)

$$(56)$$

can be obtained in the following ways

$$(57)$$

The diagrammatic rules developed in the previous section are thus applied to the two states $\sigma = \{\uparrow, \downarrow\}$, according to how the fermion lines are distributed among these electron states. The resulting integrand in Eq. (40) is given by the product of the contributions from each state. Also, in the interacting case, the phase factors b^σ_{kl}, see Eqs. (42) and (44) and Fig. 7, depend on the details of the paths of both states simultaneously. For example, the second diagrammatic contribution above is evaluated as

$$\eta^{\uparrow\prime}\eta^{\uparrow}\eta^{\downarrow\prime}\eta^{\downarrow} \, [-g^{-\zeta_1^\uparrow}_{-\eta^\uparrow}(t_3 - t_1)]b^\uparrow_{31} \, [-g^{-\zeta_1^\downarrow}_{-\eta^\downarrow}(t_4 - t_2)]b^\downarrow_{42} \, ,$$

$$(58)$$
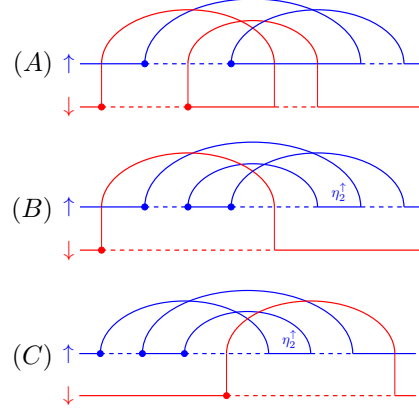
with

$$b^\uparrow_{31} = e^{-\frac{i}{\hbar}\zeta_1^\uparrow E_\uparrow(\eta^\downarrow)(t_2-t_1)}e^{-\frac{i}{\hbar}\zeta_1^\uparrow E_\uparrow(t_3-t_2)} \, ,$$
$$b^\downarrow_{42} = e^{-\frac{i}{\hbar}\zeta_1^\downarrow E_\downarrow(t_3-t_2)}e^{-\frac{i}{\hbar}\zeta_1^\downarrow E_\downarrow(\eta^{\uparrow\prime})(t_4-t_3)} \, ,$$

$$(59)$$

with $E_\sigma = \epsilon_\sigma + U/2$ and $E_\sigma(\eta) = \epsilon_\sigma + U/2(1 + \eta)$, see the scheme in Fig. 7. In the absence of interactions $E_\sigma, E_\sigma(\eta) \to \epsilon_\sigma$ and therefore $b^\uparrow_{31} \to \exp[-i\zeta_1^\uparrow\epsilon_\uparrow(t_3 - t_1)/\hbar]$ and $b^\downarrow_{42} \to \exp[-i\zeta_1^\downarrow\epsilon_\downarrow(t_4 - t_2)/\hbar]$, as in Eq. (35).

As an application of the diagrammatic rules developed in Sec. IV D to the SIAM, let us consider the three dia-

grams whose fermion lines involve both spin states

$$(60)$$

The multiplicative factor $\eta_2^\uparrow$ is brought by the overlap of more than two fermion lines of the same spin state. Consider the noninteracting case. While (A) contributes, the diagrams (B) and (C) vanish collectively once the sum over paths (specifically over $\eta_2^\uparrow$) is performed, as the phase factor $\mathcal{B}$ in the propagator is independent of the sojourn indexes, see Eq. (42) and Fig. 7. In the interacting case, (C) contributes because there is a phase factor associated to $\eta_2^\uparrow$ due to the sojourn-blip overlap, while (B) is still vanishing, as the sojourn-sojourn overlap does not contribute to the phase factors, see also Ref. [45].

V. GENERALIZED MASTER EQUATION FOR THE POPULATIONS AND THE CURRENT

In the absence of time-dependent driving, the propagator has time-translation symmetry. It is therefore convenient to Laplace-transform the population propagator order by order and obtain a generalized master equation (GME) for the populations and an integral equation for the current. The kernels of these equations are related to each other and, in turn, connected to the Green's functions. This connection will be elaborated in Sec. VII. In the following, we indicate as $\hat{f}(\lambda) = \int_0^\infty dt \exp(-\lambda t)f(t)$ the Laplace transform of a function $f(t)$.

A. GME for the populations

Due to the nested time integrals in the definition of $J^{(m)}$, Eq. (40), the reducible contributions, i.e. the ones that can be cut by a vertical line not crossing any fermion line, factorize in Laplace space. For this reason, the populations and current kernels collect the so-called irreducible diagrammatic contributions, the ones that cannot be cut by a vertical line not crossing any fermion line.

Using Eq. (48), the zeroth-order contribution to the

propagator is

$$J_{\boldsymbol{\eta'\eta}}^{(0)}(t;0) = \delta_{\boldsymbol{\eta'\eta}} , \qquad (61)$$

and its Laplace transform reads

$$\hat{J}_{\boldsymbol{\eta'\eta}}^{(0)}(\lambda) = \frac{1}{\lambda}\delta_{\boldsymbol{\eta'\eta}} . \qquad (62)$$

Let us denote with $\boldsymbol{\eta}^{(i)}$ the set of sojourn indexes associated to all states except i, namely

$$\boldsymbol{\eta}^{(i)} = (\ldots, \eta^{i-1}, \eta^{i+1}, \ldots)$$

and set the initial time $t_0 = 0$. The term $m = 1$ contains two tunneling transitions. This implies the change in the occupation of one state at most. Thus, the first-order propagator has composite indexes $\boldsymbol{\eta'}$ and $\boldsymbol{\eta}$ that differ for at most one entry. The resulting first-order propagator can be readily calculated according to the definition, Eq. (40), and the diagrammatic rules set up in Sec. IV D, yielding

$$J_{\boldsymbol{\eta'\eta}}^{(1)}(t;0) = \sum_i \int_0^t dt_2 \int_0^{t_2} dt_1 \sum_{\zeta^i} e^{-\frac{i}{\hbar}\zeta^i E_i(\boldsymbol{\eta}^{(i)})(t_2-t_1)}$$
$$\times \eta'^i \eta^i \left[-g_{-\eta^i}^{-\zeta^i}(t_2-t_1)\right]\delta_{\boldsymbol{\eta'}^{(i)}\boldsymbol{\eta}^{(i)}} . \qquad (63)$$

If, for some i, $\eta'^i \neq \eta^i$, we have $\eta'^i\eta^i = -1$ because $\eta = \pm 1$. Moreover, the sum over i collapses to a single term due to the constraint $\delta_{\boldsymbol{\eta}^{(i)'}\boldsymbol{\eta}^{(i)}}$. Taking into account Eq. (61), this implies that, up to first order,

$$J_{\boldsymbol{\eta\eta}}(t;0) = 1 - \sum_i J_{\boldsymbol{\eta'\eta}}^{(\eta'^i \neq \eta^i)}(t;0) ,$$

in agreement with the conservation of the total probability.

Let us introduce the irreducible kernel of order 1 using the explicit form for the correlator, Eq. (29),

$$\mathcal{K}_{\boldsymbol{\eta'\eta}}^{(1)}(\tau) = \prod_{j=1}^N \eta'^j\eta^j \sum_{i\zeta^i\alpha k\sigma} e^{-\frac{i}{\hbar}\zeta^i[E_i(\boldsymbol{\eta}^{(i)})-\epsilon_k]\tau}$$
$$\times \frac{-|t_{i\alpha k\sigma}|^2}{\hbar^2}f_{-\eta^i}^{\alpha}(\epsilon_k)\delta_{\boldsymbol{\eta'}^{(i)}\boldsymbol{\eta}^{(i)}} , \qquad (64)$$

where we singled out the prefactor $\prod_{j}\eta'^j\eta^j = \pm 1$, common to all orders (see the diagrammatic rules), by exploiting the property that when two sojourn indexes are the same they contribute as $(\eta^i)^2 = 1$. In Laplace space, the first-order propagator acquires then the form

$$\hat{J}_{\boldsymbol{\eta'\eta}}^{(1)}(\lambda) = \frac{1}{\lambda}\hat{\mathcal{K}}_{\boldsymbol{\eta'\eta}}^{(1)}(\lambda)\frac{1}{\lambda} , \qquad (65)$$

with

$$\hat{\mathcal{K}}_{\boldsymbol{\eta'\eta}}^{(1)}(\lambda) = \prod_{j=1}^N \eta'^j\eta^j \sum_{i\zeta^i\alpha k\sigma} \frac{-(|t_{i\alpha k\sigma}|^2/\hbar^2)\,f_{-\eta^i}^{\alpha}(\epsilon_k)}{\lambda + i\zeta^i[E_i(\boldsymbol{\eta}^{(i)})-\epsilon_k]/\hbar}\delta_{\boldsymbol{\eta'}^{(i)}\boldsymbol{\eta}^{(i)}} . \qquad (66)$$

If, for some i, $\eta'^i \neq \eta^i$, then the prefactor is -1 and the sum over i collapses to a single term, as for the first-order propagator. This entails that, from Eqs. (63) and (65), the diagonal elements of the irreducible kernel are related to the off-diagonal ones by

$$\hat{\mathcal{K}}_{\boldsymbol{\eta\eta}}^{(1)}(\lambda) = -\sum_i \hat{\mathcal{K}}_{\boldsymbol{\eta'\eta}}^{(1),\eta'^i \neq \eta^i}(\lambda) . \qquad (67)$$

Since, as we show below, the rates $\hat{\mathcal{K}}_{\boldsymbol{\eta'\eta}}^{(1)}(0)$ are the steady-state rates of the master equation for the populations in the sequential tunneling approximation [34], Eq. (67) is consistent with the conservation of the total probability.

Higher-order contributions can be calculated as well according to the diagrammatic rules given in Sec. IV D. The 2nd-order contribution to the propagator for the populations is the sum of the three classes of diagrams in Fig. 8. The first is a reducible diagram and in Laplace

FIG. 8. The three topologies of 2nd-order diagrams. Each fermion line can belong to each of the N states of the central system S. The first diagram is reducible while the second and third are irreducible.

space is the product of two lower-order diagrams

$$\hat{J}_{\overset{\frown\frown}{},\boldsymbol{\eta'\eta}}^{(2)}(\lambda) = \frac{1}{\lambda}\sum_{\boldsymbol{\eta''}}\hat{\mathcal{K}}_{\boldsymbol{\eta'\eta''}}^{(1)}(\lambda)\frac{1}{\lambda}\hat{\mathcal{K}}_{\boldsymbol{\eta''\eta}}^{(1)}(\lambda)\frac{1}{\lambda} . \qquad (68)$$

Here, the internal sum over $\boldsymbol{\eta}$ has been singled-out, allowing for the use of the matrix notation

$$\hat{\boldsymbol{J}}_{\overset{\frown\frown}{}}^{(2)}(\lambda) = \frac{1}{\lambda}\frac{\hat{\boldsymbol{\mathcal{K}}}^{(1)}(\lambda)}{\lambda} \cdot \frac{\hat{\boldsymbol{\mathcal{K}}}^{(1)}(\lambda)}{\lambda} . \qquad (69)$$

The full propagating function $\hat{\boldsymbol{J}}^{(2)}$ in Laplace space, expressed as the sum of the three diagrammatic contributions shown in Fig. 8, is given by

$$\hat{\boldsymbol{J}}^{(2)}(\lambda) = \frac{1}{\lambda}\left[\frac{\hat{\boldsymbol{\mathcal{K}}}^{(1)}(\lambda)}{\lambda} \cdot \frac{\hat{\boldsymbol{\mathcal{K}}}^{(1)}(\lambda)}{\lambda} + \frac{\hat{\boldsymbol{\mathcal{K}}}^{(2)}(\lambda)}{\lambda}\right] , \qquad (70)$$

where the irreducible kernel of 2nd order $\hat{\boldsymbol{\mathcal{K}}}^{(2)}(\lambda)$ is the sum of the two 2nd-order irreducible diagrams in Fig. 8 (the second and the third) in Laplace space. As discussed in Sec. VI below, these contributions can be written as the contraction of a matrix block with a vertex, as in Eq. (66), with the difference that the block has now internal processes. The same applies to higher-order irreducible kernels leading to the final Eq. (97) below.

Going to the 3rd-order propagator, it collects the contributions from the 15 diagrams listed in Fig. 9 where, in order to give a compact visualization, we introduce the symbols

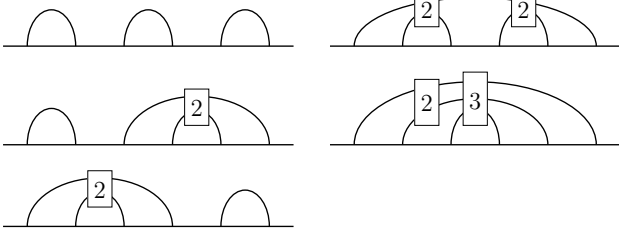$$\boxed{2} = \overline{} + \times \qquad (71)$$

FIG. 9. Compact representation for the 15 third-order diagrams. The five diagrams in the left column are reducible and can be seen as combinations of the first- and second-order ones, see Fig. 8. The ten diagrams on the right are irreducible and their explicit forms are the same as the ones listed in Appendix H for an individual degree of freedom of S. The lower-right class of diagrams vanishes when each of the three fermion lines belongs to the same state.

and

$$\boxed{3} = \overline{\overline{}} + \overline{\times} + \times\!\!\!\times \tag{72}$$

The crosses have the role of exchanging the fermion lines to produce the different topologies of diagrams. In the first column of Fig. 9 are listed the reducible 3rd-order diagrams that can be obtained by combining the two 2nd-order irreducible diagrams in Fig. 8 and a 1st-order one. The second column of Fig. 9 lists the irreducible diagrams divided for convenience in the two classes with overlap of two and three fermion lines. Irreducible diagrams containing n overlapping fermion lines are called n-tier diagrams.

Along the same lines as with the 2nd order, we can write the 3rd order propagating function in Laplace space as the sum of products of lower-order irreducible kernels plus the irreducible 3rd order kernel $\hat{\boldsymbol{\mathcal{K}}}^{(3)}(\lambda)$

$$\hat{\boldsymbol{J}}^{(3)}(\lambda) = \frac{1}{\lambda}\left[\left(\frac{\hat{\boldsymbol{\mathcal{K}}}^{(1)}(\lambda)}{\lambda}\right)^3 + \frac{\hat{\boldsymbol{\mathcal{K}}}^{(1)}(\lambda)}{\lambda}\cdot\frac{\hat{\boldsymbol{\mathcal{K}}}^{(2)}(\lambda)}{\lambda} \right.$$
$$\left. + \frac{\hat{\boldsymbol{\mathcal{K}}}^{(2)}(\lambda)}{\lambda}\cdot\frac{\hat{\boldsymbol{\mathcal{K}}}^{(1)}(\lambda)}{\lambda} + \frac{\hat{\boldsymbol{\mathcal{K}}}^{(3)}(\lambda)}{\lambda} \right], \tag{73}$$

where $\hat{\boldsymbol{\mathcal{K}}}^{(3)}(\lambda)$ collects the irreducible 3rd order diagrams in Fig. 9 (the ones in the second column).

At this point we are in the position to derive the formally exact GME for the populations and the current. The exact propagator is obtained by summing over all orders m the mth-order propagators as follows

$$\hat{\boldsymbol{J}}(\lambda) = \sum_{m=0}^{\infty} \hat{\boldsymbol{J}}^{(m)}(\lambda)$$
$$= \frac{1}{\lambda}\left[\mathbf{1} + \frac{\hat{\boldsymbol{\mathcal{K}}}^{(1)}(\lambda)}{\lambda} + \left(\frac{\hat{\boldsymbol{\mathcal{K}}}^{(1)}(\lambda)}{\lambda}\right)^2 + \frac{\hat{\boldsymbol{\mathcal{K}}}^{(2)}(\lambda)}{\lambda} \right.$$
$$\left. + \left(\frac{\hat{\boldsymbol{\mathcal{K}}}^{(1)}(\lambda)}{\lambda}\right)^3 + 2\frac{\hat{\boldsymbol{\mathcal{K}}}^{(1)}(\lambda)}{\lambda}\cdot\frac{\hat{\boldsymbol{\mathcal{K}}}^{(2)}(\lambda)}{\lambda} + \frac{\hat{\boldsymbol{\mathcal{K}}}^{(3)}(\lambda)}{\lambda} + \dots \right]$$
$$= \frac{1}{\lambda}\sum_{m=0}^{\infty}\left(\frac{\hat{\boldsymbol{\mathcal{K}}}^{(1)}(\lambda)}{\lambda} + \frac{\hat{\boldsymbol{\mathcal{K}}}^{(2)}(\lambda)}{\lambda} + \dots\right)^m$$
$$= \frac{1}{\lambda}\sum_{m=0}^{\infty}\left(\frac{\hat{\boldsymbol{\mathcal{K}}}(\lambda)}{\lambda}\right)^m$$
$$= \left[\lambda\mathbf{1} - \hat{\boldsymbol{\mathcal{K}}}(\lambda)\right]^{-1}, \tag{74}$$

where we introduced the kernel

$$\hat{\boldsymbol{\mathcal{K}}}(\lambda) = \sum_{m=1}^{\infty} \hat{\boldsymbol{\mathcal{K}}}^{(m)}(\lambda) \tag{75}$$

which collects all the irreducible contributions to $\hat{\boldsymbol{J}}$. From Eq. (74), $\lambda\hat{\boldsymbol{J}}(\lambda) - \mathbf{1} = \hat{\boldsymbol{\mathcal{K}}}(\lambda)\cdot\hat{\boldsymbol{J}}(\lambda)$. By transforming back to the time domain, this implies that $\boldsymbol{J}$ is the solution of the following GME

$$\frac{d}{dt}\boldsymbol{J}(t) = \int_0^t dt'\,\boldsymbol{\mathcal{K}}(t - t')\cdot\boldsymbol{J}(t'). \tag{76}$$

According to Eq. (19), the populations are obtained by multiplying the above matrix equation by $\mathbf{P}(0)$, the population vector at the initial time $t = 0$, which results in

$$\frac{d}{dt}\mathbf{P}(t) = \int_0^t dt'\,\boldsymbol{\mathcal{K}}(t - t')\cdot\mathbf{P}(t'). \tag{77}$$

The asymptotic populations are the solution of the equation $\mathbf{0} = \hat{\boldsymbol{\mathcal{K}}}(0)\cdot\mathbf{P}^\infty$, which is obtained upon applying to Eq. (77) the final value theorem $f(t \to \infty) = \lim_{\lambda\to 0}\lambda\hat{f}(\lambda)$.

B. Integral equation for the current

In the present situation of diagonal hybridization matrices, the current functional $\mathcal{I}_l$, Eq. (13), entering the expression for the current through the lead l via Eq. (12), specializes to

$$\mathcal{I}_l(\boldsymbol{\xi}^*, \boldsymbol{\xi}, \bar{\boldsymbol{\xi}}) = -\int_{t_0}^t dt' \sum_{i,x,y,z}\left[x\,\xi_y^z(t)\mathrm{g}_{l,xz}^{-z}(t - t')\xi_x^{-z}(t') \right]_i$$
$$\times \delta_{z,-1}\delta_{y,+1}. \tag{78}$$

The current functional has thus the same form as the phase of the influence functional except that there is no integration over the time of the last tunneling transition and there are constrains on the contributing processes. This entails that the diagrammatic unraveling of the current propagator, obtained by expanding the influence functional as a series in the tunneling transitions, goes along the same lines as the one for the populations. The differences consist in the *last* fermion line of the diagrams bearing the constraints associated with the current and the nested time integrals missing the integration over the last tunneling time. The expansion of $J^I_{l,\boldsymbol{\eta'\eta}}(t,t_0)$ starts from $m=1$ because, not being at the exponent, the current functional adds two additional transitions to the ones generated by expanding the influence functional. This also implies that, if there are no coherences in the initial state of the system, then also the paths contributing to the current start and end in sojourn states. The current propagator, in the discretized picture and in the occupation number representation, is then $J^I_{l,\boldsymbol{\eta'\eta}}(t;0) = \sum_{m=1}^{\infty} J^{I(m)}_{l,\boldsymbol{\eta'\eta}}(t;0)$, where

$$J^{I(m)}_{l,\boldsymbol{\eta'\eta}}(t;0) = \sum_{\text{paths}_m} \int \mathcal{D}^I\{t\}_m \prod_i \sum_{\mathcal{P}_i} \mathcal{B}^i_{m_i}(\mathcal{P}_i)\Phi^i_{m_i}(\mathcal{P}_i)$$
$$\times \text{ constraints },$$
(79)

with $\sum_i m_i = m$ and $\mathcal{B}^i_{m_i}$ and $\Phi^i_{m_i}$ defined in Eq. (41). To order m there are $2m$ tunneling transitions, as for the populations, however in the case of the current the last transition occurs at the final time t, yielding the definition

$$\int \mathcal{D}^I\{t\}_m := \int_{t_0}^{t} dt_{2m-1} \int_{t_0}^{t_{2m-1}} dt_{2m-2} \cdots \int_{t_0}^{t_2} dt_1 .$$
(80)

Going to the details of the constrains in the current calculations, they can be read-off from Eq. (78). The first is that the correlator of the last fermion line is not summed over the leads but has the index l of the considered lead. Further, according to Eq. (32) the Grassmann variable associated to the last transition (the paths start from and land in a sojourn) is of the type $\xi^{\zeta'}_{-\eta'\zeta'}$. Then, the constraints in Eq. (78) translate into $\zeta' = -1$ and $-\eta'\zeta' = +1$, which imply $\delta_{\eta',+1}$, namely the last sojourn of the degree of freedom i associated to the last transition has to be $+1$. Summarizing, the current constraints on the last fermion line are

- The last fermion line is specific to the lead l so that there is no contraction over the lead index α'.

- The index ζ' of the last fermion line is constrained to be $\zeta' = -1$.

- The final sojourn of the state i associated to the fermion line making the last transition must be $\eta'^i = +1$ (the sum over i accounts for all possible processes).

Examples of paths that contribute to $\mathcal{A}_l$ with associated fermion lines are shown in Fig. 10.
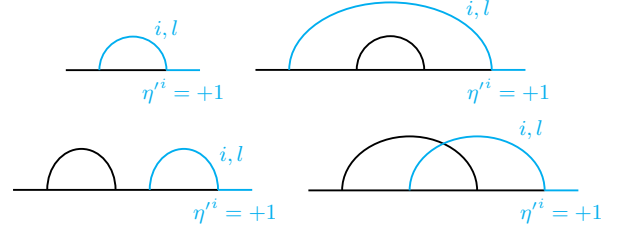
FIG. 10. Examples of irreducible diagrams contributing to $\mathcal{A}_l$. The sojourn of the degree of freedom i associated to the last transition is constrained to be $\eta^{i'} = +1$.

The explicit expression for the term $m=1$ in the expansion of the current propagator is

$$J^{I(1)}_{l,\boldsymbol{\eta'\eta}}(t;0) = \prod_{j=1}^{N} \eta'^j \eta^j \sum_i \int_0^t dt_1 \sum_{\zeta^i} e^{-\frac{i}{\hbar}\zeta^i E_i(\boldsymbol{\eta}^{(i)})(t_2-t_1)}$$
$$\times [-g^{-\zeta^i}_{l,-\eta^i}(t_2-t_1)]\delta_{\boldsymbol{\eta'}^{(i)}\boldsymbol{\eta}^{(i)}}\delta_{\zeta^i,-1}\delta_{\eta'^i,+1}$$
(81)

(cf. Eq. (63)). In Laplace space

$$\hat{\boldsymbol{J}}^{I(1)}_l(\lambda) = \hat{\boldsymbol{\mathcal{K}}}^{I(1)}_l(\lambda)\frac{1}{\lambda} .$$
(82)

Let us denote with $\hat{\boldsymbol{\mathcal{K}}}^I_l(\lambda) = \sum_m \hat{\boldsymbol{\mathcal{K}}}^{I(m)}_l(\lambda)$ the sum of all the irreducible diagrammatic contributions to $\hat{\mathcal{A}}_l(\lambda)$ with the last fermion line satisfying the constraints given by the current functional. Note that the reducible contributions to $\hat{\mathcal{A}}_l(\lambda)$ are products of ordinary irreducible kernels $\hat{\mathcal{K}}(\lambda)$ with only the last factor of the type $\hat{\boldsymbol{\mathcal{K}}}^I_l(\lambda)$. This is because only the last fermion line bears the constraints of the current calculation. Then we find that the exact current propagator is the following sum over all orders m of the m-th order propagators

$$\hat{\mathcal{A}}_l(\lambda) = \frac{\hat{\boldsymbol{\mathcal{K}}}^I_l(\lambda)}{\lambda} \cdot \left[\mathbf{1} + \frac{\hat{\boldsymbol{\mathcal{K}}}^{(1)}(\lambda)}{\lambda} + \left(\frac{\hat{\boldsymbol{\mathcal{K}}}^{(1)}(\lambda)}{\lambda}\right)^2 + \frac{\hat{\boldsymbol{\mathcal{K}}}^{(2)}(\lambda)}{\lambda} \right.$$
$$\left. + \left(\frac{\hat{\boldsymbol{\mathcal{K}}}^{(1)}(\lambda)}{\lambda}\right)^3 + \frac{\hat{\boldsymbol{\mathcal{K}}}^{(1)}(\lambda)}{\lambda} \cdot \frac{\hat{\boldsymbol{\mathcal{K}}}^{(2)}(\lambda)}{\lambda} + \dots \right]$$
$$= \hat{\boldsymbol{\mathcal{K}}}^I_l(\lambda) \cdot \left[\lambda\mathbf{1} - \hat{\mathcal{K}}(\lambda) \right]^{-1}$$
$$= \hat{\boldsymbol{\mathcal{K}}}^I_l(\lambda) \cdot \hat{\boldsymbol{J}}(\lambda) ,$$
(83)

or, in the time domain

$$\mathcal{A}_l(t) = \int_0^t dt' \, \mathcal{K}^I_l(t-t') \cdot \boldsymbol{J}(t') .$$
(84)

Similarly to the steady state-populations, the steady-state current is found by applying to Eq. (83) the final

value theorem, which results in

$$
\begin{aligned}
I_l^\infty &= e2\mathrm{Re}\,\mathrm{Tr_S}[\mathcal{A}_l^\infty] \\
&= \lim_{\lambda \to 0} e2\mathrm{Re}\,\mathrm{Tr_S}[\hat{\mathcal{K}}_l^I(\lambda) \cdot \lambda \hat{J}(\lambda)] \\
&= e2\mathrm{Re}\,\mathrm{Tr_S}[\hat{\mathcal{K}}_l^I(0) \cdot J^\infty] \\
&= e2\mathrm{Re} \sum_{\eta'\eta} \hat{\mathcal{K}}_{l,\eta'\eta}^I(0) \mathrm{P}_{\eta}^\infty ,
\end{aligned}
\tag{85}
$$

where we assumed that the matrix elements of the asymptotic propagator J^∞ are independent of their column index, i.e. that the steady-state populations are independent of their initial values. In other words, in the asymptotic propagator matrix each column is equal to the asymptotic population vector.

VI. EXACT FORMAL EXPRESSION FOR THE KERNEL

A. Block structure of the irreducible kernel

The diagrammatic contributions to the populations and current propagators display an exponential dependence on time, cf. Eqs. (29) and (42). This feature and the nested time integrals enable one to express the irreducible kernels in Laplace space as the *contraction* of products of blocks - each equipped with a matrix structure - with an initial vertex. The simplest example is provided by the first-order irreducible kernel $\hat{\mathcal{K}}^{(1)}(\lambda)$ in Eq. (66), which can be rendered by the contraction of the product of two matrices, associated to an initial vertex $\mathbf{v}$ and a block $\mathbf{h}(\lambda)$ which encompasses a free fermion line, respectively, see Fig. 11.
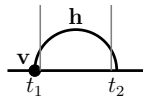
FIG. 11. Irreducible diagram of order 1. The vertex $\mathbf{v}$ is denoted by the full dot. The two ends of the fermion line are contracted, namely the indexes ζ^i, α, k, and σ are summed over. The time interval $t_2 - t_1$ is a blip only for the state associated to the fermion line. Note that the states i are summed over in contracting the fermion line, see Eq. (90).

The matrix blocks are indexed by the state index i and the associated collective index

$$
\chi := (\underbrace{\zeta^i, \alpha, k, \sigma}_{\kappa}, \eta^{(i)})
\tag{86}
$$

which includes path and leads variables (note that the components of χ depend on the state i). The scalar product between two generic blocks $\mathbf{A}$ and $\mathbf{B}$ is given

by

$$
[\mathbf{A} \cdot \mathbf{B}]_{\chi'\chi}^{i'i} = \sum_{i''\chi''} [\mathbf{A}]_{\chi'\chi''}^{i'i''} [\mathbf{B}]_{\chi''\chi}^{i''i} .
\tag{87}
$$

We denote by the symbol $\langle \cdot \rangle$ the contraction of a matrix block $\mathbf{C}$ with an initial vertex $\mathrm{v}_{-\eta^i}$. The contraction consists in summing over the initial and final index κ and κ', cf. Eq. (86), namely

$$
\langle \mathbf{C} \cdot \mathbf{v}_{-\eta^i} \rangle_{\eta'^{(i')}\eta^{(i)}}^{i'i} = \sum_{\kappa'\kappa} [\mathbf{C}]_{\chi'\chi}^{i'i} \mathrm{v}_{-\eta^i}^i(\kappa) .
\tag{88}
$$

As a result, the first-order kernel in Eq. (66) can be written as

$$
\hat{\mathcal{K}}_{\eta'\eta}^{(1)}(\lambda) = \prod_{j=1}^N \eta'^j \eta^j \sum_{i'i} \langle \mathbf{h}(\lambda) \cdot \mathbf{v}_{-\eta^i} \rangle_{\eta'^{(i')}\eta^{(i)}}^{i'i} ,
\tag{89}
$$

which is the contraction of the scalar product

$$
\langle \mathbf{h}(\lambda) \cdot \mathbf{v}_{-\eta^i} \rangle_{\eta'^{(i')}\eta^{(i)}}^{i'i} = \sum_{\kappa',\kappa} \sum_{i''\chi''} [\mathbf{h}(\lambda)]_{\chi'\chi''}^{i'i''} [\mathbf{v}_{-\eta^i}]_{\chi''\chi}^{i''i} .
\tag{90}
$$

Here, we have defined the matrix blocks of elements

$$
\begin{aligned}
[\mathbf{h}(\lambda)]_{\chi'\chi}^{i'i} &:= \frac{1}{\lambda + \mathrm{i}\zeta^i[E_i(\eta^{(i)}) - \epsilon_k]/\hbar} \delta_{i'i} \delta_{\chi'\chi} , \\
[\mathbf{v}_{\pm\eta^i}]_{\chi'\chi}^{i'i} &:= -\frac{|\mathrm{t}_{i\alpha\sigma}(\epsilon_k)|^2}{\hbar^2} f_{\pm\eta^i}^\alpha(\epsilon_k) \delta_{i'i} \delta_{\chi'\chi} \\
&\equiv \mathrm{v}_{\pm\eta^i}^i(\kappa) \delta_{i'i} \delta_{\chi'\chi} .
\end{aligned}
\tag{91}
$$

Graphically, the vertexes $\mathrm{v}_\pm$ are associated to the two processes

$$
\mathrm{v}_{-\eta^i} , \qquad \mathrm{v}_{+\eta^i} ,
\tag{92}
$$

with the $\pm$ sign of v being established directly by the form of the influence functional. Note that, since we deal with the population propagator, the paths start and end in sojourns, thus the initial vertex is always of the type $\mathrm{v}_{-\eta}$. In all diagrams, the two ends of each fermion line are contracted in this way. Analogously, the matrix element of the irreducible current kernel of first order $\mathcal{K}_l^{I(1)}(\lambda)$ reads

$$
[\hat{\mathcal{K}}_l^{I(1)}(\lambda)]_{\eta'\eta} = \prod_{j=1}^N \eta'^j \eta^j \sum_{i'i} \delta_{\eta'^i,+1} \langle \mathrm{c}_l'\mathbf{h}(\lambda)\cdot\mathbf{v}_{-\eta^i} \rangle_{\eta'^{(i')}\eta^{(i)}}^{i'i} ,
\tag{93}
$$

where $\mathrm{c}_l' := \delta_{\zeta'^i,-1}\delta_{\alpha',l}$, so that

$$
[\mathrm{c}_l'\mathbf{h}(\lambda)]_{\chi'\chi}^{i'i} := \frac{\delta_{\zeta^i,-1}\delta_{\alpha,l}}{\lambda + \mathrm{i}\zeta^i[E_i(\eta^{(i)}) - \epsilon_k]/\hbar} \delta_{i'i}\delta_{\chi'\chi} ,
\tag{94}
$$

cf. Eq. (91).
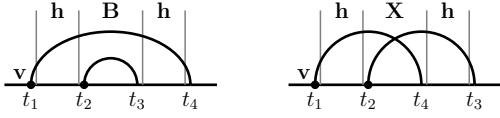
Going to orders higher than the first, consider the

FIG. 12. Irreducible diagrams contributing to $J^{(2)}$. A vertex is denoted by a full dot. The two ends of the lines connecting two blocks carry path indexes that are summed over in the connection. The first block is contracted with the vertex $\mathbf{v}$ and the right end of the last block is also contracted.
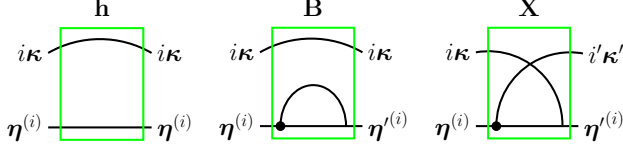

FIG. 13. The free propagator, bubble, and crossing blocks involved in the diagrams of Figs. 11 and 12.

tute the building blocks of the important resonant tunneling approximation (RTA) [47] in which diagrams with overlap of more than two overlapping fermion lines are neglected, see Eq. (106) below. The 3rd order irreducible kernel, within RTA, reads

$$\hat{\mathcal{K}}^{(3)}_{\mathrm{RTA}\boldsymbol{\eta}'\boldsymbol{\eta}}(\lambda) = \prod_{j=1}^{N} \eta'^j \eta^j \sum_{i'i} \langle \mathbf{h}(\lambda) \cdot \left[\mathbf{B}(\lambda) + \mathbf{X}(\lambda) \right] \cdot \mathbf{h}(\lambda)$$
$$\cdot \left[\mathbf{B}(\lambda) + \mathbf{X}(\lambda) \right] \cdot \mathbf{h}(\lambda) \cdot \mathbf{v}_{-\eta^i} \rangle^{i'i}_{\boldsymbol{\eta}'^{(i')}\boldsymbol{\eta}^{(i)}} \cdot$$
(96)

Including in a formal way the contributions beyond-RTA and the higher-order irreducible diagrams with overlap of arbitrarily many fermion lines, we obtain a picture where the kernel results from contraction of a dressed block, the irreducible propagator $\boldsymbol{\phi}$, whose definition is the object of the next section.

B. Diagrammatic unraveling of the kernel

The sum of all irreducible diagrams can be obtained by contracting with an initial vertex the dressed block $\boldsymbol{\phi}$ which gives the exact kernel according to

$$\hat{\mathcal{K}}_{\boldsymbol{\eta}'\boldsymbol{\eta}}(\lambda) = \prod_{j=1}^{N} \eta'^j \eta^j \sum_{i'i} \langle \boldsymbol{\phi}(\lambda) \cdot \mathbf{v}_{-\eta^i} \rangle^{i'i}_{\boldsymbol{\eta}'^{(i')}\boldsymbol{\eta}^{(i)}} \cdot \quad (97)$$

The irreducible propagator $\boldsymbol{\phi}$ can be seen as a block with an incoming and an outgoing fermion line, similar to the ones shown in Fig. 13, dressed by processes of all orders. Using the notation introduced in Sec. V, with the boxes that permute the fermion lines numbered according to the number of overlapping lines, we can give the following (symbolic) exact expression

four-transition diagrams of Fig. 12: The time slicing yields a block-product structure in Laplace space. The blocks are shown in Fig. 13. Each of them is a matrix with state indexes i, j and the two collective indexes $\boldsymbol{\chi}'$ and $\boldsymbol{\chi}$ that specify the path and lead variables according to Eq. (86).

The sum over paths is performed automatically by the matrix multiplications implied by forming the diagrams from blocks which, in turn, possibly contain internal processes. The simplest examples of the latter are given by the bubble and crossing blocks, $\mathbf{B}$ and $\mathbf{X}$, of Fig. 13. The irreducible kernel of order 2 in Laplace space acquires the following expressions in terms of the blocks defined above

$$\hat{\mathcal{K}}^{(2)}_{\boldsymbol{\eta}'\boldsymbol{\eta}}(\lambda) = \prod_{j=1}^{N} \eta'^j \eta^j \sum_{i'i} \langle \mathbf{h}(\lambda) \cdot \left[\mathbf{B}(\lambda) + \mathbf{X}(\lambda) \right]$$
$$\cdot \mathbf{h}(\lambda) \cdot \mathbf{v}_{-\eta^i} \rangle^{i'i}_{\boldsymbol{\eta}'^{(i')}\boldsymbol{\eta}^{(i)}} \cdot \quad (95)$$

The bubble and the crossing shown in Fig. 13 consti-

(98)

Notice that, for simplicity, the diagrams and the corresponding formulas above them are both ordered from left to right here, at variance with the convention used throughout the text, where formulas are ordered from

right to left. This formal unraveling of the propagator constitutes a main result of the present work. It systematically encompasses the truncation schemes based on the order in Γ (e.g. sequential tunneling and cotunneling)

and on the depth of the hierarchy of overlap of fermion lines (e.g. RTA), as we exemplify below. In Eq. (98) we have introduced $\mathbf{h}_1 \equiv \mathbf{h}$ and similarly, for the blocks with higher overlap of noncrossing fermion lines, $\mathbf{h}_n$. As in the definition of the first-order irreducible kernel in Eq. (90), the symbol $\langle \cdot \rangle$ implies the contraction with an initial vertex of a fermion line, in this case the most internal. The boxes $\boxed{2}$ and $\boxed{3}$ are defined in Eqs. (71) and (72), respectively. The box $\boxed{4}$ reads

$$\boxed{4} = \overline{\overline{\equiv}} + \overline{\overline{\asymp}} + \overline{\asymp} + \underset{\times}{\times} \, , \qquad (99)$$

and analogous definitions hold for the higher-order boxes. Finally, $\mathbf{S}_n$ contains the box $\boxed{n}$ that operates on n fermion lines by exchanging them in pairs and thus represent a class of blocks.

From the schematic expression in Eq. (98) we find in Laplace space

$$\phi = \sum_{n=0}^{\infty} \left(\mathbf{h} \langle \tilde{\mathbf{S}}_2 \mathbf{v} \rangle \right)^n \mathbf{h} \qquad (100)$$

with $\langle \mathbf{S}_2 \mathbf{v} \rangle \equiv \mathbf{B} + \mathbf{X}$, the RTA self-energy, and $\mathbf{h}_1 \equiv \mathbf{h}$, see Fig. 13. In Eq. (100), we have defined the dressed self-energies *iteratively* as

$$\tilde{\mathbf{S}}_n := \sum_{k=0}^{\infty} \left(\mathbf{h}_n \langle \tilde{\mathbf{S}}_{n+1} \mathbf{v} \rangle \right)^k \mathbf{S}_n \, . \qquad (101)$$

Summing the geometrical series in Eq. (100) we find the important result

$$\phi = [\mathbf{h}^{-1} - \langle \tilde{\mathbf{S}}_2 \mathbf{v} \rangle]^{-1} \, . \qquad (102)$$

Thus, the function ϕ is the solution of the Dyson equation

$$\phi = \mathbf{h} + \mathbf{h} \langle \tilde{\mathbf{S}}_2 \mathbf{v} \rangle \phi \, . \qquad (103)$$

The formal exact expression for ϕ generates the different approximations schemes used in literature by suitably truncating the series expression, Eq. (100), and/or the depth of the hierarchy in Eq. (101). For example, the sequential tunneling (ST) scheme, first order in Γ, is recovered by truncating Eq. (100) to $n = 0$

$$\phi_{\mathrm{ST}} = \mathbf{h} \, . \qquad (104)$$

The next-order perturbative scheme includes the cotunneling (CT) diagrams, with $n \leq 1$ in Eq. (100) and $\tilde{\mathbf{S}}_2 = \mathbf{S}_2$, so that $\langle \mathbf{S}_2 \mathbf{v} \rangle = \mathbf{B} + \mathbf{X}$. Then the irreducible propagator reads

$$\phi_{\mathrm{CT}} = \mathbf{h} + \mathbf{h}(\mathbf{B} + \mathbf{X})\mathbf{h} \, . \qquad (105)$$

Retaining all orders in the series expansion for ϕ and truncating the hierarchy in Eq. (101) to two overlapping

fermion lines, i.e. to the second tier, where $\tilde{\mathbf{S}}_2 = \mathbf{S}_2$, we obtain the Dyson equation for the RTA propagator

$$\phi_{\mathrm{RTA}} = \mathbf{h} + \mathbf{h}(\mathbf{B} + \mathbf{X})\phi_{\mathrm{RTA}} \, . \qquad (106)$$

This approximation scheme is nonperturbative in the tunnel coupling Γ and corresponds to the scheme proposed in [47]. Note that the propagator ϕ_{CT} is readily recovered by expanding ϕ_{RTA} to order Γ^2. From the RTA, neglecting the crossing blocks, we obtain the generalized dressed second order (gDSO), to be discussed below, which is the solution of

$$\phi_{\mathrm{gDSO}} = \mathbf{h} + \mathbf{h}\mathbf{B}\phi_{\mathrm{gDSO}} \qquad (107)$$

and reproduces the results obtained by Meir, Wingreen, and Lee in [39] with the equation of motion method.

C. Dyson equation for the kernel in terms of dressed bubbles and crossings

We split the exact, dressed self-energy of Eqs. (102) and (103) as $\langle \tilde{\mathbf{S}}_2 \mathbf{v} \rangle = \tilde{\mathbf{B}} + \tilde{\mathbf{X}}$, according to whether the incoming and outgoing fermion lines are the same or not. The irreducible block $\tilde{\mathbf{B}}$ is a fermion line dressed by processes of all orders. In the dressed, irreducible crossing block $\tilde{\mathbf{X}}$, the incoming and outgoing fermion lines are not the same, which implies the presence of crossings involving these lines. These two dressed blocks are shown in Fig. 14.

Let us introduce the dressed propagator ϕ_{B} obtained
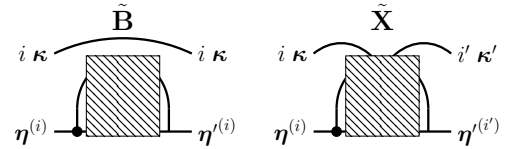

FIG. 14. Dressed, irreducible bubble and crossing blocks that generalize the ones shown in Fig. 13. Note that the difference between $\tilde{\mathbf{B}}$ and ϕ_{B} is that in the first the dressing is irreducible, and can be thought of as being the full ϕ itself, while the dressing of ϕ_{B} is the sum over all processes, reducible and irreducible.

by setting to zero the crossing block $\tilde{\mathbf{X}}$. It satisfies the same Dyson equation as ϕ, but with the dressed bubble self-energy alone; namely, in Laplace space,

$$\phi_{\mathrm{B}} = \left[\mathbf{h}^{-1} - \tilde{\mathbf{B}} \right]^{-1} \, , \qquad (108)$$

or equivalently

$$\phi_{\mathrm{B}} = \mathbf{h} + \mathbf{h}\tilde{\mathbf{B}}\phi_{\mathrm{B}} \, . \qquad (109)$$

Truncation of the hierarchy to the second tier yields the gDSO, Eq. (107), where $\tilde{\mathbf{B}} \equiv \mathbf{B}$. In terms of ϕ_{B}, we can cast the exact equation for ϕ, Eq. (103), in the form

$$\phi = \phi_{\mathrm{B}} + \phi_{\mathrm{B}}\tilde{\mathbf{X}}\phi \, . \qquad (110)$$

Due to the lack of crossings on the main fermion line, ϕ_{B} is diagonal in $\boldsymbol{\kappa}$ and in i (but not in $\boldsymbol{\eta}^{(i)}$) namely

$$[\phi_{\mathrm{B}}]^{i'i}_{\boldsymbol{\chi}'\boldsymbol{\chi}} = \varphi^{ii}_{\mathrm{B},\boldsymbol{\eta}'^{(i)}\boldsymbol{\eta}^{(i)}}(\boldsymbol{\kappa})\delta_{i'i}\delta_{\boldsymbol{\kappa}'\boldsymbol{\kappa}} . \tag{111}$$

Component-wise in $\boldsymbol{\kappa}$, retaining the matrix structure induced by $\boldsymbol{\eta}^{(i)} = (\ldots,\eta^{i-1},\eta^{i+1},\ldots)$ and with the dependence on λ left implicit, Eq. (110) reads

$$\begin{aligned}
\phi^{i'i}(\boldsymbol{\kappa}',\boldsymbol{\kappa}) &= \varphi^{ii}_{\mathrm{B}}(\boldsymbol{\kappa}')\delta_{i'i}\delta_{\boldsymbol{\kappa}'\boldsymbol{\kappa}} \\
&+ \varphi^{i'i'}_{\mathrm{B}}(\boldsymbol{\kappa}') \cdot \sum_{i''\boldsymbol{\kappa}''} \tilde{\mathbf{X}}^{i'i''}(\boldsymbol{\kappa}',\boldsymbol{\kappa}'') \cdot \phi^{i''i}(\boldsymbol{\kappa}'',\boldsymbol{\kappa}) ,
\end{aligned} \tag{112}$$

where $\varphi^{ii}_{\mathrm{B}}(\boldsymbol{\kappa})$ is the left-contracted propagator given by

$$\varphi^{ii}_{\mathrm{B}}(\boldsymbol{\kappa}) = \sum_{i'\boldsymbol{\kappa}'} \phi^{i'i}_{\mathrm{B}}(\boldsymbol{\kappa}',\boldsymbol{\kappa}) . \tag{113}$$

The steady-state population kernel can then be written as

$$\begin{aligned}
\hat{\mathcal{K}}_{\boldsymbol{\eta}'\boldsymbol{\eta}}(0) &= \prod_{j=1}^{N} \eta'^{j}\eta^{j} \sum_{i'i} \langle \boldsymbol{\phi} \cdot \mathbf{v}_{-\eta^i} \rangle^{i'i}_{\boldsymbol{\eta}'^{(i')}\boldsymbol{\eta}^{(i)}} \\
&= \prod_{j=1}^{N} \eta'^{j}\eta^{j} \sum_{i'i\boldsymbol{\kappa}'\boldsymbol{\kappa}} \phi^{i'i}_{\boldsymbol{\eta}'^{(i')}\boldsymbol{\eta}^{(i)}}(\boldsymbol{\kappa}',\boldsymbol{\kappa})\mathrm{v}^{i}_{-\eta^i}(\boldsymbol{\kappa}) .
\end{aligned} \tag{114}$$

As anticipated in Sec. V A, the steady-state populations $\mathrm{P}^{\infty}_{\boldsymbol{\eta}}$ are the solutions of the matrix equation

$$\mathbf{0} = \sum_{\boldsymbol{\eta}} \hat{\mathcal{K}}_{\boldsymbol{\eta}'\boldsymbol{\eta}}(0)\mathrm{P}^{\infty}_{\boldsymbol{\eta}} . \tag{115}$$

D. Current kernel

As shown in Sec. V B the current kernel can be calculated along the same lines as the population kernel provided that the additional constraints

$$\delta_{\eta'i',+1}\mathrm{c}'_{l} \equiv \delta_{\eta'i',+1}\delta_{\alpha',l}\delta_{\zeta',-1}$$

are introduced for the last fermion line.

According to Eq. (85), the general formula for the steady-state current on lead l is

$$I^{\infty}_{l} = e2\mathrm{Re}\sum_{\boldsymbol{\eta}'\boldsymbol{\eta}} \hat{\mathcal{K}}^{I}_{l,\boldsymbol{\eta}'\boldsymbol{\eta}}(0)\mathrm{P}^{\infty}_{\boldsymbol{\eta}} , \tag{116}$$

where the kernel is in Laplace space and calculated at $\lambda = 0$. The current kernel formally reads

$$\begin{aligned}
\hat{\mathcal{K}}^{I}_{l,\boldsymbol{\eta}'\boldsymbol{\eta}}(0) &= \prod_{j=1}^{N} \eta'^{j}\eta^{j} \sum_{i'i} \delta_{\eta'i',+1}\langle \mathrm{c}'_{l}\boldsymbol{\phi} \cdot \mathbf{v}_{-\eta^i} \rangle^{i'i}_{\boldsymbol{\eta}'^{(i')}\boldsymbol{\eta}^{(i)}} \\
&= \prod_{j=1}^{N} \eta'^{j}\eta^{j} \sum_{i'i\boldsymbol{\kappa}'\boldsymbol{\kappa}} \delta_{\eta'i',+1}\mathrm{c}'_{l}\phi^{i'i}_{\boldsymbol{\eta}'^{(i')}\boldsymbol{\eta}^{(i)}}(\boldsymbol{\kappa}',\boldsymbol{\kappa})\mathrm{v}^{i}_{-\eta^i}(\boldsymbol{\kappa}) ,
\end{aligned} \tag{117}$$

cf. Eq. (114).

Summarizing, the steady-state populations and currents of the N-state system coupled to multiple leads can be obtained via Eqs. (115) and (116), respectively. Both the population and the current kernels are in turn directly given by the irreducible propagator $\boldsymbol{\phi}$ which is calculated via the Dyson equations (109) and (110).

VII. PROPORTIONAL COUPLING AND CONNECTION WITH THE GREEN'S FUNCTIONS

Consider the situation in which the central system is connected to two leads (L and R) and the tunneling amplitudes are related by

$$|\mathrm{t}_{iR\sigma}(\epsilon)|^2 = \gamma_{iR}|\mathrm{t}_{iL\sigma}(\epsilon)|^2/\gamma_{iL}$$

with $\gamma_{iR} + \gamma_{iL} = 1$ (proportional coupling). Current conservation at the steady state $I^{\infty} = I^{\infty}_{L} = -I^{\infty}_{R}$ implies, for proportional coupling, $I^{\infty} = \sum_{i}[\gamma_{iR}I^{\infty}_{iL} - \gamma_{iL}I^{\infty}_{iR}]$, where $I^{\infty}_{i'\alpha} = e2\mathrm{Re}\sum_{\boldsymbol{\eta}'\boldsymbol{\eta}} \hat{\mathcal{K}}^{I}_{i'l,\boldsymbol{\eta}'\boldsymbol{\eta}}(0)\mathrm{P}^{\infty}_{\boldsymbol{\eta}}$ is the state-resolved steady-state current and $\hat{\mathcal{K}}^{I}_{i'l,\boldsymbol{\eta}'\boldsymbol{\eta}}(0)$ is given by Eq. (117) without the sum over the final state i'. Correspondingly, we introduce the current kernel

$$\hat{\mathcal{K}}^{I}_{\boldsymbol{\eta}'\boldsymbol{\eta}}(0) := \sum_{i'} \left[\gamma_{i'R}\hat{\mathcal{K}}^{I}_{i'L,\boldsymbol{\eta}'\boldsymbol{\eta}}(0) - \gamma_{i'L}\hat{\mathcal{K}}^{I}_{i'R,\boldsymbol{\eta}'\boldsymbol{\eta}}(0) \right] , \tag{118}$$

with the steady-state current obtained as

$$I^{\infty} = e2\mathrm{Re}\sum_{\boldsymbol{\eta}'\boldsymbol{\eta}} \hat{\mathcal{K}}^{I}_{\boldsymbol{\eta}'\boldsymbol{\eta}}(0)\mathrm{P}^{\infty}_{\boldsymbol{\eta}} . \tag{119}$$

Consider now the Dyson equation for $\boldsymbol{\phi}$, Eq. (112). To obtain the current kernel for the current on lead l we make a contraction with the vertex as in Eq. (117), which gives

$$\langle \mathrm{c}'_{l}\boldsymbol{\phi} \cdot \mathbf{v}_{-\eta^i} \rangle = \langle \mathrm{c}'_{l}\left[\phi_{\mathrm{B}} + \phi_{\mathrm{B}} \cdot \tilde{\mathbf{X}} \cdot \boldsymbol{\phi} \right] \cdot \mathbf{v}_{-\eta^i} \rangle , \tag{120}$$

or, in symbols,

$$\tag{121}$$

where we highlighted the last fermion line which bears the current constraints of the lead l. In the first term on the right-hand side, the vertex from which the last fermion line departs is the first vertex, the one explicitly appearing in the contraction. On the other hand, in the second term, this vertex is inside the dressed block with crossing of the main fermion line $\tilde{\mathbf{X}}$. Using the relation $f^{\alpha}_{-\eta}(\epsilon_k) = \delta_{\eta,+1} - \eta f^{\alpha}_{+}(\epsilon_k)$, both these vertexes (denoted with red full dots in Eq. (121)) can be split as

$$\mathrm{v}^{i}_{-\eta^i}(\boldsymbol{\kappa}) = \delta_{\eta^i,+1}\mathrm{v}^{i}(\boldsymbol{\kappa}) - \eta^i\mathrm{v}^{i}_{+}(\boldsymbol{\kappa}) , \tag{122}$$

where $\mathrm{v}^i(\boldsymbol{\kappa}) = -|\mathrm{t}_{i\alpha\sigma}(\epsilon_k)|^2/\hbar^2$ does not contain the Fermi function. Then, we can write the dressed crossing block by singling-out this internal vertex as follows

$$\tilde{\mathbf{X}}^{i'i}(\boldsymbol{\kappa}'\boldsymbol{\kappa}) = \mathrm{v}^{i'}(\boldsymbol{\kappa}')\tilde{\mathbf{x}}^{i'i}(\boldsymbol{\kappa}'\boldsymbol{\kappa}) - \mathrm{v}^{i'}_+(\boldsymbol{\kappa}')\tilde{\mathbf{x}}^{i'i}_+(\boldsymbol{\kappa}'\boldsymbol{\kappa}) . \quad (123)$$

Taking the difference in Eq. (118), the terms not containing the Fermi function, i.e. the ones with $\mathrm{v}^{i'}$, cancel out for proportional coupling, so that from (117), (120), and (123) we obtain

$$\begin{aligned}
\hat{\mathcal{K}}^I_{\boldsymbol{\eta}'\boldsymbol{\eta}}(0) &= \prod_{j=1}^N \eta'^j\eta^j \sum_{i'i} \delta_{\eta'i',+1}\Big[\gamma_{i'R}\langle \mathrm{c}'_L\boldsymbol{\phi}\cdot\mathbf{v}_{-\eta^i}\rangle^{i'i}_{\boldsymbol{\eta}'^{(i')}\boldsymbol{\eta}^{(i)}} \\
&\qquad\qquad - \gamma_{i'L}\langle \mathrm{c}'_R\boldsymbol{\phi}\cdot\mathbf{v}_{-\eta^i}\rangle^{i'i}_{\boldsymbol{\eta}'^{(i')}\boldsymbol{\eta}^{(i)}}\Big] \\
&= -\sum_{i'\boldsymbol{\kappa}'}[\gamma_{i'R}\mathrm{v}^{i'L}_+(\boldsymbol{\kappa}') - \gamma_{i'L}\mathrm{v}^{i'R}_+(\boldsymbol{\kappa}')]\Omega^{i'}_{\boldsymbol{\eta}'\boldsymbol{\eta}}(\boldsymbol{\kappa}')\delta_{\zeta',-1} ,
\end{aligned}$$
$$(124)$$

with $\mathrm{v}^{il}_+(\boldsymbol{\kappa}) = \mathrm{v}^i_+(\boldsymbol{\kappa})\delta_{\alpha,l}$ and

$$\begin{aligned}
\Omega^{i'}_{\boldsymbol{\eta}'\boldsymbol{\eta}}(\boldsymbol{\kappa}') &:= \prod_{j=1}^N \eta'^j\eta^j\delta_{\eta'i',+1}\sum_i \Big[\eta^i\boldsymbol{\varphi}^{ii}_{\mathrm{B}}(\boldsymbol{\kappa}')\delta_{i'i} \\
&+ \boldsymbol{\varphi}^{i'i'}_{\mathrm{B}}(\boldsymbol{\kappa}')\sum_{i''\boldsymbol{\kappa}''\boldsymbol{\kappa}}\tilde{\mathbf{x}}^{i'i''}_+(\boldsymbol{\kappa}',\boldsymbol{\kappa}'')\boldsymbol{\phi}^{i''i}(\boldsymbol{\kappa}'',\boldsymbol{\kappa})\mathrm{v}^i_{-\eta^i}(\boldsymbol{\kappa})\Big]_{\boldsymbol{\eta}'^{(i')}\boldsymbol{\eta}^{(i)}} ,
\end{aligned}$$
$$(125)$$

where matrix multiplication with respect to the composite sojourn indexes $\boldsymbol{\eta}^{(i)}$ is understood in the second line.

Using the above definitions and Appendix E, the stationary current with proportional coupling reads $I^\infty = -2\mathrm{Re}\mathrm{Tr}_S[\boldsymbol{\mathcal{A}}^\infty]$. From Eqs. (119) and (124)

$$\begin{aligned}
\mathrm{Tr}_S[\boldsymbol{\mathcal{A}}^\infty] &= \sum_{\boldsymbol{\eta}'\boldsymbol{\eta}}\hat{\mathcal{K}}^I_{\boldsymbol{\eta}'\boldsymbol{\eta}}(0)\mathrm{P}^\infty_{\boldsymbol{\eta}} \\
&= -\sum_i \frac{\gamma_{iL}\gamma_{iR}}{2\pi\hbar^2}\int d\epsilon[f^L_+(\epsilon) - f^R_+(\epsilon)]\Gamma_{ii}(\epsilon) \\
&\quad\times \sum_\zeta\sum_{\boldsymbol{\eta}'\boldsymbol{\eta}}\Omega^i_{\boldsymbol{\eta}'\boldsymbol{\eta}}(\zeta,\epsilon)\mathrm{P}^\infty_{\boldsymbol{\eta}}\delta_{\zeta,-1} ,
\end{aligned}$$
$$(126)$$

where we used the property $\gamma_{iL}\Gamma_{iiR}(\epsilon) = \gamma_{iR}\Gamma_{iiL}(\epsilon) = \gamma_{iL}\gamma_{iR}\Gamma_{ii}(\epsilon)$. On the other hand, from Eqs. (E3) and (E6)

$$\mathrm{Tr}_S[\boldsymbol{\mathcal{A}}^\infty] = \sum_i \frac{-\mathrm{i}\gamma_{iL}\gamma_{iR}}{2\pi\hbar}\int d\epsilon \left[f^L_+(\epsilon) - f^R_+(\epsilon)\right]\Gamma_{ii}(\epsilon)\mathcal{G}^a_{ii}(\epsilon) , \quad (127)$$

where $\mathcal{G}^a$ is the advanced Green's function of the central system. Note that the blip index ζ always multiplies the imaginary unit, as can be seen in the definition of the correlation functions g^ζ which enter the diagrammatic contributions to the propagator, see Eqs (48)-(55), along with the phase factors b_{kl} defined Eq. (42). This means that, in the time domain, ζ establishes the sign of the time variable and the real part can be obtained by removing the constraint $\delta_{\zeta,-1}$ and summing over ζ. We

can thus make the following identification with the retarded/advanced Green's functions

$$\mathcal{G}^{(\zeta)}_{ii}(\epsilon) = -\frac{\mathrm{i}\zeta}{\hbar}\sum_{\boldsymbol{\eta}'\boldsymbol{\eta}}\Omega^i_{\boldsymbol{\eta}'\boldsymbol{\eta}}(\zeta,\epsilon)\mathrm{P}^\infty_{\boldsymbol{\eta}} , \quad (128)$$

where $\zeta = +1\,(-1)$ gives the retarded (advanced) Green's function. The exact steady state current acquires, in the continuum limit, the form of the Meir-Wingreen formula [21]

$$\begin{aligned}
I^\infty &= \frac{e}{\hbar}\sum_i \int d\epsilon \left[\frac{\Gamma_L(\epsilon)\Gamma_R(\epsilon)}{\Gamma_L(\epsilon) + \Gamma_R(\epsilon)}\right]_{ii}[f^L_+(\epsilon) - f^R_+(\epsilon)] \\
&\quad\times \left[-\frac{1}{\pi}\mathrm{Im}\,\mathcal{G}^r_{ii}(\epsilon)\right] ,
\end{aligned}$$
$$(129)$$

where $\Gamma_{ii\alpha}(\epsilon) = 2\pi\sum_\sigma \varrho_{\alpha\sigma}(\epsilon)|\mathrm{t}_{i\alpha\sigma}(\epsilon)|^2$ and where we used $\mathrm{Re}[-\mathrm{i}\mathcal{G}^a_{ii}(\epsilon)] = \mathrm{Im}\mathcal{G}^a_{ii}(\epsilon) = -\mathrm{Im}\mathcal{G}^r_{ii}(\epsilon)$.

A quantity used to characterize the equilibrium ($\mu_L = \mu_R = \mu$) behavior of a transport setup is the linear conductance G, defined as the limiting value of the differential conductance $\partial I/\partial V$ for vanishing bias $eV := \mu_L - \mu_R$. Explicitly [65]

$$\begin{aligned}
G &= \frac{e^2}{\hbar}\sum_i \int d\epsilon \left[\frac{\Gamma_L(\epsilon)\Gamma_R(\epsilon)}{\Gamma_L(\epsilon) + \Gamma_R(\epsilon)}\right]_{ii}\left[-\frac{\partial f_+(\epsilon)}{\partial \epsilon}\right] \\
&\quad\times \left[-\frac{1}{\pi}\mathrm{Im}\,\mathcal{G}^r_{ii}(\epsilon)\right] ,
\end{aligned}$$
$$(130)$$

where, at equilibrium, $f^L_+(\epsilon) = f^R_+(\epsilon) = f_+(\epsilon)$ and where we used $\partial f^L_+/\partial V = -e\partial f^L_+/\partial\epsilon$ and $\partial f^R_+/\partial V = e\partial f^R_+/\partial\epsilon$.

In the following, we shall apply the general formalism developed here to two archetypal models, the resonant level model and the SIAM.

VIII. RESONANT LEVEL MODEL

Up to here, we have considered a general interacting central system connected to a number of noninteracting leads, with possibly energy- and state-dependent tunnel coupling. The only constraint has been given on the correlation matrices in the form of Eq. (29). In Sec. VII, we have specialized the discussion to the case of two leads and proportional coupling.

To exemplify the construction carried out so far, we consider in this section the resonant level model (RLM). This model describes a single, spinless level of energy ϵ_0 coupled to two noninteracting leads as shown in Fig. 15. The model Hamiltonian is

$$\begin{aligned}
H &= \epsilon_0\,a^\dagger a + \sum_{\alpha k\sigma}\epsilon_{\alpha k}c^\dagger_{\alpha k\sigma}c_{\alpha k\sigma} \\
&+ \sum_{\alpha k\sigma}\left[\mathrm{t}_{\alpha k}a^\dagger c_{\alpha k\sigma} + \mathrm{t}^*_{\alpha k}c^\dagger_{\alpha k\sigma}a\right] .
\end{aligned}$$
$$(131)$$

Due to the lack of interactions in the dot, this model admits an exact solution and has been analyzed with a
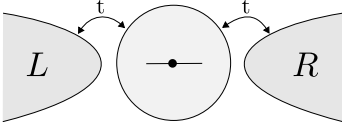
FIG. 15. Scheme of a spinless level of energy ϵ_0 tunnel-coupled to two noninteracting leads.

variety of methods in Ref. [36], see also [38]. According to the diagrammatic rules set up in Sec. IV D, the contributing diagrams for a noninteracting system can have at most two overlapping fermion lines for the same electron state. Since the dot is equipped with a single state, the RTA, discussed in Sec. VI B, provides the exact description of the resonant level. Indeed, from the diagrammatic rules we now that, in a noninteracting system, diagrams with overlap of more than two fermion lines of the same state vanish. Hence, the exact equation (110) reduces to the RTA, where the crossing block X is not dressed by internal processes and the dressed propagator ϕ_B is given by the bare propagator h dressed by the bubbles B, see Fig. 16. As a result, the exact
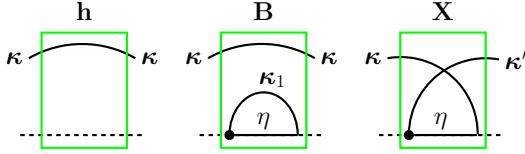
FIG. 16. Blocks involved in the propagator of the resonant level model. Full dots represent the vertexes defined in Eqs. (91) and (92). Dashed and solid lines denote blip and sojourn states, respectively. The sojourn index η assumes the values $+1$ and -1 for occupied and empty dot, respectively. These *internal* sojourns are summed over, the sum being included in the definitions of the blocks.

Dyson equation (112) specializes to

$$\phi(\kappa',\kappa) = \varphi_B(\kappa)\delta_{\kappa'\kappa} + \varphi_B(\kappa')\sum_{\kappa''}X(\kappa',\kappa'')\phi(\kappa'',\kappa) , \tag{132}$$

where the matrix structure in the sojourn index $\boldsymbol{\eta}^{(i)}$ is lost due the fact that there is a single electron state so that $\boldsymbol{\chi} \equiv \boldsymbol{\kappa}$ with

$$\boldsymbol{\kappa} = (\zeta,\alpha,k) .$$

The dressed propagator $\phi_B(\kappa',\kappa) = \varphi_B(\kappa')\delta_{\kappa'\kappa}$ is in turn given by

$$\phi_B = \left[\mathbf{h}^{-1} - \mathbf{B}\right]^{-1} , \tag{133}$$

according to Eq. (108).

In Laplace space the bare propagator $\mathbf{h}(\lambda = 0^+)$ reads

$$[\mathbf{h}]_{\kappa'\kappa} = i\hbar\frac{1}{\zeta(\epsilon_k - \epsilon_0) + i0^+}\delta_{\kappa'\kappa} , \tag{134}$$

see Eq. (91).

The bubble block, the central diagram in Fig. 16, is the contraction with a vertex of the internal fermion line (indexed with 1) of the free propagator with two overlapping fermion lines

$$[\mathbf{h}_2]_{\kappa'\kappa} = \overset{\kappa}{\underset{\eta}{\overbrace{\qquad}}}\kappa_1 = i\hbar\frac{\delta_{\zeta_1,-\zeta}}{\zeta(\epsilon_k - \epsilon_{k_1}) + i0^+}\delta_{\kappa'\kappa} . \tag{135}$$

Here, the index ζ_1 is constrained to be equal to $-\zeta$ by the diagrammatic rules, see Eq. (51) where the upper indexes of the correlation functions g_η^ζ have opposite signs. Note that the block $\mathbf{h}_2$ bears no dependence on the dot energy as the system is in a sojourn state, denoted with η, contrary to the block h in Eq. (134) where the system is in a blip state (dashed line, see the left diagram in Fig. 16). Including the sum over the internal sojourn η due to the sum-over-paths, the bubble block is evaluated as follows

$$\begin{aligned}[\mathbf{B}]_{\kappa'\kappa} &= \overset{\kappa_1}{\underset{\eta}{\overbrace{\qquad}}}\kappa = \sum_\eta \langle \mathbf{h}_2 \mathbf{v}_\eta \rangle \\ &= i\zeta\hbar\sum_{\kappa_1}\frac{\sum_\eta \mathbf{v}_\eta(\boldsymbol{\kappa}_1)\delta_{\zeta_1,-\zeta}}{\epsilon_k - \epsilon_{k_1} + i\zeta0^+}\delta_{\kappa'\kappa} \\ &= -\frac{i\zeta}{\hbar}\sum_{\alpha_1,k_1}\frac{|t_{\alpha_1}(\epsilon_{k_1})|^2}{\epsilon_k - \epsilon_{k_1} + i\zeta0^+}\delta_{\kappa'\kappa} ,\end{aligned} \tag{136}$$

where we used $\sum_\eta f_\eta(\epsilon_k) = 1$ in the vertex

$$\mathbf{v}_\eta(\boldsymbol{\kappa}) := -\frac{|t_\alpha(\epsilon_k)|^2}{\hbar^2}f_\eta^\alpha(\epsilon_k) . \tag{137}$$

In the wide-band limit (WBL), i.e. for energy independent tunneling amplitudes, using the result of Eq. (I1) we obtain

$$\begin{aligned}[\mathbf{B}]_{\kappa'\kappa} &= \zeta\frac{i}{\hbar}\sum_{\alpha_1}\varrho_{\alpha_1}|t_{\alpha_1}|^2\int d\epsilon_1 \frac{\delta_{\kappa'\kappa}}{\epsilon_1 - \epsilon_k - i\zeta0^+} \\ &= -\frac{1}{\hbar}\pi\sum_{\alpha_1}\varrho_{\alpha_1}|t_{\alpha_1}|^2\delta_{\kappa'\kappa} \\ &= -\frac{\Gamma}{2\hbar}\delta_{\kappa'\kappa} ,\end{aligned} \tag{138}$$

where $\Gamma = 2\pi\sum_\alpha \varrho_\alpha|t_\alpha|^2$. As a result, from Eq. (133),

$$\varphi_B(\zeta,k) = i\zeta\hbar\frac{1}{\epsilon_k - \epsilon_0 + i\zeta\Gamma/2} . \tag{139}$$

The block $\mathbf{X}$ is given by attaching the vertex $\mathbf{v}_\eta$ to the outgoing fermion line (with index κ') in the propagator

$$[\mathbf{h}_2^X]_{\kappa'\kappa} = i\hbar\frac{\delta_{\zeta',-\zeta}}{\zeta(\epsilon_k - \epsilon_{k'}) + i0^+} , \tag{140}$$

resulting in

$$[\mathbf{X}]_{\kappa'\kappa} = \overset{\kappa \,\,\,\,\,\, \kappa'}{\underset{\eta}{\frown}}$$

$$= \frac{i\zeta\hbar \sum_\eta v_\eta(\boldsymbol{\kappa}')}{\epsilon_k - \epsilon_{k'} + i\zeta 0^+} \delta_{\zeta',-\zeta} \qquad (141)$$

$$= -\frac{i\zeta}{\hbar} \frac{|t_{\alpha'}(\epsilon_{k'})|^2}{\epsilon_k - \epsilon_{k'} + i\zeta 0^+} \delta_{\zeta',-\zeta} \,.$$

Here, as for $\mathbf{B}$, the internal sojourn index η is summed over due to the sum-over-path with the result that $\mathbf{X}$ does not contain the Fermi function.

The retarded/advanced Green's function are given by Eq. (128) via the function $\Phi_{\eta'\eta}$ defined in Eq. (125) which, in the RLM, adapts to

$$\Omega_{\eta'\eta}(\boldsymbol{\kappa}') = \eta'\eta\delta_{\eta',+1}\Big[\eta\varphi_B(\boldsymbol{\kappa}')$$
$$+ \varphi_B(\boldsymbol{\kappa}')\sum_{\boldsymbol{\kappa}\boldsymbol{\kappa}''} x_+(\boldsymbol{\kappa}',\boldsymbol{\kappa})\phi(\boldsymbol{\kappa},\boldsymbol{\kappa}'')v_{-\eta}(\boldsymbol{\kappa}'')\Big] \,.$$
$$(142)$$

The block x_+, see Eq. (123) is easy to evaluate and from Eq. (141) reads

$$x_+ = \frac{i\zeta\hbar \sum_\eta \eta}{\epsilon_k - \epsilon_{k'} + i\zeta 0^+} \delta_{\zeta',-\zeta} = 0 \,.$$

Thus,

$$\Omega_{\eta'\eta}(\zeta,k) = \delta_{\eta',+1}\varphi_B(\zeta,k) \,,$$

and the resulting expression for the Green's function is

$$\mathcal{G}^{(\zeta)}(\epsilon_k) = -\frac{i\zeta}{\hbar}\sum_{\eta'\eta}\Omega_{\eta'\eta}(\zeta,k)P_\eta^\infty$$

$$= -\frac{i\zeta}{\hbar}\varphi_B(\zeta,k)\sum_\eta P_\eta^\infty \qquad (143)$$

$$= \frac{1}{\epsilon_k - \epsilon_0 + i\zeta\Gamma/2} \,,$$

where we used Eq. (139). Thus, as expected, the single-particle Green's function acquires a broadening $\Gamma/2$ due to the coupling of the resonant level to the leads.

Substituting $\mathcal{G}^{(\zeta=+1)}(\epsilon)$ in Eq. (129), the current for proportional coupling, $\gamma_L\Gamma_R = \gamma_R\Gamma_L$ (with $\gamma_L + \gamma_R = 1$), in the WBL reads [89]

$$I^\infty = \frac{e}{h}\int d\epsilon \,[f_+^L(\epsilon) - f_+^R(\epsilon)]\frac{\Gamma_L\Gamma_R}{(\epsilon - \epsilon_0)^2 + \Gamma^2/4}$$

$$= \frac{e}{h}\frac{\Gamma_L\Gamma_R}{\Gamma}r(\epsilon_0) \,, \qquad (144)$$

where $\Gamma = \Gamma_L + \Gamma_R$ and where we defined

$$r(x) = \mathrm{Im}\psi\left(\frac{1}{2} + i\frac{x - \mu_L - i\frac{\Gamma}{2}}{2\pi k_B T}\right)$$
$$- \mathrm{Im}\psi\left(\frac{1}{2} + i\frac{x - \mu_R - i\frac{\Gamma}{2}}{2\pi k_B T}\right) \,, \qquad (145)$$

with $\Psi(x)$ the digamma function. Equation (144) provides the exact, finite-temperature expression for the current in the RLM.

Summarizing, while the RTA gives the exact irreducible propagator ϕ and consequently the exact density matrix and current for the RLM, the crossing diagrams do not contribute to the retarded/advanced Green's functions (and to the current for proportional coupling). Note that, as the dot can host at most one electron, the system is necessarily noninteracting and consequently inelastic processes are absent. This gives the Landauer formula Eq. (144), where the temperature dependence is exclusively in the Fermi functions. Using Eq. (130) for the conductance, with the imaginary part of Eq. (143), we readily obtain the analytical expression for the conductance at $T = 0$, where $-\partial f_+/\partial\epsilon = \delta(\epsilon - \mu)$, which is of the Breit-Wigner form [22, 23]

$$G = \frac{2e^2}{h}\frac{\Gamma_L\Gamma_R/2}{(\mu - \epsilon_0)^2 + \Gamma^2/4} \,. \qquad (146)$$

For $\Gamma_\alpha = \Gamma/2$ the conductance saturates to half of the quantum of conductance $G_0 = 2e^2/h$ at resonance, i.e. for $\mu = \epsilon_0$. In the noninteracting *spinful* model, where the dot can host two electrons with opposite spin, the sum over σ yields the maximum $G_{max} = G_0$.

IX. SINGLE IMPURITY ANDERSON MODEL (SIAM)
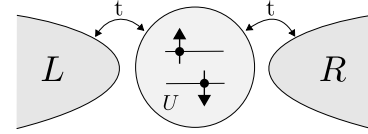
FIG. 17. Single impurity Anderson model realized by a quantum dot tunnel-coupled to two noninteracting leads.

We now specialize the discussion to the simplest, yet highly nontrivial, instance of the general model of interacting nanostructure described by Eq. (1), the single impurity Anderson model (SIAM). In the SIAM, the central system is a quantum dot that can host at most two electrons with opposite spin states, the latter being denoted by $\sigma = \uparrow,\downarrow$. The dot is connected to two leads, L and R, via a tunnel coupling which we assume here to be spin-independent. A scheme of the model is provided in Fig. 17. The resulting four many-body dot states are given by $|0\rangle$, $|\uparrow\rangle$, $|\downarrow\rangle$, and $|2\rangle$, or, in terms of the sojourn indexes $(\eta^\uparrow,\eta^\downarrow)$, by $|-1-1\rangle$, $|+1-1\rangle$, $|-1+1\rangle$, and $|+1+1\rangle$, respectively. The difference in chemical potentials produces at long times a stationary current which is essentially determined by three energy scales: The interaction energy U between the electrons in the dot, the tunnel coupling Γ, and the thermal energy $k_B T$. Despite

its simplicity, this model already displays a variety of interesting physical effects and transport regimes arising from the interplay of these energy scales, see Fig. 18 below. For example, the Kondo effect [4–6], an exquisitely nonperturbative many-body phenomenon due to the correlation between electrons in the dot and the leads, becomes relevant for temperatures around and below a certain value T_K which depends exclusively on Γ, U, and the single-particle energies ϵ_σ.

The full Hamiltonian of the setup reads

$$
\begin{aligned}
H = &\sum_\sigma \epsilon_\sigma \hat{n}_\sigma + U \hat{n}_\uparrow \hat{n}_\downarrow + \sum_{\alpha k \sigma} \epsilon_{\alpha k} c^\dagger_{\alpha k \sigma} c_{\alpha k \sigma} \\
&+ \sum_{\alpha k \sigma} \left[\mathrm{t}_{\alpha k} a^\dagger_\sigma c_{\alpha k \sigma} + \mathrm{t}^*_{\alpha k} c^\dagger_{\alpha k \sigma} a_\sigma \right] ,
\end{aligned}
\tag{147}
$$

where $\alpha = L, R$, and $\hat{n}_\sigma = a^\dagger_\sigma a_\sigma$. The single-particle energies ϵ_σ are possibly split by an externally applied magnetic field, $\epsilon_\uparrow = \epsilon_0 + \Delta_B$ and $\epsilon_\downarrow = \epsilon_0 - \Delta_B$. Note that spin-independent coupling constants $\mathrm{t}_{\alpha k}$ (and nonmagnetic leads) imply that the correlation matrices $\mathbf{g}_\pm$, Eq. (7), are not only diagonal, but also proportional to the identity, namely $[\mathbf{g}_\pm(t)]_{\sigma' \sigma} = \delta_{\sigma' \sigma}\, \mathrm{g}_\pm(t)$ with

$$
\mathrm{g}_\pm(t) = \frac{1}{\hbar^2} \sum_{\alpha k} |\mathrm{t}_{\alpha k}|^2 f^\alpha_\pm(\epsilon_k) e^{-\frac{\mathrm{i}}{\hbar}\epsilon_{\alpha k} t} .
\tag{148}
$$

In what follows we use the compact notation of Eq. (22) which, in the case considered here, adapts to

$$
\mathrm{g}^{+1}_{+1} = \mathrm{g}_+, \quad \mathrm{g}^{-1}_{+1} = \mathrm{g}^*_+, \quad \mathrm{g}^{+1}_{-1} = \mathrm{g}_-, \quad \mathrm{g}^{-1}_{-1} = \mathrm{g}^*_- .
\tag{149}
$$

In the WBL, the tunnel coupling is quantified by $\Gamma := 2\pi \sum_\alpha \varrho_\alpha |\mathrm{t}_\alpha|^2$. The collective index $\boldsymbol{\chi}$, defined for the general case in Eq. (86), specializes in the SIAM to

$$
\boldsymbol{\chi} := (\boldsymbol{\kappa}, \eta^{\bar\sigma}), \quad \text{where} \quad \boldsymbol{\kappa} = (\zeta, \alpha, k)
$$

and where $\bar\sigma$ denotes the opposite spin with respect to σ. In order to simplify the notation, from here on we make the identifications

$$
\eta^\sigma \equiv \nu \quad \text{and} \quad \eta^{\bar\sigma} \equiv \eta ,
$$

with $\bar\nu \equiv -\nu$ and $\bar\eta \equiv -\eta$, so that $\boldsymbol{\chi} := (\boldsymbol{\kappa}, \eta)$. The system energies E_i in the phase factors of Eq. (42) are in this case the path-dependent dot energies shown in Fig. 7. For the fermion lines associated to the state σ these energies read

$$
\begin{array}{ll}
E_\sigma = \epsilon_\sigma + U/2 & \bar\sigma \text{ in a blip state} \\
E_\sigma(\eta) = \epsilon_\sigma + (1 + \eta)U/2 & \bar\sigma \text{ in the sojourn } \eta .
\end{array}
\tag{150}
$$

Analogous expressions hold for $E_{\bar\sigma}$ and $E_{\bar\sigma}(\nu)$.

The retarded ($\zeta = +1$) and advanced ($\zeta = -1$) dot Green's functions, Eq. (128), adopt in the SIAM the following form

$$
\mathcal{G}^{(\zeta)}_{\sigma\sigma}(\epsilon_k) = -\frac{\mathrm{i}\zeta}{\hbar} \sum_{\boldsymbol{\eta}' \boldsymbol{\eta}} \Omega^\sigma_{\boldsymbol{\eta}' \boldsymbol{\eta}}(\zeta, k) \mathrm{P}^\infty_{\boldsymbol{\eta}} ,
\tag{151}
$$

with

$$
\begin{aligned}
\Omega^\sigma_{\boldsymbol{\eta}' \boldsymbol{\eta}}(\boldsymbol{\kappa}) = \eta' \eta \delta_{\nu',+1} &\sum_{s=\uparrow,\downarrow} \Big[\boldsymbol{\varphi}^\sigma_\mathrm{B}(\boldsymbol{\kappa}) \delta_{\sigma' \sigma} + \nu \boldsymbol{\varphi}^\sigma_\mathrm{B}(\boldsymbol{\kappa}) \\
&\times \sum_{\sigma'' \boldsymbol{\kappa}'' \boldsymbol{\kappa}'} \tilde{\mathbf{x}}^{\sigma \sigma''}_+(\boldsymbol{\kappa}, \boldsymbol{\kappa}'') \phi^{\sigma'' s}(\boldsymbol{\kappa}'', \boldsymbol{\kappa}') \mathrm{v}_{-\eta^s}(\boldsymbol{\kappa}') \Big]_{\eta' \eta^{\bar s}} ,
\end{aligned}
\tag{152}
$$

where we used $(\nu)^2 = 1$. Here, the blocks in parenthesis have a 2×2 matrix structure induced by the sojourn indexes $\eta'^{\bar\sigma'} \eta$, and the vertex is given by

$$
\mathrm{v}_{-\eta}(\boldsymbol{\kappa}) := -\frac{|\mathrm{t}_\alpha(\epsilon_k)|^2}{\hbar^2} f^\alpha_{-\eta}(\epsilon_k) .
\tag{153}
$$

The Meir-Wingreen formula, which gives the current for a general system in the case of proportional coupling with the leads, Eq. (129), adapts for the SIAM to

$$
I^\infty = \frac{e}{\hbar} \frac{\Gamma_L \Gamma_R}{\Gamma} \sum_\sigma \int d\epsilon \, [f^L_+(\epsilon) - f^R_+(\epsilon)] \left[-\frac{1}{\pi} \mathrm{Im} \mathcal{G}^r_{\sigma\sigma}(\epsilon) \right] .
\tag{154}
$$

The asymptotic population of the spin states σ is the trace over the occupation states of $\bar\sigma$ of the SIAM populations $\mathrm{P}^\infty_{\boldsymbol{\eta}}$, namely $\mathrm{p}^\sigma_\nu = \sum_\eta \mathrm{P}^\infty_{\boldsymbol{\eta}}$. In terms of the expectation value of the number operator $\hat{n}_\sigma$

$$
\mathrm{p}^\sigma_+ = \langle \hat{n}_\sigma \rangle , \qquad \mathrm{p}^\sigma_- = 1 - \langle \hat{n}_\sigma \rangle .
\tag{155}
$$

These expectation values can be calculated either by solving the master equation for $\mathrm{P}^\infty_{\boldsymbol{\eta}}$, see Eq. (115), or self-consistently, via the equations of motion technique [42], where, in the wide-band limit,

$$
\langle \hat{n}_\sigma \rangle = \frac{1}{\Gamma} \int d\epsilon \left[\Gamma_L f^L_+(\epsilon) + \Gamma_R f^R_+(\epsilon) \right] \left[-\frac{1}{\pi} \mathrm{Im} \mathcal{G}^r_{\sigma\sigma}(\epsilon) \right] ,
\tag{156}
$$

with $\Gamma = \Gamma_L + \Gamma_R$.

A. Approximation schemes

Despite the existing rich literature on the SIAM, due to the complexity of the problem, an exact analytical solution for the dot Green's function, Eq. (151), encompassing the whole regime of parameters U, Γ, and T, is not known so far. In the forthcoming sections, we show how known perturbative schemes in Γ, as well as some nonperturbative ones, are recovered within our approach. Furthermore, a novel infinite-tier approximation scheme is discussed.

In Fig. 18 we sketch the regime of validity of different analytical approaches derived from the diagrammatic unravelling of the exact irreducible propagator in Eq. (98). The sequential tunneling and cotunneling schemes are perturbative in Γ and thus valid when Γ is the smallest energy scale, namely $\Gamma \ll k_\mathrm{B} T$ for $U = 0$ and $\Gamma \ll k_\mathrm{B} T, U$ for $U \neq 0$. In order to access the regime $\Gamma \sim k_\mathrm{B} T$ one needs to include processes of all orders.

The simplest way to do this is to truncate the hierarchy of diagrams discussed in Sec. VI B to a maximum overlap of two fermion lines. We call the resulting schemes second-tier. Iterating the insertion of the bare bubble and crossing blocks defined above in the bare propagator **h** and summing the geometrical series results in the RTA [47], where ϕ is the solution of the Dyson equation (106). Neglecting the crossing blocks of the RTA, one is left with a main fermion line dressed by bubbles, a scheme which we call gDSO, as it generalizes the dressed second order (DSO), which accounts only for charge fluctuations internal to the main fermion line [49]. In our language the DSO considers the bubble blocks diagonal in the index η. On the contrary, the gDSO takes into account the full matrix structure of the bubbles and, along with the RTA, recovers the noninteracting Green's functions. These second-tier schemes display artifacts such as
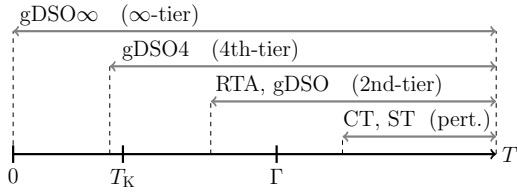
FIG. 18. The different approximation schemes for the SIAM discussed in this work, in their range of validity ($k_B = 1$). Sequential tunneling (ST) and cotunneling (CT) are perturbative in Γ (first and second order, respectively). The generalized dressed second order (gDSO) and the resonant tunneling approximation (RTA) are nonperturbative in Γ and neglect diagrams with overlap of more than two fermion lines (second-tier schemes). The first is obtained from the second by neglecting the crossing diagrams and yields the Meir-Wingreen-Lee result [39] for the retarded Green's function. Higher-tier approximation schemes deepen the hierarchy of fermion lines. We propose novel infinite-tear and fourth-tier schemes which neglect the crossings at all levels and can be seen as dressed versions of the gDSO.

the pinning of the density of states at the particle-hole symmetry point, due to the temperature-independent self-energy at this symmetry point, and do not predict the correct Kondo temperature T_K. Crossing diagrams contribute to inelastic processes but are not expected to be relevant for investigating the zero-bias anomaly. For these reasons, in Sec. IX D, we discuss an infinite-tier approximation which allows to recover the gDSO Green's function but with dressed self-energies, see Eqs. (207) and (212) below. In Sec. IX E, we explicitly evaluate such self-energies in a simplified fourth-tier scheme.

B. Perturbative schemes

1. Sequential tunneling

The simplest approximation, valid for $k_B T, U \gg \Gamma$ (or $k_B T \gg \Gamma$ if $U = 0$), consists in truncating to the low-
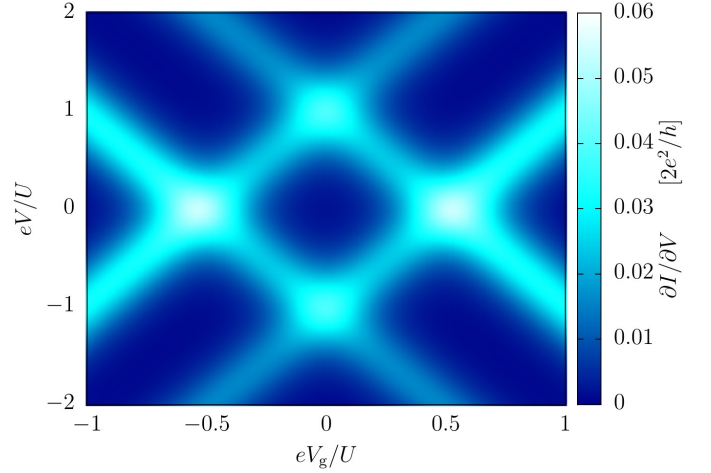
FIG. 19. Differential conductance *vs* the gate voltage V_g and bias voltage V in the sequential tunneling (ST) approximation. At low bias voltages, the current is strongly suppressed inside the regions enclosed by so-called Coulomb diamonds due to charging effects. The ST approximation does not account for virtual processes (of higher order in Γ) which enable transport of charge also inside the Coulomb diamonds. Degenerate case, $\epsilon_\sigma = \epsilon_0 = -U/2 + eV_g$, with temperature $k_B T = 0.1\ U$ and tunneling rates $\Gamma_L = \Gamma_R = 0.005\ U$.

est order in Γ the Dyson equation for the propagator ϕ, Eq. (103). This results in $\phi_{\mathrm{ST}} = \mathbf{h}$, where the bare propagator with a single fermion line reads for the SIAM $[\mathbf{h}]_{\chi'\chi}^{\sigma'\sigma} = \mathrm{h}_{\eta\eta}^\sigma \delta_{\sigma'\sigma} \delta_{\chi'\chi}$, where

$$\mathrm{h}_{\eta\eta}^\sigma = \underset{\eta}{\underset{\text{.............}}{\overset{\sigma\kappa}{\frown}}} = \mathrm{i}\hbar \frac{1}{\zeta[\epsilon_k - E_\sigma(\eta)] + \mathrm{i}0^+} \ . \qquad (157)$$

This propagator yields the current to the lowest order, namely the second order in the tunneling amplitude t (or first order in Γ). Note that the propagator ϕ_{ST} is diagonal both in the spin and in the remaining variables χ. Using Eqs. (151) and (152), the Green's functions in the ST approximation is

$$\mathcal{G}_{\sigma\sigma,\mathrm{ST}}^{(\zeta)}(\epsilon_k) = -\frac{\mathrm{i}\zeta}{\hbar} \sum_{\eta'\eta} \eta'\eta\, \varphi_{\mathrm{ST},\eta'\eta}^{\sigma\sigma}(\zeta, k)\mathrm{p}_\eta^{\bar\sigma}$$
$$= \sum_\eta \frac{\mathrm{p}_\eta^{\bar\sigma}}{\epsilon_k - E_\sigma(\eta) + \mathrm{i}\zeta0^+} \ , \qquad (158)$$

where $\mathrm{p}_\eta^{\bar\sigma} = \sum_\nu \mathrm{P}_{\boldsymbol\eta}^\infty$. Recall that $\varphi_{\mathrm{ST},\eta'\eta}^{\sigma\sigma}(\kappa) = \sum_{\sigma'\kappa'} \phi_{\mathrm{ST},\eta'\eta}^{\sigma'\sigma}(\kappa', \kappa)$, see Eq. (113). In the ST approximation, from Eqs. (155) and (158),

$$-\frac{1}{\pi}\mathrm{Im}\mathcal{G}_{\sigma\sigma}^r(\epsilon) = \delta(\epsilon - \epsilon_\sigma)(1 - \langle \hat{n}_{\bar\sigma} \rangle) + \delta(\epsilon - \epsilon_\sigma - U)\langle \hat{n}_{\bar\sigma} \rangle \ , \qquad (159)$$

where we have used $\lim_{\varepsilon \to 0^+} \varepsilon/(x^2 + \varepsilon^2) = \pi\delta(x)$, and the general formula (154) gives for the curent

$$
\begin{aligned}
I_{\mathrm{ST}}^\infty = {} & \frac{e}{\hbar} \frac{\Gamma_L \Gamma_R}{\Gamma} \sum_\sigma \Big\{ [f_+^L(\epsilon_\sigma) - f_+^R(\epsilon_\sigma)](1 - \langle \hat{n}_{\bar\sigma} \rangle) \\
& + [f_+^L(\epsilon_\sigma + U) - f_+^R(\epsilon_\sigma + U)] \langle \hat{n}_{\bar\sigma} \rangle \Big\} .
\end{aligned}
\tag{160}
$$

The levels's populations are obtained by solving Eq. (156) which yields in this case

$$
\langle \hat{n}_{\bar\sigma} \rangle = \frac{\sum_\alpha \Gamma_\alpha f_+^\alpha(\epsilon_\sigma)}{\Gamma + \sum_\alpha \Gamma_\alpha f_+^\alpha(\epsilon_\sigma) - \sum_\alpha \Gamma_\alpha f_+^\alpha(\epsilon_\sigma + U)} .
\tag{161}
$$

In Fig. 19, we show the differential conductance $\partial I/\partial V$ in the degenerate case, obtained from Eqs. (160) and (161) by using $\partial f_+^L/\partial V = -e\partial f_+^L/\partial\epsilon$ and $\partial f_+^R/\partial V = e\partial f_+^R/\partial\epsilon$. The differential conductance is shown as a function of the bias voltage $eV = \mu_L - \mu_R$, and the gate voltage, which shifts the position of the (degenerate) level via $\epsilon_0 = -U/2 + eV_{\mathrm{g}}$. Such plot, called stability diagram, highlights the resonances which form diamond-shaped regions where the differential conductance is zero. In the central regions called Coulomb diamonds, the dot populations are 0, 1, and 2, from left to right, and the current is suppressed. This effect is called Coulomb blockade and appears in the present regime of weak tunnel coupling , where the Coulomb interaction dominates and $\Gamma/k_{\mathrm{B}}T \ll 1$.

A horizontal cut ($V = 0$) of the stability diagram gives the linear conductance $G = \partial I/\partial V|_{V=0}$, see Eq. (130). The linear conductance, which is suppressed at the center of the Coulomb diamond, shows two peaks separated by the energy U, see Fig. 20 below. A straightforward extension of the ST which accounts for a Γ-broadening in the Green's function is discussed in Sec. IX C 4 below.

2. Cotunneling

The next improvement over the ST, also perturbative in Γ, is the cotunneling approximation. It allows charge transfer across the dot also in the parameter regimes where ST processes are exponentially suppressed due to the Coulomb blockade [34], i.e. around the center of the Coulomb diamond, $V_{\mathrm{g}} \sim 0$, see Fig. 19. In our diagrammatic approach, this occurs via virtual processes encoded in the bubble and crossing blocks $\mathbf{B}$ and $\mathbf{X}$, i.e., according to Eq. (105),

$$
\phi_{\mathrm{CT}} = \mathbf{h} + \mathbf{h}(\mathbf{B} + \mathbf{X})\mathbf{h} .
\tag{162}
$$

As the sequential tunneling approximation, also this scheme is valid when Γ is the smallest energy scale of the problem.

As already noticed in the case of the RLM, the diagrammatic rules in Sec. IV D and in Appendix H imply that when there are at most two overlapping fermion lines associated to the same state (in the present case to the

same spin state), the fermion line of a bubble has the index ζ opposite to the one of the main fermion line. Similarly, in a crossing, the outgoing line has the index ζ opposite to the one of the incoming line. These constraints do not apply when the spin states involved in a bubble or in a crossing block are different. It is therefore natural to distinguish these two cases.

The bubble block is obtained by contracting with a vertex the internal fermion line (indexed with 1) of the bare propagator with two overlapping fermion lines which can be of the same $[\sigma(\sigma)]$, see Eq. (163), or of opposite $[\sigma(\bar\sigma)]$ spin. The first is given by $[\mathbf{h}_2^{(\sigma)}]_{\boldsymbol{\chi'}\boldsymbol{\chi},\nu'\nu}^{\sigma'\sigma} = \mathrm{h}_2^{\sigma(\sigma)} \delta_{\sigma'\sigma} \delta_{\boldsymbol{\kappa'}\boldsymbol{\kappa}} \delta_{\boldsymbol{\eta'}\boldsymbol{\eta}}$, where

$$
\mathrm{h}_2^{\sigma(\sigma)} =
\vcenter{\hbox{}}
= \mathrm{i}\hbar \frac{\delta_{\zeta_1, -\zeta}}{\zeta(\epsilon_k - \epsilon_{k_1}) + \mathrm{i}0^+} ,
\tag{163}
$$

(cf. Eq. (135)). Note that the block $\mathbf{h}_2^{(\sigma)}$ has a 4×4 structure in the composite index $(\nu, \eta) = (\eta^\sigma, \eta^{\bar\sigma})$. The propagator with overlap of two fermion lines with opposite spin is given by the block $[\mathbf{h}_2^{(\bar\sigma)}]_{\boldsymbol{\kappa'}\boldsymbol{\kappa}}^{\sigma'\sigma} = \mathrm{h}_2^{\sigma(\bar\sigma)} \delta_{\sigma'\sigma} \delta_{\boldsymbol{\kappa'}\boldsymbol{\kappa}}$, with

$$
\mathrm{h}_2^{\sigma(\bar\sigma)} =
\vcenter{\hbox{}}
= \mathrm{i}\hbar \frac{1}{\zeta(\epsilon_k - E_\sigma) + \zeta_1(\epsilon_{k_1} - E_{\bar\sigma}) + \mathrm{i}0^+}
\tag{164}
$$

which has no structure in the sojourn indexes. The bubble block resulting from the contraction of the internal fermion lines of the two above propagators with the vertexes

$$
\mathrm{v}_{\pm\eta}(\boldsymbol{\kappa}) := -\frac{|\mathrm{t}_\alpha(\epsilon_k)|^2}{\hbar^2} f_{\pm\eta}^\alpha(\epsilon_k) ,
\tag{165}
$$

is given by $[\mathbf{B}]_{\boldsymbol{\chi'}\boldsymbol{\chi}}^{\sigma'\sigma} = \mathrm{B}_{\eta'\eta}^\sigma \delta_{\sigma'\sigma} \delta_{\boldsymbol{\kappa'}\boldsymbol{\kappa}}$. The function $\mathrm{B}_{\eta'\eta}^\sigma$ is the sum

$$
\begin{aligned}
\mathrm{B}_{\eta'\eta}^\sigma = {} & \mathrm{B}_{\eta'\eta}^{\sigma(\sigma)} + \mathrm{B}_{\eta'\eta}^{\sigma(\bar\sigma)} \\
= {} & \vcenter{\hbox{}} + \vcenter{\hbox{}} \\
= {} & \sum_{\boldsymbol{\kappa}_1} \frac{\mathrm{i}\hbar \sum_\nu \mathrm{v}_\nu(\boldsymbol{\kappa}_1) \delta_{\zeta_1, -\zeta}}{\zeta(\epsilon_k - \epsilon_{k_1}) + \mathrm{i}0^+} \delta_{\eta'\eta} \\
& + \sum_{\boldsymbol{\kappa}_1} \frac{\mathrm{i}\hbar\, \mathrm{v}_{-\eta}(\boldsymbol{\kappa}_1)}{\zeta(\epsilon_k - E_\sigma) + \zeta_1(\epsilon_{k_1} - E_{\bar\sigma}) + \mathrm{i}0^+} .
\end{aligned}
\tag{166}
$$

The first contribution, which is diagonal in all the indexes, is calculated as in Eqs. (136)-(138), and reads $\mathrm{B}_{\eta'\eta}^{\sigma(\sigma)} = -\Gamma/(2\hbar)\delta_{\eta'\eta}$ in the WBL. The second term in Eq. (166) depends on η via the vertex and can be evaluated as well in the WBL where $\sum_{\boldsymbol{\kappa}_1} \to \sum_{\zeta_1 \alpha_1} \varrho_{\alpha_1} \int d\epsilon_1$.

We obtain, see Appendix I,

$$-\frac{i}{\hbar}\sum_{\zeta_1}\zeta_1\sum_{\alpha_1}\frac{\Gamma_{\alpha_1}}{2\pi}\int_{-W}^{W}d\epsilon_1\,\frac{f_{-\eta}^{\alpha_1}(\epsilon_1)}{\epsilon_1-\mathcal{E}_{\zeta_1}+i\zeta_1 0^+}$$

$$=i\eta\sum_{\alpha}\frac{\Gamma_\alpha}{2\pi\hbar}\left[\mathrm{Re}\psi\left(\frac{1}{2}+i\frac{\mathcal{E}_{+1}-\mu_\alpha}{2\pi k_{\mathrm{B}}T}\right)\right.$$
$$\left.-\mathrm{Re}\psi\left(\frac{1}{2}+i\frac{\mathcal{E}_{-1}-\mu_\alpha}{2\pi k_{\mathrm{B}}T}\right)\right]$$
$$-\sum_{\alpha}\frac{\Gamma_\alpha}{2\hbar}\left[f_{-\eta}^\alpha(\mathcal{E}_{+1})+f_{-\eta}^\alpha(\mathcal{E}_{-1})\right]\,,\tag{167}$$

where $\mathcal{E}_{\zeta_1}:=E_{\bar\sigma}+\zeta\zeta_1(E_\sigma-\epsilon)$. All in all, the WBL expression for the bubble block reads

$$\mathrm{B}_{\eta'\eta}^\sigma=-\frac{\Gamma}{2\hbar}\delta_{\eta'\eta}$$
$$-\sum_{\alpha_1,\zeta_1}\frac{\Gamma_{\alpha_1}}{2\hbar}\left[f_{-\eta}^{\alpha_1}(\mathcal{E}_{\zeta_1})-i\frac{\eta\zeta_1}{\pi}\mathrm{Re}\psi\left(\frac{1}{2}+i\frac{\mathcal{E}_{\zeta_1}-\mu_{\alpha_1}}{2\pi k_{\mathrm{B}}T}\right)\right]\,.\tag{168}$$

Note that the second term, while depending on the sojourn index η, is independent of η'. Thus, in the WBL, the matrix elements of the bubble can be written as the sum

$$\mathrm{B}_{\eta'\eta}^\sigma=-\frac{\Gamma}{2\hbar}\delta_{\eta'\eta}+\mathrm{B}_{\bar\eta\eta}^\sigma\,.\tag{169}$$

The crossing blocks, with overlap of fermion lines with same and opposite spin, read

$$[\mathbf{X}]_{\chi'\chi}^{\sigma\sigma}=\;\underset{\eta\quad\quad\eta}{\overset{\sigma,\kappa\quad\nu\quad\sigma,\kappa'}{\,}}\;=\frac{i\hbar\sum_\nu\mathrm{v}_\nu(\kappa')}{\zeta(\epsilon_k-\epsilon_{k'})+i0^+}\delta_{\zeta',-\zeta}\delta_{\eta'\eta}\,,$$

$$[\mathbf{X}]_{\chi'\chi}^{\bar\sigma\sigma}=\;\underset{\eta\quad\quad\nu'}{\overset{\sigma,\kappa\quad\quad\bar\sigma,\kappa'}{\,}}\;=\frac{i\hbar\,\mathrm{v}_{-\eta}(\kappa')}{\zeta(\epsilon_k-E_\sigma)+\zeta'(\epsilon_{k'}-E_{\bar\sigma})+i0^+}\,,\tag{170}$$

respectively. Here, in the spin-diagonal crossing block, we include the sum over the internal sojourn ν in the definition, as done for the bubble with overlap of same-spin fermion lines, see Eq. (166).

In order to write the Green's function, we use the cotunneling irreducible propagator in Eq. (162). This yields

$$\Omega_{\eta'\eta}^{\sigma,\mathrm{CT}}(\kappa)=\eta'\eta\delta_{\nu',+1}\Big\{\mathrm{h}_{\eta\eta}^\sigma(\kappa)\delta_{\eta'\eta}$$
$$+\left[\mathbf{h}^\sigma(\kappa)\mathbf{B}^\sigma(\kappa)\mathbf{h}^\sigma(\kappa)\right]_{\eta'\eta}$$
$$+\sum_{\sigma'\kappa'}\left[\nu\mathbf{h}^\sigma(\kappa)\mathbf{x}_+^{\sigma\sigma'}(\kappa,\kappa')\mathbf{h}^{\sigma'}(\kappa')\mathrm{v}_{-\eta^{\sigma'}}(\kappa')\right]_{\eta'\eta^{\bar\sigma'}}\Big\}\,,\tag{171}$$

where, according to Eqs. (122) and (123), we split the crossing block $\mathbf{X}^{\sigma'\sigma}$ as

$$\mathbf{X}^{\sigma\sigma'}(\kappa\kappa')=\mathrm{v}(\kappa)\mathbf{x}^{\sigma\sigma'}(\kappa\kappa')-\mathrm{v}_+(\kappa)\mathbf{x}_+^{\sigma\sigma'}(\kappa\kappa')\,.\tag{172}$$

Now, from inspection of Eq. (170) we find that $\mathbf{x}_+^{\sigma\sigma}=0$ due to the sum over ν (and in analogy to the RLM case) because nothing else depends on ν. We are then left with

$$\Omega_{\eta'\eta}^{\sigma,\mathrm{CT}}(\kappa)=\eta'\eta\delta_{\nu',+1}\Big[\mathrm{h}_{\eta\eta}^\sigma(\kappa)\delta_{\eta'\eta}$$
$$+\mathrm{h}_{\eta'\eta'}^\sigma(\kappa)\mathrm{B}_{\eta'\eta}^\sigma(\kappa)\mathrm{h}_{\eta\eta}^\sigma(\kappa)$$
$$+\nu\sum_{\kappa'}\mathrm{h}_{\eta'\eta'}^\sigma(\kappa)\mathrm{x}_{+,\eta'\nu}^{\sigma\bar\sigma}(\kappa,\kappa')\mathrm{h}_{\nu\nu}^{\bar\sigma}(\kappa')\mathrm{v}_{-\eta}(\kappa')\Big]\,,\tag{173}$$

where

$$\mathbf{x}_{+,\eta'\nu}^{\sigma\bar\sigma}(\kappa,\kappa')=\frac{i\hbar\,\eta'}{\zeta(\epsilon_k-E_\sigma)+\zeta'(\epsilon_{k'}-E_{\bar\sigma})+i0^+}\,.\tag{174}$$

Using the above result and Eq. (166) we can cast $\Omega_{\mathrm{CT}}^\sigma$ in the form

$$\Omega_{\eta'\eta}^{\sigma,\mathrm{CT}}(\kappa)=\eta'\eta\delta_{\nu',+1}\bigg\{\mathrm{h}_{\eta\eta}^\sigma(\kappa)\delta_{\eta'\eta}+\mathrm{h}_{\eta'\eta'}^\sigma(\kappa)\mathrm{B}_{\eta'\eta}^{\sigma(\sigma)}(\kappa)\mathrm{h}_{\eta\eta}^\sigma(\kappa)$$
$$+i\hbar\sum_{\kappa'}\frac{\mathrm{h}_{\eta'\eta'}^\sigma(\kappa)[\mathrm{h}_{\eta\eta}^\sigma(\kappa)+\nu\eta'\mathrm{h}_{\nu\nu}^{\bar\sigma}(\kappa')]\mathrm{v}_{-\eta}(\kappa')}{\zeta(\epsilon_k-E_\sigma)+\zeta'(\epsilon_{k'}-E_{\bar\sigma})+i0^+}\bigg\}\,.\tag{175}$$

As a result, the Green's function is the sum of the ST contribution, given by the first term in Eq. (175), plus the terms of fourth order in the tunneling amplitude (second order in Γ) and reads

$$\mathcal{G}_{\sigma\sigma,\mathrm{CT}}^{(\zeta)}(\epsilon_k)=-\frac{i\zeta}{\hbar}\sum_{\eta'\eta}\Omega_{\eta'\eta,\mathrm{CT}}^\sigma(\zeta,k)\mathrm{P}_{\boldsymbol\eta}^\infty$$
$$=\mathcal{G}_{\sigma\sigma,\mathrm{ST}}^{(\zeta)}(\epsilon_k)+\mathcal{G}_{\sigma\sigma,4\mathrm{th}}^{(\zeta)}(\epsilon_k)\,.\tag{176}$$

For a comprehensive diagrammatic analysis of cotunneling effects we refer to [34]. In the recent article [86], interference phenomena at the cotunneling level, where one needs to go beyond the assumption of state-conserving tunneling, are discussed for interacting double quantum dots. In this work, we rather focus on nonperturbative schemes.

C. Nonperturbative, second-tier schemes

1. Resonant tunneling approximation (RTA)

Iterating the insertion of the cotunneling blocks $\mathbf{B}$ and $\mathbf{X}$ in the bare propagator $\mathbf{h}$, one obtains the nonperturbative RTA. The Dyson equation for the irreducible propagator $\phi_{\mathrm{RTA}}=[\mathbf{h}^{-1}-\mathbf{B}-\mathbf{X}]^{-1}$, Eq. (106), can be given in terms of the gDSO propagator $\phi_{\mathrm{gDSO}}=[\mathbf{h}^{-1}-\mathbf{B}]^{-1}$ (see the next section), as follows

$$\phi_{\mathrm{RTA}}=\phi_{\mathrm{gDSO}}+\phi_{\mathrm{gDSO}}\mathbf{X}\phi_{\mathrm{RTA}}\,.\tag{177}$$

Component-wise in κ, with the 2×2 matrix structure induced by the sojourn indexes $\eta^\uparrow,\eta^\downarrow$ left implicit, this

equation reads

$$\phi_{\mathrm{RTA}}^{\sigma'\sigma}(\boldsymbol{\kappa}',\boldsymbol{\kappa}) = \boldsymbol{\varphi}_{\mathrm{gDSO}}^{\sigma'\sigma'}(\boldsymbol{\kappa}')\delta_{\boldsymbol{\kappa}'\boldsymbol{\kappa}}\delta_{\sigma'\sigma}$$
$$+ \boldsymbol{\varphi}_{\mathrm{gDSO}}^{\sigma'\sigma'}(\boldsymbol{\kappa}') \cdot \sum_{\sigma''\boldsymbol{\kappa}''} \mathbf{X}^{\sigma'\sigma''}(\boldsymbol{\kappa}',\boldsymbol{\kappa}'') \cdot \phi_{\mathrm{RTA}}^{\sigma''\sigma}(\boldsymbol{\kappa}'',\boldsymbol{\kappa}) \, .$$
$$(178)$$

The RTA is equivalent to the second order von Neumann approach [45] and in the noninteracting case reproduces the current for the SIAM, but not the full density matrix, contrary to the case of the RLM which is fully described by the RTA. Indeed, as discussed in Sec. IV D, for $U = 0$ the contributing diagrams have at most four overlapping fermion lines, of which at most two with the same spin.

In the infinite-U limit, the RTA admits an analytical solution to be found along the lines of [47, 90]. In this limit, the blocks specialize to (consider $\zeta = +1$)

$$[\mathbf{h}]_{\boldsymbol{\chi}'\boldsymbol{\chi}}^{\sigma'\sigma} = \mathrm{i}\hbar \frac{1}{\epsilon_k - \epsilon_\sigma + \mathrm{i}0^+}\delta_{\sigma'\sigma}\delta_{\boldsymbol{\chi}'\boldsymbol{\chi}}\delta_{\eta,-1} \, ,$$

$$[\mathbf{X}]_{\boldsymbol{\chi}'\boldsymbol{\chi}}^{\sigma\sigma} = \mathrm{i}\hbar \frac{\sum_\nu \mathrm{v}_\nu^{\alpha'}(k')}{\epsilon_k - \epsilon_{k'} + \mathrm{i}0^+}\delta_{\zeta',-\zeta} \, ,$$

$$[\mathbf{X}]_{\boldsymbol{\chi}'\boldsymbol{\chi}}^{\bar\sigma\sigma} = \mathrm{i}\hbar \frac{\mathrm{v}_+^{\alpha'}(k')}{\epsilon_k - \epsilon_{k'} + \mathrm{i}0^+}\delta_{\zeta',-\zeta} \, ,$$

$$[\mathbf{B}]_{\boldsymbol{\chi}'\boldsymbol{\chi}}^{\sigma'\sigma} = \mathrm{i}\hbar \sum_{\alpha''k''} \frac{\sum_\nu \mathrm{v}_\nu^{\alpha''}(k'') + \mathrm{v}_{-\eta}^{\alpha''}(k'')}{\epsilon_k - \epsilon_{k''} + \mathrm{i}0^+}\delta_{\sigma'\sigma}\delta_{\boldsymbol{\chi}'\boldsymbol{\chi}} \, .$$
$$(179)$$

The 2×2 matrix structure of Eq. (178) is lost because η can only assume the value -1, as induced by the interaction energy appearing at the denominator of h for $\eta = +1$, namely the dot can be occupied at most by one electron. As a result, we get the following two equations for the diagonal and off-diagonal elements in the spin index (we omit the labels RTA and gDSO)

$$\phi^{\sigma\sigma}(\epsilon,\epsilon') = \varphi^{\sigma\sigma}(\epsilon)\delta(\epsilon-\epsilon')$$
$$+ \varphi^{\sigma\sigma}(\epsilon)\int d\epsilon'' \mathrm{X}^{\sigma\sigma}(\epsilon,\epsilon'')\phi^{\sigma\sigma}(\epsilon'',\epsilon)$$
$$+ \varphi^{\sigma\sigma}(\epsilon)\int d\epsilon'' \mathrm{X}^{\sigma\bar\sigma}(\epsilon,\epsilon'')\phi^{\bar\sigma\sigma}(\epsilon'',\epsilon') \, ,$$
$$\phi^{\bar\sigma\sigma}(\epsilon,\epsilon') = \varphi^{\bar\sigma\bar\sigma}(\epsilon)\int d\epsilon'' \mathrm{X}^{\bar\sigma\sigma}(\epsilon,\epsilon'')\phi^{\sigma\sigma}(\epsilon'',\epsilon)$$
$$+ \varphi^{\bar\sigma\bar\sigma}(\epsilon)\int d\epsilon'' \mathrm{X}^{\bar\sigma\bar\sigma}(\epsilon,\epsilon'')\phi^{\bar\sigma\sigma}(\epsilon'',\epsilon) \, ,$$
$$(180)$$

where $\mathrm{X}^{\bar\sigma\bar\sigma} = \mathrm{X}^{\sigma\sigma}$ and $\mathrm{X}^{\bar\sigma\sigma} = \mathrm{X}^{\sigma\bar\sigma}$, see Eq. (179). Consider now the degenerate system, $\epsilon_\uparrow = \epsilon_\downarrow = \epsilon_0$. In this case $\varphi^{\sigma\sigma} = \varphi^{\bar\sigma\bar\sigma} = \varphi^\sigma$ and, by summing the above two equations, we obtain

$$\phi^\sigma(\epsilon,\epsilon') = \varphi^\sigma(\epsilon)\delta(\epsilon-\epsilon') + \varphi^\sigma(\epsilon)\int d\epsilon'' \mathrm{X}(\epsilon,\epsilon'')\phi^\sigma(\epsilon'',\epsilon) \, ,$$
$$(181)$$

where

$$\phi^\sigma(\epsilon,\epsilon') = \sum_{\sigma'}\phi^{\sigma'\sigma}(\epsilon,\epsilon') \, ,$$
$$\mathrm{X}(\epsilon,\epsilon') = \mathrm{X}^{\sigma\sigma}(\epsilon,\epsilon') + \mathrm{X}^{\bar\sigma\sigma}(\epsilon,\epsilon')$$
$$= \mathrm{i}\hbar \sum_\alpha \frac{2\mathrm{v}_+^\alpha(\epsilon) + \mathrm{v}_-^\alpha(\epsilon)}{\epsilon - \epsilon' + \mathrm{i}0^+} \, ,$$
$$(182)$$

see Eq. (179). Solving Eq. (181), it is found that the real part of ϕ, the one which enters the current, as in Eqs. (116) and (117), reads

$$\mathrm{Re}\int d\epsilon'\phi^\sigma(\epsilon,\epsilon')\mathrm{v}_{-\eta}(\epsilon') = C_\eta \sum_\alpha [2\mathrm{v}_+^\alpha(\epsilon) + \mathrm{v}_-^\alpha(\epsilon)]|\varphi(\epsilon)|^2 \, ,$$
$$(183)$$

where C_η is a constant depending on the initial vertex $\mathrm{v}_{-\eta}$. As shown in [49] the RTA and the DSO, see Sec. IX C 3, have, in this regime of large interaction U, a qualitatively similar behavior of the linear conductance, though the RTA predicts higher peak-conductance. Moreover, the two schemes share the same prediction for the zero-bias anomaly temperature scale, which is given in Eq. (196) below.

2. Generalized dressed second-order approximation

In the gDSO, the propagator ϕ_{gDSO} is given by the Dyson equation (107). As a result, the bare ST propagator is dressed by the bubble diagrams $\mathbf{B}$, namely

$$\phi_{\mathrm{gDSO}} = \left[\mathbf{h}^{-1} - \mathbf{B}\right]^{-1} \, .$$
$$(184)$$

While being diagonal in σ and $\boldsymbol{\kappa}$, the bubble blocks $\mathbf{B}$ have a nontrivial 2×2 matrix structure in terms of the sojourn index η, see Eq. (169), a feature which accounts for charge transfer by processes internal to the main fermion line. As a result, they induce a 2×2 structure to the contracted (matrix) function $\boldsymbol{\varphi}_{\mathrm{gDSO}}^{\sigma\sigma}(\boldsymbol{\kappa})$, defined by $\phi_{\mathrm{gDSO}}^{\sigma'\sigma}(\boldsymbol{\kappa}',\boldsymbol{\kappa}) = \boldsymbol{\varphi}_{\mathrm{gDSO}}^{\sigma\sigma}(\boldsymbol{\kappa})\delta_{\boldsymbol{\kappa}'\boldsymbol{\kappa}}\delta_{\sigma'\sigma}$.

Neglecting the crossings in the main fermion lines results in the Green's function, see Eqs. (151) and (152),

$$\mathcal{G}_{\sigma\sigma}^{(\zeta)}(\epsilon_k) = -\frac{\mathrm{i}\zeta}{\hbar}\sum_{\eta'\eta}\eta'\eta\boldsymbol{\varphi}_{\mathrm{gDSO},\eta'\eta}^{\sigma\sigma}(\zeta,k)\mathrm{p}_\eta^{\bar\sigma}$$
$$= -\frac{\mathrm{i}\zeta}{\hbar}\sum_\eta \left[\boldsymbol{\varphi}_{\mathrm{gDSO},\eta\eta}^{\sigma\sigma}(\zeta,k) - \boldsymbol{\varphi}_{\mathrm{gDSO},\bar\eta\eta}^{\sigma\sigma}(\zeta,k)\right]\mathrm{p}_\eta^{\bar\sigma} \, .$$
$$(185)$$

The matrix elements of $\boldsymbol{\varphi}_\mathbf{B}$, from Eq. (184), read

$$\boldsymbol{\varphi}_{\mathrm{gDSO},\eta\eta}^{\sigma\sigma} = \frac{(\mathrm{h}_{\bar\eta\bar\eta}^\sigma)^{-1} - \mathrm{B}_{\bar\eta\bar\eta}^\sigma}{[(\mathrm{h}_{\eta\eta}^\sigma)^{-1} - \mathrm{B}_{\eta\eta}^\sigma][(\mathrm{h}_{\bar\eta\bar\eta}^\sigma)^{-1} - \mathrm{B}_{\bar\eta\bar\eta}^\sigma] - \mathrm{B}_{\eta\bar\eta}^\sigma\mathrm{B}_{\bar\eta\eta}^\sigma} \, ,$$
$$\boldsymbol{\varphi}_{\mathrm{gDSO},\bar\eta\eta}^{\sigma\sigma} = \frac{\mathrm{B}_{\bar\eta\eta}^\sigma}{[(\mathrm{h}_{\eta\eta}^\sigma)^{-1} - \mathrm{B}_{\eta\eta}^\sigma][(\mathrm{h}_{\bar\eta\bar\eta}^\sigma)^{-1} - \mathrm{B}_{\bar\eta\bar\eta}^\sigma] - \mathrm{B}_{\eta\bar\eta}^\sigma\mathrm{B}_{\bar\eta\eta}^\sigma} \, ,$$
$$(186)$$

where $h^\sigma_{\eta'\eta}$ is defined in Eq. (157) and where the dependence on $\boldsymbol{\kappa}$ of the block functions is understood. Note that the denominators are independent of η. Plugging these results in Eq. (185), with p^σ_η given by Eq. (155), the dot Green's function reads

$$
\mathcal{G}^{(\zeta)}_{\sigma\sigma} = \frac{1 - \langle \hat{n}_{\bar{\sigma}} \rangle}{\epsilon - \epsilon_\sigma - \mathrm{i}\zeta\hbar B^\sigma_{--} + \mathrm{i}\zeta\hbar B^\sigma_{+-} \frac{\epsilon - \epsilon_\sigma - \mathrm{i}\zeta\hbar[B^\sigma_{-+} + B^\sigma_{-+}]}{\epsilon - \epsilon_\sigma - U - \mathrm{i}\zeta\hbar[B^\sigma_{++} + B^\sigma_{+-}]}}
$$
$$
+ \frac{\langle \hat{n}_{\bar{\sigma}} \rangle}{\epsilon - \epsilon_\sigma - U - \mathrm{i}\zeta\hbar B^\sigma_{++} + \mathrm{i}\zeta\hbar B^\sigma_{-+} \frac{\epsilon - \epsilon_\sigma - U - \mathrm{i}\zeta\hbar[B^\sigma_{++} + B^\sigma_{+-}]}{\epsilon - \epsilon_\sigma - \mathrm{i}\zeta\hbar[B^\sigma_{--} + B^\sigma_{-+}]}} \, .
$$

$$(187)$$

In the WBL, we can simplify this expression by using the result in Eq. (169) and the property

$$
\sum_\eta B^\sigma_{\bar{\eta}\eta} = -\Gamma/\hbar \, , \tag{188}
$$

which can be checked by inspection of Eq. (168). The retarded ($\zeta = +1$) Green's function in the gDSO reads

$$
\mathcal{G}^r_{\sigma\sigma}(\epsilon) = \frac{1 - \langle \hat{n}_{\bar{\sigma}} \rangle}{\epsilon - \epsilon_\sigma + \mathrm{i}\Gamma/2 + \Sigma_{\sigma-}(\epsilon)\frac{U}{\epsilon - \epsilon_\sigma - U + \mathrm{i}3\Gamma/2}}
$$
$$
+ \frac{\langle \hat{n}_{\bar{\sigma}} \rangle}{\epsilon - \epsilon_\sigma - U + \mathrm{i}\Gamma/2 - \Sigma_{\sigma+}(\epsilon)\frac{U}{\epsilon - \epsilon_\sigma + \mathrm{i}3\Gamma/2}} \, , \tag{189}
$$

where we have identified the retarded self-energies with the off-diagonal matrix elements of the bubbles via

$$
\Sigma_{\sigma\eta}(\epsilon) := \mathrm{i}\hbar B^\sigma_{\bar{\eta}\eta}(\kappa)|_{\zeta=+1}
$$
$$
= -\sum_{\alpha_1} \frac{\Gamma_{\alpha_1}}{2\pi} \sum_{\zeta_1} \left[\eta\zeta_1 \mathrm{Re}\psi \left(\frac{1}{2} + \mathrm{i}\frac{\mathcal{E}_{\zeta_1} - \mu_{\alpha_1}}{2\pi k_B T} \right) + \mathrm{i}\pi f^{\alpha_1}_{-\eta}(\mathcal{E}_{\zeta_1}) \right] \, ,
$$

$$(190)$$

with $\mathcal{E}_{\zeta_1} := E_{\bar{\sigma}} + \zeta_1(E_\sigma - \epsilon)$ and $E_\sigma = \epsilon_\sigma + U/2$. Note that, by virtue of the property (188), which implies

$$
\Sigma_{\sigma\eta}(\epsilon) = -\Sigma_{\sigma\bar{\eta}}(\epsilon) - \mathrm{i}\Gamma \, , \tag{191}
$$

we can express the retarded Green's function in terms of a single self energy, e.g. $\Sigma_{\sigma-}(\epsilon)$. Interestingly, the result in Eq. (189) is equivalent to the one obtained by Meir, Wingreen, and Lee in [39] with the equations of motion technique.

We now summarize the properties and predictions of the gDSO. For vanishing interaction, $U = 0$, we recover the correct WBL result for the noninteracting case

$$
\mathcal{G}^r_{\sigma\sigma}(\epsilon) = \frac{1}{\epsilon - \epsilon_\sigma + \mathrm{i}\Gamma/2} \, . \tag{192}
$$

As anticipated below Eq. (146), the zero-temperature conductance in the noninteracting limit

$$
G = G_0 \frac{\Gamma_L \Gamma_R}{(\mu - \epsilon_0)^2 + \Gamma^2/4} \tag{193}
$$

saturates, at resonance and for $\Gamma_\alpha = \Gamma/2$, to the conductance quantum G_0 due to the sum over the spin degree of freedom. This can be seen by applying the general formula, Eq. (130), to the SIAM with the retarded Green's function given by Eq. (192).

For finite interaction, on the other hand, the gDSO displays a zero-bias anomaly at a characteristic temperature $T^* = T_{\mathrm{gDSO}}$. This temperature is defined as the one at which the real parts of the denominators vanish, causing a peak in the density of states $-\mathrm{Im}[\mathcal{G}^r_{\sigma\sigma}(\mu)]/\pi$. By virtue of the property (191) satisfied by the self-energies, this condition is the same for the two terms in Eq. (189) and reads

$$
(\mu - \epsilon_0)(\mu - \epsilon_0 - U) - 3\Gamma^2/4 + U \, \mathrm{Re}[\Sigma_{\sigma-}(\mu)|_{T^*}] = 0 \, . \tag{194}
$$

For sufficiently large interaction energy U, we can approximate the real part of the self-energy in Eq. (190) as

$$
\mathrm{Re}\Sigma_{\sigma-}(\mu)|_{T^*} \simeq \frac{\Gamma}{2\pi} \ln \left(\frac{U}{2\pi k_B T^*} \right) \, . \tag{195}
$$

Then, assuming $U \gg \Gamma$, solving Eq. (194) for $T^* = T_{\mathrm{gDSO}}$, we find

$$
k_B T_{\mathrm{gDSO}} \simeq \frac{U}{2\pi} e^{2\pi(\mu - \epsilon_0)(\mu - \epsilon_0 - U)/U\Gamma} \, . \tag{196}
$$

Notice that this result differs from the Kondo temperature T_K, which has the prefactor π in place of 2π at the exponent [5, 6].

Another problem of this approximation scheme is the temperature-independent behavior at the particle-hole symmetry point (sp) $\mu - \epsilon_0 = U/2$ at equilibrium in the degenerate case [40]. Indeed, since $\mathcal{E}_\pm = \mp(\epsilon - \mu)$, we have $f_+(\mathcal{E}_+) = f_-(\mathcal{E}_-)$. Also $\mathrm{Re}\psi(x + \mathrm{i}y) = \mathrm{Re}\psi(x - \mathrm{i}y)$. Thus, from Eq. (190) we find that the self-energy is purely imaginary and temperature-independent

$$
\Sigma^{\mathrm{sp}}_{\sigma\eta}(\epsilon) = -\mathrm{i}\Gamma/2 \, . \tag{197}
$$

Consequently, the retarded Green's function becomes

$$
\mathcal{G}^{r,\mathrm{sp}}_{\sigma\sigma}(\epsilon) = \frac{1 - \langle \hat{n}_{\bar{\sigma}} \rangle}{\epsilon + U/2 + \mathrm{i}\Gamma/2 - \mathrm{i}(\Gamma/2)\frac{U}{\epsilon - U/2 + \mathrm{i}3\Gamma/2}}
$$
$$
+ \frac{\langle \hat{n}_{\bar{\sigma}} \rangle}{\epsilon - U/2 + \mathrm{i}\Gamma/2 + \mathrm{i}(\Gamma/2)\frac{U}{\epsilon + U/2 + \mathrm{i}3\Gamma/2}} \, . \tag{198}
$$

This feature causes the onset of an artifact in the linear conductance G when the temperature decreases below Γ: A pinning at a temperature-independent value of G at the symmetry point. Note that inclusion of the crossings does not lift this problem: This can be seen from Fig. 3 of Ref. [44] where a scheme equivalent to the RTA, which includes the crossings, is used.

The linear conductance from the gDSO is shown in Fig. 20, for the degenerate case, as a function of the gate voltage $\epsilon_0 - \mu$ for various temperatures. At high temperatures, $k_B T > \Gamma$, there are two temperature-broadened peaks separated by the energy U, in agreement with the
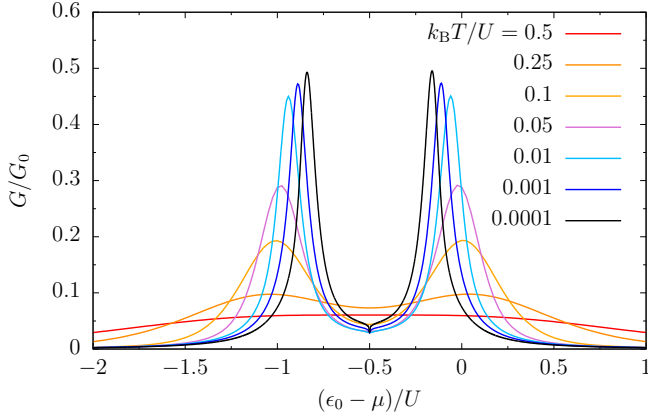
FIG. 20. Linear conductance within the gDSO, in units of the conductance quantum $G_0 = 2e^2/h$, vs the gate voltage $\epsilon_0 - \mu$ in the degenerate case $\epsilon_\sigma = \epsilon_0$. The peaks shrink and move towards the center as temperature is decreased. The curves at the lowest temperatures display an unphysical pinning at the particle-hole symmetry point. The tunnel coupling is $\Gamma = 0.1\,U$ with $\Gamma_L = \Gamma_R = \Gamma/2$.

ST result shown in Fig. 19. Upon decreasing T, the peaks get narrower and closer, witnessing the transition to Γ-broadened conductance peaks, where the dot energies are renormalized by the tunnel coupling to the leads. This is captured by the nonperturbative character of the gDSO. As anticipated above, at low temperatures, $k_BT \ll \Gamma$, the pinning of G at a temperature-independent value appears at the particle-hole symmetry point $\epsilon_0 - \mu = -U/2$. The onset of this artifact signals the breakdown of the approximation scheme. As shown in Sec. IX E, introducing higher-tier processes which dress the gDSO bubble diagrams, this problem is lifted as the dependence of the self-energies on the temperature is restored.

3. Charge fluctuations only: Dressed second order

The DSO is the simplest, nontrivial approximation scheme nonperturbative in Γ, being the dressed version of the sequential tunneling, see Eq. (104), where the main fermion line is dressed by charge fluctuations [49, 91, 92]. The diagrams retained are formally similar to the ones of the gDSO, namely they consist in dressing the main fermion lines with bare bubble diagrams. The difference is that the DSO only accounts for charge fluctuations of the main fermion line, meaning that the sojourns states before and after a bubble are the same, $\eta = \eta_1 = \cdots = \eta'$. As a consequence, the charge in the dot does not vary by more than one unit between the two ends of the main fermion line, net charge transfers being operated solely by the latter. In this scheme, the kernel connects the same states as those connected by the sequential tunneling, the states that differ by no more than one electron in occupancy. Note that the same is not true for the
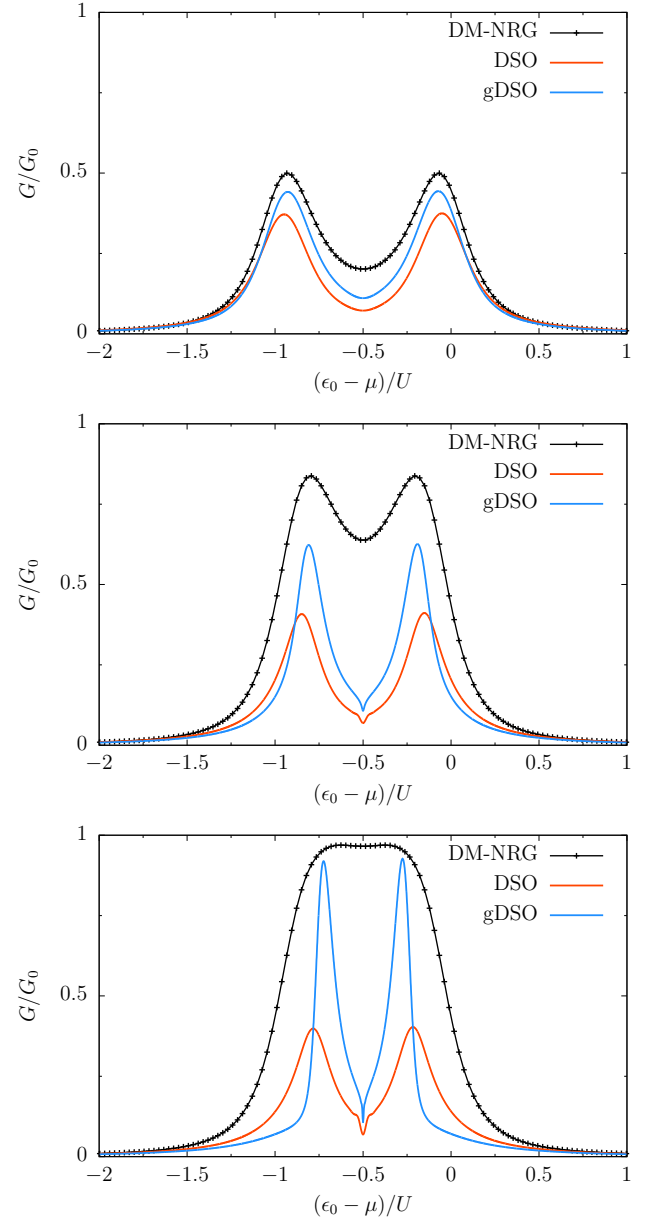
FIG. 21. Linear conductance within the gDSO and the DSO schemes compared with the curves from the numerically-exact DM-NRG. We consider the degenerate case $\epsilon_\sigma = \epsilon_0$ for three different temperatures: $k_BT = 0.04\,U$ (upper panel), $k_BT = 0.003\,U$ (central panel), and $k_BT = 0.0004\,U$ (lower panel). The tunnel coupling is $\Gamma = 0.2\,U$ with $\Gamma_L = \Gamma_R = \Gamma/2$. The parameters are chosen to allow a direct comparison with the results of [35].

gDSO, which includes also processes that vary the dot charge also within the main line (pair tunneling). The fact that the internal processes leave the intermediate sojourns unchanged means that the bubbles in the Dyson equation (205) for the function $\varphi^{\sigma\sigma}$ have a diagonal struc-

ture yielding the solution

$$\varphi^{\sigma\sigma}_{\eta'\eta,\mathrm{DSO}}(\kappa) = \frac{1}{(\mathrm{h}^{\sigma}_{\eta\eta})^{-1} - \mathrm{B}^{\sigma}_{\eta\eta}} \delta_{\eta'\eta} \ . \tag{199}$$

Thus, according to Eq. (185), the retarded DSO Green's function assumes, in the WBL, the form

$$\mathcal{G}^{r}_{\sigma\sigma}(\epsilon) = \frac{1 - \langle \hat{n}_{\bar{\sigma}} \rangle}{\epsilon - \epsilon_{\sigma} + \mathrm{i}\Gamma/2 - \Sigma_{\sigma-}(\epsilon)}$$
$$+ \frac{\langle \hat{n}_{\bar{\sigma}} \rangle}{\epsilon - \epsilon_{\sigma} - U + \mathrm{i}\Gamma/2 - \Sigma_{\sigma+}(\epsilon)} \ , \tag{200}$$

with $\Sigma_{\sigma\eta}(\epsilon)$ given by Eq. (190). Note that, contrary to the gDSO, the correct result in the noninteracting limit is *not* recovered within the DSO. However, in the limit $U \to \infty$, the DSO reproduces the gDSO result in the same limit, namely one obtains

$$\lim_{U \to \infty} \mathcal{G}^{r}_{\sigma\sigma}(\epsilon) = \frac{1 - \langle \hat{n}_{\bar{\sigma}} \rangle}{\epsilon - \epsilon_{\sigma} + \mathrm{i}\Gamma/2 - \Sigma_{\sigma-}(\epsilon)} \ . \tag{201}$$

The corresponding prediction for the Kondo-like temperature T_{DSO} is in this limit

$$k_B T_{\mathrm{DSO}} \simeq \frac{U}{2\pi} e^{-2\pi(\mu - \epsilon_0)/\Gamma} \ , \tag{202}$$

and is the same as for the gDSO, and RTA, with the wrong prefactor in the exponent. Nevertheless, the DSO is the simplest scheme, namely the one with the minimal collection of diagrams, which captures the emergence of a zero-bias anomaly at low temperatures, $k_{\mathrm{B}}T \leq \Gamma$. A comparison between the linear conductance calculated within the gDSO and the one from the DSO is shown in Fig. 21, for $k_{\mathrm{B}}T/\Gamma = 0.2$, where the linear conductance follows qualitatively the DM-NRG result, down to $k_{\mathrm{B}}T/\Gamma = 0.002$, where both schemes break down. The parameters are chosen so as to allow for a direct comparison with Fig. 6 of Ref. [35], where the scheme EOM2 (equation of motion method) behaves similarly to the gDSO.

4. Γ-broadening of the ST

Dressing the main fermion line exclusively with the temperature-independent bubble, namely the first term of Eq. (166), amounts to neglecting in the DSO retarded Green's function the temperature-dependent self-energies $\Sigma_{\sigma\pm}(\epsilon)$, see Eq. (200). The only internal process retained here corresponds to the temperature-independent diagrammatic contributions in Ref. [52]. The resulting Green's function is that of a Γ-broadened version of the ST approximation, where the single-particle energies acquire a broadening Γ due to the coupling to the leads and reads

$$G^{r}_{\sigma\sigma}(\epsilon_k) = \sum_{\eta} \frac{\mathrm{p}^{\bar{\sigma}}_{\eta}}{\epsilon_k - E_{\sigma}(\eta) + \mathrm{i}\Gamma/2} \ . \tag{203}$$
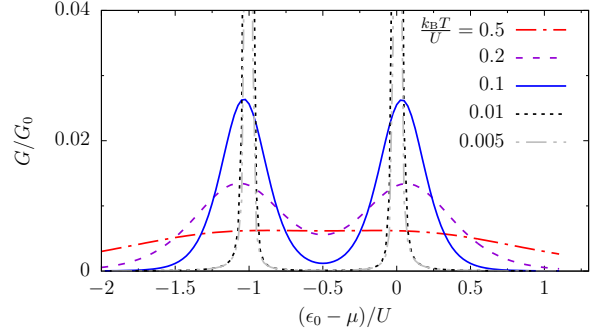
FIG. 22. Linear conductance within the Γ-broadened ST, Eq. (203) *vs* the gate voltage $\epsilon_0 - \mu$ in the degenerate case $\epsilon_{\sigma} = \epsilon_0$. Lowering the temperature, the peaks shrink until $k_{\mathrm{B}}T \simeq \Gamma$ but they do not move towards the center. Their height grows as T^{-1}. The tunnel coupling is $\Gamma = 0.01\,U$ with $\Gamma_L = \Gamma_R = \Gamma/2$.

This scheme is the same as the EOM0 reviewed in [35], which is derived with the EOM method. With this result for the Green's function, the general formula Eq. (129), gives for the current in the ST approximation

$$I^{\infty} = \frac{e}{h} \Gamma_L \Gamma_R \sum_{\sigma} \int d\epsilon\, [f^{L}_{+}(\epsilon) - f^{R}_{+}(\epsilon)]$$
$$\left[\frac{1 - \langle \hat{n}_{\bar{\sigma}} \rangle}{(\epsilon - \epsilon_{\sigma})^2 + \Gamma^2/4} + \frac{\langle \hat{n}_{\bar{\sigma}} \rangle}{(\epsilon - \epsilon_{\sigma} - U)^2 + \Gamma^2/4} \right]$$
$$= \frac{e}{h} \frac{\Gamma_L \Gamma_R}{\Gamma} \sum_{\sigma} \left[(1 - \langle \hat{n}_{\bar{\sigma}} \rangle) r(\epsilon_{\sigma}) + \langle \hat{n}_{\bar{\sigma}} \rangle r(\epsilon_{\sigma} + U) \right] , \tag{204}$$

where $r(x)$ is defined in Eq. (145).

In Fig. 22, we show the linear conductance G, obtained by plugging the retarded Green's function ($\zeta = +1$) of Eq. (203) into the general expression (130). The linear conductance is plotted, in the degenerate case, where $\epsilon_{\uparrow} = \epsilon_{\downarrow} = \epsilon_0$, against the gate voltage. Decreasing the temperature, G is suppressed around the particle-hole symmetry point $\epsilon_0 - \mu = -U/2$, the central region between the two peaks separated by the energy U, the separation being independent of the temperature, contrary to the gDSO, cf. Fig. 20.

D. An ∞-tier scheme for the SIAM

From the considerations above, the second-tier approximations well describe the behavior of the SIAM above temperatures of the order $k_{\mathrm{B}}T \sim \Gamma$. Also they capture the onset of a zero-bias anomaly at low temperature. However, artifacts occur when the temperature is lowered even further. As shown in the next sections, the problems with the Kondo temperature T_{K} and the pinning at the particle-hole symmetry point are mitigated by deepening the hierarchy of internal process including third- and fourth-tier bubble diagrams.

Let us go to the exact formal expression for ϕ, Eq. (102), and assume that the main fermion line does not undergo crossings, which yields a diagonal irreducible propagator in σ and κ. Within this assumption, the equation for ϕ becomes

$$\phi \equiv \phi_{\mathrm{B}} = [\mathbf{h}^{-1} - \tilde{\mathbf{B}}]^{-1} , \qquad (205)$$

see Eq. (108). The propagator is dressed by internal processes according to the hierarchy of Eq. (101) with $\langle \tilde{\mathbf{S}}_2 \mathbf{v} \rangle \rightarrow \tilde{\mathbf{B}}_2 \equiv \tilde{\mathbf{B}}$, where the block $[\tilde{\mathbf{B}}]^{\sigma'\sigma}_{\boldsymbol{\chi}'\boldsymbol{\chi}} = \tilde{\mathrm{B}}^{\sigma}_{\eta'\eta}(\kappa)\delta_{\sigma'\sigma}\delta_{\kappa'\kappa}$ is given by the contraction of a free propagator dressed by all possible (irreducible) processes, including crossings. The diagrammatic of this dressing is in fact the same as the exact irreducible propagator ϕ itself, see Fig. 14.

As the bare bubbles of the gDSO, the dressed bubbles are diagonal in all indexes except for η, inducing a 2×2 structure to the contracted (matrix) function $\boldsymbol{\varphi}_{\mathrm{B}}(\kappa)$. Along similar lines as in the gDSO, the matrix elements of $\boldsymbol{\varphi}_{\mathrm{B}}$ read

$$\varphi^{\sigma\sigma}_{\mathrm{B},\eta\eta} = \frac{(\mathrm{h}^{\sigma}_{\bar{\eta}\bar{\eta}})^{-1} - \tilde{\mathrm{B}}^{\sigma}_{\bar{\eta}\bar{\eta}}}{[(\mathrm{h}^{\sigma}_{\eta\eta})^{-1} - \tilde{\mathrm{B}}^{\sigma}_{\eta\eta}][(\mathrm{h}^{\sigma}_{\bar{\eta}\bar{\eta}})^{-1} - \tilde{\mathrm{B}}^{\sigma}_{\bar{\eta}\bar{\eta}}] - \tilde{\mathrm{B}}^{\sigma}_{\eta\bar{\eta}}\tilde{\mathrm{B}}^{\sigma}_{\bar{\eta}\eta}}$$

$$\varphi^{\sigma\sigma}_{\mathrm{B},\bar{\eta}\eta} = \frac{\tilde{\mathrm{B}}^{\sigma}_{\bar{\eta}\eta}}{[(\mathrm{h}^{\sigma}_{\eta\eta})^{-1} - \tilde{\mathrm{B}}^{\sigma}_{\eta\eta}][(\mathrm{h}^{\sigma}_{\bar{\eta}\bar{\eta}})^{-1} - \tilde{\mathrm{B}}^{\sigma}_{\bar{\eta}\bar{\eta}}] - \tilde{\mathrm{B}}^{\sigma}_{\eta\bar{\eta}}\tilde{\mathrm{B}}^{\sigma}_{\bar{\eta}\eta}} , \qquad (206)$$

where the bare block B has been replaced by the dressed one $\tilde{\mathrm{B}}$. Similar to Eq. (185), the dot Green's function in the ∞-tier scheme reads

$$\mathcal{G}^{(\zeta)}_{\sigma\sigma} = \frac{1 - \langle \hat{n}_{\bar{\sigma}} \rangle}{\epsilon - \epsilon_{\sigma} - \mathrm{i}\zeta\hbar\tilde{\mathrm{B}}^{\sigma}_{--} + \mathrm{i}\zeta\hbar\tilde{\mathrm{B}}^{\sigma}_{+-}\frac{\epsilon - \epsilon_{\sigma} - \mathrm{i}\zeta\hbar[\tilde{\mathrm{B}}^{\sigma}_{--}+\tilde{\mathrm{B}}^{\sigma}_{-+}]}{\epsilon - \epsilon_{\sigma} - U - \mathrm{i}\zeta\hbar[\tilde{\mathrm{B}}^{\sigma}_{++}+\tilde{\mathrm{B}}^{\sigma}_{+-}]}}$$

$$+ \frac{\langle \hat{n}_{\bar{\sigma}} \rangle}{\epsilon - \epsilon_{\sigma} - U - \mathrm{i}\zeta\hbar\tilde{\mathrm{B}}^{\sigma}_{++} + \mathrm{i}\zeta\hbar\tilde{\mathrm{B}}^{\sigma}_{-+}\frac{\epsilon - \epsilon_{\sigma} - U - \mathrm{i}\zeta\hbar[\tilde{\mathrm{B}}^{\sigma}_{++}+\tilde{\mathrm{B}}^{\sigma}_{+-}]}{\epsilon - \epsilon_{\sigma} - \mathrm{i}\zeta\hbar[\tilde{\mathrm{B}}^{\sigma}_{--}+\tilde{\mathrm{B}}^{\sigma}_{-+}]}} , \qquad (207)$$

As above, the dependence on κ is understood. Thus, neglecting the crossing of the main fermion line, we obtain a general structure for the retarded Green's function by a simple 2×2 (block) matrix inversion. The matrix elements of the dressed bubbles are schematized by

$$\tilde{\mathrm{B}}^{\sigma}_{\eta'\eta} = \quad + \quad . \qquad (208)$$

Here, the bare contribution (no internal processes) to the first bubble diagram is diagonal in $\eta'\eta$ and is also independent of the value of the sojourn η, as it does not include interactions. This bare bubble is the same as the one of the gDSO and, in the WBL, reads $\mathbf{B}^{(\sigma)} = -\mathbf{1}\Gamma/2\hbar$, see Eq. (166). In the presence of internal processes, the first dressed bubble in Eq. (208) depends in principle on the sojourn η'. This occurs when the latter has overlap with a blip of the σ path. However, in this case

the block vanishes because the overlap implies overlap of three fermion lines of the state σ, resulting in a factor ν that makes the whole diagram vanish upon summing over ν, as exemplified in the diagram (B) of Eq. (60). As a result, this block is independent of the value of the last sojourn η'. The same independence of η' holds for the second block, because the sojourn η', though involved with interactions, lies outside the block itself. On the contrary, the initial sojourn is relevant for both bubbles because it determines the vertex of the fermion line of spin $\bar{\sigma}$ according to the definition in Eq. (92). Summarizing, on the basis of the diagrammatic rules we conclude that the dressed bubble $\tilde{\mathbf{B}}$ possess the same property of the bare bubble, namely

$$\tilde{\mathbf{B}}_{\eta'\eta} = -\frac{\Gamma}{2\hbar}\mathbf{1}\delta_{\eta'\eta} + \tilde{\mathbf{B}}_{\bar{\eta}\eta} , \qquad (209)$$

where, again, boldface objects indicate diagonal matrices in the indexes σ and $\boldsymbol{\kappa}$. Exploiting the symmetry in Eq. (209), we can simplify the form of the Green's function in Eq (207). In particular, the retarded ($\zeta = +1$) Green's function in the WBL reads

$$\mathcal{G}^{r}_{\sigma\sigma}(\epsilon) = \frac{1 - \langle \hat{n}_{\bar{\sigma}} \rangle}{\epsilon - \epsilon_{\sigma} + \mathrm{i}\frac{\Gamma}{2} + \tilde{\Sigma}_{\sigma-}(\epsilon)\frac{U}{\epsilon - \epsilon_{\sigma} - U + \mathrm{i}\frac{\Gamma}{2} - \tilde{\Sigma}_{\sigma}(\epsilon)}}$$

$$+ \frac{\langle \hat{n}_{\bar{\sigma}} \rangle}{\epsilon - \epsilon_{\sigma} - U + \mathrm{i}\frac{\Gamma}{2} - \tilde{\Sigma}_{\sigma+}(\epsilon)\frac{U}{\epsilon - \epsilon_{\sigma} + \mathrm{i}\frac{\Gamma}{2} - \tilde{\Sigma}_{\sigma}(\epsilon)}} , \qquad (210)$$

where

$$\tilde{\Sigma}_{\sigma}(\epsilon) = \sum_{\eta} \tilde{\Sigma}_{\sigma\eta}(\epsilon) . \qquad (211)$$

Equation (210) is one of the main results of the present work. The problem of calculating the retarded Green's function, and thus the relevant physical properties for proportional coupling, reduces to that of determining the retarded, dressed self-energies $\tilde{\Sigma}_{\sigma\eta}$, here identified with the off-diagonal elements of the dressed bubbles via

$$\tilde{\Sigma}_{\sigma\eta}(\epsilon) := \mathrm{i}\hbar\tilde{\mathrm{B}}^{\sigma}_{\bar{\eta}\eta}(\kappa)|_{\zeta=+1} . \qquad (212)$$

The evaluation of these self-energies remains complicated due to the inner processes dressing the bubble $\tilde{\mathbf{B}}^{\sigma}$. We next introduce an approximation scheme where the internal crossings are neglected.

1. Neglecting the crossings

In the absence of crossings, the hierarchy in Eq. (101) simplifies to

$$\tilde{\mathbf{h}}_n := \sum_{k=0}^{\infty}\left(\mathbf{h}_n\langle\tilde{\mathbf{h}}_{n+1}\mathbf{v}\rangle\right)^k \mathbf{h}_n$$

$$= [\mathbf{h}_n^{-1} - \tilde{\mathbf{B}}_{n+1}]^{-1} , \qquad (213)$$

with $\mathbf{h}_n = \mathbf{1}h_n$ denoting the bare propagator with n overlapping fermion lines and $\tilde{\mathbf{h}}_n$ the corresponding propagator dressed by higher-tier bubbles $\tilde{\mathbf{B}}_n = \langle\tilde{\mathbf{h}}_n\mathbf{v}\rangle$. In particular $\tilde{\mathbf{B}}_2 = \langle\tilde{\mathbf{h}}_2\mathbf{v}\rangle \equiv \tilde{\mathbf{B}}$, where $\tilde{\mathbf{h}}_2 = [\mathbf{h}_2^{-1} - \tilde{\mathbf{B}}_3]^{-1}$. The dressed bubble $\tilde{\mathbf{B}}$ in Eq. (208) is then schematically described by the following sum of two contributions

$$\tilde{\mathrm{B}}_{\eta'\eta}^{\sigma} = \tilde{\mathrm{B}}_{\eta'\eta}^{\sigma(\sigma)} + \tilde{\mathrm{B}}_{\eta'\eta}^{\sigma(\bar{\sigma})}$$

$$\tag{214}$$

Here, the white rectangles indicate the dressing of the propagators $\mathbf{h}_2$ with two overlapping fermion lines by iteration of third-tier bubbles. Specifically, the dressed bubble of type $\sigma(\sigma)$ is given by the following contraction of a dressed propagator with 4×4 matrix structure in $\boldsymbol{\eta} = (\nu, \eta)$

$$\tilde{\mathrm{B}}_{\eta'\eta}^{\sigma(\sigma)} = \sum_\nu \langle \sum_{\nu'} [\tilde{\mathbf{h}}_2^{\sigma(\sigma)}]_{\eta'\eta} \mathrm{v}_\nu \rangle , \tag{215}$$

where $\tilde{\mathbf{h}}_2^{\sigma(\sigma)}$ is obtained by dressing the bare propagator $\mathbf{1}h_2^{\sigma(\bar{\sigma})}$, Eq. (163), with the third-tier bubble $\tilde{\mathbf{B}}_3^{\sigma(\sigma)}$, namely

$$\tilde{\mathbf{h}}_2^{\sigma(\sigma)} = \left[[\mathbf{1}h_2^{\sigma(\sigma)}]^{-1} - \tilde{\mathbf{B}}_3^{\sigma(\sigma)}\right]^{-1} . \tag{216}$$

The third-tier bubble $\tilde{\mathbf{B}}_3^{\sigma(\sigma)}$ is in turn given by the sum

$$\tag{217}$$

$$= \langle\tilde{\mathrm{h}}_{3,\nu'\nu}^{\sigma(\sigma\bar{\sigma})}\mathrm{v}_{-\eta}\rangle + \nu'\nu\langle\tilde{\mathrm{h}}_{3,\eta'\eta}^{\sigma(\sigma\sigma)}\mathrm{v}_{-\nu}\rangle .$$

The prefactor $\nu'\nu$ in the second term, which displays overlap of three fermion lines of spin σ, stems from the diagrammatic rules, see Eqs. (53)-(55) and also Eq. (H5). Note that these third-tier bubbles can in principle change the occupation state of both spin degrees of freedom. As a result, they capture spin-flip process, which are virtual processes by which the state of the dot with single occupation changes spin due to multiple (virtual) transitions as for example in

$$\uparrow \longrightarrow (\uparrow\downarrow) \longrightarrow \downarrow .$$

We anticipate that, since in the SIAM we deal with two degrees of freedom, the 4×4 structure of $\tilde{\mathbf{B}}_3^{\sigma(\sigma)}$ is the largest in the hierarchical analysis.

The other second-tier bubble in Eq. (214) is $\tilde{\mathrm{B}}^{\sigma(\bar{\sigma})}$. It is calculated as the contraction of a dressed propagator which bears no structure in the sojourn indexes

$$\tilde{\mathrm{B}}_{\eta'\eta}^{\sigma(\bar{\sigma})} = \langle\tilde{\mathrm{h}}_2^{\sigma(\bar{\sigma})}\mathrm{v}_{-\eta}\rangle , \tag{218}$$

where $\tilde{\mathrm{h}}_2^{\sigma(\bar{\sigma})}$ is obtained by dressing the bare propagator $\mathrm{h}_2^{\sigma(\bar{\sigma})}$ in Eq. (164) with the third-tier bubble $\tilde{\mathrm{B}}_3^{\sigma(\bar{\sigma})}$ according to

$$\tilde{\mathrm{h}}_2^{\sigma(\bar{\sigma})} = \left[[\mathrm{h}_2^{\sigma(\bar{\sigma})}]^{-1} - \tilde{\mathrm{B}}_3^{\sigma(\bar{\sigma})}\right]^{-1} . \tag{219}$$

The third-tier bubble entering this equation is

$$\tag{220}$$

$$= \sum_\nu \langle \sum_{\nu'} \tilde{\mathrm{h}}_{3,\nu'\nu}^{\sigma(\bar{\sigma}\sigma)}\mathrm{v}_\nu\rangle + \sum_\eta \langle \sum_{\eta'} \tilde{\mathrm{h}}_{3,\eta'\eta}^{\sigma(\bar{\sigma}\bar{\sigma})}\mathrm{v}_\eta\rangle .$$

Note that also the bubble $\tilde{\mathbf{B}}_3^{\sigma(\bar{\sigma})}$ has no structure in the sojourn indexes. Moreover, we have included the sums over the sojourns internal to the bubbles in the definitions.

In turn, the propagators $\tilde{\mathbf{h}}_3$ in Eqs. (217) and (220) are given by dressing the bare propagators $\mathbf{h}_3$ with overlap of three fermion lines with the fourth-tier bubbles $\tilde{\mathbf{B}}_4$, namely

$$\tilde{\mathbf{h}}_3 = \left[[\mathbf{h}_3]^{-1} - \tilde{\mathbf{B}}_4\right]^{-1} , \tag{221}$$

where we made no reference to the spin of the fermion lines.

The task of finding the dressed self-energies $\tilde{\Sigma}_{\sigma\eta}(\epsilon)$ has thus been reduced to the evaluation of the dressed bubbles $\tilde{\mathbf{B}}_3$ together with the inversion of the 4×4 matrix in Eq. (216). The hierarchy of internal processes proceeds similarly for higher overlaps of fermion lines. Note that the dimension associated to the matrix structure in the sojourn indexes varies between 0 and 4 (never exceeding this upper bound in the SIAM) according to the number and the spin of the overlapping fermion lines.

E. Fourth-tier scheme: gDSO4

Up to this point, the description of the hierarchy of diagrammatic contributions to the second-tier bubbles, namely to the self-energies, see Eq. (212), is exact, within the approximation of neglcting the crossings. The truncation of the hierarchy in Eq. (213) to the level $n = 3$ gives rise to a fourth-tier scheme where $\tilde{\mathbf{h}}_4 = \mathbf{h}_4$, namely $\tilde{\mathbf{B}}_4 \equiv \mathbf{B}_4$.

The fourth-tier bubbles $\mathbf{B}_4$ are the same as the gDSO second-tier bubbles $\mathrm{B}_{\eta'\eta}^\sigma$, see Eq. (166), except for the additional layers of fermion lines, and the products of sojourn indexes associated to the overlap of three fermion lines of the same spin. The 4th-tier bubbles dressing the

propagators $\tilde{h}_3$ in Eq. (217) are schematized as

$$B_{4,\nu'\nu}^{\sigma(\sigma\bar\sigma)} = \text{[diagram]} + \text{[diagram]}$$

$$= \sum_\eta \langle h_{4,\nu'\nu}^{\sigma(\sigma\bar\sigma\bar\sigma)} v_\eta \rangle + \nu'\nu \langle \tilde{h}_4^{\sigma(\sigma\sigma\sigma)} v_{-\nu} \rangle \tag{222}$$

$$B_{4,\eta'\eta}^{\sigma(\sigma\sigma)} = \text{[diagram]} + \text{[diagram]}$$

$$= \sum_\nu \langle h_{4,\eta'\eta}^{\sigma(\sigma\sigma\sigma)} v_\nu \rangle + \langle \tilde{h}_4^{\sigma(\sigma\sigma\bar\sigma)} v_{-\eta} \rangle .$$

Analogously, the propagators $\tilde{h}_3$ in Eq. (220) are dressed by the fourth-tier bubbles

$$B_{4,\nu'\nu}^{\sigma(\bar\sigma\sigma)} = \text{[diagram]} + \text{[diagram]}$$

$$= \sum_\eta \langle h_{4,\nu'\nu}^{\sigma(\bar\sigma\sigma\sigma)} v_\eta \rangle + \nu'\nu \langle h_4^{\sigma(\bar\sigma\sigma\sigma)} v_{-\nu} \rangle \tag{223}$$

$$B_{4,\eta'\eta}^{\sigma(\bar\sigma\bar\sigma)} = \text{[diagram]} + \text{[diagram]}$$

$$= \sum_\nu \langle h_{4,\eta'\eta}^{\sigma(\bar\sigma\bar\sigma\sigma)} v_\nu \rangle + \eta'\eta \langle h_4^{\sigma(\bar\sigma\bar\sigma\bar\sigma)} v_{-\eta} \rangle .$$

Note the prefactor $\eta'\eta$ in the last line which is absent in Eq. (222). The structure of the dressed propagators $\tilde{h}_3^{(\sigma)}$ is the same as the one of $\phi_{\text{gDSO}}^{\sigma\sigma}$, see Eq. (206), and their matrix elements read (we omit the reference to the spin)

$$\tilde{h}_{3,\eta\eta} = \frac{h_{3,\bar\eta\eta}^{-1} - B_{4,\bar\eta\bar\eta}}{[h_{3,\eta\eta}^{-1} - B_{4,\eta\eta}][h_{3,\bar\eta\bar\eta}^{-1} - B_{4,\bar\eta\bar\eta}] - B_{4,\eta\bar\eta}B_{4,\bar\eta\eta}}$$

$$\tilde{h}_{3,\bar\eta\eta} = \frac{B_{4,\bar\eta\eta}}{[h_{3,\eta\eta}^{-1} - B_{4,\eta\eta}][h_{3,\bar\eta\bar\eta}^{-1} - B_{4,\bar\eta\bar\eta}] - B_{4,\eta\bar\eta}B_{4,\bar\eta\eta}} . \tag{224}$$

Finally, the bare propagators with overlap of three fermion lines are diagonal 2×2 matrices with elements

$$h_{3,\nu'\nu}^{\sigma(\sigma\bar\sigma)} = \text{[diagram]} = \frac{i\hbar\delta_{\nu'\nu}}{\zeta(\epsilon_k - \epsilon_{k_1}) + \zeta_2[\epsilon_{k_2} - E_{\bar\sigma}(\nu)] + i0^+}$$

$$h_{3,\eta'\eta}^{\sigma(\sigma\sigma)} = \text{[diagram]} = \frac{i\hbar\delta_{\eta'\eta}}{\zeta(\epsilon_k - \epsilon_{k_1}) + \zeta_2[\epsilon_{k_2} - E_\sigma(\eta)] + i0^+} , \tag{225}$$

and

$$h_{3,\nu'\nu}^{\sigma(\bar\sigma\sigma)} = \text{[diagram]} = \frac{i\hbar\delta_{\nu'\nu}}{\zeta(\epsilon_k - \epsilon_{k_2}) + \zeta_1[\epsilon_{k_1} - E_{\bar\sigma}(\nu)] + i0^+}$$

$$h_{3,\eta'\eta}^{\sigma(\bar\sigma\bar\sigma)} = \text{[diagram]} = \frac{i\hbar\delta_{\eta'\eta}}{\zeta_1(\epsilon_{k_1} - \epsilon_{k_2}) + \zeta[\epsilon_k - E_\sigma(\eta)] + i0^+} , \tag{226}$$

where $E_\sigma(\eta) = \epsilon_\sigma + (1+\eta)U/2$.

In what follows, we consider a simplified version of the fourth-tier bubbles that dress the above bare propagators. This is done in order to obtain an approximate fourth-tier scheme easier to handle for analytical evaluations.

1. Approximate treatment

To provide an approximate, analytical treatment that improves on the gDSO, we start by considering a simplified version of the propagators $\tilde{h}_3$. Specifically, we neglect the second terms in Eqs. (222)-(223). This approximation yields, for all the 4th-tier bubbles, the simple result $\mathbf{B}_4 = -\Gamma/(2\hbar)\mathbf{1}$, where $\mathbf{1}$ is the two-dimensional identity in the index η or ν. As a consequence, the bare propagators in Eqs. (225)-(226) simply acquire a broadening $\Gamma/(2\hbar)$ and the dressed propagators in Eq. (224) become diagonal, as the off-diagonal parts of $\mathbf{B}_4$ are disregarded. As shown in Appendix J, the resulting third-tier bubble $\tilde{\mathbf{B}}_3^{\sigma(\sigma)}$ in Eq. (217) is approximated by

$$\tilde{B}_{3,\eta'\eta}^{\sigma(\sigma)} \simeq -\sum_\alpha \frac{\Gamma_\alpha}{\hbar}\left[\frac{1}{2} + \eta\frac{1}{\pi}\text{Im}\psi\left(\frac{1}{2} + i\frac{F_{\bar\sigma,\alpha}(\nu)}{2\pi k_B T}\right)\right]\delta_{\nu'\nu}$$
$$-\nu'\nu\sum_\alpha \frac{\Gamma_\alpha}{\hbar}\left[\frac{1}{2} + \nu\frac{1}{\pi}\text{Im}\psi\left(\frac{1}{2} + i\frac{F_{\sigma,\alpha}(\eta)}{2\pi k_B T}\right)\right]\delta_{\eta'\eta} , \tag{227}$$

where $F_{\sigma,\alpha}(\eta) =: E_\sigma(\eta) - \mu_\alpha - i\Gamma/2$ and $E_\sigma(\eta) = \epsilon_\sigma + (1+\eta)U/2$. Similarly, the third-tier bubble $\tilde{\mathbf{B}}_3^{\sigma(\bar\sigma)}$, Eq. (220), is approximated by

$$\tilde{B}_3^{\sigma(\bar\sigma)} \simeq -\sum_\alpha \frac{\Gamma_\alpha}{\hbar}\left[\frac{1}{2} - \frac{1}{2\pi}\sum_\nu \nu\text{Im}\psi\left(\frac{1}{2} + i\frac{R_{\bar\sigma,\alpha}(\nu)}{2\pi k_B T}\right)\right.$$
$$\left. - \frac{i\zeta}{2\pi}\sum_\nu \nu\text{Re}\psi\left(\frac{1}{2} + i\frac{R_{\bar\sigma,\alpha}(\nu)}{2\pi k_B T}\right)\right]$$
$$-\sum_\alpha \frac{\Gamma_\alpha}{\hbar}\left[\frac{1}{2} - \frac{1}{2\pi}\sum_\eta \eta\text{Im}\psi\left(\frac{1}{2} + i\frac{R_{\sigma,\alpha}(\eta)}{2\pi k_B T}\right)\right.$$
$$\left. - \frac{i\zeta_1}{2\pi}\sum_\eta \eta\text{Re}\psi\left(\frac{1}{2} + i\frac{R_{\sigma,\alpha}(\eta)}{2\pi k_B T}\right)\right] , \tag{228}$$

where $R_{\sigma,\alpha}(\eta) =: \zeta\zeta_1[E_\sigma(\eta) - \mu_\alpha] - i\Gamma/2$. Here, ζ and ζ_1 refer to the main and to the first internal fermion line,
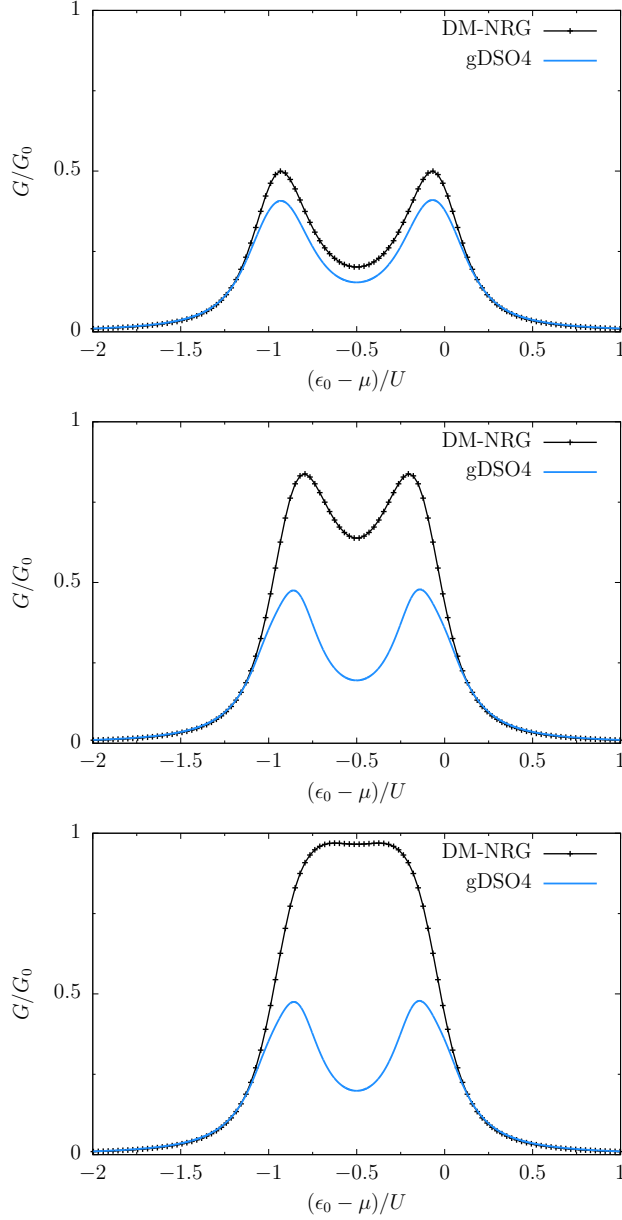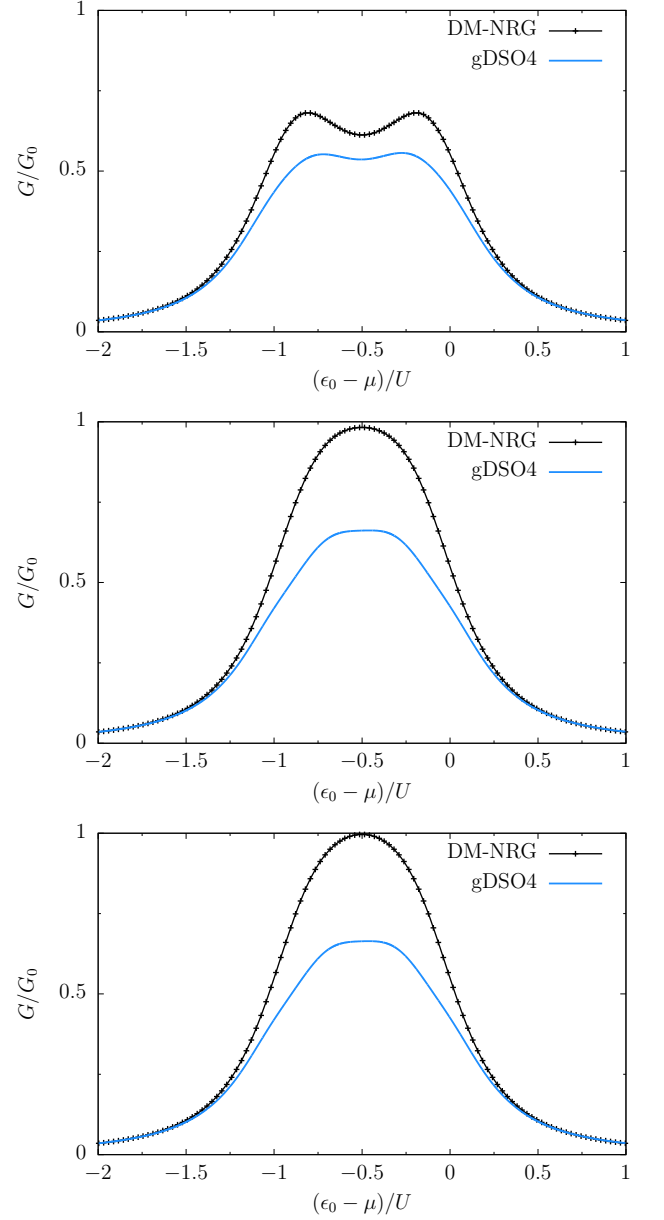
FIG. 23. gDSO4 linear conductance *vs* the gate voltage for three different temperatures: $k_\mathrm{B}T = 0.04\,U$ (upper panel), $k_\mathrm{B}T = 0.003\,U$ (central panel), and $k_\mathrm{B}T = 0.0004\,U$ (lower panel). Degenerate case, $\epsilon_\sigma = \epsilon_0$, and symmetric coupling to the leads $\Gamma_L = \Gamma_R = \Gamma/2$, with $\Gamma = 0.2\,U$. The parameters are chosen to allow a direct comparison with the results of [35]. The Kondo temperature, Eq. (235), for this choice of parameters is $k_\mathrm{B}T_\mathrm{K} \simeq 0.005\,U$. The gDSO4 conductance has a very weak dependence on temperature in the lowest two panels, a hint that the Fermi liquid regime is approached (see also Fig. 25). However, in contrast to the DM-NRG curve, the unitary limit $G = G_0$ is never approached.

FIG. 24. gDSO4 linear conductance *vs* the gate voltage for three different temperatures: $k_\mathrm{B}T = 0.04\,U$ (upper panel), $k_\mathrm{B}T = 0.003\,U$ (central panel), and $k_\mathrm{B}T = 0.0004\,U$ (lower panel). Degenerate case, $\epsilon_\sigma = \epsilon_0$, and symmetric coupling to the leads $\Gamma_L = \Gamma_R = \Gamma/2$, with $\Gamma = 0.4\,U$. The parameters are chosen to allow a direct comparison with the results of [35]. The Kondo temperature, Eq. (235), for this choice of parameters is $k_\mathrm{B}T_\mathrm{K} \simeq 0.05\,U$.

respectively.

The resulting dressed second-tier bubbles satisfy the

properties

$$\tilde{\mathrm{B}}_{\eta'\eta}^{\sigma(\sigma)} = -\frac{\Gamma}{2\hbar}\delta_{\eta'\eta} + \tilde{\mathrm{B}}_{\bar{\eta}\eta}^{\sigma(\sigma)} \quad \text{and} \quad \tilde{\mathrm{B}}_{\eta'\eta}^{\sigma(\bar{\sigma})} = \tilde{\mathrm{B}}_{\bar{\eta}\eta}^{\sigma(\bar{\sigma})} \ , \ (229)$$

see the appendices K and L. Thus the sum $\tilde{\mathrm{B}}_{\eta'\eta}^{\sigma} = \tilde{\mathrm{B}}_{\eta'\eta}^{\sigma(\sigma)} + \tilde{\mathrm{B}}_{\eta'\eta}^{\sigma(\bar{\sigma})}$ respects the property given in Eq. (209) with the
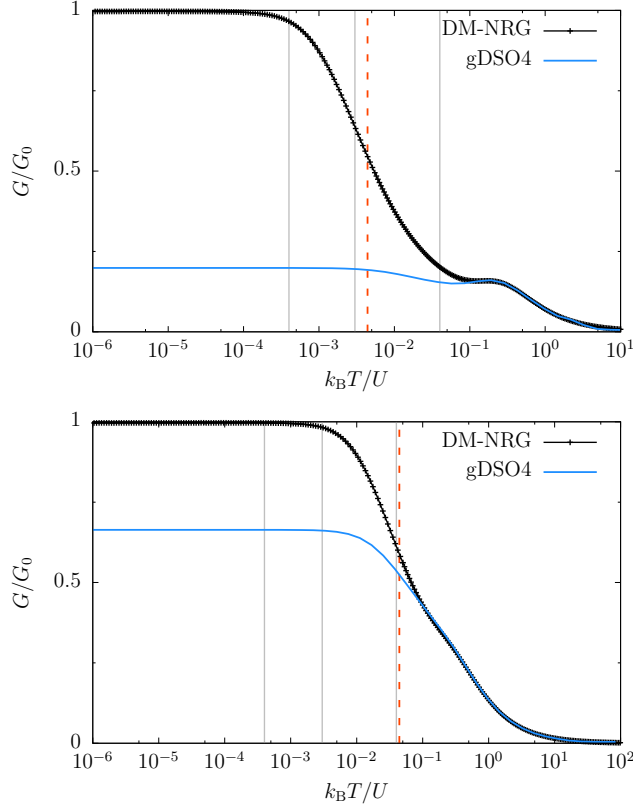
FIG. 25. Temperature dependence of the gDSO4 linear conductance at the particle-hole symmetry point $\epsilon_0 - \mu = -U/2$. Degenerate case, $\epsilon_\sigma = \epsilon_0$, and symmetric coupling to the leads $\Gamma_L = \Gamma_R = \Gamma/2$, with $\Gamma = 0.2\,U$ (upper panel) and $\Gamma = 0.4\,U$ (lower panel). The red dashed lines are at the values of the Kondo temperature $T_{\rm K}$ given by Eq. (235) while the vertical solid lines correspond to the three temperatures considered in in Figs. 23 and 24. Consistently with the DM-NRG results, well below $T_{\rm K}$ the gDSO4 curves depend only weakly on the temperature. However, the unitary value G_0 is not attained.

general non-crossing scheme. The corresponding dressed, retarded self-energies $\tilde{\Sigma}_{\sigma\eta}^{(\sigma)}(\epsilon) = i\hbar\tilde{B}_{\bar\eta\eta}^{\sigma(\sigma)}(\kappa)|_{\zeta=+1}$ entering the general expression for the Green's function, Eq. (210), via

$$\tilde{\Sigma}_{\sigma\eta} = \tilde{\Sigma}_{\sigma\eta}^{(\sigma)} + \tilde{\Sigma}_{\sigma\eta}^{(\bar\sigma)} \qquad \text{and} \qquad \sum_\eta \tilde{\Sigma}_{\sigma\eta} = \tilde{\Sigma}_\sigma \;,$$

are calculated in Appendices K and L. The dressed self-energies have the property

$$\sum_\eta \tilde{\Sigma}_{\sigma\eta}(\epsilon) = -i\Gamma \;, \qquad (230)$$

see Eqs. (K29) and (L6), the same as the one obeyed by the bare self-energies in the gDSO, Eq. (188). Therefore the gDSO4 retarded Green's function, whose general noncrossing-approximated form is provided in Eq. (210),

reads

$$\begin{aligned}
\mathcal{G}_{\sigma\sigma}^r(\epsilon) = & \frac{1 - \langle\hat{n}_{\bar\sigma}\rangle}{\epsilon - \epsilon_\sigma + i\Gamma/2 + \tilde{\Sigma}_{\sigma-}(\epsilon)\frac{U}{\epsilon - \epsilon_\sigma - U + i3\Gamma/2}} \\
& + \frac{\langle\hat{n}_{\bar\sigma}\rangle}{\epsilon - \epsilon_\sigma - U + i\Gamma/2 - \tilde{\Sigma}_{\sigma+}(\epsilon)\frac{U}{\epsilon - \epsilon_\sigma + i3\Gamma/2}} \;.
\end{aligned} \qquad (231)$$

The important difference with the gDSO is that the self-energies are now dressed by higher-level processes, and specifically by 3rd-tier bubbles, see Eqs. (215) and (218). This crucial feature, lifts the pinning problem at the symmetry point $\mu - \epsilon_0 = U/2$, as the self-energies remain temperature-dependent.

Using the sum rule $\sum_\eta \tilde{\Sigma}_{\sigma\eta}(\epsilon) = -i\Gamma$, we can give the retarded Green's function solely in terms of the self-energy $\tilde{\Sigma}_{\sigma-}$. Consider the degenerate case, $\epsilon_\uparrow = \epsilon_\downarrow = \epsilon_0$, at equilibrium, $\mu_L = \mu_R = \mu$. As for the gDSO an the DSO, a zero-bias peak in the conductance appears for temperature below a certain value $T^* = T_{\rm gDSO4}$ for which the real parts of the denominators vanish, causing a peak in the density of states $-{\rm Im}[\mathcal{G}_{\sigma\sigma}^r(\mu)]/\pi$. This condition is

$$(\mu - \epsilon_0)(\mu - \epsilon_0 - U) - 3\Gamma^2/4 + U\,{\rm Re}[\tilde{\Sigma}_{\sigma,-}(\mu)|_{T^*}] = 0 \;, \qquad (232)$$

which is formally the same as for the gDSO, except that here the self-energy is dressed. Assuming that the parameters are such that the dot is close to the center of the Coulomb diamond, i.e. $\epsilon_0 - \mu, U - \epsilon_0 + \mu \gg \Gamma$, we can approximate the self-energy in order to obtain a simple expression for the Kondo-like temperature from the condition in Eq. (232). From Eq. (L4), retaining the first term for sufficiently large U, the real part of the self-energy $\tilde{\Sigma}_{\sigma,-}^{(\bar\sigma)}$ is the same as in the gDSO, cf. Eq (195),

$$\text{Re}[\tilde{\Sigma}_{\sigma,-}^{(\bar\sigma)}(\mu)] \simeq \frac{\Gamma}{2\pi}\log\left(\frac{U}{2\pi k_{\rm B}T}\right) \;. \qquad (233)$$

As shown in Appendix K (see Eq. (K31)) the retarded self-energy of type (σ) is calculated to be

$$\tilde{\Sigma}_{\sigma,-}^{(\sigma)}(\mu) \simeq \frac{\Gamma}{4\pi}\log\left(\frac{2\Gamma}{2\pi k_{\rm B}T}\right) \;.$$

and the resulting value for the Kondo-like temperature $T^* = T_{\rm gDSO4}$ is

$$k_{\rm B}T_{\rm gDSO4} = \frac{(2U^2\Gamma)^{1/3}}{2\pi e^{\pi\Gamma/(2U)}} e^{4\pi\frac{(\mu - \epsilon_0)(\mu - \epsilon_0 - U)}{3U\Gamma}} \;, \qquad (234)$$

which essentially reproduces the result of [41]. The result of the simplified gDSO4 deviates from the true Kondo temperature $T_{\rm K}$ [5]

$$k_{\rm B}T_{\rm K} = \frac{\sqrt{U\Gamma}}{2} e^{\pi\frac{(\mu - \epsilon_0)(\mu - \epsilon_0 - U)}{U\Gamma}} \;, \qquad (235)$$

with $\lim_{U\to\infty} k_{\rm B}T_{\rm K} = \sqrt{U\Gamma/4}\exp[-\pi(\mu - \epsilon_0)/\Gamma]$. This deviation could be ascribed to the fact that, in the dressing of the third-tier bubbles, only diagonal contributions

yielding a simple structure were included. Diagrams describing spin flips involve the fourth-tier bubbles in the second column of Eqs. (222) and (223), which were not considered here. Including these contribution would imply the possibility to change both spin states, a feature which is arguably relevant in the low temperature regimes where *spin-flip* processes are dominant. Within the scheme set-up above, i.e. the simplified gDSO4, spin-flip processes are still captured by the dressed bubble $\tilde{\mathbf{B}}^{\sigma(\sigma)}$, but require both diagrams in Eq. (217).

In Figs. 23 and 24, we show the linear conductance calculated within the simplified version of the gDSO4 considered here, for $\Gamma = 0.2$ and $\Gamma = 0.4\ U$, respectively. In both cases we consider three values of the temperature. The simplified gDSO4 reproduces the DM-NRG curve quantitatively until temperatures slightly above $T_{\rm K}$ over the whole gate voltage range. After that, the conductance has only a weak temperature dependence, as expected in the fermi liquid regime [4]. However, it fails to reproduce the saturation predicted for the SIAM to the plateau value $G_0 = 2e^2/h$ for $T \to 0$. We notice that the gDSO4 has a better qualitative behavior at the larger value of Γ. As in Fig. 21, the parameters of Fig. 23 are chosen so as to allow for a direct comparison with Fig. 6 of Ref. [35], where different approximation schemes, some of which are derived with the EOM technique, are contrasted with the NRG results. Finally, Fig. 25 shows the linear conductance at the particle-hole symmetry point as a function of the temperature, for both values of Γ. In the limit $T \to 0$, the gDSO4 displays a saturation at values lower than the correct value G_0. A quantitative improvement to the gDSO4 results is expected by inclusion of the off-diagonal contributions in the fourth-tier matrices $\mathbf{B}_4$. Notice that, while the theory is applied here for simplicity to the linear conductance in the degenerate case, it has no limitations in describing the nondegenerate case and/or the presence of a voltage bias.

X. CONCLUSIONS

In summary, we have illustrated how the Feynman-Vernon approach, well-known in the study of the dissipative dynamics of quantum particles in bosonic environments [62, 77, 80, 93], is also a useful tool in the context of nonlinear transport in interacting nanojunctions. Integration over the reservoirs degrees of freedom enables one to obtain an exact path-integral representation for the reduced density matrix and the current for a general open system connected to several leads. Dealing with fermions, the path integral is given in terms of fermionic coherent states. Here, the Feynman-Vernon influence functional, a functional of the system paths, accounts exactly for the effects of the leads on the system's dynamics. While the residual integration over the Grassmann variables can be easily performed for noninteracting systems [15], this is no longer the case when local interactions are present in the nanojunction, a situation which is the topic of our

work. In its first and general part, we show how this difficulty can be overcome by expressing the path integral for the propagator in the occupation number representation. This allows for a systematic expansion of the Feynman-Vernon influence functional in the system-leads tunneling amplitude and its diagrammatic characterization. The diagrammatic expansion is carried out for a general system provided that the tunneling matrices are diagonal in the system's states, meaning that the tunneling is state-preserving. In practice, we exclude from the discussion situations like those of non-collinearly polarized leads, or when orbital coherence is important [82–84, 86–88, 94]. This assumption enables us to consider exclusively the populations of the nanojunction. Since, due to Pauli exclusion principle, a single fermionic degree of freedom can only be empty or occupied, we exploit this "two-level" character to parametrize the propagator paths in terms of "blips" and "sojourns", in analogy to the spin-boson model [77]. The diagrammatic contributions to the propagating functions for the populations are summed to yield a formally exact generalized master equation for the RDM diagonal elements. Similarly, an integral equation for the current is derived. In the last part devoted to the general formalism, we give hierarchical diagrammatic expressions for both the kernels of the GME and the one in the integral equation for the current, a major result of the general part. Due to the novelty of the approach, we have reported crucial steps of the derivations in numerous Appendices. This allows non-expert readers to get acquainted with some mathematical intricacies. At the same time, readers not interested in the elimination of the Grassmann variables, can start from the diagrammatic rules discussed in Sec. IV and continue with the derivation of the GME.

In the second part of the work, the formalism is applied to two important archetype models: the exactly solvable RLM and the SIAM. Due to the vast literature on the topic, we found it important to show how seemingly different treatments or approximation schemes can be reconciled within our formalism. For example, the nonperturbative resonant tunneling approximation proposed in [47] is soon recovered by truncating the hierarchy in the RDM kernel to the second-tier. Also, the famous Meir-Wingreen formula for the SIAM retarded Green's function, derived with the equation of motion approach [39], is obtained here within a selection of second-tier diagrams, which we call generalized dressed second order (gDSO).

While the resonant tunneling and gDSO approximations already capture the onset of the Kondo zero-bias anomaly upon decreasing temperature, they both have some drawbacks that can be overcome only by going to higher oder tier treatments. To this aim we develop first an infinite-tier approximation, whereby the evaluation of the SIAM Green's function is formally reduced to the inversion of a 4×4 self-energy matrix. Being interested in analytical solutions, we investigate the outcomes of our approximation within a fourth-tier scheme dubbed

gDSO4. Here, the Green's function self-energies become dressed by virtual tunneling transitions. This allows us a complete *analytical* treatment of the SIAM from high temperature down to temperatures of the order of the Kondo temperature T_{K} for moderate interaction. The validity of the gDSO4 in this parameter range was checked for the equilibrium SIAM against exact numerical renormalization group simulations.

An exact treatment of the gDSO4 scheme, fully accounting for the fourth-tier diagrams, seems required to satisfactorily describe the SIAM current-voltage characteristics. This amounts to inverting the 4×4 matrix Eq. (215) and performing the contraction to obtain the sought dressed self-energy. However, such task goes beyond the scope of this work and we leave it for future investigations.

Appendix A: Path integral expression for the system propagator

In the absence of an external time-dependent driving, the propagator for the quantum state of the full system, from the initial time t_0 to time t, reads

$$U(t, t_0) = e^{-\frac{i}{\hbar} H(t-t_0)} , \tag{A1}$$

with H the complete Hamiltonian of the transport setup, Eq. (1).

A path integral expression for the reduced density matrix of the central system can be obtained in the coherent-state representation [70]. The fermionic coherent states for the central system are defined as $|\boldsymbol{\xi}\rangle = \exp(-\sum_i \xi^i \hat{a}_i^\dagger)|\mathbf{0}\rangle = \prod_i \exp(-\xi^i \hat{a}_i^\dagger)|0_i\rangle = \prod_i (1 - \xi^i \hat{a}_i^\dagger)|0_i\rangle = \prod_i (|0_i\rangle - \xi^i|1_i\rangle)$, where the Grassmann variables $\boldsymbol{\xi} = (\dots, \xi^i, \dots)$ and $\boldsymbol{\xi}^* = (\dots, \xi^{i*}, \dots)$ have one component for each electronic state i defined by $\hat{a}_i|\boldsymbol{\xi}\rangle = \xi^i|\boldsymbol{\xi}\rangle$ and $\langle\boldsymbol{\xi}|\hat{a}_i^\dagger = \langle\boldsymbol{\xi}|\xi^{i*}$. The Grassmann variables obey the relations $\{\xi^i, \xi^j\} = \{\xi^i, \xi^{j*}\} = 0$, meaning that $(\xi^i)^2 = 0$. Analogous definitions hold for the leads' states $|\boldsymbol{\phi}\rangle$ in the coherent-state representation. Using the notation from Cahill and Glauber [71]

$$\int d^2\xi^i := \int d\xi^{i*} d\xi^i , \qquad \int d^2\boldsymbol{\xi} := \int \prod_i d^2\xi^i , \qquad \text{and} \qquad \boldsymbol{\xi}^* \cdot \boldsymbol{\xi} = \sum_i \xi^{i*}\xi^i , \tag{A2}$$

the identity in the Hilbert space of the central system reads

$$\hat{I} = \int d^2\boldsymbol{\xi} \, e^{-\boldsymbol{\xi}^* \cdot \boldsymbol{\xi}}|\boldsymbol{\xi}\rangle\langle\boldsymbol{\xi}| . \tag{A3}$$

The over completeness of the set of coherent states is manifest in the overlap between coherent states

$$\langle\boldsymbol{\xi}_a|\boldsymbol{\xi}_b\rangle = e^{\boldsymbol{\xi}_a^* \cdot \boldsymbol{\xi}_b} . \tag{A4}$$

The trace of an operator in the coherent-state representation is

$$\text{Tr}\{\mathcal{A}\} = \int d^2\boldsymbol{\xi} \, e^{-\boldsymbol{\xi}^* \cdot \boldsymbol{\xi}} \langle -\boldsymbol{\xi}|\mathcal{A}|\boldsymbol{\xi}\rangle , \tag{A5}$$

and the Gaussian integrals are performed via

$$\int d^2\boldsymbol{\xi} \, e^{-\boldsymbol{\xi}^* \cdot \mathcal{M} \cdot \boldsymbol{\xi} + \boldsymbol{\eta}^* \cdot \boldsymbol{\xi} + \boldsymbol{\xi}^* \cdot \boldsymbol{\psi}} = \det[\mathcal{M}] e^{\boldsymbol{\eta}^* \cdot \mathcal{M}^{-1} \cdot \boldsymbol{\psi}} . \tag{A6}$$

Assuming the factorized initial condition $\rho_{\text{tot}}(t_0) = \rho(t_0) \otimes \rho_{\text{leads}}$ for the total density matrix, the matrix element $\langle\boldsymbol{\xi}_a|\rho(t)|\boldsymbol{\xi}_b\rangle$ in the coherent-state representation of the system RDM $\rho(t)$ is given by the following trace over the leads

$$\begin{aligned}
\langle\boldsymbol{\xi}_a|\rho(t)|\boldsymbol{\xi}_b\rangle &= \langle\boldsymbol{\xi}_a|\text{Tr}_{\text{leads}}\{U(t, t_0)\rho_{\text{tot}}(t_0)U^\dagger(t, t_0)\}|\boldsymbol{\xi}_b\rangle \\
&= \int d^2\boldsymbol{\phi} \, e^{-\boldsymbol{\phi}^* \cdot \boldsymbol{\phi}} \langle -\boldsymbol{\xi}_a\boldsymbol{\phi}|U(t, t_0)\rho(t_0) \otimes \rho_{\text{leads}}(t_0)U^\dagger(t, t_0)|\boldsymbol{\phi}\boldsymbol{\xi}_b\rangle ,
\end{aligned} \tag{A7}$$

where $|\boldsymbol{\phi}\rangle$ is the state of the leads in the coherent-state representation. At this point we apply the standard procedure of dividing the time interval $t - t_0$ into K small intervals of length δt and introducing the identity for the composite system

$$I_k = \int d^2\boldsymbol{\xi}(t_k)d^2\boldsymbol{\phi}(t_k) \, e^{-\boldsymbol{\xi}^*(t_k) \cdot \boldsymbol{\xi}(t_k)} e^{-\boldsymbol{\phi}^*(t_k) \cdot \boldsymbol{\phi}(t_k)} |\boldsymbol{\phi}(t_k)\boldsymbol{\xi}(t_k)\rangle\langle\boldsymbol{\xi}(t_k)\boldsymbol{\phi}(t_k)| \tag{A8}$$

at each time instant t_k, both in the forward and in the backward propagators $U(t, t_0)$ and $U^\dagger(t, t_0)$. This results in

$$\begin{aligned}
\langle\boldsymbol{\xi}_a|\rho(t)|\boldsymbol{\xi}_b\rangle = \int d^2\boldsymbol{\phi} \, e^{-\boldsymbol{\phi}^* \cdot \boldsymbol{\phi}} \int d^2\boldsymbol{\xi}_0 d^2\boldsymbol{\phi}_0 d^2\bar{\boldsymbol{\xi}}_0 d^2\bar{\boldsymbol{\phi}}_0 \, e^{-\boldsymbol{\xi}_0^* \cdot \boldsymbol{\xi}_0 - \bar{\boldsymbol{\xi}}_0^* \cdot \bar{\boldsymbol{\xi}}_0} \, e^{-\boldsymbol{\phi}_0^* \cdot \boldsymbol{\phi}_0 - \bar{\boldsymbol{\phi}}_0^* \cdot \bar{\boldsymbol{\phi}}_0} \\
\times \langle -\boldsymbol{\xi}_a\boldsymbol{\phi}|U(t, t_0)|\boldsymbol{\phi}_0\boldsymbol{\xi}_0\rangle\langle\boldsymbol{\xi}_0\boldsymbol{\phi}_0|\rho(t_0) \otimes \rho_{\text{leads}}(t_0)|\bar{\boldsymbol{\phi}}_0\bar{\boldsymbol{\xi}}_0\rangle\langle\bar{\boldsymbol{\xi}}_0\bar{\boldsymbol{\phi}}_0|U^\dagger(t, t_0)|\boldsymbol{\phi}\boldsymbol{\xi}_b\rangle .
\end{aligned} \tag{A9}$$

Explicitly, setting $\boldsymbol{\xi}^*(t_{K+1}) \equiv \boldsymbol{\xi}_a^*$, $\bar{\boldsymbol{\xi}}(t_{K+1}) \equiv \boldsymbol{\xi}_b$, $\langle\boldsymbol{\phi}(t_{K+1})| \equiv \langle -\boldsymbol{\phi}|$, and $|\bar{\boldsymbol{\phi}}(t_{K+1})\rangle \equiv |\boldsymbol{\phi}\rangle$, the path integral expression for the matrix elements of the forward and backward propagator read

$$\begin{aligned}
\langle -\boldsymbol{\xi}_a\boldsymbol{\phi}|U(t, t_0)|\boldsymbol{\phi}_0\boldsymbol{\xi}_0\rangle = \int \prod_{k=1}^{K} d^2\boldsymbol{\xi}(t_k)d^2\boldsymbol{\phi}(t_k) e^{-\boldsymbol{\xi}^*(t_k) \cdot \boldsymbol{\xi}(t_k) - \boldsymbol{\phi}^*(t_k) \cdot \boldsymbol{\phi}(t_k)} \\
\times \prod_{k=1}^{K+1} e^{\boldsymbol{\xi}^*(t_k) \cdot \boldsymbol{\xi}(t_{k-1}) + \boldsymbol{\phi}^*(t_k) \cdot \boldsymbol{\phi}(t_{k-1})} e^{-\frac{i}{\hbar} H[\boldsymbol{\xi}^*(t_k), \boldsymbol{\phi}^*(t_k), \boldsymbol{\xi}(t_{k-1}), \boldsymbol{\phi}(t_{k-1})]\delta t}
\end{aligned} \tag{A10}$$

and

$$\langle \bar{\boldsymbol{\xi}}_0 \bar{\phi}_0 | U^\dagger(t,t_0) | \bar{\phi} \bar{\boldsymbol{\xi}}_b \rangle = \int \prod_{k=1}^K d^2 \bar{\boldsymbol{\xi}}(t_k) d^2 \bar{\phi}(t_k) e^{-\bar{\boldsymbol{\xi}}^*(t_k)\cdot\bar{\boldsymbol{\xi}}(t_k) - \bar{\phi}^*(t_k)\cdot\bar{\phi}(t_k)}$$

$$\times \prod_{k=1}^{K+1} e^{\bar{\boldsymbol{\xi}}^*(t_{k-1})\cdot\bar{\boldsymbol{\xi}}(t_k) + \bar{\phi}^*(t_{k-1})\cdot\bar{\phi}(t_k)} e^{\frac{i}{\hbar} H[\bar{\boldsymbol{\xi}}^*(t_{k-1}), \bar{\phi}^*(t_{k-1}), \bar{\boldsymbol{\xi}}(t_k), \phi(t_k)]\delta t} ,$$

(A11)

respectively. Collecting the above results, we obtain the matrix element of the RDM at time t

$$\langle \boldsymbol{\xi}_a | \rho(t) | \boldsymbol{\xi}_b \rangle = \int d^2\boldsymbol{\xi}_0 d^2\bar{\boldsymbol{\xi}}_0 \mathcal{J}(\boldsymbol{\xi}_a^*, \boldsymbol{\xi}_b, t; \boldsymbol{\xi}_0, \bar{\boldsymbol{\xi}}_0^*, t_0) \langle \boldsymbol{\xi}_0 | \rho(t_0) | \bar{\boldsymbol{\xi}}_0 \rangle ,$$

(A12)

where the propagator has the following path integral expression

$$\mathcal{J}(\boldsymbol{\xi}_a^*, \boldsymbol{\xi}_b, t; \boldsymbol{\xi}_0, \bar{\boldsymbol{\xi}}_0^*, t_0) = \int_{\boldsymbol{\xi}_0}^{\boldsymbol{\xi}_a^*} D\boldsymbol{\xi} \int_{\bar{\boldsymbol{\xi}}_0^*}^{\boldsymbol{\xi}_b} D\bar{\boldsymbol{\xi}} \ e^{\frac{i}{\hbar}[S_{\rm S}(\boldsymbol{\xi}^*,\boldsymbol{\xi}) - S_{\rm S}^*(\bar{\boldsymbol{\xi}}^*,\bar{\boldsymbol{\xi}})]} \mathcal{F}(\boldsymbol{\xi}^*, \boldsymbol{\xi}, \bar{\boldsymbol{\xi}}^*, \bar{\boldsymbol{\xi}}) .$$

(A13)

Here, the integration measures of the Grassmann-valued paths are defined by $\int D\boldsymbol{\xi} = \int \prod_{k=1}^K d\boldsymbol{\xi}_k^* d\boldsymbol{\xi}_k$ and $\int D\bar{\boldsymbol{\xi}} = \int \prod_{k=1}^K d\bar{\boldsymbol{\xi}}_k^* d\bar{\boldsymbol{\xi}}_k$. The functional containing the action of the central system is given by Eq. (5) of the main text. The Feynman-Vernon influence functional $\mathcal{F}(\boldsymbol{\xi}^*, \boldsymbol{\xi}, \bar{\boldsymbol{\xi}}^*, \bar{\boldsymbol{\xi}}) = \exp[\Phi(\boldsymbol{\xi}^*, \boldsymbol{\xi}, \bar{\boldsymbol{\xi}}^*, \bar{\boldsymbol{\xi}})]$ is a functional of the Grassmann-valued paths of the central system which encapsulates the dissipative effect due to the coupling to the leads. Its phase reads [15, 63, 72]

$$\Phi(\boldsymbol{\xi}^*, \boldsymbol{\xi}, \bar{\boldsymbol{\xi}}^*, \bar{\boldsymbol{\xi}}) = -\sum_{ij} \int_{t_0}^t dt' \int_{t_0}^{t'} dt'' \left[g_{ij}(t' - t'') \xi^{i*}(t') \xi^j(t'') + \mathcal{G}_{ji}^*(t' - t'') \bar{\xi}^{i*}(t'') \bar{\xi}^j(t') \right]$$

$$-\sum_{ij} \int_{t_0}^t dt' \int_{t_0}^t dt'' \left\{ g_{ij}(t' - t'') \bar{\xi}^{i*}(t') \xi^j(t'') - g_{+,ij}(t' - t'') \left[\xi^{i*}(t') + \bar{\xi}^{i*}(t') \right] \left[\xi^j(t'') + \bar{\xi}^j(t'') \right] \right\} ,$$

(A14)

with the temperature-independent and temperature-dependent correlation matrix of elements $g_{ij}(t)$ and $g_{+,ij}(t)$ defined as

$$g_{ij}(t) = \frac{1}{\hbar^2} \sum_{\alpha k \sigma} t_{i\alpha k} t_{j\alpha k\sigma\sigma}^* e^{-\frac{i}{\hbar}\epsilon_{\alpha k}t}$$

$$g_{+,ij}(t) = \frac{1}{\hbar^2} \sum_{\alpha k \sigma} t_{i\alpha k\sigma} t_{j\alpha k\sigma}^* f_+^\alpha(\epsilon_k) e^{-\frac{i}{\hbar}\epsilon_{\alpha k}t} ,$$

(A15)

respectively, where $f_+^\alpha(\epsilon_k) = [1 + e^{\beta_\alpha(\epsilon_{\alpha k} - \mu_\alpha)}]^{-1}$ is the Fermi function of lead α. We also define

$$g_{-,ij}(t) := g_{ij}(t) - g_{+,ij}(t)$$

$$= \frac{1}{\hbar^2} \sum_{\alpha k \sigma} t_{i\alpha k\sigma} t_{j\alpha k\sigma}^* f_-^\alpha(\epsilon_k) e^{-\frac{i}{\hbar}\epsilon_{\alpha k}t} ,$$

(A16)

where $f_-^\alpha(\epsilon_k) := 1 - f_+^\alpha(\epsilon_k)$.

Appendix B: Phase of the influence functional

The terms in Eq. (A14) can be rearranged in a convenient manner

$$\Phi(\boldsymbol{\xi}^*, \boldsymbol{\xi}, \bar{\boldsymbol{\xi}}^*, \bar{\boldsymbol{\xi}}) = -\sum_{ij} \int_{t_0}^t dt' \int_{t_0}^{t'} dt'' \left[g_{ij}(t' - t'') \xi^{i*}(t') \xi^j(t'') + \mathcal{G}_{ji}^*(t' - t'') \bar{\xi}^{i*}(t'') \bar{\xi}^j(t') \right]$$

$$+ \sum_{ij} \int_{t_0}^t dt' \int_{t_0}^t dt'' \Big[g_{+,ij}(t' - t'') \xi^{i*}(t') \xi^j(t'') + g_{+,ij}(t' - t'') \bar{\xi}^{i*}(t') \bar{\xi}^j(t'')$$

$$+ g_{+,ij}(t' - t'') \xi^{i*}(t') \bar{\xi}^j(t'') - g_{-,ij}(t' - t'') \bar{\xi}^{i*}(t') \xi^j(t'') \Big] .$$

(B1)

Further, exchanging the order of integration and using the relation $g_{ij}(-t) = g_{ji}^*(t)$, see Eq. (A15), the influence phase in Eq. (B1) can be cast in the following compact form

$$\Phi(\boldsymbol{\xi}^*, \boldsymbol{\xi}, \bar{\boldsymbol{\xi}}^*, \bar{\boldsymbol{\xi}}) = -\sum_{ij} \int_{t_0}^t dt' \int_{t_0}^{t'} dt'' \left[g_{ij}(t'-t'')\xi^{i*}(t')\xi^j(t'') + \mathcal{G}_{ji}^*(t'-t'')\bar{\xi}^{i*}(t'')\bar{\xi}^j(t') \right]$$

$$+ \sum_{ij} \int_{t_0}^t dt' \int_{t_0}^{t'} dt'' \Big[g_{+,ij}(t'-t'')\xi^{i*}(t')\xi^j(t'') + g_{+,ij}(t'-t'')\bar{\xi}^{i*}(t')\bar{\xi}^j(t'')$$

$$+ g_{+,ij}(t'-t'')\xi^{i*}(t')\bar{\xi}^j(t'') - g_{-,ij}(t'-t'')\bar{\xi}^{i*}(t')\xi^j(t'')$$

$$+ g_{+,ji}^*(t'-t'')\xi^{i*}(t'')\xi^j(t') + g_{+,ji}^*(t'-t'')\bar{\xi}^{i*}(t'')\bar{\xi}^j(t')$$

$$+ g_{+,ji}^*(t'-t'')\xi^{i*}(t'')\bar{\xi}^j(t') - g_{-,ji}^*(t'-t'')\bar{\xi}^{i*}(t'')\xi^j(t') \Big]$$

$$= -\sum_{ij} \int_{t_0}^t dt' \int_{t_0}^{t'} dt'' \Big[g_{-,ij}(t'-t'')\xi^{i*}(t')\xi^j(t'') - g_{+,ij}(t'-t'')\bar{\xi}^{i*}(t')\bar{\xi}^j(t'')$$

$$- g_{+,ij}(t'-t'')\xi^{i*}(t')\bar{\xi}^j(t'') + g_{-,ij}(t'-t'')\bar{\xi}^{i*}(t')\xi^j(t'') \tag{B2}$$

$$- g_{+,ji}^*(t'-t'')\xi^{i*}(t'')\xi^j(t') + g_{-,ji}^*(t'-t'')\bar{\xi}^{i*}(t'')\bar{\xi}^j(t')$$

$$- g_{+,ji}^*(t'-t'')\xi^{i*}(t'')\bar{\xi}^j(t') + g_{-,ji}^*(t'-t'')\bar{\xi}^{i*}(t'')\xi^j(t') \Big]$$

$$= -\int_{t_0}^t dt' \int_{t_0}^{t'} dt'' \Big[\boldsymbol{\xi}^*(t') \cdot \mathbf{g}_-(t'-t'') \cdot \boldsymbol{\xi}(t'') + \boldsymbol{\xi}(t') \cdot \mathbf{g}_+^*(t'-t'') \cdot \boldsymbol{\xi}^*(t'')$$

$$- \bar{\boldsymbol{\xi}}(t') \cdot \mathbf{g}_-^*(t'-t'') \cdot \bar{\boldsymbol{\xi}}^*(t'') - \bar{\boldsymbol{\xi}}^*(t') \cdot \mathbf{g}_+(t'-t'') \cdot \bar{\boldsymbol{\xi}}(t'')$$

$$+ \bar{\boldsymbol{\xi}}^*(t') \cdot \mathbf{g}_-(t'-t'') \cdot \boldsymbol{\xi}(t'') + \bar{\boldsymbol{\xi}}(t') \cdot \mathbf{g}_+^*(t'-t'') \cdot \boldsymbol{\xi}^*(t'')$$

$$- \boldsymbol{\xi}(t') \cdot \mathbf{g}_-^*(t'-t'') \cdot \bar{\boldsymbol{\xi}}^*(t'') - \boldsymbol{\xi}^*(t') \cdot \mathbf{g}_+(t'-t'') \cdot \bar{\boldsymbol{\xi}}(t'') \Big]$$

$$= -\int_{t_0}^t dt' \int_{t_0}^{t'} dt'' \sum_{x,y,z=\pm 1} x\, \boldsymbol{\xi}_y^z(t') \mathbf{g}_{xz}^{-z}(t'-t'') \boldsymbol{\xi}_x^{-z}(t''),$$

where we used the anticommutation property of the Grassmann variables and Eq. (A16). In the last line, we established the notation

$$\boldsymbol{\xi}_{+1}^{+1} = \boldsymbol{\xi}, \quad \boldsymbol{\xi}_{+1}^{-1} = \boldsymbol{\xi}^*, \quad \boldsymbol{\xi}_{-1}^{+1} = \bar{\boldsymbol{\xi}}, \quad \boldsymbol{\xi}_{-1}^{-1} = \bar{\boldsymbol{\xi}}^*,$$
$$\mathbf{g}_{+1}^{+1} = \mathbf{g}_+, \quad \mathbf{g}_{+1}^{-1} = \mathbf{g}_+^*, \quad \mathbf{g}_{-1}^{+1} = \mathbf{g}_-, \quad \mathbf{g}_{-1}^{-1} = \mathbf{g}_-^*. \tag{B3}$$

Equation (B2) is the form of the influence phase used throughout this work.

Appendix C: Leads' force operator correlation function

The correlation functions $g_{\pm,ij}(t)$ are related to the correlation function of the (fermion) baths force operator which appears in the quantum Langevin equation for the dot operator $a_i(t)$. Indeed, given the full Hamiltonian Eq. (1), the Heisenberg equation of motion for the leads' operators $\dot{c}_{\alpha k\sigma}(t) = \mathrm{i}[H, c_{\alpha k\sigma}(t)]/\hbar$ is solved by

$$c_{\alpha k\sigma}(t) = c_{\alpha k\sigma}(t_0)e^{-\frac{\mathrm{i}}{\hbar}\epsilon_{\alpha k}(t-t_0)} - \frac{\mathrm{i}}{\hbar}\sum_j t_{j\alpha k\sigma}^* \int_{t_0}^t dt' e^{-\frac{\mathrm{i}}{\hbar}\epsilon_{\alpha k}(t-t')} a_j(t'). \tag{C1}$$

Plugging this result in the Heisenberg equation for the system operator $a_i(t)$

$$\dot{a}_i(t) = \frac{\mathrm{i}}{\hbar}[H, a_i(t)]$$
$$= \frac{\mathrm{i}}{\hbar}[H_{\mathrm{S}}, a_i(t)] - \frac{\mathrm{i}}{\hbar}\sum_{\alpha k\sigma} t_{i\alpha k\sigma} c_{\alpha k\sigma}(t) \tag{C2}$$

we obtain the quantum Langevin equation

$$\dot{a}_i(t) = \frac{\mathrm{i}}{\hbar}[H_\mathrm{S}, a_i(t)] - \frac{1}{\hbar^2}\sum_{j\alpha k\sigma} \mathrm{t}_{i\alpha k\sigma}\mathrm{t}_{j\alpha k\sigma}^* \int_{t_0}^t dt'\, e^{-\frac{\mathrm{i}}{\hbar}\epsilon_{\alpha k}(t-t')}a_j(t') + \hat{\zeta}_i(t)\,, \tag{C3}$$

where the baths force operator reads

$$\hat{\zeta}_i(t) = -\frac{\mathrm{i}}{\hbar}\sum_{\alpha k\sigma} \mathrm{t}_{i\alpha k\sigma} e^{-\frac{\mathrm{i}}{\hbar}\epsilon_{\alpha k}(t-t_0)}c_{\alpha k\sigma}(t_0)\,, \tag{C4}$$

see, e.g., Ref. [95]. The correlation functions in Eq. (A15) are thus related to the correlation function of the baths' force operators via

$$\begin{aligned}
\langle\hat{\zeta}_i^\dagger(t)\hat{\zeta}_j(t')\rangle &= g_{+,ij}(t-t')\\
\langle\hat{\zeta}_i(t)\hat{\zeta}_j^\dagger(t')\rangle &= g_{-,ij}(t-t')\,.
\end{aligned} \tag{C5}$$

Appendix D: Path integral representation of the current and the Green's functions

Consider the current on lead l. Using the definition $f_-^l(\epsilon_k) := 1 - f_+^l(\epsilon_k)$, the current functional $\mathcal{I}$ in Eq. (13) can be rewritten as

$$\mathcal{I}_l(\boldsymbol{\xi}^*, \boldsymbol{\xi}, \bar{\boldsymbol{\xi}}) = -\int_{t_0}^t dt'\, \left\{\boldsymbol{\xi}^*(t)\mathbf{g}_l(t-t')\boldsymbol{\xi}(t') - \boldsymbol{\xi}^*(t)\tilde{\mathbf{g}}_{+,l}(t-t')[\boldsymbol{\xi}(t') + \bar{\boldsymbol{\xi}}(t')]\right\}\,, \tag{D1}$$

where

$$[\mathbf{g}_l(t)]_{ij} = [\mathbf{g}_{+,l}(t) + \mathbf{g}_{-,l}(t)]_{ij} = \frac{1}{\hbar^2}\sum_{k\sigma} \mathrm{t}_{ilk\sigma}\mathrm{t}_{jlk\sigma}^* e^{-\frac{\mathrm{i}}{\hbar}\epsilon_{lk}t}\,. \tag{D2}$$

With this expressions, recalling the relation between the operators a_i and the corresponding Grassmann variables ξ^i, the current $I_l(t) = -2\mathrm{Re}\,\mathrm{Tr}_\mathrm{S}[\mathcal{A}_l(t)]$, with the path integral representation of $\mathcal{A}_l(t)$ given by eqs. (11) and (12), can be seen as the path integral representation of the following trace over system and leads degrees of freedom

$$\begin{aligned}
\mathrm{Tr}_\mathrm{S}[\mathcal{A}_l(t)] =& -\sum_{ij}\int_{t_0}^t dt'\,\left\{g_{lij}(t-t')\mathrm{Tr}_\mathrm{tot}\left[a_i^\dagger U(t,t')a_j U(t',t_0)\rho_\mathrm{tot}(t_0)U^\dagger(t,t_0)\right]\right.\\
&\left. - g_{+,lij}(t-t')\mathrm{Tr}_\mathrm{tot}\left[a_i^\dagger U(t,t')a_j U(t',t_0)\rho_\mathrm{tot}(t_0)U^\dagger(t,t_0) + a_i^\dagger U(t,t_0)\rho_\mathrm{tot}(t_0)U^\dagger(t',t_0)a_j U^\dagger(t,t')\right]\right\}\\
=& -\sum_{ij}\int_{t_0}^t dt'\,\left[g_{lij}(t-t')\langle a_i^\dagger(t)a_j(t')\rangle - g_{+,lij}(t-t')\langle\{a_i^\dagger(t), a_j(t')\}\rangle\right]\\
=& \mathrm{i}\hbar\sum_{ij}\int_{t_0}^t dt'\,\left[g_{lij}(t-t')\mathcal{G}_{ji}^<(t'-t) - g_{+,lij}(t-t')\mathcal{G}_{ji}^a(t'-t)\right]\\
=& \mathrm{i}\hbar\int_{t_0}^t dt'\,\mathrm{Tr}\left[\mathbf{g}_l(t-t')\cdot\boldsymbol{\mathcal{G}}^<(t'-t) - \mathbf{g}_{+,l}(t-t')\cdot\boldsymbol{\mathcal{G}}^a(t'-t)\right]\,,
\end{aligned} \tag{D3}$$

where the last trace is in the matrix sense. The lesser, retarded, and advanced Green's functions are defined by

$$\begin{aligned}
[\boldsymbol{\mathcal{G}}^<(t',t)]_{ij} &= \mathrm{i}\langle a_j^\dagger(t)a_i(t')\rangle/\hbar\,,\\
[\boldsymbol{\mathcal{G}}^r(t,t')]_{ij} &= -\mathrm{i}\theta(t-t')\langle\{a_i(t), a_j^\dagger(t')\}\rangle/\hbar\,,\\
[\boldsymbol{\mathcal{G}}^a(t,t')]_{ij} &= [\boldsymbol{\mathcal{G}}^{r\dagger}(t',t)]_{ij}\\
&= \mathrm{i}\theta(t'-t)\langle\{a_j^\dagger(t'), a_i(t)\}\rangle/\hbar\,,
\end{aligned} \tag{D4}$$

respectively. Note that the Heaviside function is already taken into account in the time integral that guarantees the ordering $t' < t$.

Appendix E: Two leads and proportional coupling

Let us confine ourselves to the case of diagonal correlation matrices $\mathbf{g}_{+,\alpha}$. Having diagonal correlation matrices implies that, in the continuum limit,

$$[\mathbf{\Gamma}_\alpha(\epsilon)]_{ij} := 2\pi \sum_\sigma \varrho_{\alpha\sigma}(\epsilon)|\mathrm{t}_{i\alpha\sigma}(\epsilon)|^2 \delta_{ij} \ .$$

In a typical transport setting, the system is connected to two leads, $\alpha = L, R$. In the case of proportional coupling, the tunneling coefficients in the Hamiltonian are related by $\mathrm{t}_{iR\sigma}(\epsilon) = \sqrt{\gamma_{iR}/\gamma_{iL}}\, \mathrm{t}_{iL\sigma}(\epsilon)$ with $\gamma_{iL} + \gamma_{iR} = 1$. Since $I_L^\infty = -I_R^\infty$, the current I_L is asymptotically equal to the current $I(t) = \sum_i[\gamma_{iR}I_{iL}(t) - \gamma_{iL}I_{iR}(t)]$ which we can directly write as

$$I(t) = e2\mathrm{Re}\,\mathrm{Tr}_\mathrm{S}[\boldsymbol{\mathcal{A}}(t)] \ . \tag{E1}$$

The path integral representation for the dot operator with diagonal elements $\mathcal{A}_{ii}(t) := \gamma_{iR}\mathcal{A}_{iiL}(t) - \gamma_{iiL}\mathcal{A}_{iiR}(t)$ is formally the same as the one in Eq. (11). The current propagator $\mathcal{J}^I$ for $\mathcal{A}(t)$ is similar to $\mathcal{J}_l^I$, Eq. (12), the difference being the functional $\mathcal{I}(\boldsymbol{\xi}^*, \boldsymbol{\xi}, \bar{\boldsymbol{\xi}})$ in place of $\mathcal{I}_l(\boldsymbol{\xi}^*, \boldsymbol{\xi}, \bar{\boldsymbol{\xi}})$, where

$$\mathcal{I}(\boldsymbol{\xi}^*, \boldsymbol{\xi}, \bar{\boldsymbol{\xi}}) = \sum_i \int_{t_0}^t dt'\, \xi^{i*}(t)\left[\gamma_{iR}\mathrm{g}_{+,iiL}(t - t') - \gamma_{iL}\mathrm{g}_{+,iiR}(t - t')\right]\left[\xi^i(t') + \bar{\xi}^i(t')\right] \ . \tag{E2}$$

Here we used the property $f_-^\alpha(\epsilon) = 1 - f_+^\alpha(\epsilon)$ in the definition of the correlation matrices. In the calculation of $I(t)$ for proportional coupling, the temperature-independent term involving the lesser Green's function in Eq. (D3) drops and

$$\begin{aligned}
\mathrm{Tr}_\mathrm{S}[\boldsymbol{\mathcal{A}}(t)] &= \sum_i \left[\gamma_{iR}\mathcal{A}_{iiL}(t) - \gamma_{iL}\mathcal{A}_{iiR}(t)\right] \\
&= -\,\mathrm{i}\hbar \sum_i \int_{t_0}^t dt'\, \left[\gamma_{iR}\mathrm{g}_{+,iiL}(t - t') - \gamma_{iL}\mathrm{g}_{+,iiR}(t - t')\right]\mathcal{G}_{ii}^a(t' - t) \ .
\end{aligned} \tag{E3}$$

In the continuum limit $\sum_{k\sigma} \to \sum_\sigma \int d\epsilon \varrho_{\alpha\sigma}(\epsilon)$, with $\varrho_{\alpha\sigma}(\epsilon)$ the density of states in energy space of lead α. We define $\mathbf{\Gamma}(\epsilon) = \mathbf{\Gamma}_L(\epsilon) + \mathbf{\Gamma}_R(\epsilon)$, so that, for proportional coupling, Eq. (E3) reads

$$I(t) = e \sum_i \frac{\gamma_{iL}\gamma_{iR}}{\pi\hbar} \int d\epsilon\, \left[f_+^L(\epsilon) - f_+^R(\epsilon)\right] \mathrm{Im}\,\left[\Gamma_{ii}(\epsilon) \int_{t_0}^t dt'\, e^{-\frac{\mathrm{i}}{\hbar}\epsilon(t-t')}\mathcal{G}_{ii}^a(t' - t)\right] \ . \tag{E4}$$

Asymptotic limit

In the limit $t - t_0 \to \infty$, the time integral in Eq. (E4) yields the Fourier transform with

$$I^\infty = e \sum_i \frac{\gamma_{iL}\gamma_{iR}}{\pi\hbar} \int d\epsilon\, \left[f_+^L(\epsilon) - f_+^R(\epsilon)\right] \mathrm{Im}\,\left[\Gamma_{ii}(\epsilon)\mathcal{G}_{ii}^a(\epsilon)\right] \ . \tag{E5}$$

Taking into account the definition of the matrix $\mathbf{\Gamma}(\epsilon)$, the current formula (E5) coincides with the well-known result of Meir and Wingreen [21]. We have

$$\begin{aligned}
I^\infty &= e \sum_i \frac{\gamma_{iL}\gamma_{iR}}{\hbar} \int d\epsilon\, \left[f_+^L(\epsilon) - f_+^R(\epsilon)\right] \Gamma_{ii}(\epsilon)\frac{1}{\pi}\mathrm{Im}\,\mathcal{G}_{ii}^a(\epsilon) \\
&= \frac{e}{\hbar} \sum_i \int d\epsilon\, \left[f_+^L(\epsilon) - f_+^R(\epsilon)\right] \left[\frac{\mathbf{\Gamma}_L(\epsilon)\mathbf{\Gamma}_R(\epsilon)}{\mathbf{\Gamma}_L(\epsilon) + \mathbf{\Gamma}_R(\epsilon)}\right]_{ii} \left[-\frac{1}{\pi}\mathrm{Im}\,\mathcal{G}_{ii}^r(\epsilon)\right] \ ,
\end{aligned} \tag{E6}$$

where we used the relation $\mathrm{Im}\,\mathcal{G}_{ii}^a(\epsilon) = -\mathrm{Im}\,\mathcal{G}_{ii}^r(\epsilon)$.

Appendix F: Integrating out the Grassmann variables in the SIAM

In this appendix, we show how to trace over the Grassmann variables associated to the paths of the central system for specific instances of paths. This procedure yields ultimately the diagrammatic rules that can be traced back to the anticommutation property of Grassmann numbers. First, we exemplify the procedure for the simplest case of a central system consisting of a single, spinless level, the resonant level model. Then, we make the calculations for the more involved case of the single impurity Anderson model. Here, due to the Coulomb interaction, the phase associated to the action of the dot in the path integral expression for the propagator produces the phase factors that couple the diagrammatic contributions stemming from the individual spin paths.

In order to perform specific calculations we employ the formula that connects the coherent-state representation of the propagator for the populations to a given order m to the corresponding occupation number representation

$$J_{\boldsymbol{n'n}}^{(m)}(t,t_0) = \Pi_b(\boldsymbol{n'})\Pi_a^*(\boldsymbol{n'}) \int d^2\boldsymbol{\xi}_0 d^2\bar{\boldsymbol{\xi}}_0 \mathcal{J}^{(m)}(\boldsymbol{\xi}_a^*,\bar{\boldsymbol{\xi}}_b,t;\boldsymbol{\xi}_0,\bar{\boldsymbol{\xi}}_0^*,t_0)\langle\boldsymbol{\xi}_0|\boldsymbol{n}\rangle\langle\boldsymbol{n}|\bar{\boldsymbol{\xi}}_0\rangle \,, \tag{F1}$$

where $\boldsymbol{n} = (\ldots, n^i, \ldots)$ with $n^i = 0, 1$. The projectors are defined by

$$\Pi(\boldsymbol{n}) = \prod_{i=1}^{N} \Pi^i(n_i) \,, \qquad \Pi^*(\boldsymbol{n}) = \prod_{i=N}^{1} \Pi^{i*}(n_i) \,, \tag{F2}$$

with

$$\Pi^*(0) = \int d\xi^*\xi^* \,, \quad \Pi^*(1) = \int d\xi^* \,, \quad \Pi(0) = \int d\bar{\xi}\,\bar{\xi} \,, \quad \Pi(1) = \int d\bar{\xi} \,. \tag{F3}$$

Resonant level model

In the RLM, the central system consists of a single, spinless level with energy ϵ. We start by considering in full detail specific instances of paths with low number of transitions, situated in the forward and backward paths. In this case the occupation of the level is the single degree of freedom of the central system. Let us use Eqs. (F1) and (F2) to evaluate the contributions to the propagator at different orders in Γ given by specific instances of paths.

According to Eq. (15) we have

$$\langle\xi_0|0\rangle\langle 0|\bar{\xi}_0\rangle = 1 \quad \text{and} \quad \langle\xi_0|1\rangle\langle 1|\bar{\xi}_0\rangle = \xi^*\bar{\xi} \,.$$

To order zero, using Eq. (5) and defining $p := -i\epsilon\delta t/\hbar$

$$\begin{aligned}
J_{00}^{(0)}(t;t_0) &= \Pi_b(0)\Pi_a^*(0) \int d^2\xi_0 d^2\bar{\xi}_0 \mathcal{J}^{(0)}(\xi_a^*,\bar{\xi}_b,t;\xi_0,\bar{\xi}_0^*,t_0)\langle\xi_0|0\rangle\langle 0|\bar{\xi}_0\rangle \\
&= \int d\bar{\xi}_{N+1}\bar{\xi}_{N+1}d\xi_{N+1}^*\xi_{N+1}^* \prod_{n=0}^{N} d^2\xi_n d^2\bar{\xi}_n e^{-\xi_n^*\xi_n}e^{-\bar{\xi}_n^*\bar{\xi}_n} \prod_{n=1}^{N+1} e^{\xi_n^*\xi_{n-1}p_n}e^{\bar{\xi}_{n-1}^*\bar{\xi}_n p_n^*} \\
&= \int d\bar{\xi}_{N+1}\bar{\xi}_{N+1}d\xi_{N+1}^*\xi_{N+1}^* \prod_{n=0}^{N} d^2\xi_n d^2\bar{\xi}_n e^{-\xi_n^*\xi_n}e^{-\bar{\xi}_n^*\bar{\xi}_n} \\
&= 1 \,,
\end{aligned} \tag{F4}$$

with $\xi_{N+1}^* \equiv \xi_a^*$ and $\bar{\xi}_{N+1} \equiv \xi_b$. Here we have used the property $\exp(\psi) = 1 + \psi$ and Eq. (14). These properties imply that, for all n, the terms in the rightmost product contribute as 1, otherwise there would be either products of same Grassmann numbers ($\psi^2 = 0$) or integrations not compensated by the corresponding Grassmann numbers in the integrand ($\int d\psi = 0$), see Eq. (14).

On the other hand, along the same lines one can see that a path with no transitions cannot join two states with different occupation, namely

$$\begin{aligned}
J_{10}^{(0)}(t;t_0) &= \Pi_b(1)\Pi_a^*(1) \int d^2\xi_0 d^2\bar{\xi}_0 \mathcal{J}^{(0)}(\xi_a^*,\bar{\xi}_b,t;\xi_0,\bar{\xi}_0^*,t_0)\langle\xi_0|0\rangle\langle 0|\bar{\xi}_0\rangle \\
&= \int d\bar{\xi}_{N+1}d\xi_{N+1}^* \prod_{n=0}^{N} d^2\xi_n d^2\bar{\xi}_n e^{-\xi_n^*\xi_n}e^{-\bar{\xi}_n^*\bar{\xi}_n} \prod_{n=1}^{N+1} e^{\xi_n^*\xi_{n-1}p_n}e^{\bar{\xi}_{n-1}^*\bar{\xi}_n p_n^*} \\
&= 0 \,,
\end{aligned} \tag{F5}$$

where, again, we used the properties of the Grassmann integrals, Eq. (14). In the following we associate the color red to the tunneling times and the colors black and blue to the sojourn and blip times, respectively. These are the time intervals when the RDM is in a diagonal (resp. off-diagonal) state, see Fig. 5.

Going to first order in Γ, we first consider the path in Fig. 26(a) with tunneling transitions in the forward branch.
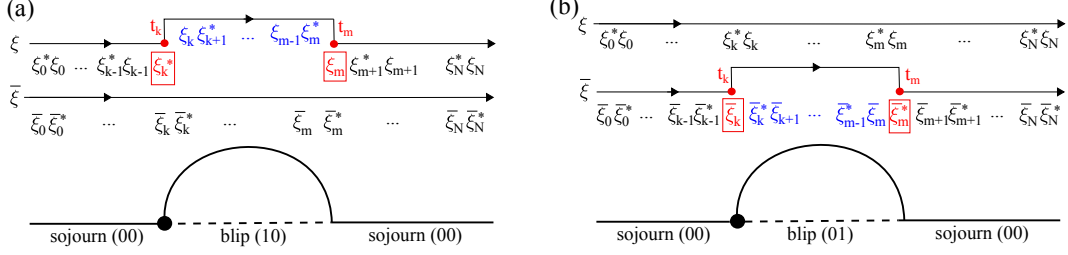
FIG. 26. Two examples of paths with two transitions, either in the forward (a) or in the backward (b) time branch. The Grassmann variables boxed in red are the ones appearing in the influence functional for the examples of paths considered. Note that we use the same time direction for the two branches with the consequence that $\bar{\xi}$ and $\bar{\xi}^*$ creates and annihilates an electron in the dot, respectively.

Specifically, an electron is created in the central system at time t_k and subsequently annihilated at time t_m. The path is thus identified by the sequence ξ_k^*, ξ_m, see Fig. 6. Using the preliminary results

$$
\begin{aligned}
\prod_{n=k}^{m} d^2\xi_n &= d\xi_k^* \left(\prod_{n=k+1}^{m} d\xi_{n-1} d\xi_n^* \right) d\xi_m \\
\prod_{n=k}^{m} d^2\bar{\xi}_n &= \prod_{n=m}^{k} d^2\bar{\xi}_n = d\bar{\xi}_m^* \left(\prod_{n=m}^{k+1} d\bar{\xi}_n d\bar{\xi}_{n-1}^* \right) d\bar{\xi}_k ,
\end{aligned}
\tag{F6}
$$

the contribution from path (a) in Fig. 26 is obtained as

$$
\begin{aligned}
J^{(1)}_{(a),00}(t;t_0) =& \Pi_b(0)\Pi_a^*(0) \int d^2\xi_0 d^2\bar{\xi}_0 \mathcal{J}^{(1)}_{(a)}(\xi_a^*, \bar{\xi}_b, t; \xi_0, \bar{\xi}_0^*, t_0) \langle \xi_0 | 0 \rangle \langle 0 | \bar{\xi}_0 \rangle \\
=& \int_{t_0}^{t} dt_m \int_{t_0}^{t_m} dt_k \int d\bar{\xi}_{N+1} \bar{\xi}_{N+1} d\xi_{N+1}^* \xi_{N+1}^* \prod_{n=0}^{N} d^2\xi_n d^2\bar{\xi}_n e^{-\xi_n^* \xi_n} e^{-\bar{\xi}_n^* \bar{\xi}_n} \\
& \times \prod_{n=1}^{N+1} e^{\xi_n^* \xi_{n-1} p_n} e^{\bar{\xi}_{n-1}^* \bar{\xi}_n p_n^*} \xi_m [-\mathrm{g}_+^*(t_m - t_k)] \xi_k^* \\
=& \int_{t_0}^{t} dt_m \int_{t_0}^{t_m} dt_k \, [-\mathrm{g}_+^*(t_m - t_k)] \int d\xi_{N+1}^* d\bar{\xi}_{N+1} \bar{\xi}_{N+1} \xi_{N+1}^* \prod_{n=0}^{N} d^2\bar{\xi}_n e^{-\bar{\xi}_n^* \bar{\xi}_n} \prod_{n=0}^{k-1} d^2\xi_n e^{-\xi_n^* \xi_n} \prod_{n=m+1}^{N} d^2\xi_n e^{-\xi_n^* \xi_n} \\
& \times d\xi_k^* \left(\prod_{n=k+1}^{m} d\xi_{n-1} d\xi_n^* \right) d\xi_m \left(\prod_{n=k+1}^{m} \xi_n^* \xi_{n-1} p_n \right) \xi_m \xi_k^* \\
=& \int_{t_0}^{t} dt_m \int_{t_0}^{t_m} dt_k \, [-\mathrm{g}_+^*(t_m - t_k)] \prod_{n=k+1}^{m} p_n \underbrace{\int d\xi_k^* d\xi_m \xi_m \xi_k^*}_{=1} \\
\longrightarrow & \int_{t_0}^{t} dt_2 \int_{t_0}^{t_2} dt_1 \, [-\mathrm{g}_+^*(t_2 - t_1)] e^{-\frac{i}{\hbar}\epsilon(t_2 - t_1)} .
\end{aligned}
\tag{F7}
$$

Similarly, the contribution from path (b) in Fig. 26 is

$$
\begin{aligned}
J^{(1)}_{(b),00}(t;t_0) =& \Pi_b(0)\Pi_a^*(0)\int d^2\xi_0 d^2\bar{\xi}_0 \mathcal{J}^{(1)}_{(b)}(\xi_a^*,\bar{\xi}_b,t;\xi_0,\bar{\xi}_0^*,t_0)\langle\xi_0|0\rangle\langle 0|\bar{\xi}_0\rangle \\
=& \int_{t_0}^{t}dt_m\int_{t_0}^{t_m}dt_k\int d\bar{\xi}_{N+1}\bar{\xi}_{N+1}d\xi_{N+1}^*\xi_{N+1}^* \prod_{n=0}^{N}d^2\xi_n d^2\bar{\xi}_n e^{-\xi_n^*\xi_n}e^{-\bar{\xi}_n^*\bar{\xi}_n} \\
& \times \prod_{n=1}^{N+1}e^{\xi_n^*\xi_{n-1}p_n}e^{\bar{\xi}_{n-1}^*\bar{\xi}_n p_n^*}\,\bar{\xi}_m^*\,\mathrm{g}_+(t_m-t_k)\bar{\xi}_k \\
=& \int_{t_0}^{t}dt_m\int_{t_0}^{t_m}dt_k\,\mathrm{g}_+(t_m-t_k)\int d\xi_{N+1}^*d\bar{\xi}_{N+1}\bar{\xi}_{N+1}\xi_{N+1}^* \prod_{n=0}^{N}d^2\xi_n e^{-\xi_n^*\xi_n} \\
& \times \prod_{n=0}^{k-1}d^2\bar{\xi}_n e^{-\bar{\xi}_n^*\bar{\xi}_n}\prod_{n=m+1}^{N}d^2\bar{\xi}_n e^{-\bar{\xi}_n^*\bar{\xi}_n}d\bar{\xi}_m^*\left(\prod_{n=m}^{k+1}d\bar{\xi}_n d\bar{\xi}_{n-1}^*\right)d\bar{\xi}_k\left(\prod_{n=k+1}^{m}\bar{\xi}_{n-1}^*\bar{\xi}_n p_n^*\right)\bar{\xi}_m^*\bar{\xi}_k \\
=& \int_{t_0}^{t}dt_m\int_{t_0}^{t_m}dt_k\,\mathrm{g}_+(t_m-t_k)\prod_{n=k+1}^{m}p_n^*\underbrace{\int d\bar{\xi}_m^*d\bar{\xi}_k\bar{\xi}_m^*\bar{\xi}_k}_{=-1} \\
\longrightarrow& \int_{t_0}^{t}dt_2\int_{t_0}^{t_2}dt_1\,[-\mathrm{g}_+(t_2-t_1)]e^{\frac{i}{\hbar}\epsilon(t_2-t_1)}\,.
\end{aligned}
\tag{F8}
$$

Hence, the two propagators for the specific paths (a) and (b) are the complex conjugated of each other.

Next we consider the two paths contributing to $J^{(1)}(1,t;0,t_0)$ which are depicted in Fig. 27.
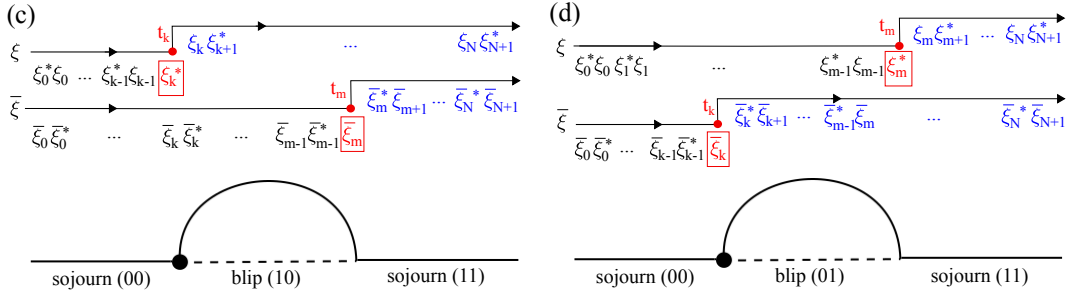
FIG. 27. Paths with two transitions, one in the forward and the other in the backward branch. The boxed Grassmann variables in red are the ones appearing in the influence functional for the examples of paths considered.

The contribution of path (c) is evaluated similarly to those of paths (a) and (b). Explicitly

$$
\begin{aligned}
J^{(1)}_{(c),10}(t;t_0) =& \Pi_b(1)\Pi_a^*(1)\int d^2\xi_0 d^2\bar{\xi}_0 \mathcal{J}^{(1)}_{(c)}(\xi_a^*,\bar{\xi}_b,t;\xi_0,\bar{\xi}_0^*,t_0)\langle\xi_0|0\rangle\langle 0|\bar{\xi}_0\rangle \\
=& \int_{t_0}^{t}dt_m\int_{t_0}^{t_m}dt_k\int d\bar{\xi}_{N+1}d\xi_{N+1}^* \prod_{n=0}^{N}d^2\xi_n d^2\bar{\xi}_n e^{-\xi_n^*\xi_n}e^{-\bar{\xi}_n^*\bar{\xi}_n}\prod_{n=1}^{N+1}e^{\xi_n^*\xi_{n-1}p_n}e^{\bar{\xi}_{n-1}^*\bar{\xi}_n p_n^*}\bar{\xi}_m[-\mathrm{g}_+^*(t_m-t_k)]\xi_k^* \\
=& \int_{t_0}^{t}dt_m\int_{t_0}^{t_m}dt_k\,[-\mathrm{g}_+^*(t_m-t_k)]\int d\bar{\xi}_{N+1}d\xi_{N+1}^*\prod_{n=0}^{k-1}d^2\xi_n e^{-\xi_n^*\xi_n}\prod_{n=0}^{m-1}d^2\bar{\xi}_n e^{-\bar{\xi}_n^*\bar{\xi}_n} \\
& \times d\xi_k^*\left(\prod_{n=k+1}^{N}d\xi_{n-1}d\xi_n^*\right)d\xi_N\left(\prod_{n=k+1}^{N}\xi_n^*\xi_{n-1}p_n\right)\xi_{N+1}^*\xi_N p_{N+1} \\
& \times d\bar{\xi}_N^*\left(\prod_{n=N}^{m+1}d\bar{\xi}_n d\bar{\xi}_{n-1}^*\right)d\bar{\xi}_m\left(\prod_{n=m+1}^{N}\bar{\xi}_{n-1}^*\bar{\xi}_n p_n^*\right)\bar{\xi}_N^*\bar{\xi}_{N+1}p_{N+1}^*\bar{\xi}_m\xi_k^*
\end{aligned}
$$

$$
= -\int_{t_0}^{t} dt_m \int_{t_0}^{t_m} dt_k \left[-\mathrm{g}_+^*(t_m - t_k)\right] \int \prod_{n=0}^{k-1} d^2\xi_n e^{-\xi_n^*\xi_n} \prod_{n=0}^{m-1} d^2\bar\xi_n e^{-\bar\xi_n^*\bar\xi_n}
$$

$$
\times \left(\prod_{n=k+1}^{N} d\xi_{n-1} d\xi_n^*\right)\left(\prod_{n=k+1}^{N} \xi_n^*\xi_{n-1} p_n\right) p_{N+1}
$$

$$
\times \left(\prod_{n=N}^{m+1} d\bar\xi_n d\bar\xi_{n-1}^*\right)\left(\prod_{n=m+1}^{N} \bar\xi_{n-1}^*\bar\xi_n p_n^*\right) p_{N+1}^* \int d\xi_k^* d\bar\xi_m \bar\xi_m \xi_k^*
$$

$$
= -\int_{t_0}^{t} dt_m \int_{t_0}^{t_m} dt_k \left[-\mathrm{g}_+^*(t_m - t_k)\right] \prod_{n=k+1}^{N+1} p_n \prod_{n=m+1}^{N+1} p_n^* \int d\xi_k^* d\bar\xi_m \bar\xi_m \xi_k^*
$$

$$
= -\int_{t_0}^{t} dt_m \int_{t_0}^{t_m} dt_k \left[-\mathrm{g}_+^*(t_m - t_k)\right] \prod_{n=k+1}^{m} p_n
$$

$$
\longrightarrow -\int_{t_0}^{t} dt_2 \int_{t_0}^{t_2} dt_1 \left[-\mathrm{g}_+^*(t_2 - t_1)\right] e^{-\frac{i}{\hbar}\epsilon(t_2 - t_1)} \tag{F9}
$$

Analogously, for the path (d) in Fig. 27 we obtain

$$
J^{(1)}_{(d)10}(t;,t_0) = \Pi_b(1)\Pi_a^*(1) \int d^2\xi_0 d^2\bar\xi_0 \mathcal{J}^{(1)}_{(\bar\sigma)}(\xi_a^*, \bar\xi_b, t; \xi_0, \bar\xi_0^*, t_0)\langle\xi_0|0\rangle\langle 0|\bar\xi_0\rangle
$$

$$
= \int_{t_0}^{t} dt_m \int_{t_0}^{t_m} dt_k \int d\bar\xi_{N+1} d\xi_{N+1}^* \prod_{n=0}^{N} d^2\xi_n d^2\bar\xi_n e^{-\xi_n^*\xi_n} e^{-\bar\xi_n^*\bar\xi_n} \prod_{n=1}^{N+1} e^{\xi_n^*\xi_{n-1}p_n} e^{\bar\xi_{n-1}^*\bar\xi_n p_n^*} \xi_m^* \mathrm{g}_+(t_m - t_k)\bar\xi_k
$$

$$
= \int_{t_0}^{t} dt_m \int_{t_0}^{t_m} dt_k \, \mathrm{g}_+(t_m - t_k) \int d\bar\xi_{N+1} d\xi_{N+1}^* \prod_{n=0}^{k-1} d^2\xi_n e^{-\xi_n^*\xi_n} \prod_{n=0}^{m-1} d^2\bar\xi_n e^{-\bar\xi_n^*\bar\xi_n}
$$

$$
\times d\xi_m^* \left(\prod_{n=m+1}^{N} d\xi_{n-1} d\xi_n^*\right) d\xi_N \left(\prod_{n=m+1}^{N} \xi_n^*\xi_{n-1} p_n\right) \xi_{N+1}^*\xi_N p_{N+1}
$$

$$
\times d\bar\xi_N^* \left(\prod_{n=N}^{k+1} d\bar\xi_n d\bar\xi_{n-1}^*\right) d\bar\xi_k \left(\prod_{n=k+1}^{N} \bar\xi_{n-1}^*\bar\xi_n p_n^*\right) \bar\xi_N^*\bar\xi_{N+1} p_{N+1}^* \xi_m^*\bar\xi_k
$$

$$
= -\int_{t_0}^{t} dt_m \int_{t_0}^{t_m} dt_k \, \mathrm{g}_+(t_m - t_k) \int \prod_{n=0}^{k-1} d^2\xi_n e^{-\xi_n^*\xi_n} \prod_{n=0}^{m-1} d^2\bar\xi_n e^{-\bar\xi_n^*\bar\xi_n}
$$

$$
\times d\xi_m^* \left(\prod_{n=m+1}^{N} d\xi_{n-1} d\xi_n^*\right) d\xi_N d\xi_{N+1}^* \left(\prod_{n=m+1}^{N} \xi_n^*\xi_{n-1} p_n\right) \xi_{N+1}^*\xi_N p_{N+1}
$$

$$
\times d\bar\xi_{N+1} d\bar\xi_N^* \left(\prod_{n=N}^{k+1} d\bar\xi_n d\bar\xi_{n-1}^*\right) d\bar\xi_k \left(\prod_{n=k+1}^{N} \bar\xi_{n-1}^*\bar\xi_n p_n^*\right) \bar\xi_N^*\bar\xi_{N+1} p_{N+1}^* \xi_m^*\bar\xi_k
$$

$$
= -\int_{t_0}^{t} dt_m \int_{t_0}^{t_m} dt_k \, \mathrm{g}_+(t_m - t_k) \prod_{n=m+1}^{N+1} p_n \prod_{n=k+1}^{N+1} p_n^* \int d\xi_m^* d\bar\xi_k \xi_m^*\bar\xi_k
$$

$$
= -\int_{t_0}^{t} dt_m \int_{t_0}^{t_m} dt_k \left[-\mathrm{g}_+(t_m - t_k)\right] \prod_{n=k+1}^{m} p_n^*
$$

$$
\longrightarrow -\int_{t_0}^{t} dt_2 \int_{t_0}^{t_2} dt_2 \left[-\mathrm{g}_+(t_2 - t_1)\right] e^{\frac{i}{\hbar}\epsilon(t_2 - t_1)} \tag{F10}
$$

We notice that Eqs. (F7) and (F9) only differ by a sign and the same holds for Eqs. (F8) and (F10).

Now we consider the specific four-transition path (second order in Γ) individuated by the ordered sequence of Grassmann variables $\{\xi_{k_1}^*, \bar\xi_{k_2}, \bar\xi_{k_3}^*, \xi_{k_4}\}$ and shown in Fig. 28.

(e)
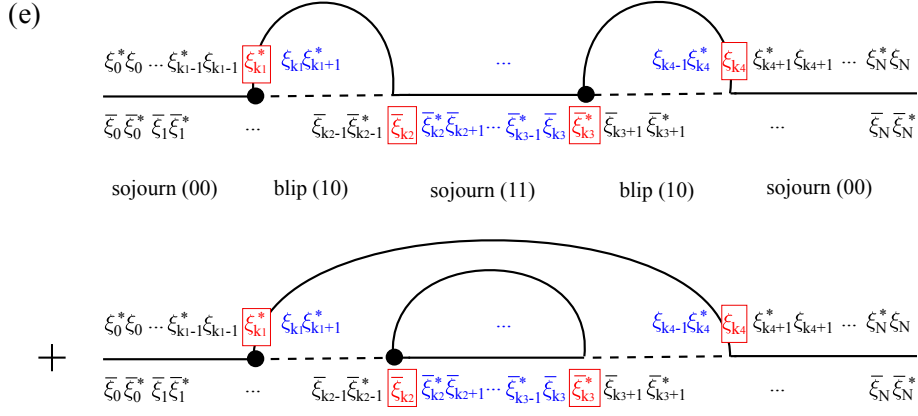
FIG. 28. Path with four transitions, two in the forward and the others in the backward branch. Here, only the collective path is represented, with diagonal and off-diagonal states depicted with continuous and dashed lines, respectively. The boxed Grassmann variables in red are the ones appearing in the influence functional in this example.

The contribution of this path to $J_{00}^{(2)}(t;t_0)$ is evaluated along the same lines as above

$$
\begin{aligned}
J_{(e),00}^{(2)}(t;t_0) =& \Pi_b(0)\Pi_a^*(0)\int d^2\xi_0 d^2\bar\xi_0 \mathcal{J}_{(e)}^{(2)}(\xi_a^*,\bar\xi_b,t;\xi_0,\bar\xi_0^*,t_0)\langle\xi_0|0\rangle\langle 0|\bar\xi_0\rangle \\
=& \int_{t_0}^{t} dt_{k_4}\cdots\int_{t_0}^{t_{k_2}} dt_{k_1}\ \int d\bar\xi_{N+1}\bar\xi_{N+1} d\xi_{N+1}^*\xi_{N+1}^* \prod_{n=0}^{k_1-1} d^2\xi_n e^{-\xi_n^*\xi_n}\prod_{n=k_4+1}^{N} d^2\xi_n e^{-\xi_n^*\xi_n} \\
&\times \prod_{n=0}^{k_2-1} d^2\bar\xi_n e^{-\bar\xi_n^*\bar\xi_n}\prod_{n=k_3+1}^{N} d^2\bar\xi_n e^{-\bar\xi_n^*\bar\xi_n} \\
&\times d\xi_{k_1}^*\left(\prod_{n=k_1+1}^{k_4} d\xi_{n-1}d\xi_n^*\right)d\xi_{k_4}\left(\prod_{n=k_1+1}^{k_4}\xi_n^*\xi_{n-1}p_n\right) \\
&\times d\bar\xi_{k_3}^*\left(\prod_{n=k_3}^{k_2+1} d\bar\xi_n d\bar\xi_{n-1}^*\right)d\bar\xi_{k_2}\left(\prod_{n=k_2+1}^{k_3}\bar\xi_{n-1}^*\bar\xi_n p_n^*\right) \\
&\times\left\{\bar\xi_{k_2}[-g_+^*(t_{k_2}-t_{k_1})]\xi_{k_1}^*\xi_{k_4}g_-^*(t_{k_4}-t_{k_3})\bar\xi_{k_3}^*\right. \\
&\left.+\xi_{k_4}[-g_+^*(t_{k_4}-t_{k_1})]\xi_{k_1}^*\bar\xi_{k_3}^* g_+(t_{k_3}-t_{k_2})\bar\xi_{k_2}\right\} \\
=& \int_{t_0}^{t} dt_{k_4}\cdots\int_{t_0}^{t_{k_2}} dt_{k_1}\int d\xi_{k_1}^* d\xi_4 d\bar\xi_{k_3}^* d\bar\xi_{k_2}\left\{\bar\xi_{k_2}\xi_{k_1}^*\xi_{k_4}\bar\xi_{k_3}^*[-g_+^*(t_{k_2}-t_{k_1})]g_-^*(t_{k_4}-t_{k_3})\right. \\
&\left.+\xi_{k_4}\xi_{k_1}^*\bar\xi_{k_3}^*\bar\xi_{k_2}[-g_+^*(t_{k_4}-t_{k_1})]g_+(t_{k_3}-t_{k_2})\right\}\prod_{n=k_1+1}^{k_2}p_n\prod_{n=k_3+1}^{k_4}p_n \\
=& \int_{t_0}^{t} dt_4\cdots\int_{t_0}^{t_2} dt_1\left\{[-g_+^*(t_2-t_1)][-g_-^*(t_4-t_3)]+[-g_+^*(t_4-t_1)][-g_+(t_3-t_2)]\right\} \\
&\times e^{-\frac{i}{\hbar}\epsilon(t_2-t_1)}e^{-\frac{i}{\hbar}\epsilon(t_4-t_3)}\ .
\end{aligned}
\tag{F11}
$$

Note that a product of the type $g(t_4-t_2)g(t_3-t_1)$, implying a crossing of the fermion lines, is not present for this specific path because we have fixed the Grassmann variables at the transition times and the form of the influence functional prevents the fermion lines from joining two starred or two non-starred charges, see Eq. (6).

From the examples above we can draw some conclusions

- Integrations over the *sojourn* time intervals yield an overall phase factor 1.
- Integrations over the *blip* time intervals yield the phase factors $\exp(-\zeta i\epsilon\tau/\hbar)$, where τ is the blip length and $\zeta=\pm 1$, depending on the nature of the blip.

Once the trivial integrations over the sojourns/blip time intervals are performed, we are left with a final integration over the Grassmann variables associated to the transitions. As a result of this procedure, neither the Grassmann variables in the integration measures nor the ones in the integrands are time-ordered. Specifically,

- In the integration measure, the backward variables appear to the right of the forward and, within this two classes, starred variables are to the left of the non-starred ones. This reflects the original order of the integrations.

- In the integrand, the Grassmann variables appear as a sequence of pairs whose order depends on how they are coupled by the functions $g(t_j - t_i)$.

SIAM

We now generalize the procedure used for the RLM by analyzing specific instances of paths involving both spin states in the SIAM. To avoid adding further indexes we denote the Grassmann variables associated to $\sigma = \uparrow$ with the usual ξ and the ones associated to $\sigma = \downarrow$ with the letter ψ. As for the RLM, instead of using the collective sojourn index $\boldsymbol{\eta} = (\eta^\uparrow, \eta^\downarrow)$, we indicate the initial and final occupation of the spin states of the dot in the argument of the propagator. The integration measure has the property $d^2\boldsymbol{\xi} = d\xi^* d\psi^* d\xi d\psi = -d\xi^* d\xi d\psi^* d\psi$, so that $d^2\boldsymbol{\xi} d^2\bar{\boldsymbol{\xi}} = d\xi^* d\xi d\psi^* d\psi d\bar{\xi}^* d\bar{\xi} d\bar{\psi}^* d\bar{\psi} = d^2\xi d^2\bar{\xi} d^2\psi d^2\bar{\psi}$. We use this property to factorize the integrations over the Grassmann variables for the two degrees of freedom.

For the SIAM, the coherent states are expressed, in terms of occupation number states, as

$$
\begin{aligned}
|\boldsymbol{\xi}\rangle =& (1 - \xi \hat{a}_\uparrow^\dagger)(1 - \psi \hat{a}_\downarrow^\dagger)|0_\uparrow 0_\downarrow\rangle \\
=& |0_\uparrow 0_\downarrow\rangle + |1_\uparrow 0_\downarrow\rangle \xi + |0_\uparrow 1_\downarrow\rangle \psi + |1_\uparrow 1_\downarrow\rangle \psi\xi \\
\langle\boldsymbol{\xi}| =& \langle 0_\downarrow 0_\uparrow|(1 - \hat{a}_\downarrow \psi^*)(1 - \hat{a}_\uparrow \xi^*) \\
=& \langle 0_\downarrow 0_\uparrow| + \psi^*\langle 1_\downarrow 0_\uparrow| + \xi^*\langle 0_\downarrow 1_\uparrow| + \xi^*\psi^*\langle 1_\downarrow 1_\uparrow| .
\end{aligned}
\tag{F12}
$$

As a result, the populations are found by calculating the matrix element of the impurity RDM

$$
\langle\boldsymbol{\xi}|\rho|\bar{\boldsymbol{\xi}}\rangle = P_{00} + \cdots + \psi^*\bar{\psi}\, P_{01} + \cdots + \xi^*\bar{\xi}\, P_{10} + \cdots + \xi^*\psi^*\bar{\psi}\bar{\xi}\, P_{11}
\tag{F13}
$$

and applying the projectors defined in Eq. (F2) via $P_{\boldsymbol{n}} \equiv \rho_{\boldsymbol{nn}} = \Pi_b(\boldsymbol{n})\Pi_a^*(\boldsymbol{n})\langle\boldsymbol{\xi}|\rho|\bar{\boldsymbol{\xi}}\rangle$.

Let us introduce the abbreviations

$$
\begin{aligned}
\text{overlap} \quad O_n^\uparrow =& e^{-\xi_n^* \xi_n} & \bar{O}_n^\uparrow =& e^{-\bar{\xi}_n^* \bar{\xi}_n} \\
O_n^\downarrow =& e^{-\psi_n^* \psi_n} & \bar{O}_n^\downarrow =& e^{-\bar{\psi}_n^* \bar{\psi}_n} \\
H_0 \quad \mathcal{P}_n^\uparrow =& e^{\xi_n^* \xi_{n-1} p_n^\uparrow} & \bar{\mathcal{P}}_n^\uparrow =& e^{\bar{\xi}_{n-1}^* \bar{\xi}_n p_n^{*\uparrow}} \\
\mathcal{P}_n^\downarrow =& e^{\psi_n^* \psi_{n-1} p_n^\downarrow} & \bar{\mathcal{P}}_n^\downarrow =& e^{\bar{\psi}_{n-1}^* \bar{\psi}_n p_n^{*\downarrow}} \\
\text{interaction} \quad \mathcal{U}_n =& e^{\xi_n^* \xi_{n-1} \psi_n^* \psi_{n-1} u_n} & \bar{\mathcal{U}}_n =& e^{\bar{\xi}_{n-1}^* \bar{\xi}_n \bar{\psi}_{n-1}^* \bar{\psi}_n u_n^*} ,
\end{aligned}
\tag{F14}
$$

where $p_n^\sigma := 1 - (\mathrm{i}/\hbar)\epsilon_\sigma \delta t_n$ and $u_n := -(\mathrm{i}/\hbar)U\delta t_n$, with U the interaction energy. Consider the path in Fig. 29. From Eqs. (F1) and (F2), the contribution to $J_{10,00}^{(2)}(t; t_0)$ given by the path reads
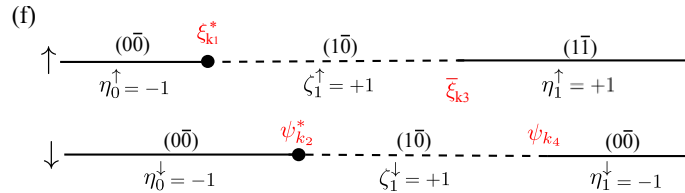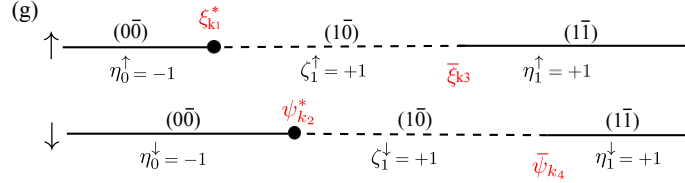

FIG. 29. Path with four transitions distributed in the two sub-paths of the spin variables $\uparrow$ and $\downarrow$. Note that the path for $\sigma = \uparrow$ is of the type (c) in Fig. 27, while $\sigma = \downarrow$ undergoes a sequence of the type (a) in Fig. 26.

$$J_{(f),10,00}^{(2)}(t;t_0) = \Pi_b^\uparrow(1)\Pi_b^\downarrow(0)\Pi_a^{\downarrow*}(0)\Pi_a^{\uparrow*}(1)\int d^2\boldsymbol{\xi}_0 d^2\bar{\boldsymbol{\xi}}_0 \mathcal{J}_{(f)}^{(2)}(\boldsymbol{\xi}_a^*,\bar{\boldsymbol{\xi}}_b,t;\boldsymbol{\xi}_0,\bar{\boldsymbol{\xi}}_0^*,t_0)\langle\boldsymbol{\xi}_0|\mathbf{0}\rangle\langle\mathbf{0}|\bar{\boldsymbol{\xi}}_0\rangle$$

$$= \int_{t_0}^t dt_{k_4}\cdots\int_{t_0}^{t_{k_2}} dt_{k_1}\int d\bar{\xi}_{N+1}d\bar{\psi}_{N+1}\,\bar{\psi}_{N+1}d\psi_{N+1}^*\psi_{N+1}^*d\xi_{N+1}^*\prod_{n=0}^N d^2\xi_n d^2\psi_n d^2\bar{\xi}_n d^2\bar{\psi}_n O_n^\uparrow O_n^\downarrow \bar{O}_n^\uparrow \bar{O}_n^\downarrow$$

$$\times\prod_{n=1}^{N+1}\mathcal{P}_n^\uparrow \mathcal{P}_n^\downarrow \bar{\mathcal{P}}_n^\uparrow \bar{\mathcal{P}}_n^\downarrow \mathcal{U}_n \bar{\mathcal{U}}_n \bar{\xi}_{k_3}[-\mathrm{g}_+^{\uparrow*}(t_{k_3}-t_{k_1})]\xi_{k_1}^*\psi_{k_4}[-\mathrm{g}_+^{\downarrow*}(t_{k_4}-t_{k_2})]\psi_{k_2}^*$$

$$= \int_{t_0}^t dt_{k_4}\cdots\int_{t_0}^{t_{k_2}} dt_{k_1}\int d\bar{\xi}_{N+1}d\xi_{N+1}^*\left(\prod_{n=0}^{k_1-1} d\xi_n^* d\xi_n O_n^\uparrow\right)d\xi_{k_1}^*\left(\prod_{n=k_1+1}^N d\xi_{n-1}d\xi_n^*\mathcal{P}_n^\uparrow\right)d\xi_N\mathcal{P}_{N+1}^\uparrow$$

$$\times\bar{\mathcal{P}}_{N+1}^\uparrow d\bar{\xi}_N^*\left(\prod_{n=N}^{k_3+1} d\bar{\xi}_n d\bar{\xi}_{n-1}^*\bar{\mathcal{P}}_n^\uparrow\right)d\bar{\xi}_{k_3}\left(\prod_{n=k_3-1}^0 d\bar{\xi}_n^* d\bar{\xi}_n \bar{O}_n^\uparrow\right)\bar{\xi}_{k_3}[-\mathrm{g}_+^{*\uparrow}(t_{k_3}-t_{k_1})]\xi_{k_1}^*$$

$$\times d\bar{\psi}_{N+1}\,\bar{\psi}_{N+1}d\psi_{N+1}^*\psi_{N+1}^*\left(\prod_{n=0}^N d\bar{\psi}_n^* d\bar{\psi}_n \bar{O}_n^\downarrow\right)\left(\prod_{n=0}^{k_2-1} d\psi_n^* d\psi_n O_n^\downarrow\right)d\psi_{k_2}^*$$

$$\times\left(\prod_{n=k_2+1}^{k_4} d\psi_{n-1}d\psi_n^*\mathcal{P}_n^\downarrow\mathcal{U}_n\right)d\psi_{k_4}\left(\prod_{n=k_4+1}^N d\psi_n^* d\psi_n O_n^\downarrow\right)\psi_{k_4}[-\mathrm{g}_+^{*\downarrow}(t_{k_4}-t_{k_2})]\psi_{k_2}^* .$$

$$\text{(F15)}$$

Now, since (see Eq. (F14))

$$\prod_n d\xi_n^* d\xi_n O_n = \prod_n d\xi_n^* d\xi_n e^{-\bar{\xi}_n^*\bar{\xi}_n} = 1$$

$$\text{and}\qquad \prod_n d\xi_{n-1}d\xi_n^*\mathcal{P}_n = \prod_n d\xi_{n-1}d\xi_n^* e^{\xi_n^*\xi_{n-1}p_n} = \prod_n p_n ,$$

$$\text{(F16)}$$

we get

$$J_{(f),10,00}^{(2)}(t;t_0) = \int_{t_0}^t dt_{k_4}\cdots\int_{t_0}^{t_{k_2}} dt_{k_1}\prod_{n=k_1+1}^N p_n^\uparrow\prod_{n=k_2+1}^{k_4}(p_n^\downarrow+u_n)\prod_{n=k_3+1}^N p_n^{\uparrow*}[-\mathrm{g}_+^{\uparrow*}(t_{k_3}-t_{k_1})][-\mathrm{g}_+^{\downarrow*}(t_{k_4}-t_{k_2})]$$

$$\times\int d\bar{\xi}_{N+1}d\xi_{N+1}^* d\xi_{k_1}^* d\xi_N \mathcal{P}_{N+1}^\uparrow \bar{\mathcal{P}}_{N+1}^\uparrow d\bar{\xi}_N^* d\bar{\xi}_{k_3}\bar{\xi}_{k_3}\xi_{k_1}^*$$

$$\times d\bar{\psi}_{N+1}\,\bar{\psi}_{N+1}d\psi_{N+1}^*\psi_{N+1}^* d\psi_{k_2}^* d\psi_{k_4}\psi_{k_4}\psi_{k_2}^*$$

$$= -\int_{t_0}^t dt_{k_4}\cdots\int_{t_0}^{t_{k_2}} dt_{k_1}\prod_{n=k_1+1}^{N+1} p_n^\uparrow\prod_{n=k_2+1}^{k_4}(p_n^\downarrow+u_n)\prod_{n=k_3+1}^{N+1} p_n^{\uparrow*}[-\mathrm{g}_+^{\uparrow*}(t_{k_3}-t_{k_1})][-\mathrm{g}_+^{\downarrow*}(t_{k_4}-t_{k_2})]$$

$$\times\int d\xi_{k_1}^* d\bar{\xi}_{k_3}\bar{\xi}_{k_3}\xi_{k_1}^* d\psi_{k_2}^* d\psi_{k_4}\psi_{k_4}\psi_{k_2}^*$$

$$= -\int_{t_0}^t dt_4\cdots\int_{t_0}^{t_2} dt_1\, e^{-\frac{i}{\hbar}\epsilon_\uparrow(t_3-t_1)}e^{-\frac{i}{\hbar}(\epsilon_\downarrow+U)(t_4-t_2)}[-\mathrm{g}_+^{\uparrow*}(t_3-t_1)][-\mathrm{g}_+^{\downarrow*}(t_4-t_2)] ,$$

$$\text{(F17)}$$

where we have used Eq. (F6) and the properties that couples of Grassmann variables commute with other Grassmann variables and that variables belonging to different spins anticommute.

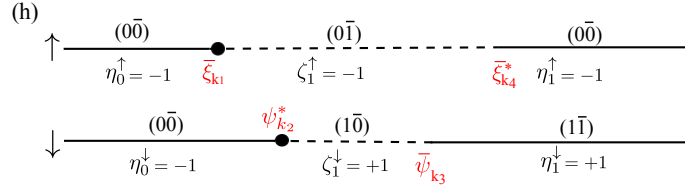Next we consider the process depicted in Fig. 30, which contributes to $\rho_{11,11}$. As above, we have

FIG. 30. Path with four transitions distributed in the two sub-paths of the spin variables $\uparrow$ and $\downarrow$. Note that the sub-paths are both of the type (c) in Fig. 27.

$$J_{(g)11,00}^{(2)}(t;t_0) = \Pi_b^\uparrow(1)\Pi_b^\downarrow(1)\Pi_a^{\downarrow*}(1)\Pi_a^{\uparrow*}(1)\int d^2\boldsymbol{\xi}_0 d^2\bar{\boldsymbol{\xi}}_0 \mathcal{J}_{(g)}^{(2)}(\boldsymbol{\xi}_a^*,\bar{\boldsymbol{\xi}}_b,t;\boldsymbol{\xi}_0,\bar{\boldsymbol{\xi}}_0^*,t_0)\langle\boldsymbol{\xi}_0|\mathbf{0}\rangle\langle\mathbf{0}|\bar{\boldsymbol{\xi}}_0\rangle$$

$$= \int_{t_0}^{t} dt_{k_4}\cdots\int_{t_0}^{t_{k_2}} dt_{k_1}\int d\bar{\xi}_{N+1}d\bar{\psi}_{N+1}\,d\psi_{N+1}^*d\xi_{N+1}^*\prod_{n=0}^{N}d^2\xi_n d^2\psi_n d^2\bar{\xi}_n d^2\bar{\psi}_n O_n^\uparrow O_n^\downarrow \bar{O}_n^\uparrow \bar{O}_n^\downarrow$$

$$\times \prod_{n=1}^{N+1}\mathcal{P}_n^\uparrow\mathcal{P}_n^\downarrow\bar{\mathcal{P}}_n^\uparrow\bar{\mathcal{P}}_n^\downarrow\mathcal{U}_n\bar{\mathcal{U}}_n\bar{\xi}_{k_3}[-\mathrm{g}_+^{\uparrow*}(t_{k_3}-t_{k_1})]\xi_{k_1}^*\bar{\psi}_{k_4}[-\mathrm{g}_+^{\downarrow*}(t_{k_4}-t_{k_2})]\psi_{k_2}^*$$

$$= \int_{t_0}^{t} dt_{k_4}\cdots\int_{t_0}^{t_{k_2}} dt_{k_1}\int d\bar{\xi}_{N+1}d\xi_{N+1}^*\left(\prod_{n=0}^{k_1-1}d\xi_n^*d\xi_n O_n^\uparrow\right)d\xi_{k_1}^*\left(\prod_{n=k_1+1}^{N}d\xi_{n-1}d\xi_n^*\mathcal{P}_n^\uparrow\right)d\xi_N \mathcal{P}_{N+1}^\uparrow$$

$$\times \bar{\mathcal{P}}_{N+1}^\uparrow d\bar{\xi}_N^*\left(\prod_{n=N}^{k_3+1}d\bar{\xi}_n d\bar{\xi}_{n-1}^*\bar{\mathcal{P}}_n^\uparrow\right)d\bar{\xi}_{k_3}\left(\prod_{n=k_3-1}^{0}d\bar{\xi}_n^*d\bar{\xi}_n \bar{O}_n^\uparrow\right)\bar{\xi}_{k_3}[-\mathrm{g}_+^{\uparrow*}(t_{k_3}-t_{k_1})]\xi_{k_1}^*$$

$$\times d\bar{\psi}_{N+1}d\psi_{N+1}^*\left(\prod_{n=0}^{k_2-1}d\psi_n^*d\psi_n O_n^\downarrow\right)d\psi_{k_2}^*\left(\prod_{n=k_2+1}^{N}d\psi_{n-1}d\psi_n^*\mathcal{P}_n^\downarrow\mathcal{U}_n\right)d\psi_N\mathcal{P}_{N+1}^\downarrow\mathcal{U}_{N+1}$$

$$\times \bar{\mathcal{P}}_{N+1}^\downarrow\bar{\mathcal{U}}_{N+1}d\bar{\psi}_N^*\left(\prod_{n=N}^{k_4+1}d\bar{\psi}_n d\bar{\psi}_{n-1}^*\bar{\mathcal{P}}_n^\downarrow\bar{\mathcal{U}}_n\right)d\bar{\psi}_{k_4}\left(\prod_{n=k_4-1}^{0}d\bar{\psi}_n^*d\bar{\psi}_n\bar{O}_n^\downarrow\right)\bar{\psi}_{k_4}[-\mathrm{g}_+^{\downarrow*}(t_{k_4}-t_{k_2})]\psi_{k_2}^* \,.$$

(F18)

Again we use the definitions of $\mathcal{P}_n$ and $\mathcal{O}_n$ to integrate out the terms in parenthesis and get

$$J_{(g)11,00}^{(2)}(t;t_0) = \int_{t_0}^{t} dt_{k_4}\cdots\int_{t_0}^{t_{k_2}} dt_{k_1}\prod_{n=k_1+1}^{N}p_n^\uparrow\prod_{n=k_2+1}^{N}(p_n^\downarrow+u_n)\prod_{n=k_3+1}^{N}p_n^{\uparrow*}\prod_{n=k_4+1}^{N}(p_n^{\downarrow*}+u_n^*)$$

$$\times [-\mathrm{g}_+^{\uparrow*}(t_{k_3}-t_{k_1})][-\mathrm{g}_+^{\downarrow*}(t_{k_4}-t_{k_2})]$$

$$\times \int d\bar{\xi}_{N+1}d\xi_{N+1}^*d\xi_{k_1}^*d\xi_N\mathcal{P}_{N+1}^\uparrow\bar{\mathcal{P}}_{N+1}^\uparrow d\bar{\xi}_N^*d\bar{\xi}_{k_3}\bar{\xi}_{k_3}\xi_{k_1}^*$$

$$\times d\bar{\psi}_{N+1}d\psi_{N+1}^*d\psi_{k_2}^*d\psi_N\mathcal{P}_{N+1}^\downarrow\mathcal{U}_{N+1}\bar{\mathcal{P}}_{N+1}^\downarrow\bar{\mathcal{U}}_{N+1}d\bar{\psi}_N^*d\bar{\psi}_{k_4}\bar{\psi}_{k_4}\psi_{k_2}^*$$

$$= \int_{t_0}^{t} dt_{k_4}\cdots\int_{t_0}^{t_{k_2}} dt_{k_1}\prod_{n=k_1+1}^{N+1}p_n^\uparrow\prod_{n=k_2+1}^{N+1}(p_n^\downarrow+u_n)\prod_{n=k_3+1}^{N+1}p_n^{\uparrow*}\prod_{n=k_4+1}^{N+1}(p_n^{\downarrow*}+u_n^*)$$

$$\times [-\mathrm{g}_+^{\uparrow*}(t_{k_3}-t_{k_1})][-\mathrm{g}_+^{\downarrow*}(t_{k_4}-t_{k_2})]\int d\xi_{k_1}^*d\bar{\xi}_{k_3}\bar{\xi}_{k_3}\xi_{k_1}^*d\psi_{k_2}^*d\bar{\psi}_{k_4}\bar{\psi}_{k_4}\psi_{k_2}^*$$

$$= \int_{t_0}^{t} dt_4\cdots\int_{t_0}^{t_2} dt_1\, e^{-\frac{i}{\hbar}\epsilon_\uparrow(t_3-t_1)}e^{-\frac{i}{\hbar}(\epsilon_\downarrow+U)(t_4-t_2)}[-\mathrm{g}_+^{\uparrow*}(t_3-t_1)][-\mathrm{g}_+^{\downarrow*}(t_4-t_2)] \,.$$

(F19)

It is already apparent that the interaction is present in the time intervals where both spin states are occupied either in the forward or in the backward branch. Simultaneous double occupation in the two branches, as it is the case for the sojourn states (11,11), leads to a cancellation due to the sum of u_n and u_n^* at the exponent. To better clarify this

(h)

FIG. 31. Path with four transitions distributed in the two sub-paths of the spin variables $\uparrow$ and $\downarrow$. Note that the sub-path $\sigma = \; \uparrow$ is of the type (b) in Fig. 26, while $\sigma = \; \downarrow$ undergoes a sequence of the type (c), see Fig. 27.

point, consider the example in Fig. (31). This path contributes to $J^{(2)}_{01,00}(t;t_0)$, the contribution being

$$
\begin{aligned}
J^{(2)}_{(h)01,00}(t;t_0) =& \Pi^{\uparrow}_b(0)\Pi^{\downarrow}_b(1)\Pi^{\downarrow*}_a(1)\Pi^{\uparrow*}_a(0)\int d^2\boldsymbol{\xi}_0 d^2\bar{\boldsymbol{\xi}}_0 \mathcal{J}^{(2)}_{(h)}(\boldsymbol{\xi}^*_a,\bar{\boldsymbol{\xi}}_b,t;\boldsymbol{\xi}_0,\bar{\boldsymbol{\xi}}^*_0,t_0)\langle\boldsymbol{\xi}_0|\mathbf{0}\rangle\langle\mathbf{0}|\bar{\boldsymbol{\xi}}_0\rangle \\
=& \int_{t_0}^{t} dt_{k_4}\cdots\int_{t_0}^{t_{k_2}} dt_{k_1}\ \int d\bar{\xi}_{N+1}\bar{\xi}_{N+1}d\bar{\psi}_{N+1}\ d\psi^*_{N+1}d\xi^*_{N+1}\xi^*_{N+1}\prod_{n=0}^{N}d^2\xi_n d^2\psi_n d^2\bar{\xi}_n d^2\bar{\psi}_n O^{\uparrow}_n O^{\downarrow}_n \bar{O}^{\uparrow}_n \bar{O}^{\downarrow}_n \\
& \times \prod_{n=1}^{N+1}\mathcal{P}^{\uparrow}_n\mathcal{P}^{\downarrow}_n\bar{\mathcal{P}}^{\uparrow}_n\bar{\mathcal{P}}^{\downarrow}_n\mathcal{U}_n\bar{\mathcal{U}}_n\bar{\xi}^*_{k_4}\mathrm{g}^{\uparrow}_+(t_{k_4}-t_{k_1})\bar{\xi}_{k_1}\bar{\psi}_{k_3}[-1\mathrm{g}^{\downarrow*}_+(t_{k_3}-t_{k_2})]\psi^*_{k_2} \\
=& \int_{t_0}^{t} dt_{k_4}\cdots\int_{t_0}^{t_{k_2}} dt_{k_1}\ \int d\xi^*_{N+1}d\bar{\xi}_{N+1}\bar{\xi}_{N+1}\xi^*_{N+1}\left(\prod_{n=0}^{N}d\xi^*_n d\xi_n O^{\uparrow}_n\right)\left(\prod_{n=N}^{k_4+1}d\bar{\xi}^*_n d\bar{\xi}_n \bar{O}^{\uparrow}_n\right)d\bar{\xi}^*_{k_4} \\
& \times \left(\prod_{n=k_4}^{k_1+1}d\bar{\xi}_n d\bar{\xi}^*_{n-1}\bar{\mathcal{P}}^{\uparrow}_n\right)d\bar{\xi}_1\left(\prod_{n=k_1-1}^{0}d\bar{\xi}^*_n d\bar{\xi}_n \bar{O}^{\uparrow}_n\right)\bar{\xi}^*_{k_4}[-\mathrm{g}^{\uparrow}_+(t_{k_4}-t_{k_1})]\bar{\xi}_{k_1} \\
& \times d\psi^*_{N+1}d\bar{\psi}_{N+1}\left(\prod_{n=0}^{k_2-1}d\psi^*_n d\psi_n O^{\downarrow}_n\right)d\psi^*_{k_2}\left(\prod_{n=k_2+1}^{N}d\psi_{n-1}d\psi^*_n \mathcal{P}^{\downarrow}_n\right)d\psi_N \mathcal{P}^{\downarrow}_{N+1} \\
& \times d\bar{\psi}^*_N\bar{\mathcal{P}}^{\downarrow}_{N+1}\left(\prod_{n=N}^{k_3+1}d\bar{\psi}_n d\bar{\psi}^*_{n-1}\bar{\mathcal{P}}^{\downarrow}_n\right)d\bar{\psi}_{k_3}\left(\prod_{n=k_3-1}^{0}d\bar{\psi}^*_n d\bar{\psi}_n \bar{O}^{\downarrow}_n\right)\prod_{n=k_3+1}^{k_4}\bar{\mathcal{U}}_n \\
& \times \bar{\psi}_{k_3}[-\mathrm{g}^{\downarrow*}_+(t_{k_3}-t_{k_2})]\psi^*_{k_2}\ .
\end{aligned}
$$

$$(F20)$$

Once the trivial integrations are carried out as before, we are left with

$$
\begin{aligned}
J^{(2)}_{(h)01,00}(t;t_0) =& \int_{t_0}^{t} dt_{k_4}\cdots\int_{t_0}^{t_{k_2}} dt_{k_1}\prod_{n=k_2+1}^{N}p^{\downarrow}_n\prod_{n=k_1+1}^{k_4}p^{\uparrow*}_n\prod_{n=k_3+1}^{k_4}(p^{\downarrow*}_n+u^*_n)\prod_{n=k_4+1}^{N}p^{\downarrow*}_n[-\mathrm{g}^{\uparrow}_+(t_{k_4}-t_{k_1})][-\mathrm{g}^{\downarrow*}_+(t_{k_3}-t_{k_2})] \\
& \times \int d\xi^*_{N+1}d\bar{\xi}_{N+1}\bar{\xi}_{N+1}\xi^*_{N+1}d\bar{\xi}^*_{k_4}d\bar{\xi}_1\bar{\xi}^*_{k_4}\bar{\xi}_{k_1}d\psi^*_{N+1}d\bar{\psi}_{N+1}d\psi^*_{k_2}d\psi_N \mathcal{P}^{\downarrow}_{N+1}d\bar{\psi}^*_N\bar{\mathcal{P}}^{\downarrow}_{N+1}d\bar{\psi}_{k_3}\bar{\psi}_{k_3}\psi^*_{k_2} \\
=& \int_{t_0}^{t} dt_{k_4}\cdots\int_{t_0}^{t_{k_2}} dt_{k_1}\prod_{n=k_2+1}^{N+1}p^{\downarrow}_n\prod_{n=k_1+1}^{k_4}p^{\uparrow*}_n\prod_{n=k_3+1}^{k_4}(p^{\downarrow*}_n+u^*_n)\prod_{n=k_4+1}^{N+1}p^{\downarrow*}_n[-\mathrm{g}^{\uparrow}_+(t_{k_4}-t_{k_1})][-\mathrm{g}^{\downarrow*}_+(t_{k_3}-t_{k_2})] \\
& \times \int d\bar{\xi}^*_{k_4}d\bar{\xi}_1\bar{\xi}^*_{k_4}\bar{\xi}_{k_1}d\psi^*_{k_2}d\bar{\psi}_{k_3}\bar{\psi}_{k_3}\psi^*_{k_2} \\
=& -\int_{t_0}^{t} dt_4\cdots\int_{t_0}^{t_2} dt_1\ e^{\frac{i}{\hbar}\epsilon_{\uparrow}(t_4-t_1)}e^{-\frac{i}{\hbar}\epsilon_{\downarrow}(t_3-t_2)}e^{\frac{i}{\hbar}U(t_4-t_3)}[-\mathrm{g}^{\uparrow}_+(t_4-t_1)][-\mathrm{g}^{\downarrow*}_+(t_3-t_2)]\ .
\end{aligned}
$$

$$(F21)$$

In the above examples the phase factors stemming from the action of the dot have been factorized as $\prod_{j=1}^{n}\exp[-\frac{i}{\hbar}E_j\tau_j]$ in order to reflect the time intervals τ_j between transitions. One can recognize that these phase factors are related to the blip/sojourn states of the underlying spin paths according to the example in Fig. 7.

Appendix G: Integration measure $\int \mathcal{D}\{\xi\}$

To see how the parametrization of the integrals over the Grassmann variables associated to the transition times works, consider the example of path shown in Fig. 32(b). Following Eq. (46), the integration measure reads
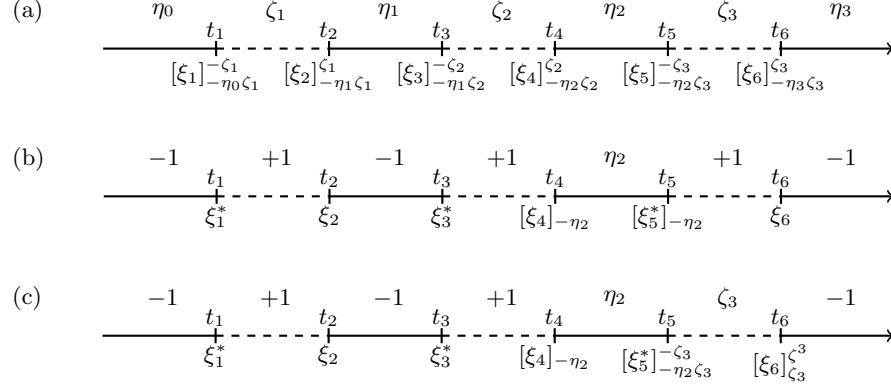
FIG. 32. Six-transition path. General case (a) and two specific examples: In the first η_2 is left unspecified while $\eta_0 = \eta_1 = \eta_3 = -1$ and $\zeta_1 = \zeta_2 = \zeta_3 = +1$ (b). In the second also ζ_3 is left unspecified (c).

$$
\begin{aligned}
&- \eta_2 d\xi_1^* d\xi_2 d\xi_3^* (d\xi_4)_{-\eta_2} (d\xi_5^*)_{-\eta_2} d\xi_6 \\
&= \begin{cases} d\xi_1^* d\xi_2 d\xi_3^* d\xi_4 d\xi_5^* d\xi_6 \ , & \eta_2 = -1 \\ d\xi_1^* d\xi_2 d\xi_3^* d\xi_6 d\bar{\xi}_5^* d\bar{\xi}_4 \ , & \eta_2 = +1 \end{cases}
\end{aligned}
\tag{G1}
$$
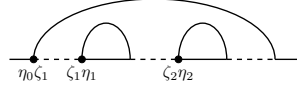
As a further example, we leave also ζ_3 unspecified, see Fig. 32(c), so that the integration measure reads

$$
\begin{aligned}
&- \eta_2 \zeta_3 d\xi_1^* d\xi_2 d\xi_3^* (d\xi_4)_{-\eta_2} (d\xi_5)_{-\eta_2 \zeta_3}^{-\xi_3} (d\xi_6)_{\zeta_3}^{\zeta_3} \\
&= \begin{cases} d\xi_1^* d\xi_2 d\xi_3^* d\xi_4 d\xi_5^* d\xi_6 \ , & \eta_2 = -1, \zeta_3 = +1 \\ d\xi_1^* d\xi_2 d\xi_3^* d\xi_6 d\bar{\xi}_5^* d\bar{\xi}_4 \ , & \eta_2 = +1, \zeta_3 = +1 \\ d\xi_1^* d\xi_2 d\xi_3^* d\xi_4 d\bar{\xi}_6^* d\bar{\xi}_5 \ , & \eta_2 = -1, \zeta_3 = -1 \\ d\xi_1^* d\xi_2 d\xi_3^* d\xi_5 d\bar{\xi}_6^* d\bar{\xi}_4 \ , & \eta_2 = +1, \zeta_3 = -1 \end{cases}
\end{aligned}
\tag{G2}
$$
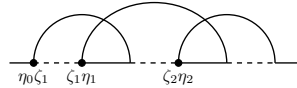
Carrying out an integration over the Grassmann variables associated to the tunneling transitions is straightforward in the present derivation: The integral yields simply an overall sign, due to the order of the variables to be integrated, times the factors $(-\eta_k \zeta_k)$.

Appendix H: Further examples of diagrammatic contributions from an individual state

For the sake of compactness, in the following expressions we set $(t_j - t_i) \equiv (j, i)$. Then, the ten third-order irreducible diagrammatic contributions $\mathcal{B}^i_{m_i}(\mathcal{P}_i)\Phi^i_{m_i}(\mathcal{P}_i)$, see Eq. (40), take the form

$$(+1)\prod_{n=1}^{3}(-\zeta_n\eta_n)\ [\eta_0\zeta_1 g_{-\eta_0}^{-\zeta_1}(6,1)]b_{61}\ [\zeta_1\eta_1 g_{\eta_1}^{\zeta_1}(3,2)]b_{32}\ [\zeta_2\eta_2 g_{\eta_2}^{\zeta_2}(5,4)]b_{54}\ \delta_{\zeta_3,\zeta_1}\delta_{\zeta_2,\zeta_1}$$

$$= \eta'\eta\ [-g_{-\eta}^{-\zeta_1}(6,1)]b_{61}\ [-g_{\eta_1}^{\zeta_1}(3,2)]b_{32}\ [-g_{\eta_2}^{\zeta_1}(5,4)]b_{54}\ \delta_{\zeta_3,\zeta_1}\delta_{\zeta_2,\zeta_1}\ ,$$

$$(-1)\prod_{n=1}^{3}(-\zeta_n\eta_n)\ [\eta_0\zeta_1 g_{-\eta_0}^{-\zeta_1}(5,1)]b_{51}\ [\zeta_1\eta_1 g_{\eta_1}^{\zeta_1}(3,2)]b_{32}\ [\zeta_2\eta_2 g_{\eta_2}^{\zeta_2}(6,4)]b_{64}\ \delta_{\zeta_3,-\zeta_1}\delta_{\zeta_2,\zeta_1}$$

$$= \eta'\eta\ [-g_{-\eta}^{-\zeta_1}(5,1)]b_{51}\ [-g_{\eta_1}^{\zeta_1}(3,2)]b_{32}\ [-g_{\eta_2}^{\zeta_1}(6,4)]b_{64}\ \delta_{\zeta_3,-\zeta_1}\delta_{\zeta_2,\zeta_1}\ ,$$

$$(-1)\prod_{n=1}^{3}(-\zeta_n\eta_n)\ [\eta_0\zeta_1 g_{-\eta_0}^{-\zeta_1}(3,1)]b_{31}\ [\zeta_1\eta_1 g_{\eta_1}^{\zeta_1}(6,2)]b_{62}\ [\zeta_2\eta_2 g_{\eta_2}^{\zeta_2}(5,4)]b_{54}\ \delta_{\zeta_3,-\zeta_1}\delta_{\zeta_2,\zeta_1}$$

$$= \eta'\eta\ [-g_{-\eta}^{-\zeta_1}(3,1)]b_{31}\ [-g_{\eta_1}^{\zeta_1}(6,2)]b_{62}\ [-g_{\eta_2}^{\zeta_1}(5,4)]b_{54}\ \delta_{\zeta_3,-\zeta_1}\delta_{\zeta_2,\zeta_1}\ ,$$

$$(\text{H1})$$
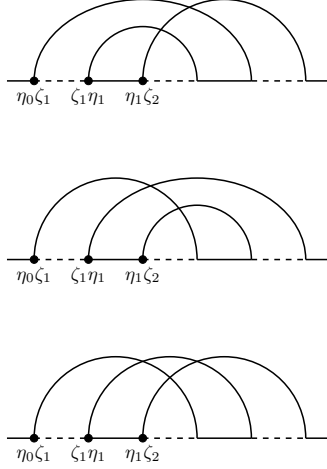
$$(+1)\prod_{n=1}^{3}(-\zeta_n\eta_n)\ [\eta_0\zeta_1 g_{-\eta_0}^{-\zeta_1}(3,1)]b_{31}\ [\zeta_1\eta_1 g_{\eta_1}^{\zeta_1}(5,2)]b_{52}\ [\zeta_2\eta_2 g_{\eta_2}^{\zeta_2}(6,4)]b_{64}\ \delta_{\zeta_3,\zeta_1}\delta_{\zeta_3,-\zeta_2}$$

$$= \eta'\eta\ [-g_{-\eta}^{-\zeta_1}(3,1)]b_{31}\ [-g_{\eta_1}^{\zeta_1}(5,2)]b_{52}\ [-g_{\eta_2}^{-\zeta_1}(6,4)]b_{64}\ \delta_{\zeta_3,\zeta_1}\delta_{\zeta_2,-\zeta_1}\ ,$$

$$(\text{H2})$$
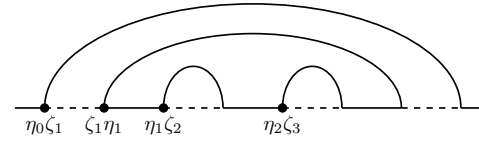
$$\prod_{k=1}^{3}(-\zeta_k\eta_k)[\eta_0\zeta_1\ g_{-\eta_0}^{-\zeta_1}(6,1)]b_{61}\ [\zeta_1\eta_1 g_{\eta_1}^{\zeta_1}(5,2)]b_{52}\ [\eta_1\zeta_2 g_{-\eta_1}^{-\zeta_2}(4,3)]b_{43}\delta_{\zeta_3,\zeta_1}$$

$$= \eta'\eta\eta_1\eta_2\ [-g_{-\eta}^{-\zeta_1}(6,1)]b_{61}\ [-g_{\eta_1}^{\zeta_1}(5,2)]b_{52}[-g_{-\eta_1}^{-\zeta_2}(4,3)]b_{43}\delta_{\zeta_3,\zeta_1}\ ,$$

$$(-1)\prod_{k=1}^{3}(-\zeta_k\eta_k)[\eta_0\zeta_1\ g_{-\eta_0}^{-\zeta_1}(6,1)]b_{61}\ [\zeta_1\eta_1 g_{\eta_1}^{\zeta_1}(4,2)]b_{42}\ [\eta_1\zeta_2 g_{-\eta_1}^{-\zeta_2}(5,3)]b_{53}\delta_{\zeta_3,-\zeta_2}\delta_{\zeta_2,-\zeta_1}$$

$$= -\eta'\eta\eta_1\eta_2\ [-g_{-\eta}^{-\zeta_1}(6,1)]b_{61}\ [-g_{\eta_1}^{\zeta_1}(4,2)]b_{42}[-g_{-\eta_1}^{-\zeta_2}(5,3)]b_{53}\ \delta_{\zeta_3,\zeta_1}\delta_{\zeta_2,-\zeta_1}\ ,$$

$$(-1)\prod_{k=1}^{3}(-\zeta_k\eta_k)[\eta_0\zeta_1\ g_{-\eta_0}^{-\zeta_1}(5,1)]b_{51}\ [\zeta_1\eta_1 g_{\eta_1}^{\zeta_1}(6,2)]b_{62}\ [\eta_1\zeta_2 g_{-\eta_1}^{-\zeta_2}(4,3)]b_{43}\delta_{\zeta_3,-\zeta_1}$$

$$= \eta'\eta\eta_1\eta_2\ [-g_{-\eta}^{-\zeta_1}(5,1)]b_{51}\ [-g_{\eta_1}^{\zeta_1}(6,2)]b_{62}[-g_{-\eta_1}^{-\zeta_2}(4,3)]b_{43}\ \delta_{\zeta_3,-\zeta_1}\ ,$$

$$(\text{H3})$$

$$(+1)\prod_{k=1}^{3}(-\zeta_k\eta_k)[\eta_0\zeta_1 \; g_{-\eta_0}^{-\zeta_1}(5,1)]b_{51} \; [\zeta_1\eta_1 g_{\eta_1}^{\zeta_1}(4,2)]b_{42} \; [\eta_1\zeta_2 g_{-\eta_1}^{-\zeta_2}(6,3)]b_{63}\delta_{\zeta_3,-\zeta_1}\delta_{\zeta_2,-\zeta_1}$$

$$= -\eta'\eta\eta_1\eta_2 \; [-g_{-\eta}^{-\zeta_1}(5,1)]b_{51} \; [-g_{\eta_1}^{\zeta_1}(4,2)]b_{42}[-g_{-\eta_1}^{-\zeta_2}(6,3)]b_{63} \; \delta_{\zeta_3,-\zeta_1} \; \delta_{\zeta_2,-\zeta_1} \; ,$$

$$(+1)\prod_{k=1}^{3}(-\zeta_k\eta_k)[\eta_0\zeta_1 \; g_{-\eta_0}^{-\zeta_1}(4,1)]b_{41} \; [\zeta_1\eta_1 g_{\eta_1}^{\zeta_1}(6,2)]b_{62} \; [\eta_1\zeta_2 g_{-\eta_1}^{-\zeta_2}(5,3)]b_{53}\delta_{\zeta_3,-\zeta_1}\delta_{\zeta_2,\zeta_1}$$

$$= -\eta'\eta\eta_1\eta_2 \; [-g_{-\eta}^{-\zeta_1}(4,1)]b_{41} \; [-g_{\eta_1}^{\zeta_1}(6,2)]b_{62}[-g_{-\eta_1}^{-\zeta_1}(5,3)]b_{53} \; \delta_{\zeta_3,-\zeta_1} \; \delta_{\zeta_2,\zeta_1} \; ,$$

$$(-1)\prod_{k=1}^{3}(-\zeta_k\eta_k)[\eta_0\zeta_1 \; g_{-\eta_0}^{-\zeta_1}(3,1)]b_{31} \; [\zeta_1\eta_1 g_{\eta_1}^{\zeta_1}(4,2)]b_{52} \; [\eta_1\zeta_2 g_{-\eta_1}^{-\zeta_2}(6,3)]b_{63}\delta_{\zeta_3,\zeta_2}\delta_{\zeta_2,\zeta_1}$$

$$= -\eta'\eta\eta_1\eta_2[-g_{-\eta}^{-\zeta_1}(4,1)]b_{41} \; [-g_{\eta_1}^{\zeta_1}(5,2)]b_{52} \; [-g_{-\eta_1}^{-\zeta_1}(6,3)]b_{63}\delta_{\zeta_3,\zeta_1}\delta_{\zeta_2,\zeta_1} \; .$$

(H4)

We also evaluate the following irreducible fourth-order diagram, which is relevant for the scheme gDSO4 introduced in Sec. IX E,

(H5)

$$(+1)\prod_{k=1}^{4}(-\zeta_k\eta_k) \; [\eta_0\zeta_1 g_{-\eta_0}^{-\zeta_1}(8,1)]b_{81} \; [\zeta_1\eta_1 g_{\eta_1}^{\zeta_1}(7,2)]b_{72} \; [\eta_1\zeta_2 g_{-\eta_1}^{-\zeta_2}(4,3)]b_{43} \; [\eta_2\zeta_3 g_{-\eta_2}^{-\zeta_3}(6,5)]b_{65} \; \delta_{\zeta_4,\zeta_1}$$

$$= \eta'\eta\eta_1\eta_3 \; [-g_{-\eta}^{-\zeta_1}(8,1)]b_{81} \; [-g_{\eta_1}^{\zeta_1}(7,2)]b_{72} \; [-g_{-\eta_1}^{-\zeta_2}(4,3)]b_{43} \; [-g_{-\eta_2}^{-\zeta_3}(6,5)]b_{65} \; \delta_{\zeta_4,\zeta_1} \; .$$

Appendix I: Contraction integrals in the wide-band limit

- Integral not involving the Fermi function ($\zeta = \pm 1$)

$$I_0(\mathcal{E}; \zeta) = \int_{-W}^{W} dx \frac{1}{x - \mathcal{E}' + i\zeta\, \mathcal{E}''}$$
$$\simeq -i\zeta\pi \qquad (W \gg \mathcal{E}').$$

- Integral involving $f_{-\eta}(x)$, where $\eta = \pm 1$, with $f_+(x) = [e^{\beta(x-\mu)}+1]^{-1}$ the Fermi function and $f_-(x) = 1 - f_+(x)$. Assume $\mathcal{E}$ independent of x, with $\mathcal{E}'' > 0$, and $W \gg \mathcal{E}', \mu$

$$
\begin{aligned}
I_+(\mathcal{E}) &= \int_{-W}^{W} d\epsilon \frac{f_+(\epsilon)}{\epsilon - \mathcal{E}' + i\mathcal{E}''} \\
&= \int_{-\bar{W}}^{\bar{W}} dx \frac{\bar{f}_+(x)}{x - (\mathcal{E}' - \mu)/k_B T + i\mathcal{E}''/k_B T} \qquad [\bar{f}_+(x) = (e^x + 1)^{-1}, \qquad \bar{W} \simeq W/k_B T] \\
&= 2\pi i \sum_j \text{Res}_j \left\{ \frac{\bar{f}_+(z)}{z - (\mathcal{E}' - \mu)/k_B T + i\mathcal{E}''/k_B T} \right\} \\
&= -2\pi i \sum_{k=0}^{k_{\bar{W}}} \frac{1}{2\pi i(k + 1/2) - (\mathcal{E}' - \mu)/k_B T + i\mathcal{E}''/k_B T} - i\frac{\pi}{2} \\
&= -\sum_{k=0}^{k_{\bar{W}}} \frac{1}{k + 1/2 + \mathcal{E}''/(2\pi k_B T) + i(\mathcal{E}' - \mu)/(2\pi k_B T)} - i\frac{\pi}{2}.
\end{aligned}
$$

Now, since $W \to \infty$, the sum can be extended to infinity. Following Ref. [48], if $\mathcal{E}$ is independent of ϵ, we single out the $k = 0$ term in the sum over k and add and subtract the Euler-Mascheroni constant $\gamma_E = \lim_{K\to\infty} \sum_{k=1}^{K} 1/k - \ln(K)$. At this point, using the definition of digamma function $\psi(z) = -\gamma_E - 1/z - \sum_{k=1}^{\infty} [1/(k+z) - 1/k]$, we obtain

$$
\begin{aligned}
I_+(\mathcal{E}) &= \text{Re}\psi\left(\frac{1}{2} + i\frac{\mathcal{E}' - i\mathcal{E}'' - \mu}{2\pi k_B T}\right) - \ln\frac{W}{2\pi k_B T} - i\left[\frac{\pi}{2} - \text{Im}\psi\left(\frac{1}{2} + i\frac{\mathcal{E}' - i\mathcal{E}'' - \mu}{2\pi k_B T}\right)\right] \\
I_-(\mathcal{E}) &= \int_{-W}^{W} dx \frac{f_-(x)}{x - \mathcal{E}' + i\mathcal{E}''} = \int_{-W}^{W} dx \frac{1 - f_+(x)}{x - \mathcal{E}' + i\mathcal{E}''} \\
&= -\text{Re}\psi\left(\frac{1}{2} + i\frac{\mathcal{E}' - i\mathcal{E}'' - \mu}{2\pi k_B T}\right) + \ln\frac{W}{2\pi k_B T} - i\left[\frac{\pi}{2} + \text{Im}\psi\left(\frac{1}{2} + i\frac{\mathcal{E}' - i\mathcal{E}'' - \mu}{2\pi k_B T}\right)\right],
\end{aligned}
$$

where we used Eq. (I1). Thus

$$
\begin{aligned}
I(\mathcal{E}; \eta) &= \int_{-W}^{W} dx \frac{f_{-\eta}(x)}{x - \mathcal{E}' + i\mathcal{E}''} \\
&= -\eta\left[\text{Re}\psi\left(\frac{1}{2} + i\frac{\mathcal{E}' - i\mathcal{E}'' - \mu}{2\pi k_B T}\right) - \ln\frac{W}{2\pi k_B T}\right] - i\left[\frac{\pi}{2} + \eta\text{Im}\psi\left(\frac{1}{2} + i\frac{\mathcal{E}' - i\mathcal{E}'' - \mu}{2\pi k_B T}\right)\right]
\end{aligned}
$$

Further

$$
\begin{aligned}
I^*(\mathcal{E}; \eta) &= \int_{-W}^{W} dx \frac{f_{-\eta}(x)}{x - \mathcal{E}' - i\mathcal{E}''} \\
&= -\eta\left[\text{Re}\psi\left(\frac{1}{2} + i\frac{\mathcal{E}' - i\mathcal{E}'' - \mu}{2\pi k_B T}\right) - \ln\frac{W}{2\pi k_B T}\right] + i\left[\frac{\pi}{2} + \eta\text{Im}\psi\left(\frac{1}{2} + i\frac{\mathcal{E}' - i\mathcal{E}'' - \mu}{2\pi k_B T}\right)\right]
\end{aligned}
$$

Then, collecting the above results we can give the **compact expression**

$$
\begin{aligned}
I(\mathcal{E}; \zeta, \eta) &= \int_{-W}^{W} dx \frac{f_{-\eta}(x)}{x - \mathcal{E}' + i\zeta\mathcal{E}''} \\
&= -\eta\left[\text{Re}\psi\left(\frac{1}{2} + i\frac{\mathcal{E}' - i\mathcal{E}'' - \mu}{2\pi k_B T}\right) - \ln\frac{W}{2\pi k_B T}\right] - i\zeta\left[\frac{\pi}{2} + \eta\text{Im}\psi\left(\frac{1}{2} + i\frac{\mathcal{E}' - i\mathcal{E}'' - \mu}{2\pi k_B T}\right)\right]
\end{aligned}
$$

(I1)

(I2)

(I3)

(I4)

(I5)

(I6)

- Special case: $\mathcal{E}'' = 0^+$.

$$\int_{-W}^{W} dx \frac{f_{-\eta}(x)}{x - \mathcal{E}' + i\zeta\, 0^+} = -\eta \left[\mathrm{Re}\psi \left(\frac{1}{2} + i\frac{\mathcal{E}' - \mu}{2\pi k_{\mathrm{B}}T} \right) - \ln \frac{W}{2\pi k_{\mathrm{B}}T} \right] - i\zeta\pi f_{-\eta}(\mathcal{E}') \,, \tag{I7}$$

see also Eq. (E1) of Ref. [48]. Here we used the property

$$\frac{1}{2} \mp \frac{1}{\pi}\mathrm{Im}\psi \left(\frac{1}{2} + i\frac{\mathcal{E}' - \mu}{2\pi k_{\mathrm{B}}T} \right) = f_{\pm}(\mathcal{E}') \tag{I8}$$

and also $f_{-\eta}(x) = \delta_{\eta,+1} - \eta f_{+}(x)$. Note that

$$\int_{-W}^{W} dx \frac{1}{x - \mathcal{E}' + i\zeta\, 0^+} = \sum_{\eta} \int_{-W}^{W} dx \frac{f_{-\eta}(x)}{x - \mathcal{E}' + i\zeta\, 0^+} = -i\zeta\pi \,,$$

in agreement with Eq. (I1).

- We assume that, in general, $\mathcal{E} = \mathcal{E}(\zeta, \eta)$ and consider the distinct cases $\mathcal{E}(\eta) = \mathcal{E}_{\eta}$ and $\mathcal{E}(\zeta) = \mathcal{E}_{\zeta}$. In the first case, summing over η

$$\begin{aligned}
\sum_{\eta} I(\mathcal{E}_{\eta}; \zeta, \eta) = {}& -\left[\mathrm{Re}\psi \left(\frac{1}{2} + i\frac{\mathcal{E}'_{+} - i\mathcal{E}''_{+} - \mu}{2\pi k_{\mathrm{B}}T} \right) - \mathrm{Re}\psi \left(\frac{1}{2} + i\frac{\mathcal{E}'_{-} - i\mathcal{E}''_{-} - \mu}{2\pi k_{\mathrm{B}}T} \right) \right] \\
& - i\zeta \left[\pi + \mathrm{Im}\psi \left(\frac{1}{2} + i\frac{\mathcal{E}'_{+} - i\mathcal{E}''_{+} - \mu}{2\pi k_{\mathrm{B}}T} \right) - \mathrm{Im}\psi \left(\frac{1}{2} + i\frac{\mathcal{E}'_{-} - i\mathcal{E}''_{-} - \mu}{2\pi k_{\mathrm{B}}T} \right) \right] \,.
\end{aligned} \tag{I9}$$

Note that if $\mathcal{E}$ is independent of η, then $\sum_{\eta} I(\mathcal{E}; \zeta, \eta) = -i\zeta\pi$. Likewise, when $\mathcal{E} = \mathcal{E}_{\zeta}$

$$\begin{aligned}
\sum_{\zeta} \zeta\, I(\mathcal{E}_{\zeta}; \zeta, \eta) = {}& -\eta \left[\mathrm{Re}\psi \left(\frac{1}{2} + i\frac{\mathcal{E}'_{+} - i\mathcal{E}''_{+} - \mu}{2\pi k_{\mathrm{B}}T} \right) - \mathrm{Re}\psi \left(\frac{1}{2} + i\frac{\mathcal{E}'_{-} - i\mathcal{E}''_{-} - \mu}{2\pi k_{\mathrm{B}}T} \right) \right] \\
& - i \left[\pi + \eta\mathrm{Im}\psi \left(\frac{1}{2} + i\frac{\mathcal{E}'_{+} - i\mathcal{E}''_{+} - \mu}{2\pi k_{\mathrm{B}}T} \right) + \eta\mathrm{Im}\psi \left(\frac{1}{2} + i\frac{\mathcal{E}'_{-} - i\mathcal{E}''_{-} - \mu}{2\pi k_{\mathrm{B}}T} \right) \right] \,.
\end{aligned} \tag{I10}$$

If $\mathcal{E}$ is independent of ζ, then $\sum_{\zeta} \zeta I(\mathcal{E}; \zeta, \eta) = 2i\zeta\mathrm{Im}I(\mathcal{E}; \zeta, \eta)$.

Appendix J: Evaluation of the dressed third-tier bubbles in the simplified gDSO4

The fermion lines are labeled as κ, κ_1, and κ_2, from the most external to the most internal. Recalling that $\eta \equiv \eta^{\bar\sigma}$, the third-tier bubble diagrams are obtained by contracting the internal fermion lines (κ_2) with a vertex. The 3rd-tier bubble of type $\sigma(\sigma)$ is the sum of bubbles of two kinds, according to the spin of the most internal fermion line. In the gDSO4 it is obtained by contracting the propagators in Eq. (225) dressed by the simplified bubbles $B_4 \sim -\Gamma/2$ with the vertex $v_{-x} = -|t_\alpha(\epsilon_k)|^2 f^\alpha_{-x}(\epsilon_k)/\hbar^2$, where x stands for η or ν. The result is

$$
\tilde{B}^{\sigma(\sigma)}_{3,\boldsymbol{\eta'\eta}} \simeq \quad \text{[diagram]} \quad + \quad \text{[diagram]}
$$

$$
= \sum_{\kappa_2} \frac{\hbar\, v^{\alpha_2}_{-\eta}(\epsilon_{k_2})\delta_{\nu'\nu}}{\Gamma/2 - i\zeta(\epsilon_k - \epsilon_{k_1}) - i\zeta_2[\epsilon_{k_2} - E_{\bar\sigma}(\nu)]} + \nu'\nu \sum_{\kappa_2} \frac{\hbar\, v^{\alpha}_{-\nu}(\epsilon_{k_2})\delta_{\eta'\eta}}{\Gamma/2 - i\zeta(\epsilon_k - \epsilon_{k_1}) - i\zeta_2[\epsilon_{k_2} - E_\sigma(\eta)]} \tag{J1}
$$

$$
= -\frac{i}{\hbar} \sum_{\alpha_2} \varrho_{\alpha_2}|t_{\alpha_2}|^2 \sum_{\zeta_2} \zeta_2 \int_{-W}^{W} d\epsilon_2 \frac{f^{\alpha_2}_{-\eta}(\epsilon_2)\delta_{\nu'\nu}}{\epsilon_2 - [E_{\bar\sigma}(\nu) - \zeta_2\zeta(\epsilon-\epsilon_1)] + i\zeta_2\Gamma/2}
$$

$$
- \nu'\nu \frac{i}{\hbar} \sum_{\alpha_2} \varrho_{\alpha_2}|t_{\alpha_2}|^2 \sum_{\zeta_2} \zeta_2 \int_{-W}^{W} d\epsilon_2 \frac{f^{\alpha_2}_{-\nu}(\epsilon_2)\delta_{\eta'\eta}}{\epsilon_2 - [E_\sigma(\eta) - \zeta_2\zeta(\epsilon-\epsilon_1)] + i\zeta_2\Gamma/2} \ ,
$$

where $E_{\bar\sigma}(\nu) = \epsilon_{\bar\sigma} + (1+\nu)U/2$ and $E_\sigma(\eta) = \epsilon_\sigma + (1+\eta)U/2$. Here, the vertex $v_\eta(\boldsymbol{\kappa})$ is defined in Eq. (153) and the width $\Gamma/2\hbar$ is given by summing the geometrical series

$$
\text{[diagram]} = \text{[diagram]} + \text{[diagram]} + \text{[diagram]} + \quad \dots \tag{J2}
$$

where each of the bubble is evaluated to be $B_4 = -\Gamma/(2\hbar)$. The resulting internal dressing is indicated as the dashed rectangle. Using Eq. (I6) to solve the integrals we obtain

$$
\tilde{B}^{\sigma(\sigma)}_{3,\boldsymbol{\eta'\eta}} \simeq \frac{i}{\hbar}\delta_{\nu'\nu} \sum_\alpha \frac{\Gamma_\alpha}{2\pi}\Bigg\{ \eta\bigg[\mathrm{Re}\psi\left(\frac{1}{2} + i\frac{\zeta(\epsilon_1-\epsilon) + E_{\bar\sigma}(\nu) - i\Gamma/2 - \mu_\alpha}{2\pi k_B T}\right) - \mathrm{Re}\psi\left(\frac{1}{2} + i\frac{\zeta(\epsilon-\epsilon_1) + E_{\bar\sigma}(\nu) - i\Gamma/2 - \mu_\alpha}{2\pi k_B T}\right)\bigg]
$$

$$
+ i\bigg[\pi + \eta\mathrm{Im}\psi\left(\frac{1}{2} + i\frac{\zeta(\epsilon_1-\epsilon) + E_{\bar\sigma}(\nu) - i\Gamma/2 - \mu_\alpha}{2\pi k_B T}\right) + \eta\mathrm{Im}\psi\left(\frac{1}{2} + i\frac{\zeta(\epsilon-\epsilon_1) + E_{\bar\sigma}(\nu) - i\Gamma/2 - \mu_\alpha}{2\pi k_B T}\right)\bigg]\Bigg\}
$$

$$
+ \nu'\nu\frac{i}{\hbar}\delta_{\eta'\eta} \sum_\alpha \frac{\Gamma_\alpha}{2\pi}\Bigg\{ \nu\bigg[\mathrm{Re}\psi\left(\frac{1}{2} + i\frac{\zeta(\epsilon_1-\epsilon) + E_\sigma(\eta) - i\Gamma/2 - \mu_\alpha}{2\pi k_B T}\right) - \mathrm{Re}\psi\left(\frac{1}{2} + i\frac{\zeta(\epsilon-\epsilon_1) + E_\sigma(\eta) - i\Gamma/2 - \mu_\alpha}{2\pi k_B T}\right)\bigg]
$$

$$
+ i\bigg[\pi + \nu\mathrm{Im}\psi\left(\frac{1}{2} + i\frac{\zeta(\epsilon_1-\epsilon) + E_\sigma(\eta) - i\Gamma/2 - \mu_\alpha}{2\pi k_B T}\right) + \nu\mathrm{Im}\psi\left(\frac{1}{2} + i\frac{\zeta(\epsilon-\epsilon_1) + E_\sigma(\eta) - i\Gamma/2 - \mu_\alpha}{2\pi k_B T}\right)\bigg]\Bigg\} \ , \tag{J3}
$$
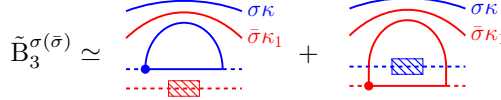
where $\Gamma_\alpha = 2\pi\varrho_\alpha|t_\alpha|^2$ and $\sum_\alpha \Gamma_\alpha = \Gamma$. Fixing the argument $\epsilon_1 = \epsilon$, we have

$$
\tilde{B}^{\sigma(\sigma)}_{3,\boldsymbol{\eta'\eta}} \simeq -\sum_\alpha \frac{\Gamma_\alpha}{\hbar}\left[\frac{1}{2} + \eta\frac{1}{\pi}\mathrm{Im}\psi\left(\frac{1}{2} + i\frac{F_{\bar\sigma,\alpha}(\nu)}{2\pi k_B T}\right)\right]\delta_{\nu'\nu} - \nu'\nu\sum_\alpha \frac{\Gamma_\alpha}{\hbar}\left[\frac{1}{2} + \nu\frac{1}{\pi}\mathrm{Im}\psi\left(\frac{1}{2} + i\frac{F_{\sigma,\alpha}(\eta)}{2\pi k_B T}\right)\right]\delta_{\eta'\eta} \ , \tag{J4}
$$

where $F_{\sigma,\alpha}(\eta) =: E_\sigma(\eta) - \mu_\alpha - i\Gamma/2$.

The 3rd-tier bubble of type $\sigma(\bar\sigma)$ does not have a matrix structure and is given by the contraction of the propagators in Eq. (226), dressed by the simplified fourth-tier bubble $B_4 = -\Gamma/2$, with the vertex $v_x = -|t_\alpha(\epsilon_k)|^2 f^\alpha_x(\epsilon_k)/\hbar^2$, where

x stands for η or ν. It is the composite bubble

$$\tilde{B}_3^{\sigma(\bar\sigma)} \simeq \quad \text{(diagram)} \quad + \quad \text{(diagram)}$$

$$=\hbar \sum_{\kappa_2}\left[\sum_\nu \frac{v_\nu^{\alpha_2}(\epsilon_{k_2})\delta_{\zeta_2,-\zeta}}{\Gamma/2-i\zeta(\epsilon_k-\epsilon_{k_2})-i\zeta_1[\epsilon_{k_1}-E_{\bar\sigma}(\nu)]}+\sum_\eta \frac{v_\eta^{\alpha_2}(k_2)\delta_{\zeta_2,-\zeta_1}}{\Gamma/2-i\zeta_1(\epsilon_{k_1}-\epsilon_{k_2})-i\zeta[\epsilon_k-E_\sigma(\eta)]}\right]$$

$$=\frac{i\zeta}{\hbar}\sum_{\alpha_2}\varrho_{\alpha_2}|t_{\alpha_2}|^2\sum_\nu\int_{-W}^{W}d\epsilon_2\,\frac{f_\nu^{\alpha_2}(\epsilon_2)}{\epsilon_2-\epsilon+\zeta\zeta_1[E_{\bar\sigma}(\nu)-\epsilon_1]-i\zeta\Gamma/2}$$

$$+\frac{i\zeta_1}{\hbar}\sum_{\alpha_2}\varrho_{\alpha_2}|t_{\alpha_2}|^2\sum_\eta\int_{-W}^{W}d\epsilon_2\,\frac{f_\eta^{\alpha_2}(\epsilon_2)}{\epsilon_2-\epsilon_1+\zeta\zeta_1[E_\sigma(\eta)-\epsilon]-i\zeta_1\Gamma/2}\,, \tag{J5}$$

where $E_\sigma(\eta)=\epsilon_\sigma+(1+\eta)U/2$. From Eq. (I6) we obtain

$$\tilde{B}_3^{\sigma(\bar\sigma)}\simeq\frac{i}{\hbar}\sum_\alpha\frac{\Gamma_\alpha}{2\pi}\left\{\zeta\mathrm{Re}\psi\left(\frac{1}{2}+i\frac{\epsilon-\zeta\zeta_1(\epsilon_{\bar\sigma}+U-\epsilon_1)-i\Gamma/2-\mu_\alpha}{2\pi k_B T}\right)-\zeta\mathrm{Re}\psi\left(\frac{1}{2}+i\frac{\epsilon-\zeta\zeta_1(\epsilon_{\bar\sigma}-\epsilon_1)-i\Gamma/2-\mu_\alpha}{2\pi k_B T}\right)\right.$$

$$+\zeta_1\mathrm{Re}\psi\left(\frac{1}{2}+i\frac{\epsilon_1-\zeta\zeta_1(\epsilon_\sigma+U-\epsilon)-i\Gamma/2-\mu_\alpha}{2\pi k_B T}\right)-\zeta_1\mathrm{Re}\psi\left(\frac{1}{2}+i\frac{\epsilon_1-\zeta\zeta_1(\epsilon_\sigma-\epsilon)-i\Gamma/2-\mu_\alpha}{2\pi k_B T}\right)$$

$$+i\left[2\pi-\mathrm{Im}\psi\left(\frac{1}{2}+i\frac{\epsilon-\zeta\zeta_1(\epsilon_{\bar\sigma}+U-\epsilon_1)-i\Gamma/2-\mu_\alpha}{2\pi k_B T}\right)+\mathrm{Im}\psi\left(\frac{1}{2}+i\frac{\epsilon-\zeta\zeta_1(\epsilon_{\bar\sigma}-\epsilon_1)-i\Gamma/2-\mu_\alpha}{2\pi k_B T}\right)\right.$$

$$\left.\left.-\mathrm{Im}\psi\left(\frac{1}{2}+i\frac{\epsilon_1-\zeta\zeta_1(\epsilon_\sigma+U-\epsilon)-i\Gamma/2-\mu_\alpha}{2\pi k_B T}\right)+\mathrm{Im}\psi\left(\frac{1}{2}+i\frac{\epsilon_1-\zeta\zeta_1(\epsilon_\sigma-\epsilon)-i\Gamma/2-\mu_\alpha}{2\pi k_B T}\right)\right]\right\}. \tag{J6}$$

Taking $\epsilon=\epsilon_1=\mu$

$$\tilde{B}_3^{\sigma(\bar\sigma)}\simeq-\sum_\alpha\frac{\Gamma_\alpha}{\hbar}\left[\frac{1}{2}-\frac{1}{2\pi}\sum_\nu\nu\mathrm{Im}\psi\left(\frac{1}{2}+i\frac{R_{\bar\sigma,\alpha}(\nu)}{2\pi k_B T}\right)-\frac{i\zeta}{2\pi}\sum_\nu\nu\mathrm{Re}\psi\left(\frac{1}{2}+i\frac{R_{\bar\sigma,\alpha}(\nu)}{2\pi k_B T}\right)\right]$$

$$-\sum_\alpha\frac{\Gamma_\alpha}{\hbar}\left[\frac{1}{2}-\frac{1}{2\pi}\sum_\nu\eta\mathrm{Im}\psi\left(\frac{1}{2}+i\frac{R_{\sigma,\alpha}(\eta)}{2\pi k_B T}\right)-\frac{i\zeta_1}{2\pi}\sum_\eta\eta\mathrm{Re}\psi\left(\frac{1}{2}+i\frac{R_{\sigma,\alpha}(\eta)}{2\pi k_B T}\right)\right], \tag{J7}$$

where $R_{\sigma,\alpha}(\eta)=:\zeta\zeta_1[E_\sigma(\eta)-\mu_\alpha]-i\Gamma/2$. At equilibrium, in the degenerate case, $\epsilon_\uparrow=\epsilon_\downarrow=\epsilon_0$, and taking $\zeta=+1$ (retarded self-energies)

$$\tilde{B}_{3,\zeta_1=+1}^{\sigma(\bar\sigma)}\simeq-\frac{\Gamma}{\hbar}\left[1-\frac{1}{\pi}\mathrm{Im}\psi\left(\frac{1}{2}+\frac{\Gamma/2}{2\pi k_B T}-i\frac{\epsilon_0+U-\mu}{2\pi k_B T}\right)+\frac{1}{\pi}\mathrm{Im}\psi\left(\frac{1}{2}+\frac{\Gamma/2}{2\pi k_B T}-i\frac{\epsilon_0-\mu}{2\pi k_B T}\right)\right]$$

$$+i\frac{\Gamma}{\hbar\pi}\left[\mathrm{Re}\psi\left(\frac{1}{2}+\frac{\Gamma/2}{2\pi k_B T}-i\frac{\epsilon_0+U-\mu}{2\pi k_B T}\right)-\mathrm{Re}\psi\left(\frac{1}{2}+\frac{\Gamma/2}{2\pi k_B T}-i\frac{\epsilon_0-\mu}{2\pi k_B T}\right)\right] \tag{J8}$$

$$\tilde{B}_{3,\zeta_1=-1}^{\sigma(\bar\sigma)}\simeq-\frac{\Gamma}{\hbar}\left[1-\frac{1}{\pi}\mathrm{Im}\psi\left(\frac{1}{2}+\frac{\Gamma/2}{2\pi k_B T}+i\frac{\epsilon_0+U-\mu}{2\pi k_B T}\right)+\frac{1}{\pi}\mathrm{Im}\psi\left(\frac{1}{2}+\frac{\Gamma/2}{2\pi k_B T}+i\frac{\epsilon_0-\mu}{2\pi k_B T}\right)\right].$$

Appendix K: Dressing the bubble $B^{\sigma(\sigma)}$ in the simplified gDSO4

The dressed bubble $\tilde{\mathbf{B}}^{\sigma(\sigma)}$ in Eq. (214) is obtained by contracting the dressed propagator $\tilde{\mathbf{h}}_2^{\sigma(\sigma)}$ according to

$$\tilde{B}_{\eta'\eta}^{\sigma(\sigma)} = \underbrace{\quad}_{\eta \quad \tilde{\mathbf{h}}_2^{\sigma(\sigma)} \quad \eta'} = \sum_\nu \Big\langle \sum_{\nu'} [\tilde{\mathbf{h}}_2^{\sigma(\sigma)}]_{\boldsymbol{\eta}'\boldsymbol{\eta}} v_\nu \Big\rangle \, , \tag{K1}$$

where the vertex is defined by

$$v_\eta = -\frac{|t_\alpha(\epsilon_k)|^2}{\hbar^2} f_\eta^\alpha(\epsilon_k) \, . \tag{K2}$$

Here, $\tilde{\mathbf{h}}_2^{\sigma(\sigma)}$ has a 4×4 structure in the collective sojourn index $\boldsymbol{\eta} = (\nu, \eta)$ induced by the third-tier bubble $\tilde{\mathbf{B}}_3^{\sigma(\sigma)}$.

In order to avoid the inversion of a four-dimensional matrix in

$$\tilde{\mathbf{h}}_2^{\sigma(\sigma)} = \left[[\mathbf{1}\mathrm{h}_2^{\sigma(\sigma)}]^{-1} - \tilde{\mathbf{B}}_3^{\sigma(\sigma)} \right]^{-1} \, , \quad \text{where} \quad \mathrm{h}_2^{\sigma(\sigma)} = i\hbar \frac{\delta_{\zeta_1, -\zeta}}{\zeta(\epsilon_k - \epsilon_{k_1}) + i0^+} \, , \tag{K3}$$

we exploit the specific form of the third-tier bubbles forming $\tilde{\mathbf{B}}_3^{\sigma(\sigma)}$ in the simplified gDSO4. Specifically, to dress the propagator $\mathbf{1}\mathrm{h}_2^{(\sigma)}$ we retain the 2×2 matrix structure in the sojourn index η of the spin path $\bar{\sigma}$ while using explicitly the structure in ν of the third-tier bubble. To this aim, we write the third-tier bubble in Eq. (J4) as

$$\tilde{\mathbf{B}}_{3,\boldsymbol{\eta}'\boldsymbol{\eta}}^{\sigma(\sigma)} \simeq \underbrace{\quad}_{\eta \quad \quad \eta'}^{\nu \quad \quad \nu} + \underbrace{\quad}_{\eta \quad \quad \eta}^{\nu \quad \quad \nu'} = \tilde{B}_{3,\eta'\eta}^A(\nu)\delta_{\nu'\nu} + \nu'\nu\tilde{B}_{3,\eta'\eta}^B(\nu) \, , \tag{K4}$$

where

$$\begin{aligned}
\tilde{B}_{3,\eta'\eta}^A(\nu) &= -\sum_\alpha \frac{\Gamma_\alpha}{\hbar} \left[\frac{1}{2} + \eta \frac{1}{\pi} \mathrm{Im}\psi \left(\frac{1}{2} + i\frac{F_{\bar{\sigma},\alpha}(\nu)}{2\pi k_B T} \right) \right] \, , \\
\tilde{B}_{3,\eta'\eta}^B(\nu) &= -\sum_\alpha \frac{\Gamma_\alpha}{\hbar} \left[\frac{1}{2} + \nu \frac{1}{\pi} \mathrm{Im}\psi \left(\frac{1}{2} + i\frac{F_{\sigma,\alpha}(\eta)}{2\pi k_B T} \right) \right] \delta_{\eta'\eta} \, ,
\end{aligned} \tag{K5}$$

and where $F_{\sigma,\alpha}(\eta) =: E_\sigma(\eta) - \mu_\alpha - i\Gamma/2$. The following properties hold

$$\begin{aligned}
\tilde{B}_{3,\eta\eta}^A(\nu) &= \tilde{B}_{3,\bar{\eta}\eta}^A(\nu) \, , \\
\sum_\eta \tilde{B}_{3,\eta'\eta}^A(\nu) &= -\Gamma/\hbar \, , \\
\sum_\nu \tilde{B}_{3,\eta'\eta}^B(\nu) &= -\Gamma/\hbar \delta_{\eta'\eta} \, .
\end{aligned} \tag{K6}$$

Note that while in $\tilde{B}_{3,\eta'\eta}^A(\nu)$ the index ν is related to the interaction energy, in $\tilde{B}_{3,\eta'\eta}^B(\nu)$ the same index is related to the vertex and vice-versa for η.

The dressed bubble is then obtained as the contraction

$$\tilde{B}_{\eta'\eta}^{\sigma(\sigma)} = \sum_\nu \langle \tilde{\mathrm{h}}_{2,\eta'\eta}^{\sigma(\sigma)}(\nu) v_\nu \rangle$$

$$= \underbrace{\quad}_{\tilde{\mathbf{h}}_2^A} + \underbrace{\quad}_{\tilde{\mathbf{h}}_2^A \quad \tilde{\mathbf{B}}_3^B \quad \tilde{\mathbf{h}}_2^A} + \dots \, , \tag{K7}$$

where $\tilde{\mathrm{h}}_{2,\eta'\eta}^{\sigma(\sigma)}(\nu) = \sum_{\nu'}[\tilde{\mathbf{h}}_2^{\sigma(\sigma)}]_{\boldsymbol{\eta}'\boldsymbol{\eta}}$ has a two-dimensional structure in η and is obtained by adopting a two-stage procedure: First we iterate the third-tier bubble $\tilde{\mathbf{B}}_3^A$ to obtain the dressed propagator $\tilde{\mathbf{h}}_2^A$ and then insert iteratively

the bubbles $\tilde{\mathbf{B}}_3^B$ accounting for the multiplicative factors $\nu'\nu$ in Eq. (K4). The dressed propagator $\tilde{\mathbf{h}}_2^A(\nu)$ is given by the series

$$
\begin{aligned}
\tilde{\mathbf{h}}_2^A(\nu) =& \mathbf{1}\mathrm{h}_2^{\sigma(\sigma)} + \mathrm{h}_2^{(\sigma)}\tilde{\mathbf{B}}_3^A(\nu)\mathrm{h}_2^{\sigma(\sigma)} + \ldots \\
=& \left[\mathbf{1}[\mathrm{h}_2^{\sigma(\sigma)}]^{-1} - \tilde{\mathbf{B}}_3^A(\nu)\right]^{-1} .
\end{aligned}
\tag{K8}
$$

Note that, while the non-dressed block $\mathbf{h}_2^{(\sigma)} = \mathbf{1}\mathrm{h}_2^{(\sigma)}$ is still diagonal in η, the dressed block $\tilde{\mathbf{h}}_2^A$ acquires a structure in η due to the bubbles $\tilde{\mathbf{B}}_3^A$ that can change the charge state in the dot. Using the properties of $\tilde{\mathbf{B}}_3^A$ in Eq. (K6), the diagonal and off-diagonal matrix elements read

$$
\begin{aligned}
\tilde{\mathrm{h}}_{2,\eta\eta}^A(\nu) =& \frac{[\mathrm{h}_2^{\sigma(\sigma)}]^{-1} - \tilde{\mathrm{B}}_{3,\bar{\eta}\bar{\eta}}^A(\nu)}{\left[[\mathrm{h}_2^{\sigma(\sigma)}]^{-1} - \tilde{\mathrm{B}}_{3,\eta\eta}^A(\nu)\right]\left[[\mathrm{h}_2^{\sigma(\sigma)}]^{-1} - \tilde{\mathrm{B}}_{3,\bar{\eta}\bar{\eta}}^A(\nu)\right] - \tilde{\mathrm{B}}_{3,\eta\bar{\eta}}^A(\nu)\tilde{\mathrm{B}}_{3,\bar{\eta}\eta}^A(\nu)} \\
=& \mathrm{h}_2^{\sigma(\sigma)} + \frac{\tilde{\mathrm{B}}_{3,\bar{\eta}\eta}^A(\nu)}{[\mathrm{h}_2^{\sigma(\sigma)}]^{-1}\left[[\mathrm{h}_2^{\sigma(\sigma)}]^{-1} + \Gamma/\hbar\right]}
\end{aligned}
\tag{K9}
$$

$$
\text{and} \qquad \tilde{\mathrm{h}}_{2,\bar{\eta}\eta}^A(\nu) = \frac{\tilde{\mathrm{B}}_{3,\bar{\eta}\eta}^A(\nu)}{[\mathrm{h}_2^{\sigma(\sigma)}]^{-1}\left[[\mathrm{h}_2^{\sigma(\sigma)}]^{-1} + \Gamma/\hbar\right]} ,
$$

respectively. Thus

$$
\begin{aligned}
\tilde{\mathbf{h}}_2^A(\nu) =& \left[\mathbf{1}[\mathrm{h}_2^{\sigma(\sigma)}]^{-1} - \tilde{\mathbf{B}}_3^A(\nu)\right]^{-1} \\
=& \mathbf{1}\mathrm{h}_2^{\sigma(\sigma)} + \frac{\mathrm{h}_2^{\sigma(\sigma)}}{[\mathrm{h}_2^{\sigma(\sigma)}]^{-1} + \Gamma/\hbar}\tilde{\mathbf{B}}_3^A(\nu) \\
=& \mathbf{1}\mathrm{h}_2^{\sigma(\sigma)} + \mathrm{h}_2^{\sigma(\sigma)}\tilde{\mathrm{h}}_2^{\sigma(\sigma)}\tilde{\mathbf{B}}_3^A(\nu) ,
\end{aligned}
\tag{K10}
$$

where

$$
\tilde{\mathrm{h}}_2^{\sigma(\sigma)} = \frac{1}{[\mathrm{h}_2^{\sigma(\sigma)}]^{-1} + \Gamma/\hbar} \qquad \text{and} \qquad \mathrm{h}_2^{\sigma(\sigma)}\tilde{\mathrm{h}}_2^{\sigma(\sigma)} = \frac{1}{\Gamma/\hbar}\left[\mathrm{h}_2^{\sigma(\sigma)} - \frac{1}{[\mathrm{h}_2^{\sigma(\sigma)}]^{-1} + \Gamma/\hbar}\right] .
\tag{K11}
$$

Including iteratively the third-tier bubbles $\tilde{\mathbf{B}}_3^B$, and accounting for the factors ν and ν' associated to the first and last sojourn in the presence of overlap of three fermion lines of the same spin, the full dressed propagator in Eq. (K7) is the series

$$
\begin{aligned}
\tilde{\mathbf{h}}_2^{\sigma(\sigma)}(\nu) =& \tilde{\mathbf{h}}_2^A(\nu) + \sum_{\nu'}\nu'\tilde{\mathbf{h}}_2^A(\nu')\tilde{\mathbf{B}}_3^B(\nu)\nu\tilde{\mathbf{h}}_2^A(\nu) \\
& + \sum_{\nu'}\nu'\tilde{\mathbf{h}}_2^A(\nu')\sum_{\nu''}\tilde{\mathbf{B}}_3^B(\nu'')\tilde{\mathbf{h}}_2^A(\nu'')\tilde{\mathbf{B}}_3^B(\nu)\nu\tilde{\mathbf{h}}_2^A(\nu) + \ldots \\
=& \tilde{\mathbf{h}}_2^A(\nu) + \sum_{\nu'}\nu'\tilde{\mathbf{h}}_2^A(\nu')\frac{\mathbf{1}}{\mathbf{1} - \sum_{\nu''}\tilde{\mathbf{B}}_3^B(\nu'')\tilde{\mathbf{h}}_2^A(\nu'')}\tilde{\mathbf{B}}_3^B(\nu)\nu\tilde{\mathbf{h}}_2^A(\nu) \\
=& \tilde{\mathbf{h}}_2^A(\nu) + \nu\mathbf{H}(\nu) ,
\end{aligned}
\tag{K12}
$$

where $\Delta\tilde{\mathbf{h}}_2^A = \tilde{\mathbf{h}}_2^A(+1) - \tilde{\mathbf{h}}_2^A(-1) = \mathrm{h}_2^{\sigma(\sigma)}\tilde{\mathrm{h}}_2^{\sigma(\sigma)}[\tilde{\mathbf{B}}_3^A(+1) - \tilde{\mathbf{B}}_3^A(-1)]$, and where we have defined

$$
\mathbf{H}(\nu) := \Delta\tilde{\mathbf{h}}_2^A\frac{\mathbf{1}}{\mathbf{1} - \sum_{\nu''}\tilde{\mathbf{B}}_3^B(\nu'')\tilde{\mathbf{h}}_2^A(\nu'')}\tilde{\mathbf{B}}_3^B(\nu)\tilde{\mathbf{h}}_2^A(\nu) .
\tag{K13}
$$

Note that, in agreement with the results of the diagrammatic rules, in the absence of interaction, the function $\mathbf{H}(\nu)$ vanishes, as it contains the contribution of more than two overlapping fermion lines.

The dressed fermion line block, whose contraction yields the dressed bubble $\tilde{\mathbf{B}}^{\sigma(\sigma)}$ according to Eq. (K7), has the first term proportional to the identity, see Eq. (K10), and the remaining part which is independent of the index η', as can be seen by using the properties of the third-tier bubbles in Eq. (K6). This ensures that the resulting bubble has

the general property Eq. (209), which ultimately allows for expressing the self-energies in terms of the off-diagonal elements of the bubbles, namely

$$\tilde{\Sigma}^{(\sigma)}_{\sigma\eta}(\epsilon) := i\hbar \tilde{B}^{\sigma(\sigma)}_{\bar{\eta}\eta}(\kappa)|_{\zeta=+1} \ . \tag{K14}$$

We can now evaluate the dressed bubble $\tilde{\mathbf{B}}^{\sigma(\sigma)}$ via Eq. (K7) by using Eq. (K12) and splitting the vertex as

$$v_\nu = \delta_{\nu,-1}v + \nu v_+ \ , \tag{K15}$$

where $v = -|t_{\alpha\sigma}(\epsilon_k)|^2/\hbar^2$, and $v_\pm = f_\pm(\epsilon_k)v$, and where we used the relation $f_+(\epsilon) = 1 - f_-(\epsilon)$. The resulting expression is

$$\begin{aligned}
\tilde{\mathbf{B}}^{\sigma(\sigma)} &= \sum_\nu \langle \tilde{\mathbf{h}}^{\sigma(\sigma)}_2(\nu)v_\nu \rangle \\
&= \sum_\nu \langle \tilde{\mathbf{h}}^A_2(\nu)v_\nu \rangle + \sum_\nu \langle \nu \mathbf{H}(\nu)v_\nu \rangle \\
&= \langle \tilde{\mathbf{h}}^A_2(-1)v \rangle + \langle \Delta \tilde{\mathbf{h}}^A_2 v_+ \rangle - \langle \mathbf{H}(-1)v \rangle + \sum_\nu \langle \mathbf{H}(\nu)v_+ \rangle \ .
\end{aligned} \tag{K16}$$

The sum over ν in the last term yields the following simplification

$$\begin{aligned}
\Delta\tilde{\mathbf{h}}^A_2 + \sum_\nu \mathbf{H}(\nu) &= \Delta\tilde{\mathbf{h}}^A_2 + \Delta\tilde{\mathbf{h}}^A_2 \frac{\mathbf{1}}{\mathbf{1} - \sum_{\nu''} \tilde{\mathbf{B}}^B_3(\nu'')\tilde{\mathbf{h}}^A_2(\nu'')} \sum_\nu \tilde{\mathbf{B}}^B_3(\nu)\tilde{\mathbf{h}}^A_2(\nu) \\
&= \Delta\tilde{\mathbf{h}}^A_2 \frac{\mathbf{1}}{\mathbf{1} - \sum_\nu \tilde{\mathbf{B}}^B_3(\nu)\tilde{\mathbf{h}}^A_2(\nu)} \\
&= \Delta\tilde{\mathbf{h}}^A_2 \frac{\mathbf{1}}{\mathbf{1}(1 + \mathrm{h}^{(\sigma)}_2 \Gamma/\hbar) - \mathrm{h}^{(\sigma)}_2 \tilde{\mathrm{h}}^{(\sigma)}_2 \sum_\nu \tilde{\mathbf{B}}^B_3(\nu)\tilde{\mathbf{B}}^A_3(\nu)} \\
&= \Delta\tilde{\mathbf{B}}^A_3 \frac{\mathbf{1}}{\mathbf{1}([\mathrm{h}^{(\sigma)}_2]^{-1} + \Gamma/\hbar)^2 - \sum_\nu \tilde{\mathbf{B}}^B_3(\nu)\tilde{\mathbf{B}}^A_3(\nu)} \\
&\equiv \mathbf{K} \ ,
\end{aligned} \tag{K17}$$

where $\Delta\tilde{\mathbf{B}}^A_3 := \tilde{\mathbf{B}}^A_3(+1) - \tilde{\mathbf{B}}^A_3(-1)$. Using the explicit expressions in Eq. (K5) for the third-tier bubbles, it is possible to cast the matrix $\sum_\nu \tilde{\mathbf{B}}^B_3(\nu)\tilde{\mathbf{B}}^A_3(\nu)$ as the sum of a term proportional to the identity and a second term $\mathbf{P}$ with the symmetry $\mathrm{P}_{\eta\eta} = \mathrm{P}_{\bar{\eta}\eta}$. As a result

$$\sum_\nu \tilde{\mathbf{B}}^B_3(\nu)\tilde{\mathbf{B}}^A_3(\nu) = \mathbf{1}\Delta\mathrm{b}_\sigma\Delta\mathrm{b}_{\bar{\sigma}} + \mathbf{P} \ , \tag{K18}$$

where

$$\begin{aligned}
\Delta\mathrm{b}_{\bar{\sigma}} &= -\sum_\alpha \frac{\Gamma_\alpha}{\hbar}\left[\frac{1}{\pi}\mathrm{Im}\psi\left(\frac{1}{2} + \frac{\Gamma/2}{2\pi k_B T} + i\frac{\epsilon_{\bar{\sigma}} + U - \mu_\alpha}{2\pi k_B T}\right) - \frac{1}{\pi}\mathrm{Im}\psi\left(\frac{1}{2} + \frac{\Gamma/2}{2\pi k_B T} + i\frac{\epsilon_{\bar{\sigma}} - \mu_\alpha}{2\pi k_B T}\right)\right] \ , \\
\Delta\mathrm{b}_\sigma &= -\sum_\alpha \frac{\Gamma_\alpha}{\hbar}\left[\frac{1}{\pi}\mathrm{Im}\psi\left(\frac{1}{2} + \frac{\Gamma/2}{2\pi k_B T} + i\frac{\epsilon_\sigma + U - \mu_\alpha}{2\pi k_B T}\right) - \frac{1}{\pi}\mathrm{Im}\psi\left(\frac{1}{2} + \frac{\Gamma/2}{2\pi k_B T} + i\frac{\epsilon_\sigma - \mu_\alpha}{2\pi k_B T}\right)\right] \ .
\end{aligned} \tag{K19}$$

Using the explicit expression for the matrix elements of $\Delta\tilde{\mathbf{B}}^A_3$, namely $\Delta\tilde{\mathbf{B}}^A_{3,\eta'\eta} = \eta\Delta\mathrm{b}_{\bar{\sigma}}$, the matrix elements of $\mathbf{K}$ read

$$\begin{aligned}
\mathrm{K}_{\eta'\eta} &= \eta\frac{\Delta\mathrm{b}_{\bar{\sigma}}}{([\mathrm{h}^{(\sigma)}_2]^{-1} + \Gamma/\hbar)^2 - \Delta\mathrm{b}_\sigma\Delta\mathrm{b}_{\bar{\sigma}}} \\
&= \eta\frac{\Delta\mathrm{b}_{\bar{\sigma}}}{2\sqrt{\Delta\mathrm{b}_\sigma\Delta\mathrm{b}_{\bar{\sigma}}}}\left[\frac{1}{[\mathrm{h}^{(\sigma)}_2]^{-1} + \Gamma/\hbar - \sqrt{\Delta\mathrm{b}_\sigma\Delta\mathrm{b}_{\bar{\sigma}}}} - \frac{1}{[\mathrm{h}^{(\sigma)}_2]^{-1} + \Gamma/\hbar + \sqrt{\Delta\mathrm{b}_\sigma\Delta\mathrm{b}_{\bar{\sigma}}}}\right] \ .
\end{aligned} \tag{K20}$$

The dressed bubble of type $\sigma(\sigma)$, Eq. (K16), is thus the following sum of three terms

$$\begin{aligned}
\tilde{\mathbf{B}}^{\sigma(\sigma)} &= \langle \tilde{\mathbf{h}}^A_2(-1)v \rangle - \langle \mathbf{H}(-1)v \rangle + \langle \mathbf{K}v_+ \rangle \\
&= -\frac{\Gamma}{2\hbar}\mathbf{1} + \langle \mathrm{h}^{\sigma(\sigma)}_2 \tilde{\mathrm{h}}^{\sigma(\sigma)}_2 v \rangle \tilde{\mathbf{B}}^A_3(-1) - \langle \mathbf{H}(-1)v \rangle + \langle \mathbf{K}v_+ \rangle \ ,
\end{aligned} \tag{K21}$$

where we used Eq. (K10) and the result of Eqs. (136) and (138) for the first term.

We are interested in the off-diagonal elements of this dressed bubble which yields the corresponding retarded self-energies according to Eq. (K14). The second term of Eq. (K21) vanishes because of the contraction with the vertex $v = v_+ + v_-$. Indeed, using the definition in Eq. (K3) and Eq. (K11) for the product $h_2^{\sigma(\sigma)}\tilde{h}_2^{\sigma(\sigma)}$, the contraction yields

$$
\begin{aligned}
\langle h_2^{\sigma(\sigma)}\tilde{h}_2^{\sigma(\sigma)}v\rangle =& \frac{i\zeta}{\hbar}\frac{1}{\Gamma/\hbar}\sum_{\alpha_1}\varrho_{\alpha_1}|t_{\alpha_1}|^2\sum_\nu\int_{-W}^{W}d\epsilon_1\left[\frac{f_\nu^{\alpha_1}(\epsilon_1)}{\epsilon_1-\epsilon-i\zeta 0^+}-\frac{f_\nu^{\alpha_1}(\epsilon_1)}{\epsilon_1-\epsilon-i\zeta\Gamma}\right] \\
=&\frac{i\zeta}{2\pi}\sum_\alpha\frac{\Gamma_\alpha}{\Gamma}\sum_\nu\nu\left\{\mathrm{Re}\psi\left(\frac{1}{2}+i\frac{\epsilon-\mu_\alpha}{2\pi k_B T}\right)-\mathrm{Re}\psi\left(\frac{1}{2}+\frac{\Gamma}{2\pi k_B T}+i\frac{\epsilon-\mu_\alpha}{2\pi k_B T}\right)\right. \\
&\left.-i\zeta\left[\mathrm{Im}\psi\left(\frac{1}{2}+i\frac{\epsilon-\mu_\alpha}{2\pi k_B T}\right)-\mathrm{Im}\psi\left(\frac{1}{2}+\frac{\Gamma}{2\pi k_B T}+i\frac{\epsilon-\mu_\alpha}{2\pi k_B T}\right)\right]\right\}=0\,,
\end{aligned}
\tag{K22}
$$

where we used Eq. (I6) to solve the integral. The third term in Eq. (K21) is evaluated as follows. According to Eq. (K13) and the second line of Eq. (K17), the matrix block $\mathbf{H}(-1)$ can be expressed as the sum of two terms

$$
\begin{aligned}
\mathbf{H}(-1) =&\mathbf{K}\tilde{\mathbf{B}}_3^B(-1)\tilde{h}_2^A(-1)\\
=&h_2^{\sigma(\sigma)}\mathbf{K}\tilde{\mathbf{B}}_3^B(-1)+h_2^{\sigma(\sigma)}\tilde{h}_2^{\sigma(\sigma)}\mathbf{K}\tilde{\mathbf{B}}_3^B(-1)\tilde{\mathbf{B}}_3^A(-1)\,.
\end{aligned}
\tag{K23}
$$

The functions of ϵ_1 to be integrated upon performing the contraction, in the first and second term are of the type

$$
\begin{aligned}
&\frac{h_2^{\sigma(\sigma)}}{[h_2^{\sigma(\sigma)}]^{-1}+\Gamma_\pm/\hbar}=\frac{1}{\Gamma_\pm/\hbar}\left[h_2^{\sigma(\sigma)}-\frac{1}{[h_2^{\sigma(\sigma)}]^{-1}+\Gamma_\pm/\hbar}\right]\\
\text{and}\quad&\frac{h_2^{\sigma(\sigma)}\tilde{h}_2^{\sigma(\sigma)}}{[h_2^{\sigma(\sigma)}]^{-1}+\Gamma_\pm/\hbar}=\frac{1}{\Gamma_\pm/\hbar}\left[h_2^{\sigma(\sigma)}\tilde{h}_2^{\sigma(\sigma)}-\frac{\tilde{h}_2^{\sigma(\sigma)}}{[h_2^{(\sigma)}]^{-1}+\Gamma_\pm/\hbar}\right]\,,
\end{aligned}
\tag{K24}
$$

respectively, where $\Gamma_\pm=\Gamma\pm\hbar\sqrt{\Delta b_\sigma\Delta b_{\bar\sigma}}$. Expanding the functions in the second line as done in the first line, we end up with integrals of the same type of Eq. (K22) which vanish.

Thus, we are left with

$$
\tilde{\mathbf{B}}^{\sigma(\sigma)}=-\frac{\Gamma}{2\hbar}\mathbf{1}+\langle\mathbf{K}v_+\rangle\,.
\tag{K25}
$$

Since $K_{\eta'\eta}$ is independent of η', see Eq. (K20), as already noted above, the bubble $\tilde{\mathbf{B}}^{\sigma(\sigma)}$ has the property

$$
\tilde{B}_{\eta'\eta}^{\sigma(\sigma)}=-\frac{\Gamma}{2\hbar}\delta_{\eta'\eta}+\tilde{B}_{\bar\eta\eta}^{\sigma(\sigma)}\,.
\tag{K26}
$$

Noting that $\Delta b_{\bar\sigma/\sigma}=-|\Delta b_{\bar\sigma/\sigma}|$, the off-diagonal elements are

$$
\begin{aligned}
\tilde{B}_{\bar\eta\eta}^{\sigma(\sigma)}=&\langle K_{\bar\eta\eta}v_+\rangle\\
=&-\frac{i\zeta}{\hbar}\frac{\eta}{2}\sqrt{\frac{|\Delta b_{\bar\sigma}|}{|\Delta b_\sigma|}}\sum_{\alpha_1}\varrho_{\alpha_1}|t_{\alpha_1}|^2\int_{-W}^{W}d\epsilon_1\left[\frac{f_+^{\alpha_1}(\epsilon_1)}{\epsilon_1-\epsilon-i\zeta\Gamma_-}-\frac{f_+^{\alpha_1}(\epsilon_1)}{\epsilon_1-\epsilon-i\zeta\Gamma_+}\right]\,.
\end{aligned}
\tag{K27}
$$

Using Eq. (I5) to perform the integrations we obtain for the corresponding retarded self-energies

$$
\begin{aligned}
\tilde{\Sigma}_{\sigma\eta}^{(\sigma)}(\epsilon)=&\frac{\eta}{2}\sqrt{\frac{|\Delta b_{\bar\sigma}|}{|\Delta b_\sigma|}}\sum_\alpha\frac{\Gamma_\alpha}{2\pi}\left\{\mathrm{Re}\psi\left(\frac{1}{2}+\frac{\Gamma_-}{2\pi k_B T}+i\frac{\epsilon-\mu_\alpha}{2\pi k_B T}\right)-\mathrm{Re}\psi\left(\frac{1}{2}+\frac{\Gamma_+}{2\pi k_B T}+i\frac{\epsilon-\mu_\alpha}{2\pi k_B T}\right)\right.\\
&\left.-i\left[\mathrm{Im}\psi\left(\frac{1}{2}+\frac{\Gamma_-}{2\pi k_B T}+i\frac{\epsilon-\mu_\alpha}{2\pi k_B T}\right)-\mathrm{Im}\psi\left(\frac{1}{2}+\frac{\Gamma_+}{2\pi k_B T}+i\frac{\epsilon-\mu_\alpha}{2\pi k_B T}\right)\right]\right\}\,.
\end{aligned}
\tag{K28}
$$

Note that these self-energies have the property

$$
\sum_\eta\tilde{\Sigma}_{\sigma\eta}^{(\sigma)}(\epsilon)=0\,.
\tag{K29}
$$

At equilibrium, $\mu_L = \mu_R = \mu$, and at $\epsilon = \mu$

$$\tilde{\Sigma}_{\sigma\eta}^{(\sigma)}(\mu) = \frac{\eta}{2}\sqrt{\frac{|\Delta b_{\bar{\sigma}}|}{|\Delta b_\sigma|}}\frac{\Gamma}{2\pi}\left[\mathrm{Re}\psi\left(\frac{1}{2}+\frac{\Gamma_-}{2\pi k_\mathrm{B}T}\right) - \mathrm{Re}\psi\left(\frac{1}{2}+\frac{\Gamma_+}{2\pi k_\mathrm{B}T}\right)\right] . \tag{K30}$$

Consider the degenerate case, $\epsilon_\uparrow = \epsilon_\downarrow = \epsilon_0$. The self-energies are well-behaved in the limit $T \to 0$, though they do not yield the correct unitary limit for the conductance. Moreover, the correct behavior for the exponent of the expression for Kondo temperature is not captured by this scheme. Indeed, around the center of the Coulomb diamond, namely for $\mu - \epsilon_0, U - \mu + \epsilon_0 \gg \Gamma$, from Eq. (K19) $\Delta b_{\bar{\sigma}} = \Delta b_\sigma \sim -\Gamma/\hbar$ and the dressed self-energy $\tilde{\Sigma}_{\sigma-}^{(\sigma)}(\mu)$ is approximated, at low temperature, by

$$\begin{aligned}
\tilde{\Sigma}_{\sigma,-}^{(\sigma)}(\mu) &\simeq -\frac{\Gamma}{4\pi}\left[\mathrm{Re}\psi\left(\frac{1}{2}\right) - \mathrm{Re}\psi\left(\frac{1}{2}+\frac{2\Gamma}{2\pi k_\mathrm{B}T}\right)\right] \\
&\simeq \frac{\Gamma}{4\pi}\mathrm{Re}\psi\left(\frac{1}{2}+\frac{2\Gamma}{2\pi k_\mathrm{B}T}\right) .
\end{aligned} \tag{K31}$$

As shown in the main text, the prefactor yields an incorrect exponent in the Kondo temperature.

Appendix L: Evaluation of the dressed bubble $\tilde{\mathbf{B}}^{\sigma(\bar{\sigma})}$ in the simplified gDSO4

The dressed bubble $\tilde{\mathbf{B}}^{\sigma(\bar{\sigma})}$ is given by iteratively inserting the composite 3rd-level bubble $\tilde{\mathrm{B}}_3^{\sigma(\bar{\sigma})}$ in Eq (J5) which results in the geometrical series

$$\tilde{\mathrm{B}}_{\eta'\eta}^{\sigma(\bar{\sigma})} = \left\langle \frac{1}{[\mathrm{h}_2^{\sigma(\bar{\sigma})}]^{-1} - \tilde{\mathrm{B}}_3^{\sigma(\bar{\sigma})}}\mathrm{v}_{-\eta}\right\rangle , \tag{L1}$$

where the bare propagator $\mathrm{h}_2^{\sigma(\bar{\sigma})}$ is given by

$$\mathrm{h}_2^{\sigma(\bar{\sigma})} = i\hbar\frac{1}{\zeta(\epsilon_k - E_\sigma) + \zeta_1(\epsilon_{k_1} - E_{\bar{\sigma}}) + i0^+} \tag{L2}$$

and $E_\sigma = \epsilon_\sigma - U/2$. From Eq. (L1), the retarded ($\zeta = +1$), dressed self-energy of type $(\bar{\sigma})$ reads

$$\begin{aligned}
\tilde{\Sigma}_{\sigma,\eta}^{(\bar{\sigma})}(\epsilon) &\equiv i\zeta\hbar\tilde{\mathrm{B}}_{\bar{\eta}\eta}^{\sigma(\bar{\sigma})}(\kappa)|_{\zeta=+1} \\
&= i\zeta\hbar^2\sum_{\kappa_1}\frac{-(|\mathrm{t}_{\alpha_1}(\epsilon_{k_1})|^2/\hbar^2)f_{-\eta}^{\alpha_1}(\epsilon_{k_1})}{-i\zeta(\epsilon_k - \epsilon_\sigma - U/2\hbar) - i\zeta_1(\epsilon_{k_1} - \epsilon_{\bar{\sigma}} - U/2\hbar) - \hbar\tilde{\mathrm{B}}_3^{\sigma(\bar{\sigma})}|_{\zeta=+1}} \\
&= \sum_{\alpha_1}\varrho_{\alpha_1}|\mathrm{t}_{\alpha_1}|^2\sum_{\zeta_1}\zeta_1\int_{-W}^W d\epsilon_1\frac{f_{-\eta}^{\alpha_1}(\epsilon_1)}{\epsilon_1 - [\epsilon_{\bar{\sigma}} + \zeta_1(\epsilon_\sigma - \epsilon) + \delta_{\zeta_1,+1}U] - i\zeta_1\hbar\tilde{\mathrm{B}}_3^{\sigma(\bar{\sigma})}|_{\zeta=+1}} .
\end{aligned} \tag{L3}$$

As an approximation, assuming the 3rd-tier self-energies to be constant with respect to ϵ_1 as in Eqs. (J7)-(J8), the integral in Eq. (L3) is readily solved as

$$\begin{aligned}
\tilde{\Sigma}_{\sigma\eta}^{(\bar{\sigma})}(\epsilon) &\simeq \sum_\alpha\varrho_\alpha|\mathrm{t}_\alpha|^2\sum_{\zeta_1}\zeta_1\int_{-W}^W d\epsilon_1\frac{f_{-\eta}^\alpha(\epsilon_1)}{\epsilon_1 - \mathcal{E}_{\zeta_1} - i\zeta_1\hbar\mathrm{Re}\,\tilde{\mathrm{B}}_3^{\sigma(\bar{\sigma})}} \\
&= \sum_\alpha\varrho_\alpha|\mathrm{t}_\alpha|^2\sum_{\zeta_1}\zeta_1\int_{-W}^W d\epsilon_1\frac{f_{-\eta}^\alpha(\epsilon_1)}{\epsilon_1 - \mathcal{E}_{\zeta_1} + i\zeta_1\hbar|\mathrm{Re}\,\tilde{\mathrm{B}}_3^{\sigma(\bar{\sigma})}|} \\
&= \sum_\alpha\frac{\Gamma_\alpha}{2\pi}\Bigg\{-\eta\left[\mathrm{Re}\psi\left(\frac{1}{2}+i\frac{\mathcal{E}_{+1} - i\hbar|\mathrm{Re}\,\tilde{\mathrm{B}}_{3,\zeta_1=+1}^{\sigma(\bar{\sigma})}| - \mu_\alpha}{2\pi k_\mathrm{B}T}\right) - \mathrm{Re}\psi\left(\frac{1}{2}+i\frac{\mathcal{E}_{-1} - i\hbar|\mathrm{Re}\,\tilde{\mathrm{B}}_{3,\zeta_1=-1}^{\sigma(\bar{\sigma})}| - \mu_\alpha}{2\pi k_\mathrm{B}T}\right)\right] \\
&\quad - i\left[\pi + \eta\mathrm{Im}\psi\left(\frac{1}{2}+i\frac{\mathcal{E}_{+1} - i\hbar|\mathrm{Re}\,\tilde{\mathrm{B}}_{3,\zeta_1=+1}^{\sigma(\bar{\sigma})}| - \mu_\alpha}{2\pi k_\mathrm{B}T}\right) + \eta\mathrm{Im}\psi\left(\frac{1}{2}+i\frac{\mathcal{E}_{-1} - i\hbar|\mathrm{Re}\,\tilde{\mathrm{B}}_{3,\zeta_1=-1}^{\sigma(\bar{\sigma})}| - \mu_\alpha}{2\pi k_\mathrm{B}T}\right)\right]\Bigg\} ,
\end{aligned} \tag{L4}$$

where, in the second line, we used explicitly the fact that the real part of $\tilde{B}_3^{\sigma(\bar{\sigma})}$ is negative, see Eqs. (J7)-(J8). Here, the energies in the arguments of the digamma functions read

$$\mathcal{E}_{\zeta_1} = \epsilon_{\bar{\sigma}} + \zeta_1(\epsilon_\sigma - \epsilon) + \delta_{\zeta_1,+1}U - \zeta_1\hbar\mathrm{Im}\,\tilde{B}_{3,\zeta_1}^{\sigma(\bar{\sigma})} \; . \tag{L5}$$

Note that

$$\sum_\eta \tilde{\Sigma}_{\sigma\eta}^{(\bar{\sigma})}(\epsilon) = -\mathrm{i}\Gamma \; . \tag{L6}$$

This is a general property, not due to the approximate evaluation of the integral in Eq. (L4). Indeed, it can be obtained directly from the integral form, Eq. (L3), by summing over η and applying Eq. (I1).

---

[1] P. W. Anderson, "Localized Magnetic States in Metals," Phys. Rev. **124**, 41–53 (1961).

[2] T. K. Ng and P. A. Lee, "On-Site Coulomb Repulsion and Resonant Tunneling," Phys. Rev. Lett. **61**, 1768–1771 (1988).

[3] L. Glazman and M. Rahik, "Resonant Kondo transparency of a barrier with quasilocal impurity states," JETP Lett. **11**, 2389 (1988).

[4] A.P. Hewson, *The Kondo problem to heavy fermions* (Cambridge University Press, Cambridge, 1993).

[5] W. G. van der Wiel, S. De Franceschi, T. Fujisawa, J. M. Elzerman, S. Tarucha, and L. P. Kouwenhoven, "The Kondo Effect in the Unitary Limit," Science **289**, 2105 (2000).

[6] L. Kouwenhoven and L. Glazman, "Revival of the Kondo effect," Physics World **14**, 33–38 (2001).

[7] K. G. Wilson, "The renormalization group: Critical phenomena and the Kondo problem," Rev. Mod. Phys. **47**, 773–840 (1975).

[8] R. Bulla, T. A. Costi, and T. Pruschke, "Numerical renormalization group method for quantum impurity systems," Rev. Mod. Phys. **80**, 395–450 (2008).

[9] S. R. White, "Density matrix formulation for quantum renormalization groups," Phys. Rev. Lett. **69**, 2863–2866 (1992).

[10] U. Schollwöck, "The density-matrix renormalization group in the age of matrix product states," Ann. Phys. **326**, 96–192 (2011).

[11] F. B. Anders and A. Schiller, "Real-Time Dynamics in Quantum-Impurity Systems: A Time-Dependent Numerical Renormalization-Group Approach," Phys. Rev. Lett. **95**, 196801 (2005).

[12] F. Heidrich-Meisner, A. E. Feiguin, and E. Dagotto, "Real-time simulations of nonequilibrium transport in the single-impurity Anderson model," Phys. Rev. B **79**, 235336 (2009).

[13] S. Weiss, J. Eckel, M. Thorwart, and R. Egger, "Iterative real-time path integral approach to nonequilibrium quantum transport," Phys. Rev. B **77**, 195316 (2008).

[14] L. Mühlbacher and E. Rabani, "Real-Time Path Integral Approach to Nonequilibrium Many-Body Quantum Systems," Phys. Rev. Lett. **100**, 176403 (2008).

[15] J. Jin, X. Zheng, and Y. J. Yan, "Exact dynamics of dissipative electronic systems and quantum transport: Hierarchical equations of motion approach," J. Chem. Phys. **128**, 234703 (2008).

[16] C. Schinabeck, A. Erpenbeck, R. Härtle, and M. Thoss, "Hierarchical quantum master equation approach to electronic-vibrational coupling in nonequilibrium transport through nanosystems," Phys. Rev. B **94**, 201407 (2016).

[17] E. Arrigoni, M. Knap, and W. von der Linden, "Nonequilibrium Dynamical Mean-Field Theory: An Auxiliary Quantum Master Equation Approach," Phys. Rev. Lett. **110**, 086403– (2013).

[18] A. Dorda, M. Nuss, W. von der Linden, and E. Arrigoni, "Auxiliary master equation approach to nonequilibrium correlated impurities," Phys. Rev. B **89**, 165105 (2014).

[19] D. M Fugger, A. Dorda, F. Schwarz, J. von Delft, and E. Arrigoni, "Nonequilibrium Kondo effect in a magnetic field: auxiliary master equation approach," New J. Phys. **20**, 013030 (2018).

[20] J. Eckel, F. Heidrich-Meisner, S. G. Jakobs, M. Thorwart, M. Pletyukhov, and R. Egger, "Comparative study of theoretical methods for non-equilibrium quantum transport," New J. Phys. **12**, 043042 (2010).

[21] Y. Meir and N. S. Wingreen, "Landauer formula for the current through an interacting electron region," Phys. Rev. Lett. **68**, 2512–2515 (1992).

[22] H. J. W. Haug and A.-P. Jahuo, *Quantum Kinetics in transport and optics of semiconductors, Springer Series in Solid-State Science* (Springer-Verlag, Berlin 2nd Ed., 2008).

[23] E. Scheer and J. C. Cuevas, *Molecular electronics: an introduction to theory and experiment* (World Scientific, Singapore, 2010).

[24] D. Ryndyk, *Theory of Quantum Transport at Nanoscale* (Springer, New York, 2016).

[25] M. Thoss and F. Evers, "Perspective: Theory of quantum transport in molecular junctions," J. Chem. Phys. **148**, 030901 (2018).

[26] G. Cohen and M. Galperin, "Green's function methods for single molecule junctions," J. Chem. Phys. **152**, 090901 (2020).

[27] F. Evers, R. Korytár, S. Tewari, and J. M. van Ruitenbeek, "Advances and challenges in single-molecule electron transport," Rev. Mod. Phys. **92**, 035001 (2020).

[28] K. Blum, *Density matrix theory and applications*, Vol. 64 (Springer, Berlin, 2012).

[29] H. Schoeller, "Transport Theory of Interacting Quantum Dots," in *Mesoscopic Electron Transport*, Nato Science Series E (Kluwer, Dordrecht, 1997) pp. 291–330.

[30] C. Timm, "Tunneling through molecules and quantum dots: Master-equation approaches," Phys. Rev. B **77**, 195416 (2008).

[31] C. Timm, "Time-convolutionless master equation for quantum dots: Perturbative expansion to arbitrary order," Phys. Rev. B **83**, 115416 (2011).

[32] S. Andergassen, V. Meden, H. Schoeller, J. Splettstoesser, and M. R. Wegewijs, "Charge transport through single molecules, quantum dots and quantum wires," Nanotechnology **21**, 272001 (2010).

[33] T. J. Levy and E. Rabani, "Symmetry breaking and restoration using the equation-of-motion technique for nonequilibrium quantum impurity models," J. Phys.: Condens. Matter **25**, 115302 (2013).

[34] S. Koller, M. Grifoni, M. Leijnse, and M. R. Wegewijs, "Density-operator approaches to transport through interacting quantum dots: Simplifications in fourth-order perturbation theory," Phys. Rev. B **82**, 235307 (2010).

[35] B. de Souza Melo, L. G. G. V. Dias da Silva, A. R. Rocha, and C. Lewenkopf, "Quantitative comparison of Anderson impurity solvers applied to transport in quantum dots," J. Phys.: Condens. Matter **32**, 095602 (2019).

[36] V. Reimer, M. R. Wegewijs, K. Nestmann, and M. Pletyukhov, "Five approaches to exact open-system dynamics: Complete positivity, divisibility, and time-dependent observables," J. Chem. Phys. **151**, 044101 (2019).

[37] C J. Lindner, F. B. Kugler, V. Meden, and H. Schoeller, "Renormalization group transport theory for open quantum systems: Charge fluctuations in multilevel quantum dots in and out of equilibrium," Phys. Rev. B **99**, 205142 (2019).

[38] M. S. Ferguson, O. Zilberberg, and G. Blatter, "Open quantum systems beyond Fermi's golden rule: Diagrammatic expansion of the steady-state time-convolutionless master equation," arXiv:2010.09838 (2020).

[39] Y. Meir, N. S. Wingreen, and P. A. Lee, "Transport through a strongly interacting electron system: Theory of periodic conductance oscillations," Phys. Rev. Lett. **66**, 3048–3051 (1991).

[40] V. Kashcheyevs, A. Aharony, and O. Entin-Wohlman, "Applicability of the equations-of-motion technique for quantum dots," Phys. Rev. B **73**, 125338 (2006).

[41] R. Van Roermund, S-Y. Shiau, and M. Lavagna, "Anderson model out of equilibrium: Decoherence effects in transport through a quantum dot," Phys. Rev. B **81**, 165115 (2010).

[42] M. Lavagna, "Transport through an interacting quantum dot driven out-of-equilibrium," J. Phys.: Conf. Ser. **592**, 012141 (2015).

[43] U. Eckern and K. I Wysokiński, "Two- and three-terminal far-from-equilibrium thermoelectric nanodevices in the Kondo regime," New J. Phys. **22**, 013045 (2020).

[44] J. N. Pedersen and A. Wacker, "Tunneling through nanosystems: Combining broadening with many-particle states," Phys. Rev. B **72**, 195330 (2005).

[45] O. Karlström, C. Emary, P. Zedler, J. N. Pedersen, C. Bergenfeldt, P. Samuelsson, T. Brandes, and A. Wacker, "A diagrammatic description of the equations of motion, current and noise within the second-order von Neumann approach," J. Phys. A: Math. Theor. **46**, 065301 (2013).

[46] H. Schoeller and G. Schön, "Mesoscopic quantum transport: Resonant tunneling in the presence of a strong Coulomb interaction," Phys. Rev. B **50**, 18436–18452 (1994).

[47] J. König, J. Schmid, H. Schoeller, and G. Schön, "Resonant tunneling through ultrasmall quantum dots: Zero-bias anomalies, magnetic-field dependence, and boson-assisted transport," Phys. Rev. B **54**, 16820–16837 (1996).

[48] M. Leijnse and M. R. Wegewijs, "Kinetic equations for transport through single-molecule transistors," Phys. Rev. B **78**, 235424 (2008).

[49] J. Kern and M. Grifoni, "Transport across an Anderson quantum dot in the intermediate coupling regime," EPJB **86**, 384 (2013).

[50] J. Jin, J. Li, Y. Liu, X-Q Li, and YJ Yan, "Improved master equation approach to quantum transport: From Born to self-consistent Born approximation," J. Chem. Phys **140**, 244111 (2014).

[51] R. B. Saptsov and M. R. Wegewijs, "Fermionic superoperators for zero-temperature nonlinear transport: Real-time perturbation theory and renormalization group for Anderson quantum dots," Phys. Rev. B **86**, 235432 (2012).

[52] R. B. Saptsov and M. R. Wegewijs, "Time-dependent quantum transport: Causal superfermions, exact fermion-parity protected decay modes, and Pauli exclusion principle for mixed quantum states," Phys. Rev. B **90**, 045407 (2014).

[53] H. Schoeller and J. König, "Real-Time Renormalization Group and Charge Fluctuations in Quantum Dots," Phys. Rev. Lett. **84**, 3686–3689 (2000).

[54] A. Rosch, J. Paaske, J. Kroha, and P. Wölfle, "Nonequilibrium Transport through a Kondo Dot in a Magnetic Field: Perturbation Theory and Poor Man's Scaling," Phys. Rev. Lett. **90**, 076804 (2003).

[55] J. Paaske, A. Rosch, and P. Wölfle, "Nonequilibrium transport through a Kondo dot in a magnetic field: Perturbation theory," Phys. Rev. B **69**, 155330 (2004).

[56] J. Paaske, A. Rosch, J. Kroha, and P. Wölfle, "Nonequilibrium transport through a Kondo dot: Decoherence effects," Phys. Rev. B **70**, 155301 (2004).

[57] A. Rosch, J. Paaske, J. Kroha, and P. Wölfle, "The Kondo Effect in Non-Equilibrium Quantum Dots: Perturbative Renormalization Group," J. Phys. Soc. Japan **74**, 118–126 (2005).

[58] M. Pletyukhov and H. Schoeller, "Nonequilibrium Kondo model: Crossover from weak to strong coupling," Phys. Rev. Lett. **108**, 260601 (2012).

[59] C. Karrasch, T. Enss, and V. Meden, "Functional renormalization group approach to transport through correlated quantum dots," Phys. Rev. B **73**, 235337 (2006).

[60] A. Altland and B. D. Simons, *Condensed Matter Field Theory* (Cambridge University Press, 2010).

[61] A. Kamenev, in *Nanoscopic Quantum Transport, Proceedings of the Les Houches Summer School of Theoretical Physics, 2004*, Vol. 81 (Elsevier, Amsterdam, 2005) pp. 177–246.

[62] U. Weiss, *Quantum Dissipative Systems* (World Scientific, Singapore, 2012, 4th ed.).

[63] J. Jin, M. W.-Y. Tu, W.-M. Zhang, and Y. J. Yan, "Non-equilibrium quantum theory for nanodevices based on the Feynman–Vernon influence functional," New J. Phys. **12**, 083013 (2010).

[64] A. Altland and R. Egger, "Nonequilibrium Dephasing in Coulomb Blockaded Quantum Dots," Phys. Rev. Lett. **102**, 026805 (2009).

[65] N. S. Wingreen and Y. Meir, "Anderson model out of equilibrium: Noncrossing-approximation approach to transport through a quantum dot," Phys. Rev. B **49**, 11040–11052 (1994).

[66] S. Smirnov and M. Grifoni, "Nonequilibrium Kondo transport through a quantum dot in a magnetic field," New J. Phys. **15**, 073047 (2013).

[67] D. R. Schmid, S. Smirnov, M. Margańska, A. Dirnaichner, P. L. Stiller, M. Grifoni, A. K. Hüttel, and C. Strunk, "Broken SU(4) symmetry in a Kondo-correlated carbon nanotube," Phys. Rev. B **91**, 155435 (2015).

[68] M. Niklas, S Smirnov, D. Mantelli, M. Margańska, N.-V. Nguyen, W. Wernsdorfer, J.-P. Cleuziou, and M. Grifoni, "Blocking transport resonances via Kondo many-body entanglement in quantum dots," Nat. Commun. **7**, 12442 (2016).

[69] A. Lahiri, T. Hata, S. Smirnov, M. Ferrier, T. Arakawa, M. Niklas, M. Marganska, K. Kobayashi, and M. Grifoni, "Unraveling a concealed resonance by multiple Kondo transitions in a quantum dot," Phys. Rev. B **101**, 041102 (2020).

[70] J. W. Negele and H. Orland, *Quantum Many-Particle Systems* (Addison-Wesley Publishing Company, Redwood City, California, 1988).

[71] K. E. Cahill and R. J. Glauber, "Density operators for fermions," Phys. Rev. A **59**, 1538–1555 (1999).

[72] M. W.-Y. Tu and W.-M. Zhang, "Non-Markovian decoherence theory for a double-dot charge qubit," Phys. Rev. B **78**, 235311 (2008).

[73] W.-M. Zhang, P.-Y. Lo, H.-N. Xiong, M. W.-Y. Tu, and F. Nori, "General Non-Markovian Dynamics of Open Quantum Systems," Phys. Rev. Lett. **109**, 170402 (2012).

[74] P.-Y. Yang and W.-M. Zhang, "Master equation approach to transient quantum transport in nanostructures," Front. Phys. **12**, 127204 (2016).

[75] H. Grabert and M. H. Devoret (Eds.), *Single Charge Tunneling*, Nato Science Series B (Springer, 1992).

[76] Y. Meir, N. S. Wingreen, and P. A. Lee, "Low-temperature transport through a quantum dot: The Anderson model out of equilibrium," Phys. Rev. Lett. **70**, 2601–2604 (1993).

[77] A. J. Leggett, S. Chakravarty, A. T. Dorsey, Matthew P. A. Fisher, Anupam Garg, and W. Zwerger, "Dynamics of the dissipative two-state system," Rev. Mod. Phys. **59**, 1–85 (1987).

[78] R. Hanson, L. P. Kouwenhoven, R. J. Petta, S. Tarucha, and K. L. M. Vandersypen, "Spins in few-electron quantum dots," Rev. Mod. Phys. **79**, 1217–1265 (2007).

[79] A. E. Laird, F. Kuemmeth, G. A. Steele, K. Grove-Rasmussen, J. Nygård, K. Flensberg, and L. P. Kouwenhoven, "Quantum transport in carbon nanotubes," Rev. Mod. Phys. **87**, 703–764 (2015).

[80] M. Grifoni and P. Hänggi, "Driven quantum tunneling," Phys. Rep. **304**, 229–354 (1998).

[81] M. Schiro and O. Scarlatella, "Quantum impurity models coupled to Markovian and non-Markovian baths," J. Chem. Phys. **151**, 044102 (2019).

[82] J. König and J. Martinek, "Interaction-Driven Spin Precession in Quantum-Dot Spin Valves," Phys. Rev. Lett. **90**, 166602 (2003).

[83] M. Braun, J. König, and J. Martinek, "Frequency-dependent current noise through quantum-dot spin valves," Phys. Rev. B **74**, 075328 (2006).

[84] R. Hornberger, S. Koller, G. Begemann, A. Donarini, and M. Grifoni, "Transport through a double-quantum-dot system with noncollinearly polarized leads," Phys. Rev. B **77**, 245313 (2008).

[85] A. Rezaei, R. Hussein, A. Kamra, and W. Belzig, "Phase-controlled spin and charge currents in a superconductor-ferromagnet hybrid," Phys. Rev. Research **2**, 033336 (2020).

[86] C. Rohrmeier and A. Donarini, "Pseudospin resonances reveal synthetic spin-orbit interaction," arXiv:2008.09857 (2021).

[87] D. Darau, G. Begemann, A. Donarini, and M. Grifoni, "Interference effects on the transport characteristics of a benzene single-electron transistor," Phys. Rev. B **79**, 235404 (2009).

[88] A. Donarini, M. Niklas, M. Schafberger, N. Paradiso, C. Strunk, and M. Grifoni, "Coherent population trapping by dark state formation in a carbon nanotube quantum dot," Nat. Commun. **10**, 381 (2019).

[89] This integral can be solved by noting that the denominator in the integral splits as $\left\{ [(\epsilon - \epsilon_0) - i\Gamma/2]^{-1} - [(\epsilon - \epsilon_0) + i\Gamma/2]^{-1} \right\} / i\Gamma$ and by applying Eq. (I6).

[90] J. König, Master's thesis, Universität Karlsruhe (1995).

[91] S. Koller, M. Grifoni, and J. Paaske, "Sources of negative tunneling magnetoresistance in multilevel quantum dots with ferromagnetic contacts," Phys. Rev. B **85**, 045313 (2012).

[92] A. Dirnaichner, M. Grifoni, A. Prüfling, D. Steininger, A. K. Hüttel, and C. Strunk, "Transport across a carbon nanotube quantum dot contacted with ferromagnetic leads: Experiment and nonperturbative modeling," Phys. Rev. B **91**, 195402 (2015).

[93] H. Grabert, P. Schramm, and G.-L. Ingold, "Quantum Brownian motion: the functional integral approach," Phys. Rep. **168**, 115–207 (1988).

[94] H. A. Nilsson, O. Karlström, M. Larsson, P. Caroff, J. N. Pedersen, L. Samuelson, A. Wacker, L. E. Wernersson, and H. Q. Xu, "Correlation-induced conductance suppression at level degeneracy in a quantum dot," Phys. Rev. Lett. **104**, 186804 (2010).

[95] S. Kohler, S. Camalet, M. Strass, J. Lehmann, G.-L. Ingold, and P. Hänggi, "Charge transport through a molecule driven by a high-frequency field," Chem. Phys. **296**, 243–249 (2004).